2007

Oil bypassing by water invasion to wells: mechanisms and remediation

Juan Carlos Hernandez
Louisiana State University and Agricultural and Mechanical College, jhern14@lsu.edu

OIL BYPASSING BY WATER INVASION TO WELLS: MECHANISMS AND REMEDIATION

A Dissertation

Submitted to the Graduate Faculty of the
Louisiana State University and
Agricultural and Mechanical College
in partial fulfillment of the
requirements for the degree of
Doctor of Philosophy

In

The Department of Petroleum Engineering

By
Juan C. Hernandez
B.S., Universidad de Oriente, Venezuela, 1998
MPhil, Imperial College of Science, Technology and Medicine, London, 2001
August, 2007

DEDICATION

To God, my best friend…

To my son, my motivation and inspiration…

To my wife, because you are still the air I want to breathe…

To my parents, who give me strength and taught me the value of faith and love…

To my parents in law, who love me like their own son and are always there when I need…

To my family and friends, who have always supported me with endless love and care…

ACKNOWLEDGEMENTS

The author expresses special gratitude and appreciation to Dr. Andrew K. Wojtanowicz, for his patience, guidance and knowledge. Dr. Wojtanowicz gave me the opportunity of pursuing doctoral studies in a difficult moment in my life, which I will always remember and appreciate. He was always willing to discuss new ideas and offer valuable help.

A deep appreciation is also extended to Dr. Chris White for his guidance and supervision through my research work here at LSU. Dr. White helped me to obtain my first internship, which I will never forget. I am also very thankful to my other examining committee members, Dr. Julius Langlinais, who was always there when I needed advice and Dr. Richard Hughes, who was always kind and open to discussions.

I wish to express my gratitude to the LSU Craft and Hawkins Department of Petroleum Engineering and the State of Louisiana for providing financial support to my graduate studies. I also want to thank Dr. John McMullan for his advice and for giving me the opportunity of teaching the numerical simulation class.

Finally, I want to extend my most deep appreciation to all other faculty members and graduate students in the Department. You made these years at LSU some of the best years in my life!

TABLE OF CONTENTS

LIST OF TABLES

LIST OF FIGURES

ABSTRACT

This study addresses oil bypassing caused by water invasion to wells in edge and bottom water-drive oil reservoirs – a significant problem worldwide. It is shown that the amount of by-passed (not recovered) oil is significant and could be predicted analytically and reduced by modifying well's completion. A large statistical sample from the population of possible reservoir-well systems with edge and bottom-water has been created theoretically using several databases of actual reservoirs properties worldwide. Dimensional analysis allowed converting reservoir properties distributions into dimensionless group distributions. Then, the amount of by-passed oil was correlated with the dimensionless groups using designed experiments conducted on a reservoir simulator. The resulting correlations determine the percent amount of movable oil that could be recovered by the end of well's operation, when the water cut value reaches its maximum limit. They also show how operational parameters such as well spacing, penetration and production rate may affect oil recovery. From the sensitivity analysis, the end-point mobility ratio appears to control more than 55 percent of the oil bypassing process –far more than other groups. The statistical results also show that half of the typical edge and bottom-water well-reservoir systems would have at least 17% or 25% of their movable oil bypassed, respectively.

The effect of reservoir heterogeneity defined by permeability stratification has been studied for edge-water systems having transgressive, regressive and serrated depositional sequences with a Dykstra-Parsons coefficient of 0.75. Oil bypassing showed to be qualitatively more significant in the transgressive sequences. It was also found that the effect of reservoir heterogeneity is more significant for reservoirs with high end-point mobility ratios.

Numerical reservoir simulation is also used to investigate improved recovery of well's completions of different penetration and dual-completed wells with segregated inflow from the

top and bottom (water sink) completions. It appears that short completions perform best in reservoirs with large end-point mobility ratios produced at low rates by delaying water breakthrough and improving the amount of oil recovered per barrel of fluid produced. For most reservoirs with water drive, however, the results show that the best single completion strategy is the use of fully penetrating wells, since they improve the recovery rate.

Dual well completions with "water sink" (DWS) enable independent (although synchronized) rate schedules at the two completions. This study offers a new method to operate DWS systems by using variable rates at the bottom completion for a constant production rate - with limited maximum water cut - at the top completion over the entire life of the well. The method provides better distribution of produced fluids, as it controls water saturation outside the well. When compared with conventional "short" completion, DWS well recovers oil faster and may also produce oil-free water for re-injection. However, a comparison with long single completion of similar length based on the same total fluid rate does not give different recovery rates but shows that DWS well operates at different pressure drawdowns and produces two streams of fluids having substantially different compositions. It is, then, concluded that the recovery performance of the two types of wells may be different if the basis for comparison is a maximum pressure drawdown rather than same total fluid rate.

CHAPTER 1. INTRODUCTION

1.1. Background and Purpose

Oil bypassing is a significant problem in U.S. reservoirs. Of the 582 billion barrels of oil in-place in discovered fields in the U.S., 208 billions have been already produced or proven, leaving behind 374 billion barrels of oil (Advanced Resources International, 2006), or 64.3% of the oil in place. Water invasion is known to be a major contributor to this problem. On average in the United States, more than seven barrels of water are produced for each barrel of oil (R. Lee, 2002).

The problem of oil bypassing by water invasion can be caused by different reasons in different wells and reservoirs. Displacement of oil by water is controlled by viscous forces, gravity forces, capillary forces and heterogeneities. These mechanisms or forces may interact with each other during displacements and natural water influx. The water originates from the formation of multiple fingers, water channeling, gravity underrunning (formation of a water tongue) and/or water coning. The two most typical geological scenarios of abnormal water sweeping in homogeneous reservoirs are horizontal or anticline structures with oil underlain by bottom water (bottom-water systems) and dipping reservoirs with attic oil and side water drive (edge-water systems). Water coning is the main source of abnormal sweeping in the structures with bottom-water, whereas the combined effect of water under-running (formation of a water tongue) and coning plays a significant role in the abnormal sweeping of side water reservoirs. Water under-running and coning also have an important effect in the abnormal sweeping of heterogeneous reservoirs. The existence of permeability barriers, channels, and other heterogeneities, however, may aggravate the bypassing of oil. Understanding the mechanisms of

water invasion and oil bypassing in edge and bottom water-drive reservoirs is, therefore, of capital importance since it would allow identifying potential solutions.

Knowledge of the motion of the oil-water interface is needed in reservoir engineering in order to determine the amount of oil that will be recovered by the end of the well's operation. For low flow velocities, gravity forces tend to dominate the displacement and a stable (constant slope) interface occurs. A stable interface is desirable because it results in high recovery factors. However, the required flow velocity may be so low that the corresponding critical production rate would not be economical. Generally, production rates needed for economical recovery exceed the critical rates. Therefore, the interface becomes unstable and a cone and/or water tongue develops, causing early water breakthrough and oil bypassing. Also, most of the well's production life is plagued by very high water cut. When instability occurs, the less viscous water creates paths into the more viscous oil, leaving zones with original oil bypassed. Determining the volume of oil that may be bypassed in unstable displacements is of paramount importance. This is because a secondary recovery method and/or a technology for the control of the produced water can be planned as a result of such determination.

The most well known analytical models for the determination of the motion of the oil-water interface in edge-water systems are the models presented by Richardson and Blackwell (1971), Dake (1978), Dietz (1953), Outmans (1962) and Sheldon and Fayers (1962). The most popular method for the prediction of oil bypassing in bottom-water systems was developed by Kuo and DesBrisay (1983). Potential use of these models for well's recovery prediction is important due to their simplicity when compared to reservoir simulations. Despite their convenience, analytical models are poor estimators of the water breakthrough time (Hernandez and Wojtanowicz, 2005). Moreover, these models are based on assumptions that may not

represent the real physics of the water-oil displacement. For example, these analytical models assume completely segregated flow, i.e., they neglect the smearing, separation or diffusion of water saturation fronts that occurs as a consequence of fractional flow effects at high mobility ratios. There is a need, therefore, for accurate correlations for rapid prediction of the water breakthrough time and amount of by-passed oil in structures with edge and bottom-water advancement.

Once the amount of bypassed oil is quantified, efforts should be directed towards identifying possible solutions to the problem. Over the years, there have been many attempts to reduce and/or manage the amount of water produced, thus reducing oil bypassing. Typically, they have been classified as mechanical and chemical methods. Mechanical methods commonly involve the use of packers, bridge plugs, well abandonment, infill drilling, pattern flow control and horizontal wells. Among the most commonly used chemical methods are cement, sand, calcium carbonate, gels, resins, foams, emulsions, particulates, precipitates, microorganisms and polymers. Thus, the effective strategy for selecting a proper method should involve a careful diagnosis of the excessive water problem. Seright et al. (2003) proposed a methodology to attack the various types of water problems by categorizing them from the least to most difficult. Water coning and underruning were considered the most difficult with no easy, low-cost solution. The authors maintained that gel treatments will almost never work for coning and underruning problems. Their observation was based on extensive reservoir and completion engineering studies and analyses of many field applications.

Gel treatments target the reduction of water inflow to wells implicitly assuming that oil inflow would increase. In case of water coning and underruning, the flow of water is an integral part of flow deliverability and, as such, cannot be stopped or reduced without reducing the oil

flow. Thus, strategies studied in this research address the increased/accelerated oil recovery, instead of reduced water production. The oil and gas industry is increasingly using smart well completions to increase well productivity and reduce water-handling problems. Two different methods for recovery improvement are studied using numerical simulation: changes in well penetration and dual completion installation featuring the Downhole Water Sink (DWS) technology (Wojtanowicz, 2004). DWS uses completions deliberately installed below the water-oil interface to control water coning. The bottom completion drains water and keeps the top completion open to oil inflow. The technology has demonstrated to be an effective method in controlling and delaying water coning in bottom-water systems (Shirman et al., 1998; Wojtanowicz et al., 1999; Inikori et al, 2002). However, the reservoir and operational conditions that would result in maximized recovery using the technology for such systems are not entirely understood. On the other hand, the feasibility of DWS in edge-water systems has not been determined.

The main objectives of this research can be summarized as follows: first, to understand the dynamics of water production in the main types of producing systems (edge and bottom-water systems). In other words, why and how is oil bypassed? Second, to quantify the amount of unrecovered reserves associated with oil bypassing due to water coning/underruning. In other words, how much oil can be by-passed in typical production scenarios? Third, to create prediction tools for the estimation of oil bypassing. The idea is to create correlations that are quite easy to use and, therefore, useful to operators. Finally, to propose techniques to improve oil recovery in reservoirs subject to water coning/underruning. Obviously, demonstrating the ability of these techniques may have an important economical impact for the oil industry and significant benefits for operators.

1.2. Significance of This Research

The significance of this research and contributions to Petroleum Engineering can be summarized as follows:

- This research allows a better understanding of the dynamics of water production in edge water and bottom-water reservoirs.
- This research presents new correlations for the prediction of oil bypassing in edge and bottom-water drive reservoirs.
- The research prioritizes the properties and groups with the largest effect on oil bypassing.
- The research provides clues on the effect of capillary pressure, relative permeability and aquifer strength on oil bypassing and water invasion.
- The research presents a statistical quantification, based on a database of reservoir properties, of the amount of bypassed oil in typical edge and bottom-water reservoirs.
- The research gives insights on the effect of rock heterogeneity on oil bypassing and water invasion in edge-water systems
- The effect of well penetration on oil bypassing is studied in detail. This research presents results on the best well completion strategy (i.e., degree of well penetration) for both edge and bottom-water systems.
- The research clarifies the feasibility of Down Hole Water Sink (DWS) in edge and bottom-water reservoirs.
- Finally, a new method is proposed to enhance DWS operation in vertical wells. The method includes material balance calculations for comparison with simulation results. The method combines simplicity and accuracy.

1.3 Research Methods

The objectives of this work have been accomplished using the following methods:

Numerical Experiments: in the context of this research, an experiment is a numerical simulation. All the numerical experiments have been completed using the black oil reservoir simulator "IMEX", developed by Computer Modeling Group (CMG).

Experimental Design: Experimental design is a strategy in which the input variables are varied simultaneously in a series of experimental runs according to a predetermined pattern to obtain the experimental response. In other words, each experimental run will have a specific combination of input variable levels based on the design matrix. Then, the results are analyzed using statistical equation modeling methods, so as to extract the relationship between the input variables and the output response(s) (Yaw Peng and Gupta, 2003). In the experimental design methodology, parameters are varied simultaneously instead of the relatively inefficient one variable-at-a-time approach (Friedmann et al., 2001).

Analysis of Variance (ANOVA): is used to discern which factors are contributing to the variability of a response. It is an excellent procedure to screen variables at an early stage of a study, and it is a standard method for analysis of experimental designs (Armenta et al., 2003). In this research, the main responses analyzed are the water breakthrough time, percentage of by-passed oil at breakthrough and percentage of by-passed oil at abandonment conditions. A significance level of 5% has been used in all ANOVA calculations in this research.

Response Surface Methodology (White et al., 2001): A response surface model is an empirical fit of experimental or computed responses. The responses are usually measured or computed at factor combinations specified by an experimental design. The model is usually a polynomial fit with linear regression. Each term in the polynomial is a function of one or more

factors. The coefficients in the polynomial are the factor effects and the interactions.

Scaling/Inspectional Analysis: In fluid flow thru permeable media, scaling means that such quantities as dimensionless pressures and saturations are identical at all scales. Scaling also reduces the number of parameters in the problem statement. This reduction is particularly useful in experimental work, where minimization reduces the number of experiments. Also, scaling removes the need to convert between systems of units (Shook et al., 1992).

Inspectional Analysis (IA) consists in transforming the equations of a problem, differential or otherwise, so that all the variables are dimensionless. Simple inspection then shows how these dimensionless variables are related. This method makes use of physical information contained in initial conditions and boundary conditions (Ruark, 1935).

Some of the advantages of inspectional analysis over the well known dimensional analysis (Buckingham, 1914) are: it gives a clearer physical insight (Ruark, 1935). It is stronger since it is based on the underlying physical laws, usually expressed in form of partial differential equations and boundary conditions (Shook et al., 1992). IA can be done even with an incomplete set of equations (Shook et al., 1992). IA is capable of yielding all the information that can be obtained by dimensional analysis and more (Ruark, 1935). IA guards us against writing down too many dimensionless constants (Ruark, 1935).

1.4 Dissertation Outline

This study is divided into six chapters. This introductory chapter (Chapter 1) presents an overview of the problem of oil bypassing due to water invasion. It also presents a cohesive summary of the potential solutions to the problem reported in the literature.

Chapter 2 describes the main geological scenarios where oil bypassing may occur as a consequence of water invasion. It also presents a literature review on the mechanisms of oil

bypassing. The chapter ends with a description of the main existing analytical models used for the prediction of the amount of bypassed oil in edge and bottom-water reservoirs.

Chapter 3 presents the results of analytical and numerical simulation studies undertaken to validate the analytical models described in Chapter 2. The main emphasis of Chapter 3 is on the identification of the limitations of these analytical models.

Chapter 4 deals with the prediction of oil bypassing in edge and bottom-water dive reservoirs. Numerical simulation and statistical analysis are used to establish rough guidelines for the parameters promoting oil bypassing. Simulation results are then used to create simplified correlations for the prediction of the amount of by-passed oil in these systems. The correlations were obtained using dimensionless groups and experimental design. The levels of the dimensionless groups in the design were obtained using an extensive database of reservoir conditions created for this study. The database contains information on reservoirs from all around the world. Numerical simulation is also used to quantify the amount of oil that can be bypassed in typical edge and bottom-water reservoirs.

Chapter 5 investigates the well completion strategies that would improve oil recovery in edge and bottom-water systems. First, the most efficient degree of well penetration in these systems is investigated. Then, a comparison is made between single and dual well completions (DWS) for different reservoir conditions.

Chapter 6 provides the conclusions from this research work and recommendations for future research.

CHAPTER 2. LITERATURE REVIEW

Horizontal or anticline structures with oil underlain by bottom water (bottom-water systems) and dipping reservoirs with attic oil and side water drive (edge-water systems) are the two most typical geological scenarios of abnormal water sweeping leading to oil bypassing. This chapter presents a brief description of these two geological scenarios. It also presents a literature review on the mechanisms of oil bypassing and the main existing analytical models used for the prediction of the amount of bypassed oil.

2.1 Oil Bypassing in Edge-Water Drive Reservoirs

2.1.1 Description of Geological Scenario

Many petroleum reservoirs obtain a major part of their natural producing energy from water located at the flanks or edges of the reservoir. Water generally comes from an aquifer adjacent to the oil zone (Kumar, 1977). These reservoirs are called edge water-drive reservoirs, and are mainly characterized by (1) a small surface area of contact between the oil and water zone, (2) a water movement that is essentially parallel to the bedding plane, (3) Small thickness/length and width/length ratios. Figures 1 and 2 show imaginary views of edge-water systems.

2.1.2 Mechanisms

In an oil reservoir with edge-water drive, the two fluids are separated by gravity. As shown in Figure 3, initially, the oil/water interface is mostly horizontal, although slight inclination may occur due to capillary pressure effects.

After production starts, the interface moves towards the producing well. Its shape would be controlled by viscous, capillary and gravity forces, as well as by rock heterogeneity. For low flow velocities, gravity forces tend to dominate the displacement. In this case, the density

difference would act to keep the interface moving up dip as a smooth plane with constant slope (stable interface).

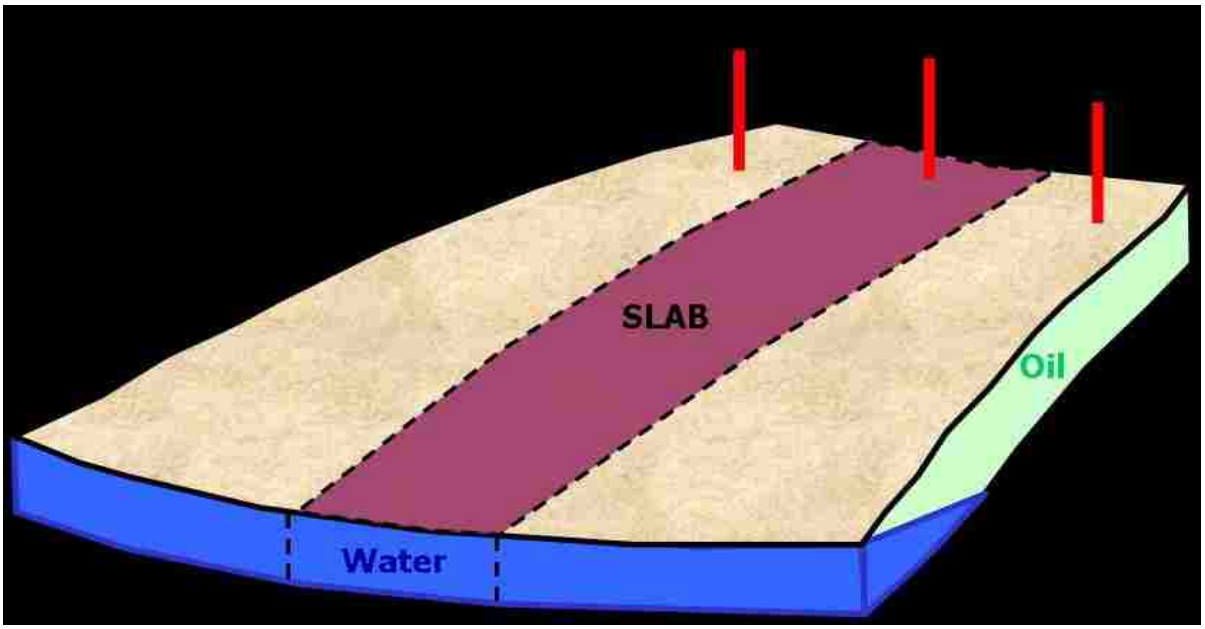

Figure 1: Imaginary 3D View of an Edge Water-Drive Reservoir

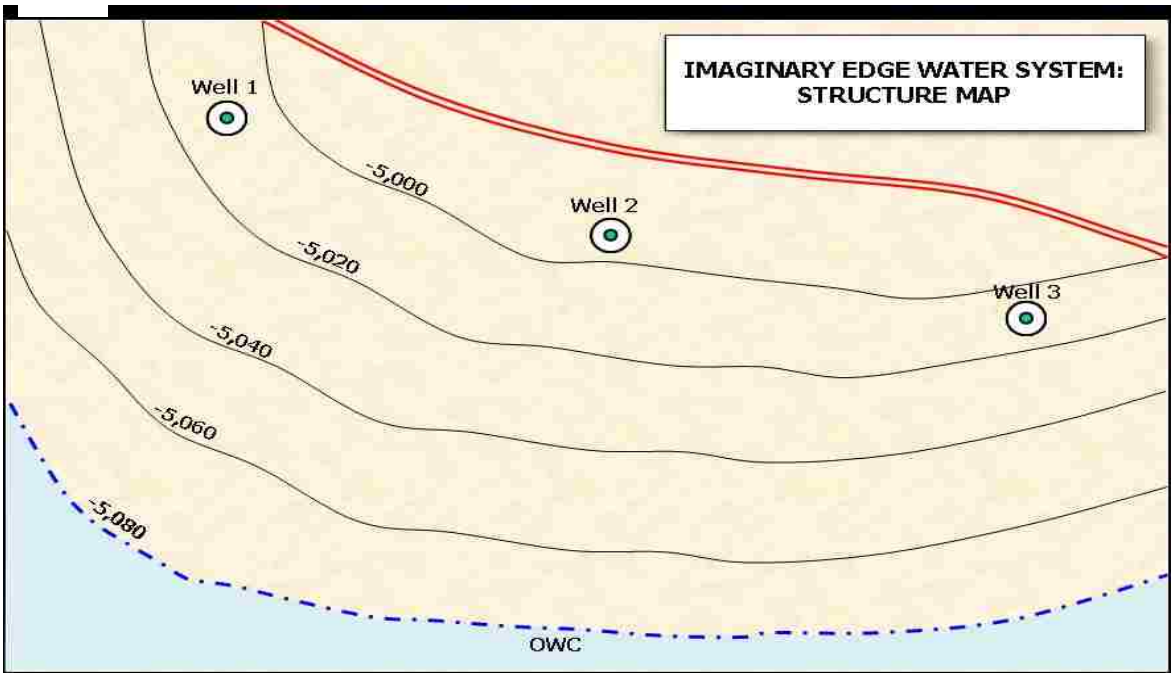

Figure 2: Typical Map View of an Edge Water-Drive Reservoir

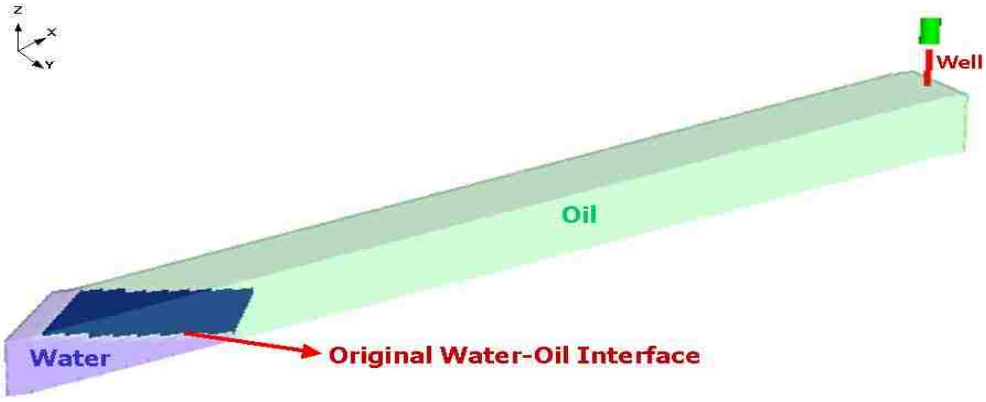

Figure 3: Horizontal Oil-Water Contact at Time=0 Days

Although a stable front is always beneficial for recovery, the required critical flow velocity may be so low that the corresponding production rate is not economical. Typically, the economical production rates exceed the critical rates (Richardson and Blackwell, 1971). In such cases, the combination of gravity and viscous forces results in the development of a water tongue along the bottom of the structure, as shown in Figure 4. Since the water has higher mobility than the oil, it tends to channel and bypass the oil, but since the water is normally denser than the oil, it seeks the bottom of the layer creating a water tongue (Richardson and Blackwell, 1971). This mechanism is known as gravity underruning, and is the main source of oil bypassing in edge water-drive reservoirs.

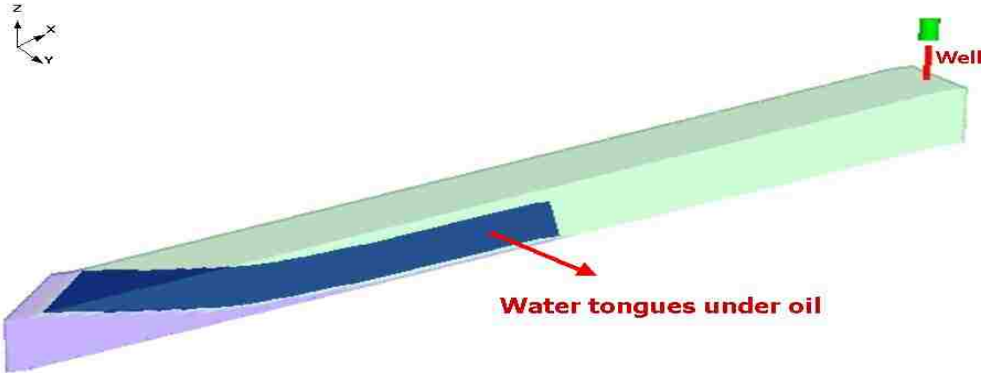

Figure 4: Formation of a Gravity Tongue

When the water tongue approaches the production well, the pressure drawdown at the well causes the formation of a water salient (Arslan, 2005) or areal tongue (Figure 5) and/or a cone (Figure 6). Shapes of the tongue, the salient and the cone depend on the operational conditions and properties of the reservoir and its fluids. For example, Slobod and Howlett (1963) suggested that, for very high flow rates, the displacement is dominated by the formation of multiple fingers instead of a gravity tongue. The mechanisms affecting gravity underruning are essentially the same that affect viscous fingering. The formation of a single water tongue or multiple fingers depends on reservoir heterogeneity and the magnitude of the forces acting on the system.

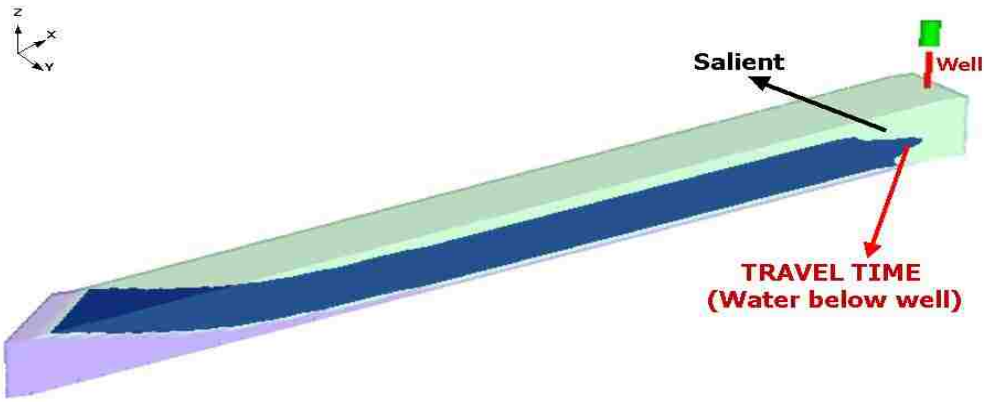

Figure 5: Formation of a Salient or Areal Tongue

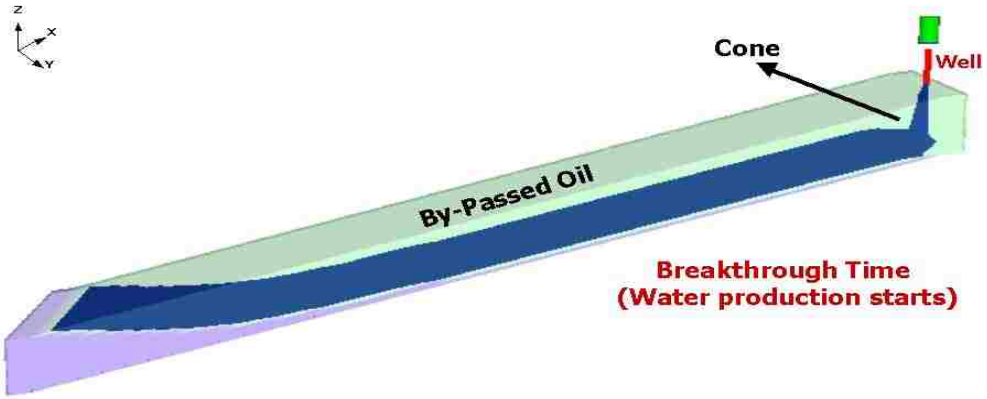

Figure 6: Formation of a Water Cone

After water breakthrough occurs, water cut at the well starts to increase - sometimes dramatically - and, eventually, the well may have to be shut off because of high water production (it would not be economical to produce at such small oil rates and such high water rates) leaving behind bypassed oil.

2.1.3 Analytical Models

The main existing analytical models for the estimation of the development of the oil/water contact with time and, therefore, oil bypassing in edge-water systems are briefly described in this section.

Richardson and Blackwell's Model (1971)

Probably the simplest model for water underrunning was proposed by Richardson and Blackwell. The model is based on the following basic assumptions:

- The water layer is of constant thickness, as shown in the 2D (X-Z) cross-section presented in Figure 7.
- At a particular time, the fraction of the total thickness occupied by water is *X* and the fraction occupied by oil is *1-X*.
- The water layer moves vertically with no resistance as the oil is produced.
- The oil and water flow horizontally.

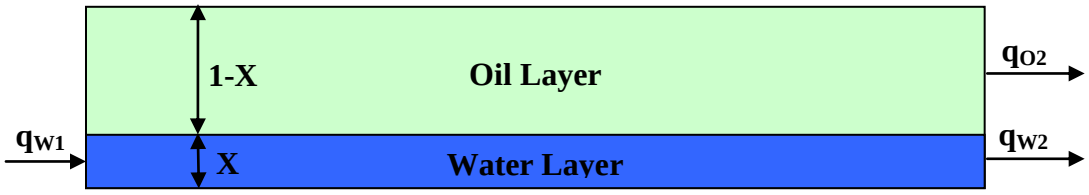

Figure 7: Richardson and Blackwell (1971) Model for Water Underrunning.

The cumulative oil recovery, N_p, in displaceable pore volumes (PV) can be estimated by:

$N_p = X$……..(2.1)

And the water influx, W_e, can be calculated as follows:

$W_e = W_p + X$……..(2.2)

The total water production, W_p, is given by:

$$W_p = \frac{K_{w,ro}}{2K_o}[X - \ln(1+X)] - \frac{X}{2} \quad \text{……..(2.3)}$$

After breakthrough, the instantaneous produced water-oil ratio can be calculated by the expression:

$$WOR = \frac{q_w}{q_o} = \frac{K_{w,ro}}{2K_o}\left[\frac{X}{1+X} + \ln(1+X) - \frac{1}{2}\right] \quad \text{……(2.4)}$$

Where μ_o is oil viscosity (cp), μ_w is water viscosity (cp), $K_{w,ro}$ is the effective permeability to water at residual oil and K_o is the effective permeability to oil in darcies.

The water cut is given by:

$$Water\ Cut(\%) = \frac{WOR}{WOR+1} * 100 \quad \text{……..(2.5)}$$

This is a very simple model that can be quickly applied in calculations by hand and that does not require a detailed knowledge of the reservoir. The authors claim that the model successfully reproduced the recoveries and water cuts obtained from 2 different fields.

Dake's Model (1978)

In 1978, Dake proposed a modification of the Buckley-Leverett theory in order to estimate oil recovery in homogeneous dipping reservoirs. Dake recognized that gravity underrunning is not a one-dimensional problem, but reduced the mathematical description to one dimension by

using average saturations and saturation dependent relative permeabilities over the reservoir thickness. The most important assumptions of the model are:

- The displacement occurs under segregated flow conditions, as shown in Figure 8. There is a distinct interface with no capillary transition zone.
- The average saturations and relative permeabilities are obtained using the fractional thickness of the water, b (Figure 8).
- Flow can be assumed to occur along the centerline of the reservoir.
- The displacement is governed by vertical equilibrium; i.e., gravity alone is responsible for the distribution of the fluids in the dip-normal direction.
- The reservoir is considered to be homogeneous.
- The displacement is considered to be linear and incompressible.

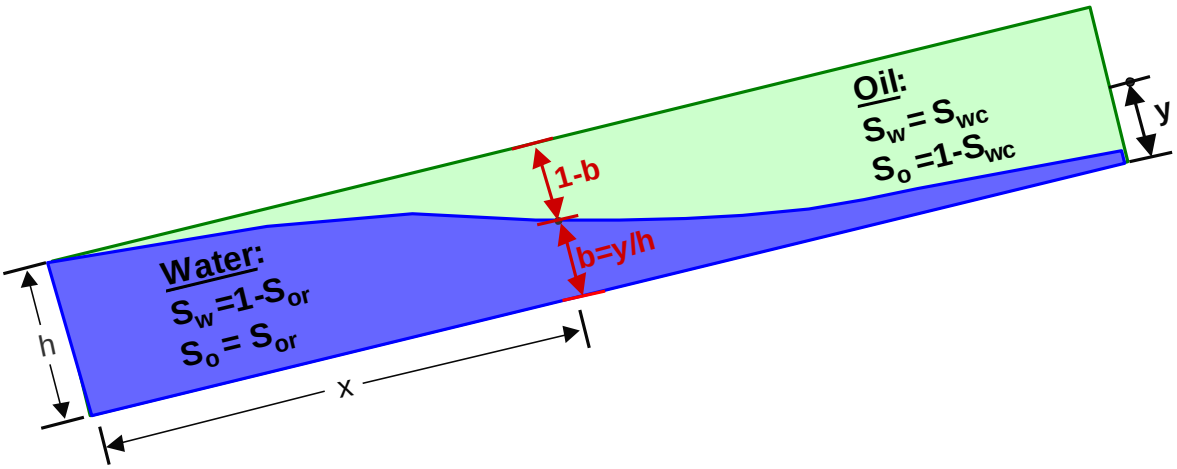

Figure 8: Dake's (1978) Model for Water Underrunning

Dake's model incorporates Dietz (1953) stability criteria in the recovery calculations. According to Dietz (1953), a displacement is stable if the angle between the oil-water interface and the direction of the flow remains constant through the displacement, or:

$$\frac{dy}{dx} \blacksquare \tan \blacksquare \quad \text{.....(2.6)}$$

For stable displacement, the oil recovery before the breakthrough is equal to the volume of water injected. After breakthrough, the oil recovery for stable displacements can be calculated from simple geometrical considerations as follows (see Figure 9):

$$N_{PD} \blacksquare \frac{(h \blacksquare_e)^2}{2\,h\,L \tan \blacksquare} \quad \text{.....(2.7)}$$

Where, N_{PD} is the oil recovery in Movable Oil Volumes (MOV), h is the thickness and L is the length of the reservoir.

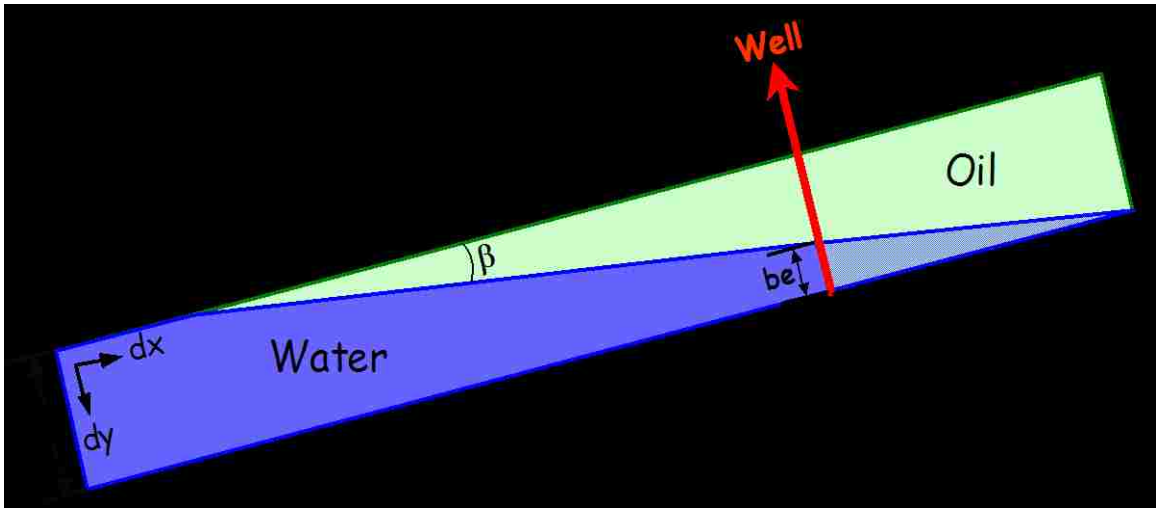

Figure 9: Stable, Segregated Displacement of Oil by Water (After Dake (1978))

The water cut or fractional flow of water can be estimated as follows:

$$f_{we} \blacksquare \frac{(N_{PD} \blacksquare_e)}{W_{ID}} \quad \text{.....(2.8)}$$

Where b_e is the fractional thickness of water at the producing end ($b_e = y_e/h$). The number of MOV's of water injected, W_{ID} is:

$$W_{ID} = N_{PD} \frac{(y_e)^2}{2\,h\,L\tan}$$ .....(2.9)

And the production time is related to the water influx, expressed in pore volumes (PV's), by the equation:

$$Time\,(days) = \frac{W_{ID}(PV).h.w.L.}{q_i.5.615}$$ .....(2.10)

Where w is the distance between injection wells, ϕ is the porosity (fraction) and q_i is the injection rate in b/d/well.

For unstable displacements (dy/dx not constant), oil recovery before breakthrough is also equal to the volume of water injected. After breakthrough, however, oil recovery (N_{pD}, expressed in Movable Oil Volumes (MOV's)), can be calculated using the formula:

$$N_{pD} = \frac{1}{M}\left[2\sqrt{W_{iD}\,M\left[1-\frac{G}{M}\right]+\left[1-\frac{W_{iD}G}{M}\right]}-W_{iD}\left[2-\frac{(M-1)}{(M-1)}G\right]\right]$$ ..(2.11)

Where, W_{iD} is the cumulative water injection, also expressed in MOV's. M is the end point mobility ratio, which can be expressed as:

$$M = \left[k_{rw}' \Big/ k_{ro}'\right]$$ .....(2.12)

And G is the dimensionless gravity number, which in field units is:

$$G = \left[4.9*10^{-} \frac{k.k_{rw}.A.\sin}{q_t.}\right]$$ .....(2.13)

The relationship between Movable Oil Volumes (MOV's) and Pore Volumes (PV's) is:

$$MOV = PV(1-S_{wc}-S_{or})$$ .....(2.14)

Where S_{wc} is the connate water saturation and S_{or} is the residual oil saturation. The water cut or fractional flow of water is:

$$f_{we} = \frac{M.b_e - b_e(1 -)G}{1 + M( )b_e} \quad \text{.....(2.15)}$$

One of the main advantages of this model is that it has quite simple mathematical expressions that can be solved analytically in short time. The main concern with the model is its accuracy. This is because the assumptions made are not always justified. For example, the model considers that there is not capillary transition zone, which can only be justified when the thickness of this transition zone can be disregarded.

Dietz Model (1953)

In 1953, Dietz proposed a two-dimensional model for water encroachment in a monoclinal field. The model is based on the following assumptions:

- There is a distinct interface rather than a capillary transition zone between the oil bearing and the flooded part of the formation.
- The absolute permeability will be considered constant throughout the formation (homogeneous reservoir)
- The displacement is considered to be incompressible.

These assumptions are quite similar to the assumptions made by Dake (1978), which were shown previously. Dietz (1953) proposed the following equation for the maximum rate of oil production for stable displacement:

$$q_{critical} = V_{critical} \frac{h.g( )\sin }{(/ k_o)(/ k_w)} \quad \text{.....(2.16)}$$

Where $q_{critical}$ is the critical rate of inflow per unit width. Equation 2.16 is very important because it defines the maximum flow rate allowed to keep a stable front. Below the critical rate, the difference in specific gravity will cause the interface to remain at a constant slope. Above the critical rate, equilibrium is not possible and a water tongue will be formed.

Before production starts (time=0), the equation for the oil/water interface proposed by Dietz (1953) is:

$$x_t = \frac{y}{\tan\alpha} \qquad \text{.....(2.17)}$$

And, for a given time after production starts:

$$x_t = \frac{y}{\tan\alpha} - \frac{a \cdot h}{[a(h - y)]\, y^2}\,(1 - S_{or} - S_{wc}) \qquad \text{.....(2.18)}$$

Where Q is the cumulative inflow per unit volume and $a=1/M$.

The subsurface volume of oil displaced by the water tongue can be calculated as follows (see Figure 10):

$$Qo = (1 - S_{or} - S_{wc}).y_{ec.\lim} * \left[x_{crest} - \frac{y_{ec.\lim}}{2\tan} - \frac{Q.a.h}{1} \frac{1}{a(h - y)\, y} \right]_{y_{ec.\lim}}^{h} \qquad \text{..... (2.19)}$$

Where x_{crest} is the distance between the original water table and the producing well and $y_{ec.\,lim}$ is the thickness of the water tongue at the well. The water cut can be expressed as:

$$\frac{q_w}{q} = \frac{y}{a(h - y)\, y} \qquad \text{.....(2.20)}$$

It is very important to mention that gravity effects were neglected in the equations shown above. Dietz (1953) justified this by saying that if gravity effects were considered, a partial differential equation of second order would have to be solved, which could complicate the model

considerably. In addition, Dietz (1953) suggested that when the production rate is several times the critical rate, as may happen most of the time in the field, gravity effects are not important.

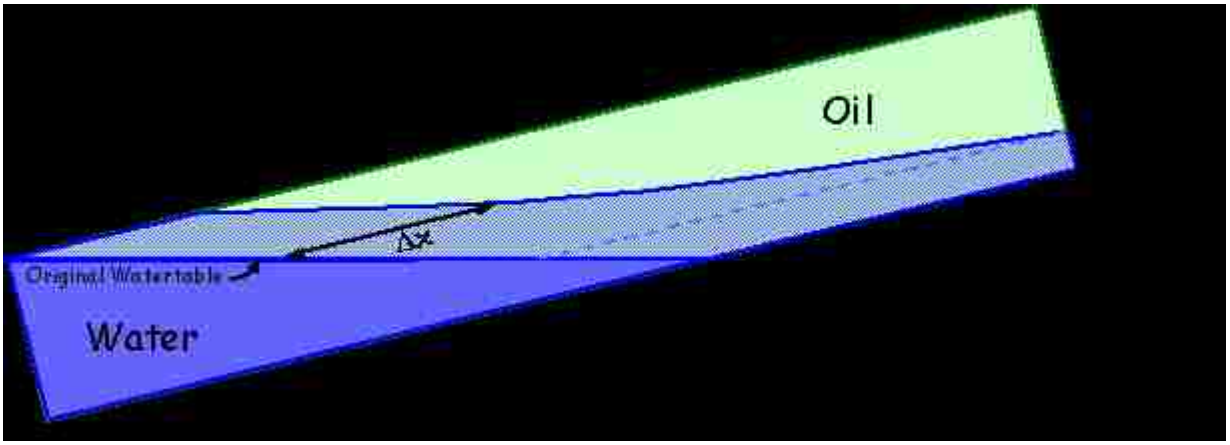

Figure 10: Dietz Model, Volume of Oil Displaced by Water (After Dietz (1953))

Outmans' Model (1962)

In 1962, Outmans introduced the concept of transient interfaces during the displacement of oil by water in porous media. Outmans indicated that the concept of transient interfaces is justified because the changes in the production rate in a reservoir may not be followed by an instantaneous adjustment of the interface to the new rate, but by a transition period during which the interface evolves from one equilibrium condition to the other. Outmans also mentioned that if the displacement exceeds a given critical rate, no equilibrium is possible and viscous fingers are formed. Outman's critical rate can be expressed as:

$$Vc_{Outmans} = Vc_{Dietz} \quad \text{.....(2.21)}$$

Where:

$$a = \frac{T_e}{(M)(h^*)^2} \quad \text{.....(2.22)}$$

T_e is the effective interfacial tension, λ'_w is defined as $k_w / (\mu_w . \phi . (1-S_{or}-S_{wc}))$ and h^* is the total thickness of the layer. Because the calculation of "*a*" involves the inverse square of the thickness of the medium (*h**), the value of "*a*" can be assumed to be negligible in typical reservoirs ($Vc_{Outmans} \approx Vc_{Dietz}$).

Other assumptions of the model are:

- Homogeneous reservoir.
- A surface (interface) can be defined where the saturation changes discontinuously.
- The fluids are of negligible compressibility within the range of pressures considered, and Darcy's law is valid throughout.
- A constant pressure drop across the interface due to capillary pressure does not affect the calculations and, therefore, is omitted.

The shape of the interface can be calculated by higher-order approximations. If "*a*" is neglected, the position (*x**) of the interface for a given thickness (*y**) and time (*t**) is (see Figure 11):

*x** [redacted](*y**, *t**) [redacted])*h** / [redacted]……(2.23)

Where:

[redacted]$\cot$[redacted](1[redacted]*n*)e^{t} [redacted]*n*] cos *y* ……(2.24)

[redacted]$\cot$[redacted](1[redacted]*n*)e^{3t} [redacted]*n*] $\frac{\cos 3y}{9}$ ……(2.25)

$$\eta_3 = \frac{1}{8}(1+m)\left(\frac{4}{\pi}\cot\alpha\right)^2\left[2m^2 t\, e^t - (1+2m+3m^2)e^t + 4m(1+m)e^{2t} - (1+m)^2 e^{3t}\right]\cos y$$

$$+\frac{1}{9}(1+m)\left(\frac{4}{\pi}\cot\alpha\right)^2\left[2m\, e^t - (1+3m)e^{2t} + (1+m)e^{4t}\right]\cos 2y$$

$$+\left(\frac{4}{\pi}\cot\alpha\right)^2(1+m)]e^{5t} + m\frac{\cos 5y}{25} \quad \text{.....(2.26)}$$

And:

$$m = \frac{Vc}{V^*} \quad \text{.....(2.27)}$$

$$V^* = Vc - V \quad \text{.....(2.28)}$$

$$y = \pi y^*/h^* \quad \text{.....(2.29)}$$

$$t = \frac{1}{1+M}\left(\frac{M}{1+M}\right)^2 t^* / h^* \quad \text{.....(2.30)}$$

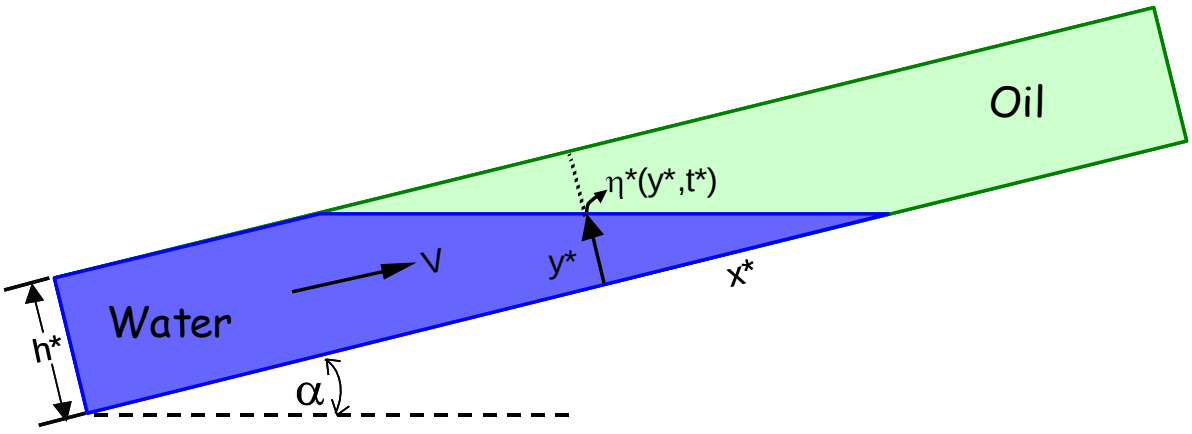

Figure 11: Outmans Model: Position of the Interface (After Outmans (1962))

The following practical observations can be derived from Outmans' paper (1962):

- Transient interfaces approaching equilibrium occur only if:

- $V<Vc_{Outmans}$ for any M.
- $M<1$ for any V.

- If $Vc_{Dietz}<V<Vc_{Outmans}$, a single finger of increasing length forms along the bottom of the model. This single finger is not an unstable interface, but a transient interface that will eventually approach equilibrium. However, because the interfacial tension term "*a*" can be neglected in most of the reservoirs, it is interpreted that Outmans suggests that this single finger would mainly occur in experimental models. In addition, Dietz (1953) indicated that, because the single finger is nearly parallel to the boundaries, its length is very large compared with the thickness of the formation, which means that the simulation of such equilibrium interface in the reservoir would require models of unusual length.
- If $V>Vc_{Outmans}$ and $M>1$, the mathematical model indicates viscous fingering across the entire interface. It is believed that Outmans' model (1962) was not developed for these conditions and, therefore, it should not be used (transient interfaces approaching equilibrium will not occur).

Sheldon and Fayers' Model (1962)

After Dietz (1953) developed equations of motion for the interface in a water-oil displacement, a number of authors have tried to develop similar equations in an attempt to model the movement of the water through the reservoir and the amount of by-passed oil in a water-oil system. The equations described in this section were developed by Sheldon and Fayers (1962). The principle is the same that was used by Dietz (1953), but Sheldon and Fayers considered density difference contributions that were previously neglected.

The general equation describing the motion of the interface developed by Sheldon and

Fayers (1962) is (see Figure 12):

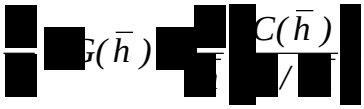

.....(2.31)

Where

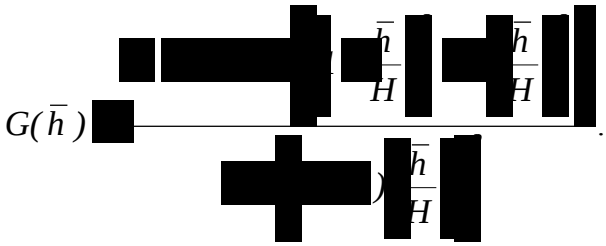

.....(2.32)

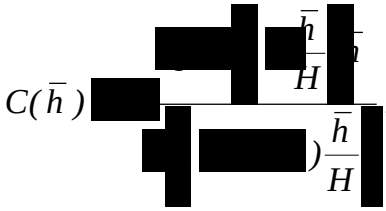

.....(2.33)

These equations were derived to express the downward displacement of fluid 1 by fluid 2 (for example, oil being displaced by gas). In order to describe the upward displacement of oil by water, the equations should have $\bar{h}$ replaced by $H-\bar{h}$ and $\Delta\rho$ by $-\Delta\rho$.

The nomenclature of the equations is as follows:

 = Velocity of a point on the interface.

 = Derivative of the interface at that point.

$C(\bar{h})$ = Curvature term in Sheldon and Fayers equation.

$G(\bar{h})$ = Density term in Sheldon and Fayers equation.

$\bar{h}$ = Normal distance from the lower boundary to the interface.

H = Total thickness of the reservoir.

[redacted] = Reciprocal mobility ratio ([redacted]).

[redacted] = Product of porosity and change in water saturation across interface.

[redacted] = Inclination of reservoir with respect to the horizontal.

[redacted] = Density difference between fluids 1 and 2.

q = Flow rate per unit area.

[redacted] = Mobility of the fluid.

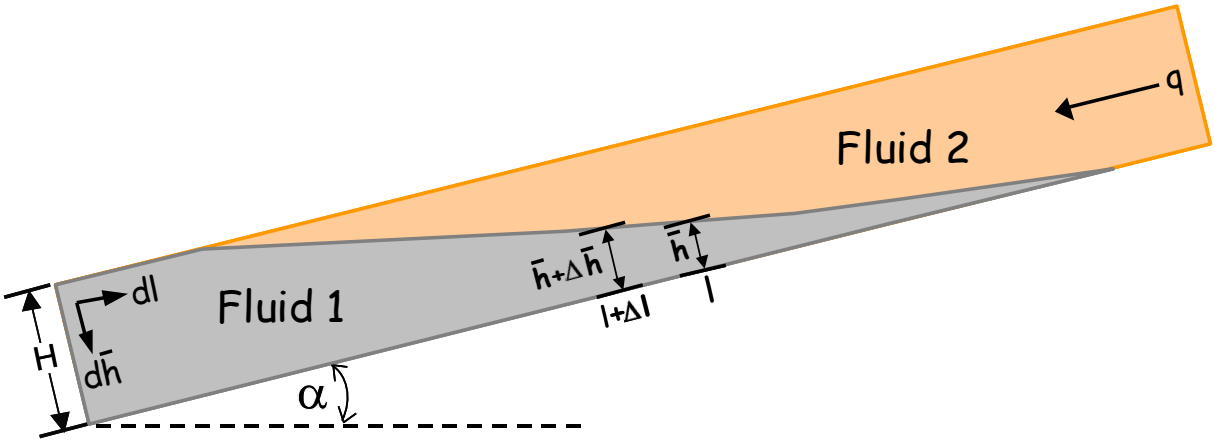

Figure 12: Schematic of the Interface: Sheldon and Fayers Model
(After Sheldon and Fayers (1962))

Sheldon and Fayers (1962) also derived the following equations for the velocities of the trailing and leading edges:

For the trailing edge:

[redacted] ……...……...(2.34)

For the leading edge:

[redacted] ……..……...(2.35)

For steady-state conditions, the interface is a straight line that can be expressed by:

[redacted] ……..……...……(2.36)

This steady state shape does not occur if [redacted] (additional details about this method and the stability conditions for the interface can be obtained in their paper. For the purpose of the calculations shown in Chapter 3, it was decided not to include Sheldon and Fayers' Model (1962). This is because Equation (2.31) cannot be readily solved analytically and a finite difference technique is required, which complicates the calculations.

2.2 Oil Bypassing in Bottom-Water Drive Reservoirs

2.2.1 Description of Geological Scenario

As shown diagrammatically in Figures 13 and 14, classic bottom-water systems are anticlines where nearly the entire reservoir is underlain by the oil-water contact. An anticline is a fold structure, with a concave-downward shape in which the sides of the fold slope apart. The largest oilfields occur in large, gentle anticlines in thick sedimentary rock sequences (Alden, 2007).

2.2.2 Mechanisms

Under static conditions in bottom-water systems, oil stays on top of water due to the density difference in both fluids. Once the well is put on production, a pressure gradient is created around the wellbore and oil starts to flow into the well. This pressure gradient may cause the oil/water interface to deform into a cone shape, as shown in Figure 15. The gravity force,

which is dependent on the density difference between oil and water, is opposing the movement of water upwards and counteracts the pressure gradients at the wellbore. As production continues, however, the cone shaped profile may become unstable due to high pressure drawdown around the wellbore causing water breakthrough into the well (Figure 16). After water breakthrough, water cut may increase dramatically and, eventually, the well may have to be shut because of excessive water production (the well reaches its economic water cut), leaving behind bypassed oil (Figure 17).

Three different stages of cone development have been observed in experimental studies using Hele-Shaw and Pie-shaped models (Siddiqi, 2001). Stage one consists of the initial bending of the oil-water contact. Stage two is the accelerated movement of the cone to the well just before water breakthrough. Stage three is the lateral growth of the cone. Water coning is one of the most widely studied phenomena in the oil industry. There seems to be a gap of knowledge, however, on the quantification of the effect of coning on oil bypassing for different combinations of well/reservoir properties.

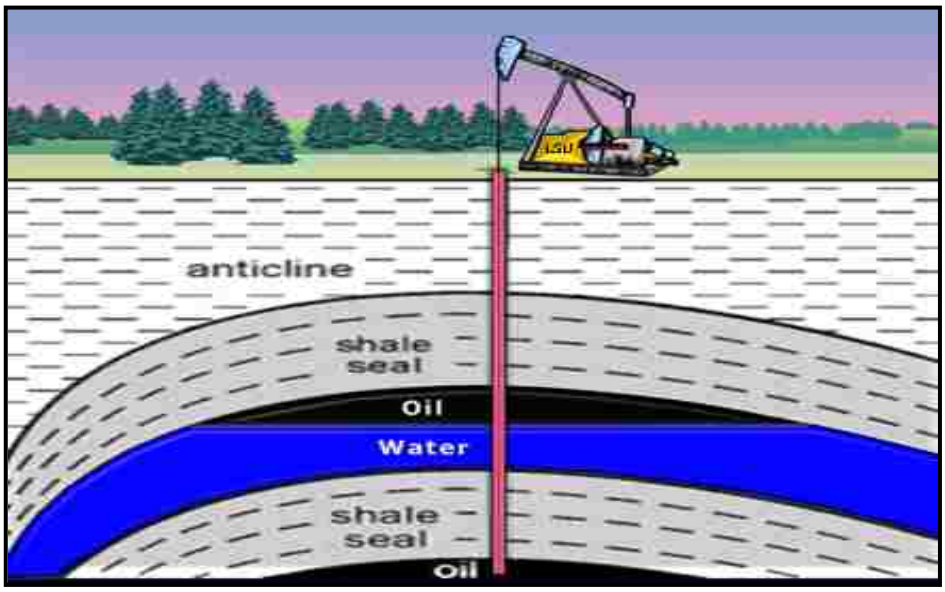

Figure 13: Typical Cross Section of a Bottom-Water System

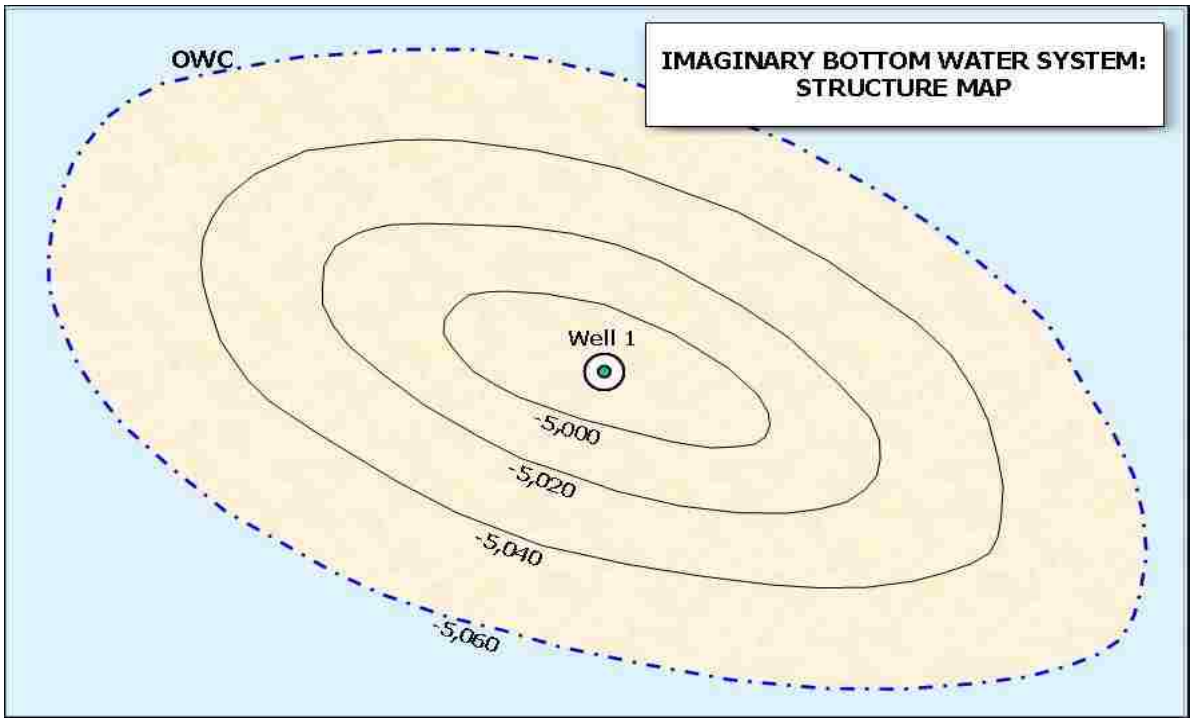

Figure 14: Typical Map View of a Bottom-Water System

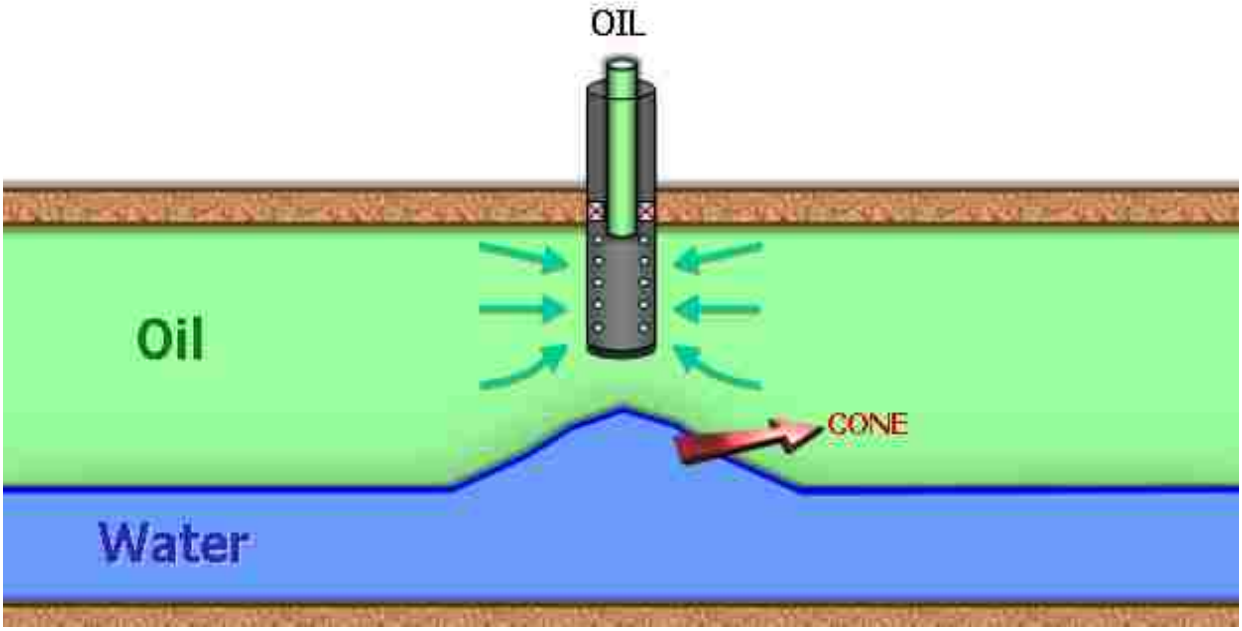

Figure 15: Oil-Water Interface Deformation into a Cone Shape

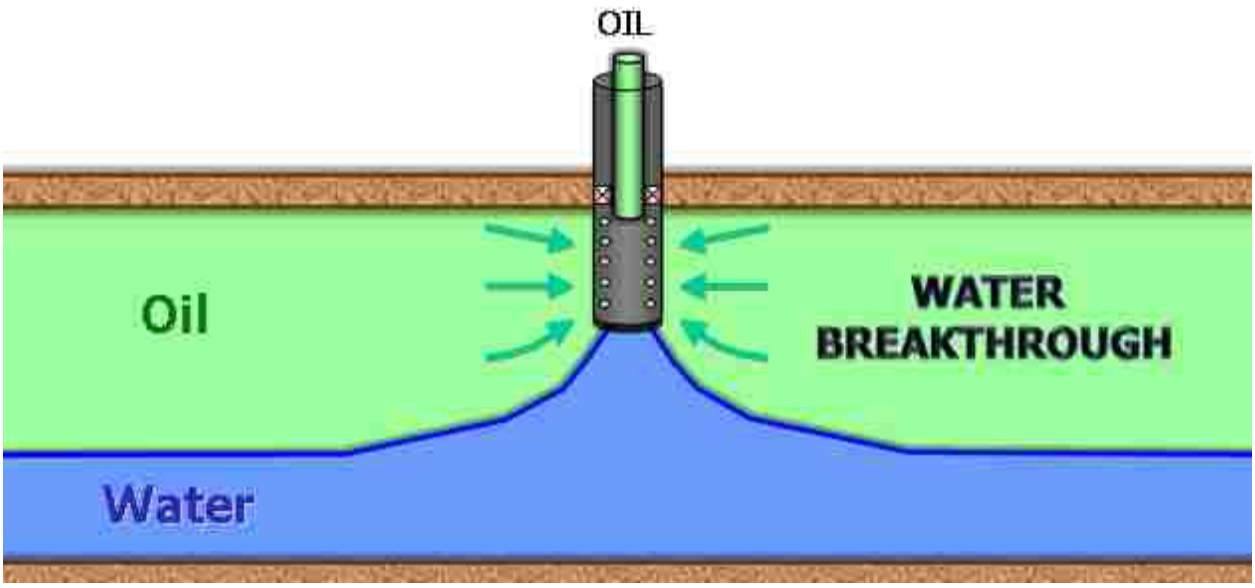

Figure 16: Water Breakthrough Caused by Coning

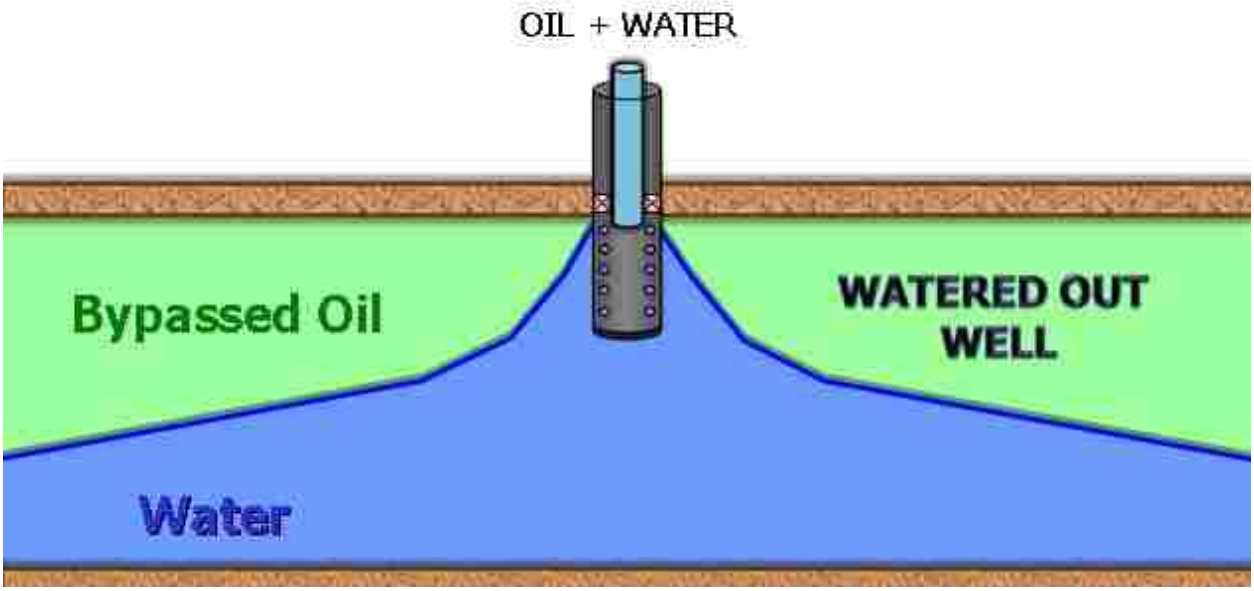

Figure 17: Oil Bypassing as a Result of Water Coning in Bottom-Water Systems

2.2.3 Analytical Models

Perhaps the most widely used analytical model for prediction water cut (and oil recovery) for bottom-water reservoirs is the method formulated by Kuo and DesBrisay (1983), which is

based upon a generalization of computer-generated production histories. The method requires good knowledge of reservoir properties, some of which might be difficult to find (vertical permeability, for example). To develop their model, Kuo and DesBrisay ran a series of numerical experiments. The simulation results were then used to develop three correlations for water coning predictions. The parameters varied during the experiments were the ratio of vertical to horizontal permeability (from 0.01 to 1.0), the completion penetration (from 20% to 80% of the oil column), the production rate (from 500 to 2000 rb/d), and the mobility ratio of water and oil (from 1.0 to 10). The resultant relation was developed in a normalized, dimensionless form. To make the normalization, two parameters were defined: a dimensionless time and a dimensionless water cut. These parameters are defined as follows:

$$t_D = \frac{t}{t_{BT}} \qquad \text{.....(2.37)}$$

$$WC_D = \frac{WC}{WC_{ul}} \qquad \text{.....(2.38)}$$

The water breakthrough time must be determined in order to calculate the dimensionless time (see Equation (2.37)). To develop their method, Kuo and DesBrisay (1983) used the correlation of Bournazel and Jeanson (1971) for the evaluation of the breakthrough time. This correlation is based in experimental results and can be expressed as:

$$t_{BT} = \frac{[illegible]\ln(t_D)_{BT}}{0.00137([illegible])k_v(1[illegible]M)} \qquad \text{.....(2.39)}$$

Where:

t_{BT} = breakthrough time, days

μ_o = oil viscosity, cp

ϕ = porosity, fraction

h = oil column thickness, ft

ρ_w = water density, gm/cc

ρ_o = oil density, gm/cc

k_v = vertical permeability, md

M = water-oil mobility ratio= $[\mu_o(k_w)_{or}/\mu_w(k_o)_{wc}]$, where (k_w) is the effective permeability to water at residual oil saturation and $(k_o)_{wc}$ is the effective permeability to oil at connate water saturation

α = 0.5 for $M < 1$ and 0.6 for $1 < M < 10$.

$(t_D)_{BT}$ = Dimensionless breakthrough time,

According to Bournazel and Jeanson (1971), the dimensionless breakthrough time is given by:

$$(t_D)_{BT} = \frac{z}{3 - 0.7z} \quad \text{.....(2.40)}$$

Another equation for the estimation of the dimensionless breakthrough time was introduced by Sobocinski and Cornelius (1975):

$$(t_D)_{BT} = \frac{z}{4}\left[1 - \frac{0.6 - 0.7z}{7 - 2z}\right] \quad \text{.....(2.41)}$$

z is defined as the dimensionless cone height, and is expressed as follows (Kuo and DesBrisay (1983):

$$z = \frac{0.00307(\rho_w - \rho_o)k_h\, h\,(h - h_p)}{\mu_o\, q_o\, B_o} \quad \text{.....(2.42)}$$

Where:

k_h = horizontal permeability, md

h_p = perforated interval, ft

B_o = oil formation volume factor, rb/stb

q_o = oil production rate, stb/day

The ultimate dimensionless water cut, WC_{ul}, required in Equation (2.38), can be calculated by the expression:

$$WC_{ul} \frac{M \frac{h_w}{h_o}}{M \frac{h_w}{h_o}} \quad \text{.....(2.43)}$$

Where M is the mobility ratio and h_o and h_w are the current thicknesses of the oil and water columns, respectively.

Kuo and DesBrisay (1983) combined all results from their numerical experiments in the dimensionless plot presented in Figure 18. They described the pattern of dimensionless water cut development using three equations valid within three different intervals of dimensionless time:

WC_D for $t_D < 0.5$.....(2.44)

WC_D $.94 \log t_D$ $.29$ for $0.5 < t_D < 5.7$.....(2.45)

WC_D for $t_D > 5.7$.....(2.46)

The following procedure by Kuo and DesBrisay (1983) can be used to calculate the development of water cut and oil recovery over time for a given total fluid production rate in a vertical well.

1. Calculate dimensionless breakthrough time t_D using Equation (2.37)
2. Estimate the limiting water cut for the reservoir using Equation (2.43). The thicknesses of oil and water can be calculated by material balance as follows:

h_W H_W H_O M_D .....(2.47)

$$h_o = H_o (1 - M_D) \quad \text{.....(2.48)}$$

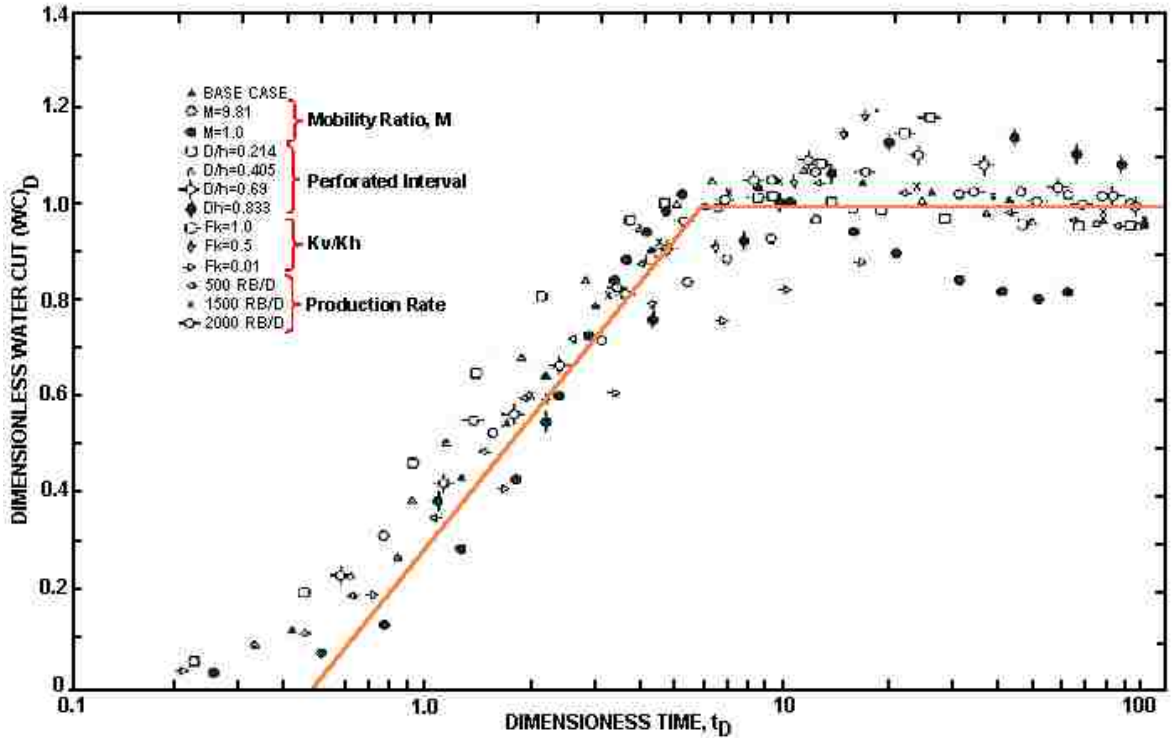

Figure 18: Water Production History in Dimensionless Formulation
(after Kuo and DesBrisay (1983))

Where:

$$M_D = (N_p / N)(1 - S_{wc}) / (1 - S_{or} - S_{wc}) \quad \text{.....(2.49)}$$

And:

H_w = initial water zone thickness, ft.

H_o = initial oil zone thickness, ft.

S_{wc} = connate water saturation, fraction.

S_{or} = residual oil saturation, fraction.

N = oil in place, stb.

N_p = cumulative oil production, stb.

For the first time step (before water breakthrough), N_p can be estimated as the total (oil) rate multiplied by the production time. For the subsequent time steps, N_p could be obtained using an iterative procedure as follows:

$$N_{p(n+1)} = N_{p(n)} + (t_{(n+1)} - t_{(n)}) * \frac{(q_{(n+1)} + q_n)}{2} \quad \text{.....(2.50)}$$

Where *n+1* refers to the current time step and *n* denotes the previous time step.

3. Calculate new dimensionless water cuts using Equations (2.44), (2.45) or (2.46).
4. Obtain the actual water-cut fraction using Equation (2.38).
5. Calculate water and oil rates as

$$q_w = fw \cdot q_T \quad \text{.....(2.51)}$$

$$q_o = q_T - q_w \quad \text{.....(2.52)}$$

Where q_T, q_w and q_o represent total flow rate, water flow rate, and oil flow rate, respectively. Obviously, recovery can be estimated as:

$$R(\%) = N_p/N \quad \text{.....(2.53)}$$

And the percentage of bypassed oil (BPO) is defined as:

$$BPO(\%) = 100 - R(\%) \quad \text{.....(2.54)}$$

CHAPTER 3. VALIDATION OF ANALYTICAL MODELS

The objective of this chapter is to validate the best-known analytical models for the prediction of the motion of the oil-water interface in edge and bottom-water systems. The validation study includes: first, the analysis of the results of calculations performed with the models to identify their weaknesses and strengths. Second, the modification of some of the models to ensure consistency in the calculations. Third, a comparison between analytical and simulation results.

3.1 Validation of Analytical Models for Edge-Water Reservoirs

3.1.1 Analytical Calculations

Five different analytical models for the prediction of the motion of the water-oil interface and calculation of final recovery in the dipping structures were presented in Chapter 2. The study of these methods is important because of their simplicity compared with numerical simulations, which can be time consuming. In addition, knowledge of the motion of the water-oil interface and final recovery are needed in reservoir engineering in order to determine the volume of oil that will be recovered, and the amount of oil that will be by-passed by the end of a well's life. In this section, calculations performed with the models are presented for a dipping homogeneous reservoir with side-water advancement. The main objective of these calculations is to evaluate the main strengths and weaknesses of the models. It was decided not to include Sheldon and Fayers' Model (1962) in the calculations presented in this Chapter. This is because Equation (2.31) cannot be readily solved analytically and a finite difference technique is required.

Input Data and Description of Cases

The properties of the rock and the fluids and the water-oil relative permeabilities used in

the calculations are shown in Tables 1 and 2, respectively. The parameters related to the geometry of the reservoir, as well as the injection/production rates used, are shown in Table 3. As can be noted, calculations were performed for oil viscosities of 0.67 cp, 3 cp, 5 cp and 10 cp, dip angles of the reservoir of 5, 25 and 40 degrees and injection/production rates of 260 and 3000 b/d. This was done in order to measure the effect of different variables on the oil recovery and the water inflow performance. A summary of the cases analyzed is shown in Table 4. This table also shows end point mobility ratios, dimensionless gravity numbers and critical rates calculated using Equations (2.12), (2.13) and (2.16), respectively.

Table 1: Rock and Fluid Properties Used in Analytical Calculations

B_o (rb/stb)=	1.3
B_w (rb/stb)=	1.0
μ_o (cp)=	0.67, 5 and 10
μ_w (cp)=	0.5
γ_o=	0.81
γ_w=	1.04
K_{abs} (darcies)=	2
ϕ (fraction)=	0.18
S_{wc} (fraction)=	0.2
S_{or} (fraction)=	0.2

Calculations Using Richardson and Blackwell's Model (1971)

Results of the calculations completed using Richardson and Blackwell's model for the cases presented in Table 4 are shown in Table 5. The blank spaces in Table 5 are justified by the fact that the model can only be applied for calculations at and after the breakthrough time (which is symbolized with bold characters). The thickness of the horizontal water layer, X (which is also the oil recovery as a fraction of the displaceable oil), was introduced to the model as an input parameter. Then, the water production, W_p, and the water influx, W_e, were obtained using

Equations (2.3) and (2.2), respectively. Finally, the water cut was calculated using Equation (2.5).

Table 2: Relative Permeabitities Used in the Analytical Calculations

S_w	k_{rw}	k_{ro}	k_{ro}/k_{rw}
0.20	0.00	0.80	-
0.25	0.00	0.61	305.00
0.30	0.01	0.47	52.22
0.35	0.02	0.37	18.50
0.40	0.03	0.29	8.64
0.45	0.05	0.22	4.31
0.50	0.08	0.16	2.17
0.55	0.10	0.12	1.20
0.60	0.13	0.08	0.61
0.65	0.17	0.05	0.29
0.70	0.21	0.03	0.13
0.75	0.25	0.01	0.04
0.80	0.30	0.00	0.00

Table 3: Reservoir Geometry and Other Properties

Dip Angle (degrees)	5, 25 and 40
Reservoir Thickness (ft)	40
Distance between Injection/Production Wells (ft)	625
Distance Between Injectors and Producers (ft)	2000
Injection/Production Rate (b/d/well)	260, 3000

Table 4: Description of Cases Used in the Analytical Calculations

Case	M	G	q (b/d)	q_c (b/d)	Dip Angle
1	3.75	5.50	260.00	519.58	25
2	0.50	5.50	260.00	-2857.70	25
3	0.50	1.13	260.00	-589.30	5
4	7.50	5.50	260.00	219.80	25
5	7.50	1.13	260.00	45.30	5
6	2.25	0.72	3000.00	1738.57	40

Table 5: Results of Analytical Calculations Using Richardson and Blackwell's Model

% By Passed Oil (1-X)	μ_o = 0.67 cp (Cases 2, 3)		μ_o = 3 cp (Case 6)		μ_o = 5 cp (Case 1)		μ_o = 10 cp (Cases 4, 5)	
	Water Influx (MOV)	Water Cut (%)	Water Influx (MOV)	Water Cut (%)	Water Influx (MOV)	Water Cut (%)	Water Influx (MOV)	Water Cut (%)
70							**0.32**	**44.00**
60							0.53	60.00
55					**0.45**	**42.11**	0.67	66.15
50					0.54	50.00	0.83	71.43
40					0.77	63.64	1.25	80.00
38			**0.62**	**49.20**	0.83	66.07	1.35	81.46
30			0.80	61.54	1.11	75.00	1.86	86.67
20			1.13	75.61	1.61	84.62	2.83	92.00
10			1.71	88.37	2.55	92.86	4.66	96.36
5			2.32	94.32	3.54	96.55	6.61	98.26
3	**0.99**	**85.71**	2.77	96.62	4.29	97.96	8.09	98.97
0	2.15	100.00	7.89	100.00	12.82	100.00	25.13	100.00

The model predicts that, at the water breakthrough, the amount of by-passed oil (BPO) is 3%, 38%, 55% and 70% of the displaceable oil for oil viscosities of 0.67 cp, 3 cp, 5 cp and 10 cp, respectively. For the cases with the lowest oil viscosity there is a favorable endpoint mobility ratio (M<1) and, therefore, the amount of BPO at breakthrough is much smaller. For the cases with the highest oil viscosity; however, the amount of BPO at breakthrough is more than 20 times larger than for the cases with the lowest oil viscosity.

The Richardson and Blackwell model has a simple mathematical formulation and it can be easily applied using hand calculations. In fact, the only input data needed are the oil and water viscosities, the connate water saturation, the residual oil saturation, the effective permeability of oil and the relative permeability of water at the residual oil saturation. However, the model does not differentiate between stable displacements and unstable ones and it does not take into

account the effect of dip angle and capillary forces on the calculations. In addition, the assumptions made are probably too simplistic. For example, the assumptions that the water layer is of constant thickness does not seem to agree with experimental results for the water underrunning phenomena obtained by authors such as Fayers and Muggeridge (1990). Also, some inconsistencies were found in the results. For example, the model predicts no water production before breakthrough despite the fact that there is a fractional thickness of water, X.

Thus, the use of Richardson and Blackwell model is only recommended as a quick first approach for the prediction of the oil recovery at the water breakthrough, and not for detailed calculations of the volume of by-passed oil or the water inflow in time, which require a deeper knowledge of the shape of the water-oil interface.

Calculations Using Dake's Model (1978)

As indicated in Chapter 2, Dake's model includes equations for the calculation of the oil recovery for stable displacements (Equation (2.7)) and unstable displacements (Equation (2.11)). In order to distinguish between both types of displacements, the equation of critical velocity of Dietz (1953) (Equation (2.16)), can be used. According to Dietz' criteria, Cases 1 to 3 in Table 4 are stable displacement cases and Cases 4 to 6 are unstable displacement cases.

Dake's Model: Calculations for Stable Displacement

Table 6 shows the results the calculations performed using Dake's model for Cases 1, 2 and 3 (stable displacement). The breakthrough time is shown with bold characters. The fractional thickness of the water tongue at the producing end, b_e, was introduced as an input parameter in all the calculations. The oil recovery, water cut and time were estimated using Equations (2.7), (2.8) and (2.10), respectively.

It can be noted that for the reservoir with a 25° dip (Case 2), breakthrough occurred later

and the maximum recovery (0% BPO) was obtained sooner than for the reservoir with a 5 degree dip (Case 3). Therefore, it seems that the gravity forces in a reservoir with a 25° dip have a very favorable effect on delaying the breakthrough time in comparison with a reservoir with a 5° dip.

Table 6: Results of Analytical Calculations Using Dake's Model. Cases 1 to 3 (stable displacement)

be	BPO (% MOV)	Water Cut (Fraction)	Time (Days)
CASE 1 (M=3.75, q=260 b/d, α=25°)			
0.00	**4.29**	**0.00**	**3540.10**
0.125	3.29	0.13	3579.80
0.25	2.41	0.26	3619.49
0.50	1.07	0.51	3698.88
0.75	0.27	0.76	3778.27
1.00	0.00	1.00	3857.66
CASE 2 (M=0.5, q=260 b/d, α=25°)			
0.00	**1.97**	**0.00**	**3626.17**
0.125	1.51	0.13	3644.35
0.25	1.11	0.25	3662.53
0.50	0.49	0.50	3698.88
0.75	0.12	0.75	3735.24
1.00	0.00	1.00	3771.59
CASE 3 (M=0.5, q=260 b/d, α=5°)			
0.00	**7.93**	**0.00**	**3405.52**
0.125	6.07	0.13	3478.86
0.25	4.46	0.27	3552.20
0.50	1.98	0.52	3698.88
0.75	0.50	0.76	3845.57
1.00	0.00	1.00	3992.25

The effect of the end-point mobility ratio, M, is clear from the comparison of Cases 1 and 2. As expected, for the case with the lowest mobility ratio (Case 2), the breakthrough occurs later and the amount of BPO at breakthrough is smaller. It is also important to mention that the

interface predicted by the model at all times for these three cases of stable displacement is a straight line, as shown in Figure 9.

Dake's Model: Calculations for Unstable Displacement

Table 7 shows the results the calculations performed using Dake's Model for Cases 4, 5 and 6 (unstable displacement). For these cases, the oil recovery, water cut and time were estimated using Equations (2.11), (2.15) and (2.10), respectively.

Table 7: Results of Analytical Calculations Using Dake's Model. Cases 4 to 6 (unstable displacement)

be	BPO (% MOV)	Water Cut (Fraction)	Time (Days)
CASE 4 (M=7.5, q=260 b/d, α=25°)			
0.00	**50.11**	**0.00**	**1845.30**
0.04	37.45	0.07	2330.42
0.09	25.68	0.14	2815.54
0.16	14.95	0.23	3300.66
0.30	5.67	0.37	3785.77
1.00	0.00	1.00	4270.89
CASE 5 (M=7.5, q=260 b/d, α=5°)			
0.00	**84.29**	**0.00**	**580.98**
0.22	44.77	0.60	3065.57
0.39	23.66	0.75	5550.16
0.56	10.33	0.85	8034.75
0.76	2.61	0.92	10519.34
1.00	0.00	1.00	13003.93
CASE 6 (M=2.25, q=3000 b/d, α=40°)			
0.00	**34.45**	**0.00**	**210.13**
0.13	22.69	0.19	251.76
0.29	13.29	0.37	293.39
0.47	6.23	0.55	335.02
0.69	1.67	0.75	376.65
1.00	0.00	1.00	418.28

A comparison between the results given in Table 7 with the results presented in Table 6

shows that, as expected, the amount of by-passed oil at breakthrough for the cases in which the displacement is unstable is much higher than for the cases in which the displacement is stable.

Table 7 also shows that, for the case with a 25° dip (Case 4), breakthrough occurred later and the maximum recovery (0% BPO) was obtained sooner than for the case with 5 degrees (Case 5). This confirms the favorable effect gravity forces have on water inflow performance. However, despite the fact that the dip angle for Case 6 is higher, both the water breakthrough and the maximum recovery occurred sooner than in all the other five cases. This is because the injection/production rate for Case 6 is more than ten times higher than for the other cases and, therefore, the water-oil interface travels much faster.

Calculations Using Dietz' Model (1953, Unstable Displacement)

The results of the calculations undertaken using Dietz' model for Cases 4, 5 and 6 are shown in Table 8. The results at breakthrough are shown with bold characters. Dietz' model was specially formulated to predict the development of the water inflow in time when the critical rate defined by Equation (2.16) is exceeded, a condition satisfied by Cases 4, 5 and 6 (unstable displacement). In Cases 1, 2 and 3, the displacement is stable and, therefore, the interface remains at a constant slope. A brief description of the procedure used for the calculations follows. The initial interface (t=0), was calculated with Equation (2.17) introducing values for the thickness (y) from 0 to h (thickness of the reservoir). Because the cumulative inflow per unit volume (Q) before breakthrough is equal to the volume of water injected, Equation (2.18) was used to estimate the position of the water tongue (x). After the water breakthrough, both the thickness of the water tongue (y) and x are known, therefore, Equation (2.18) was used to estimate Q. Finally, the volume of displaced oil and the water cut were estimated from Equations (2.19) and (2.20), respectively.

Table 8: Results of Analytical Calculations Using Dietz's Model. Cases 4 to 6 (unstable displacement)

b_e	BPO (% MOV)	Water Cut (Fraction)	Time (Days)
CASE 4 (M=7.5, q=260 b/d, α=25°)			
0.00	**86.96**	**0.00**	**472.03**
0.13	66.94	0.52	1559.38
0.25	49.45	0.71	3289.03
0.50	22.21	0.88	8717.11
0.75	5.61	0.96	16840.04
1.00	0.00	1.00	27741.63
CASE 5 (M=7.5, q=260 b/d, α=5°)			
0.00	**88.39**	**0.00**	**380.44**
0.13	69.81	0.52	1296.11
0.25	52.86	0.71	2815.70
0.50	24.89	0.88	7889.94
0.75	6.57	0.96	16049.73
1.00	0.00	1.00	27741.63
CASE 6 (M=2.25, q=3000 b/d, α=40°)			
0.00	**56.09**	**0.00**	**139.08**
0.13	43.07	0.24	186.50
0.25	31.74	0.43	241.05
0.50	14.19	0.69	371.74
0.75	3.57	0.87	531.65
1.00	0.00	1.00	721.28

A comparison of the results of Tables 7 and 8 shows that breakthrough times for Dietz' model are lower than for Dake's model. Because Dietz' model neglects gravity forces, it results in thinner and longer water tongues that reach the well faster. It can also be noticed that Dietz' model predicts a larger amount of by-passed oil at breakthrough and a longer time for the water to displace all the movable oil from the reservoir than Dake's model.

Figure 19 displays a cross section of the slab showing the movement of the oil-water interface predicted using Dietz' model for Case 4. The water tongue progressively penetrates

into the oil zone until it reaches the producing end of the system. It can also be noted that the length of the interface increases with time (from approximately 85 ft at t=0 to about 1970 ft at breakthrough). The straight line shown in blue represents the initial horizontal interface, which is defined by Equation (2.17). Water breakthrough for Case 4 occurs in only 472 days, which is about 25% of the breakthrough time predicted by Dake's model. Similar shapes (thin and elongated tongues) for the water-oil interface were also obtained for Cases 5 and 6.

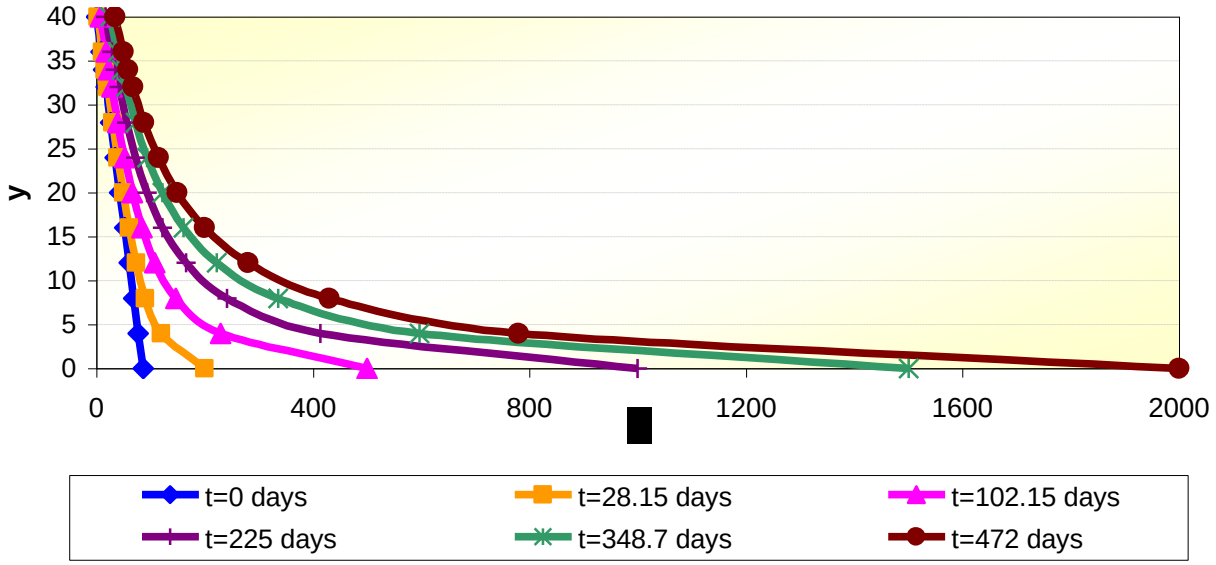

Figure 19: Prediction of the Movement of the Oil-Water Interface Using Dietz' Model for Case 4 (M=7.5, q=260 b/d, α=25°). Slab has been rotated for visualization purposes

The dip angle of the reservoir for Case 5 (5 degrees) is smaller than for Case 4 (25 degrees). Therefore, a more favorable effect of the gravity forces and a much higher breakthrough time may be expected for Case 4. Using Dake's model, the breakthrough times obtained for Cases 4 and 5 were 1845 days and 581 days; respectively, which confirms the favorable effect of the gravity forces. Using Dietz' model; however, the breakthrough time obtained for Case 4 was 472 days, which is very close to the 380 days obtained by the model for

Case 5. This small difference between the breakthrough times obtained using Dietz' model for Cases 4 and 5 is probably caused by the fact that the model neglects the gravity effects.

Table 8 also shows that, for Case 6, the breakthrough time is lower than for Cases 4 and 5. This is because for Case 6 the injection/production rate is much higher and, therefore, the oil-water interface travels much faster. In addition, it can be noted that the breakthrough time predicted using Dietz' model for this case - 139 days - is quite close to the breakthrough time predicted by Dake's model - 210 days. This is mainly because at high rates the viscous forces dominate over the gravity forces. In other words, for the rates under consideration for this case, the gravity forces do not seem to have an important effect on the results.

The results presented here showed that, even if coning does not exist in the reservoir, the formation of a water tongue could lead to substantial water inflow and large amounts of by-passed oil to be abandoned in the reservoir for economical reasons. For example Table 8 shows that, for Case 4, it takes the water approximately 9 years (3285 days) to displace the initial 50% of the oil in the reservoir and about 67 years (24455 days) to displace the remaining 50%. It can also be noted that this remaining oil would have to be produced with water cuts above 70%. This does not seem feasible from an economical perspective and probably most of this remaining oil may never be recovered. The effect of coning on these results will be studied with the help of a numerical simulator, as explained later.

Calculations Using Outmans' Model (1962)

Calculations for Stable Displacement (Transient Interfaces Approaching Equilibrium)

The results of the calculations performed using Outmans' model for Cases 1, 2 and 3 are shown in Table 9. These cases satisfy the conditions stated in Chapter 2, (Section 2.1.3) for transient interfaces approaching stable equilibrium, namely $V<Vc_{Outmans}$ for any M (satisfied by

Case 1); and $M<1$ for any V (satisfied by Cases 2 and 3). The term "a" (Equation 2.22) was neglected in the calculations (effect of interfacial tension may be insignificant in the reservoir when compared to laboratory models). This implies that, according to Equation (2.21), $Vc_{Outmans} \approx Vc_{Dietz}$. The shape of the interface was calculated using Equations (2.23) to (2.30), where the thickness of the reservoir (y^*) and the time of injection before breakthrough (t^*) were introduced as input parameters. Because the interfaces obtained at breakthrough for all three cases approached straight lines, the oil recovery, water cut and the time of injection/production after the breakthrough were calculated from simple geometrical considerations using Equations (2.7), (2.8) and (2.10), respectively.

It can be seen that, for Cases 1, 2 and 3, the results obtained using Outmans' model are similar to the results obtained using Dake's model. This is because, for displacements below the Dietz critical rate (defined by Equation (2.16)), the shapes and dip angles of the interfaces predicted by both models are very similar. Table 9 also shows that breakthrough times predicted by Outmans' model are slightly lower than the ones predicted by Dake's model. One reason for this may be the fact that Outmans' model considers that there is an initial horizontal interface in the reservoir while Dake's model does not consider an initial interface and, therefore, water needs to displace more pore volume in order to get to the producer.

Figure 20 shows the movement of the interface predicted using Outmans' model from the beginning of the injection/producer until the breakthrough for Case 1. The interface moves with a velocity V. As can be noted, breakthrough is reached in 3478 days. It can also be noted that, at breakthrough time, the interface estimated by Outmans' model approaches a straight line, which indicates that it is approaching stable equilibrium. Similar shapes of the oil-water interface were

obtained for Cases 2 and 3, which also satisfy the conditions stated in Chapter 2 for transient interfaces approaching stable equilibrium.

Table 9: Results of Analytical Calculations Using Outmans' Model. Cases 1 to 3 (transient interfaces approaching equilibrium)

be	BPO (% MOV)	Water Cut (Fraction)	Time (Days)
CASE 1 (M=3.75, q=260 b/d, α=25°)			
0.00	**4.03**	**0.00**	**3478.70**
0.13	3.09	0.13	3515.24
0.25	2.27	0.26	3551.79
0.50	1.01	0.51	3624.87
0.75	0.25	0.76	3697.96
1.00	0.00	1.00	3771.04
CASE 2 (M=0.5, q=260 b/d, α=25°)			
0.00	**1.77**	**0.00**	**3560.73**
0.13	1.35	0.13	3576.76
0.25	1.00	0.25	3592.80
0.50	0.44	0.50	3624.87
0.75	0.11	0.75	3656.94
1.00	0.00	1.00	3689.01
CASE 3 (M=0.5, q=260 b/d, α=5°)			
0.00	**8.26**	**0.00**	**3031.51**
0.13	6.32	0.13	3099.73
0.25	4.65	0.27	3167.95
0.50	2.06	0.52	3304.40
0.75	0.52	0.76	3440.85
1.00	0.00	1.00	3577.30

Outmans' Model: Unstable Displacement (Transient Interfaces Not Approaching Equilibrium)

The main purpose of the Outmans' model is related to the study of the water inflow in time when the conditions that cause transient interfaces approaching equilibrium are satisfied. This is, $V<Vc_{Outmans}$ for any M (satisfied by Case 1); and $M<1$ for any V (satisfied by Cases 2 and

3). Because Cases 4, 5 and 6 do not satisfy these conditions, it is believed that Outmans' model should not be used for the prediction of the water inflow in time for these cases.

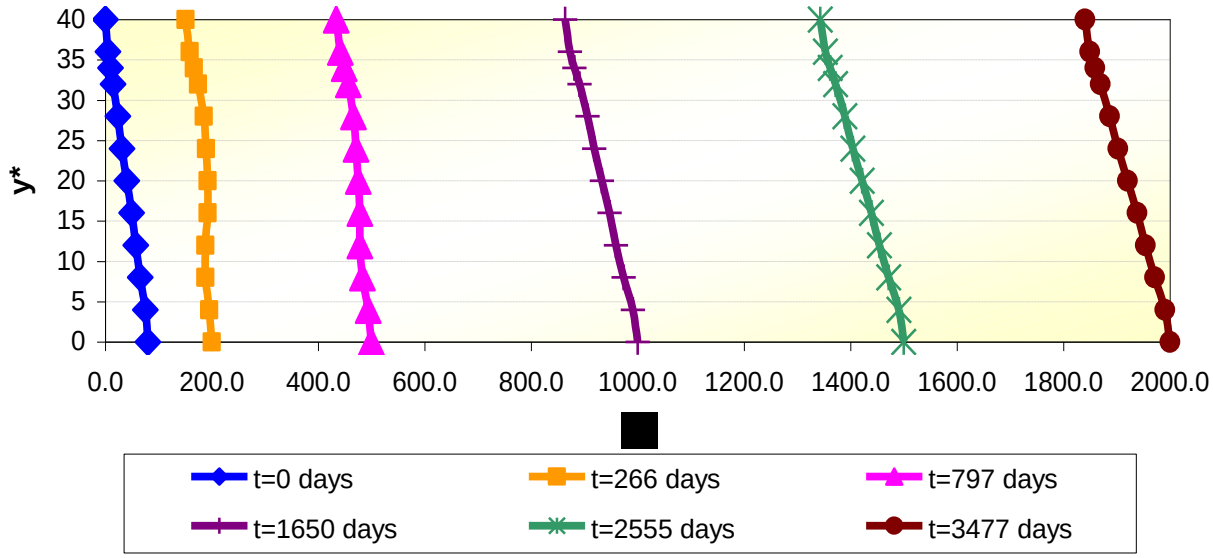

Figure 20: Prediction of the Movement of the Oil-Water Interface Using Outmans Model for Case 1 (M=3.75, q=260 b/d, α=25°).

Water Cut Plots Interpretation

Figures 21, 22, and 23 show the water cut profiles obtained using Dake's and Outmans' models for Cases 1, 2 and 3; respectively. The shape of the water cut plots is a straight line due to the fact that the shape of the interfaces at and after breakthrough for these three cases is also a straight line (stable displacement). It can also be noted that, for all three cases, Outmans' model predicts an earlier breakthrough time than Dake's model. As indicated before, one reason for this may be the fact that Outmans' model considers that there is an initial horizontal interface in the reservoir while Dake's model does not consider an initial interface and, therefore, water needs to displace more pore volume in order to get to the producer end of the system.

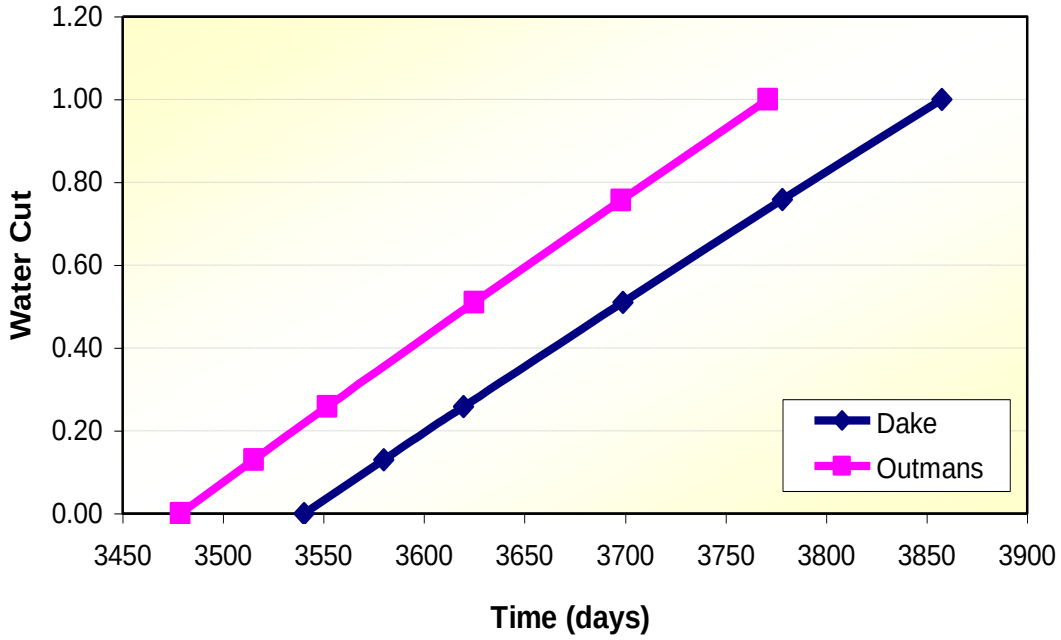

Figure 21: Water Cut Predicted Using Dake's and Outmans' Models for Case 1 (M=3.75, q=260 b/d, α=25°).

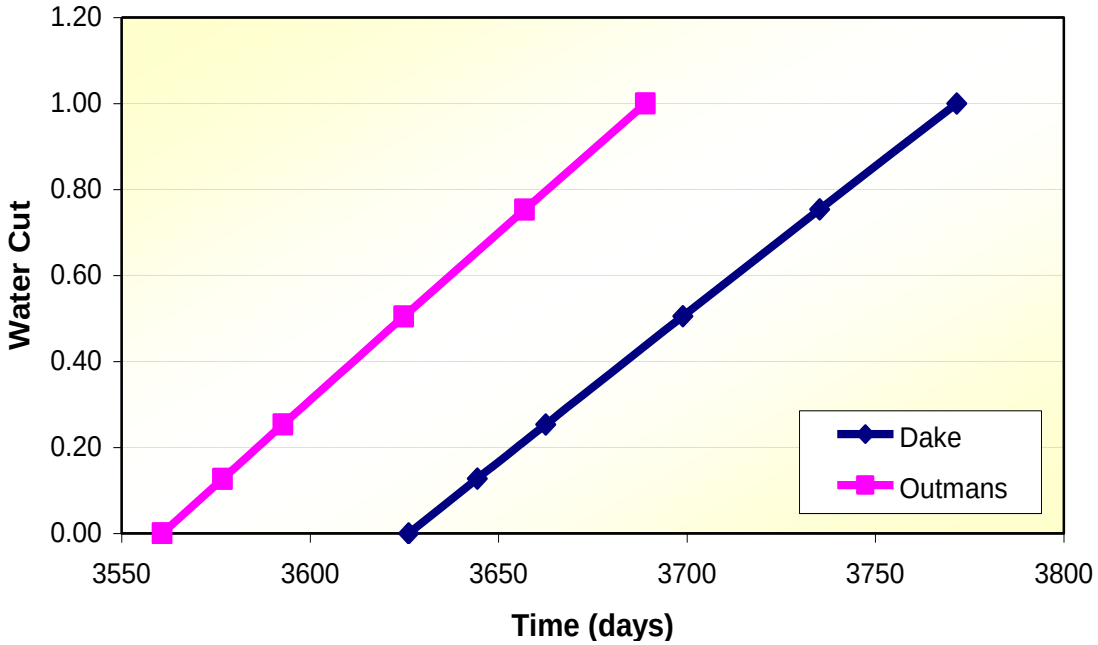

Figure 22: Water Cut Predicted Using Dake's and Outmans' Models for Case 2 (M=0.5, q=260 b/d, α=25°).

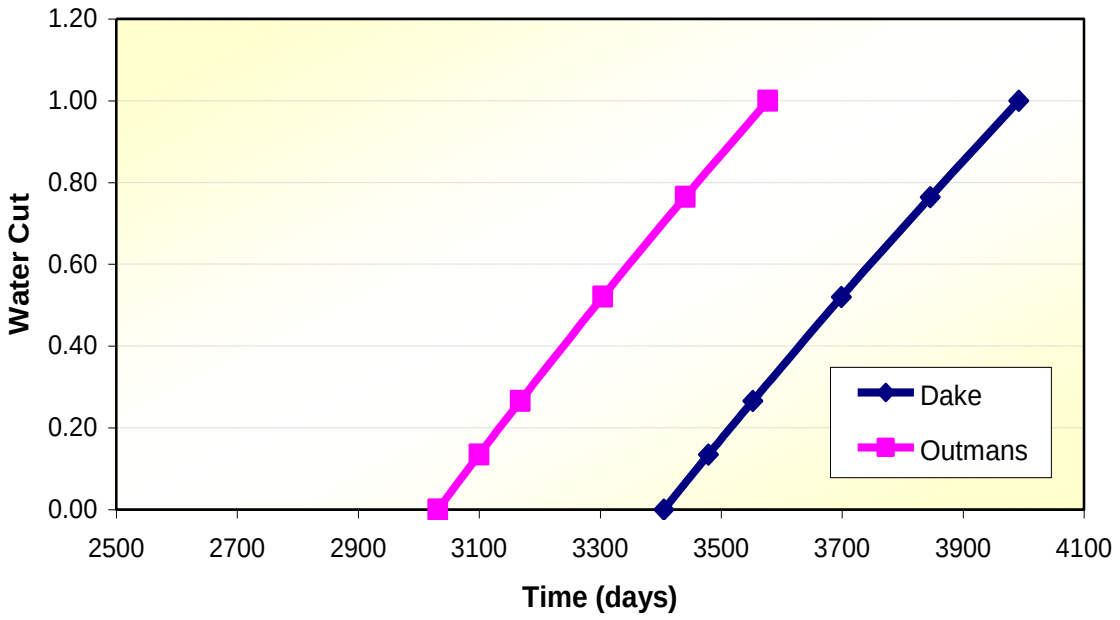

Figure 23: Water Cut Predicted Using Dake's and Outmans' Models for Case 3 (M=0.5, q=260 b/d, α=5°).

Figures 24, 25 and 26 show the water cut profiles predicted using Dake's and Dietz' models for Cases 4, 5 and 6; respectively. As it was indicated before, for these three cases the displacement can be considered unstable and, therefore, the water cut plots are not straight lines.

The effect of the dip angle over Dake's calculations can be deduced from Figures 24 and 25. For small dip angles and, therefore, small gravity forces (Case 5, Figure 25), the water cut profile obtained using Dake's method has a higher curvature than the one obtained for a larger dip angle and larger gravity forces (Case 4, see Figure 24). Therefore, it seems that the larger the dip angle and gravity forces, the smaller the curvature of the water cut profile estimated using Dake's model.

The effect of the dip angle over the water cut profiles obtained with Dietz' model can also be deduced from Figures 24 and 25. Obviously, because Dietz' model neglects the effect of gravity forces, there is no noticeable difference between the water cut curves obtained for Cases

4 and 5 (the only difference in the input data between these cases is the dip angle, which mainly affects the gravity forces).

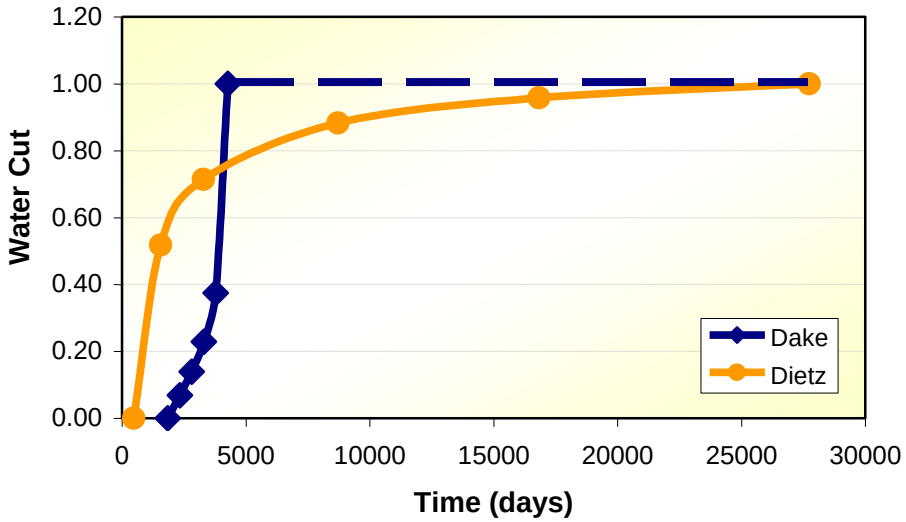

Figure 24: Water Cut Predicted Using Dake's and Dietz' Models for Case 4 (M=7.5, q=260 b/d, α=25°).

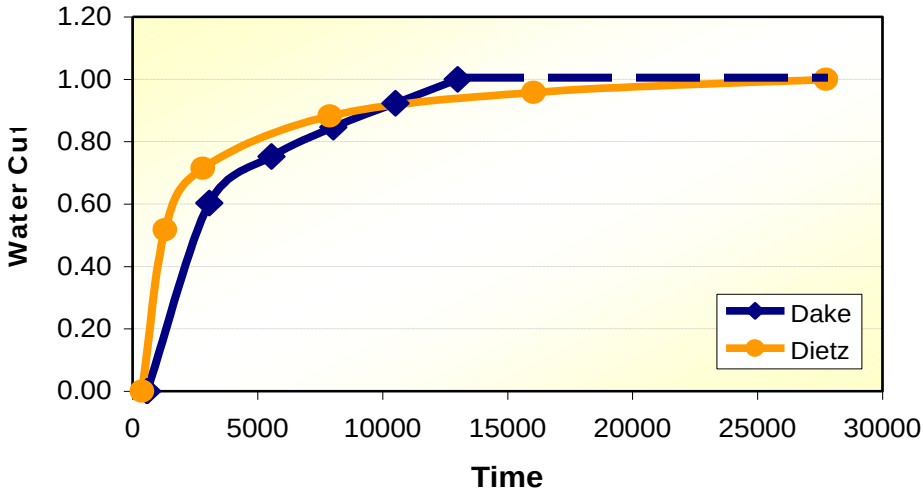

Figure 25: Water Cut Predicted Using Dake's and Dietz' Models for Case 5 (M=7.5, q=260 b/d, α=5°).

An analysis of the results obtained using Dake's model also shows that the curvature of

the water cut plots is smaller for low mobility ratios and/or small injection/production rates. Furthermore, for low mobility ratios, the effect of the gravity forces on the curvature of the water cut plots was found to be quite small. These results suggest that the calculations performed using Dake's model are quite sensitive to changes in both the gravity and the viscous forces. A review of Figures 24, 25 and 26 also suggests that; however, water cut profiles obtained by Dietz's model are not as sensitive to the changes in the mobility ratio and/or rate as the profiles obtained using Dake's model.

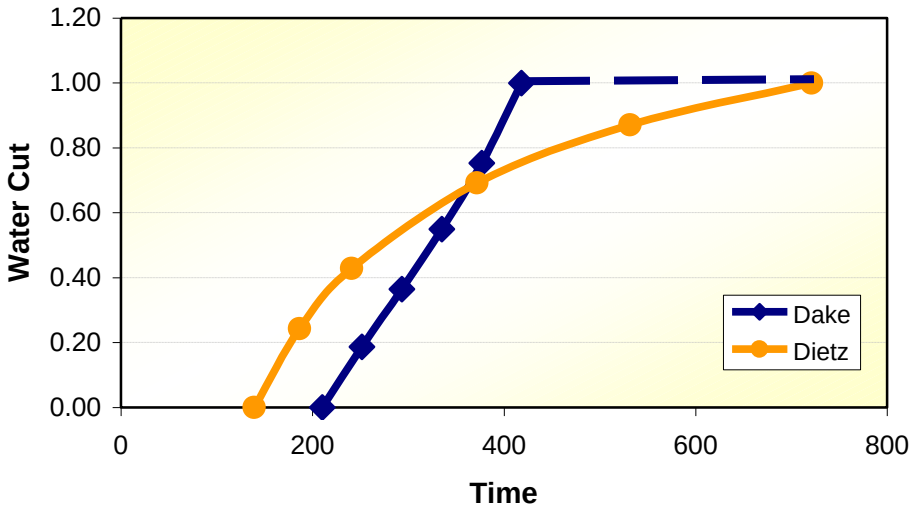

Figure 26: Water Cut Predicted Using Dake's and Dietz' Models for Case 6 (M=2.25, q=3000 b/d, α=40°).

By-passed Oil at Breakthrough

A summary of the volume of by-passed oil at breakthrough estimated using the different models studied in this section is shown in Table 10. Logically, because the shape of the interface for the cases in which the displacement can be regarded as stable (Cases 1, 2 and 3) is a straight line, the volume of by-passed oil at breakthrough for these cases is very small (less than 20% of the MOV). The only exception is the volume of by-passed oil at breakthrough obtained using

Richardson and Blackwell's model for Case 1, which is much higher than the volume estimated using the other methods. This is probably because Richardson and Blackwell's model showed to be quite sensitive to the mobility ratio and does not consider the effect of the dip angle of the reservoir. The table also shows that Dake's and Outmans' models give about the same volume of by-passed oil at breakthrough for each one of the stable Cases (Cases 1, 2 and 3). This is because for each of these cases the angle between the interface and the bedding predicted by both models at breakthrough is very similar.

Table 10: By-Passed Oil (% of Movable Oil Volume) at Breakthrough for Cases 1 to 6

Model Name	**Case 1** M=3.75, q=260 b/d, α=25°	**Case 2** M=0.5, q=260 b/d, α=25°	**Case 3** M=0.5, q=260 b/d, α=5°	**Case 4** M=7.5, q=260 b/d, α=25°	**Case 5** M=7.5, q=260 b/d, α=5°	**Case 6** M=2.25, q=3000 b/d, α=40°
Richardson and Blackwell	55.00	3.00	3.00	70.00	70.00	38.00
Dake	4.29	1.97	7.93	50.11	84.29	34.45
Dietz	-	-	-	86.96	88.39	56.09
Outmans	4.03	1.77	8.26	-	-	-

It can also be noted that, for the cases in which the displacement can be regarded as unstable (Cases 4, 5 and 6), the volume of by-passed oil at breakthrough calculated using the different models studied is higher than 30% of the MOV and, in most of the cases, the volume of by-passed at breakthrough oil is more than half of the maximum volume of movable oil.

Because Dietz' model does not take into account the effect of gravity forces, the volumes of by-passed oil at breakthrough obtained for Cases 4 and 5 are very similar. The small difference in the by-passed oil between both cases is due to the way in which the initial interfaces were considered (see Figure 27). For a dip angle of 5 degrees (Case 5), the fraction of

the slab occupied by water is larger than for the case with 25 degrees (Case 4) and, therefore, the volume of oil that can be displaced by water (and the volume of oil that can be by-passed) is larger for this later case.

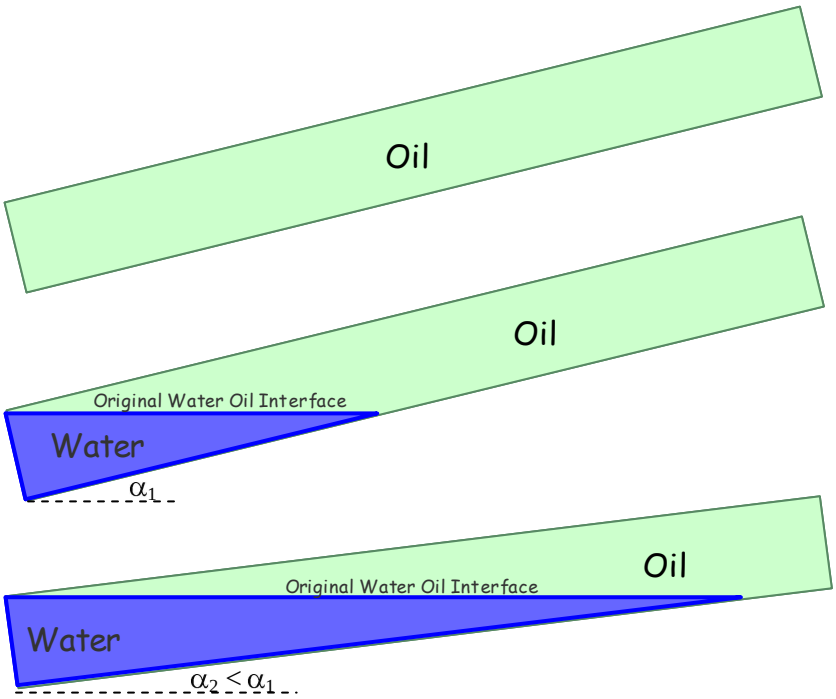

Dake's model considers no initial interface.

Outmans' and Dietz' models consider an initial interface. The volume occupied by the initial interface is larger for the smaller dip angle.
The volume of oil that can be displaced by water is higher for the larger angle.

Figure 27: Initial Interface: Difference between Dake's, Outmans' and Dietz' Models.

Obviously, the large volumes of by-passed oil at breakthrough obtained for the cases in which the displacement can be regarded as unstable (Cases 4, 5 and 6) are a consequence of the shape of the water-oil interface predicted by the models. Unfortunately, most of the water-oil displacements are believed to be unstable because of the high rates required for the economical exploitation of the reservoirs. Then, the use of methods for the control of the produced water, such as the Down Hole Water Sink (DWS) technology, could be encouraged in order to extend the productive life of the reservoirs.

Summary

Four models for the prediction of the amount of by-passed oil in a dipping homogeneous reservoir with side-water advancement have been briefly studied in this section. The first model studied, the Richardson and Blackwell's model, is only recommended as a quick first approach for the prediction of the water breakthrough, and not for detailed calculations of the volume of by-passed oil. The second model analyzed, Dake's model, is a very versatile method that can be easily applied and it has expressions for both stable and unstable displacement. However, in order to express the mathematical description of the problem in one dimension, the flow is assumed to occur along the centerline of the reservoir, which does not represent the real physics of the water oil displacement in dipping structures. This model can be used for comparison purposes and as a reference for more detailed calculations.

The third model studied, Outmans' model, is perhaps the best model for water displacements below the critical rate. This is because Outmans' model introduces the concept of transient interfaces approaching equilibrium, which is considered a very useful and realistic concept due to the fact that stable tilts may not exist in the reservoir after the beginning of the production. However, it was found that both Dake's and Outmans' models estimated the same amounts of by-passed oil for the cases in which stable displacement is expected to occur, which suggest that the impact of using one or the other can be insignificant for stable conditions.

The last model analyzed, Dietz' model; can be recommended for very high values of the injection/production rate (above the critical rate). This model gives very high values for the volume of by-passed oil at breakthrough and it predicts very long recovery times at higher water cuts, which may be expected in unstable water-oil displacements where a water tongue is formed. For low injection/production rates; however, the effect of the gravity forces, which are

neglected by the model, can be significant and the model may give very inaccurate results. Additional work is then needed in order to determine the minimum injection/production rates at which Dietz's model can give acceptable results. It is believed that Dietz' model may be accurate for injection/production rates about 10 times higher than the critical rate and that Dake's model may be used for injections/production rates just above the critical. However, this is purely hypothetical.

The models analyzed in this section provide a simple and quick approach for the calculation of the water inflow in time and the volume of by-passed oil in systems with side-water flood. Some general guidelines about their use are summarized in Table 11. According to the results presented here, the best known methods for predicting the motion of the water-oil interface in dipping structures could be those by Dietz (1953) and Dake (1978). However, it is important to mention that, despite the fact that each one of the models presented in Table 11 works reasonably well under specific conditions, there is no single satisfactory model for the calculation of the by-passed oil for the whole range of conditions that can exist in hydrocarbon reservoirs. In addition, it is also important to indicate that no analytical model was found in the literature for the determination of the motion of the water-oil interface when **both water conning and gravity underruning occur in the reservoir**. Finally, the results presented in this section showed that the formation of a water tongue in a side water reservoir could cause substantial amounts of by-passed oil at breakthrough. Obviously, higher amounts of by-passed oil may be expected if coning is also included. The combined effect of gravity underrunning and coning in side water systems need to be studied with the help of numerical simulation.

The next sections present the results of a simulation study completed with the objective of understanding the role of coning and further validating Dietz and Dake's models. The study

includes: first, the selection of the best geometry to be used in the simulator. Second, a grid sensitivity analysis designed to improve run times without compromising accuracy. Third, a brief description of the aquifer modeling method employed in the simulations. Fourth, a description of the simulation model used and the cases considered. Finally, a discussion of the results and a summary of the most important findings.

Table 11: Summary of Guidelines for the Use of Analytical Models for the Calculation of By-passed Oil in Edge-Water Drive Reservoirs

Model	Recommended For:
Richardson and Blackwell (1971)	- Calculation of volume of displaced oil at and after the breakthrough where precision is not important.
Dake (1978)	- Can be used for both stable and unstable displacements. - General comparisons with other models. - Injection/Production rates just above the critical rate
Outmans (1962)	- Stable Displacement where transient interfaces may occur (for example, it may be useful in cases where the injection/production rates change significantly).
Dietz (1953)	- Very high injection/production rates (above the critical), where gravity effects are not important

3.1.2 Selection of Grid Geometry

Angular Slab vs. Rectangular Slab

A 3D (X, Y, Z) simulation model was constructed to represent an idealized one-well element of an edge water-drive reservoir. The model constitutes a slab with the well completed at the upper end of the structure. Only one well was considered since all other wells may have a symmetrical behavior (Figure 1). The model has been created using the reservoir simulator "IMEX", developed by Computer Modeling Group (CMG). Two different grid geometries were

tested for the slab: angular and rectangular grid geometries. The angular geometry was achieved by building a radial simulation grid and assigning a porosity of zero to the grid blocks up dip of the area to be modeled. This is shown in Figure 28-a (XY view). The rectangular geometry was obtained by using regular Cartesian grid blocks. This can be seen in Figure 28-b (XY view). Both geometries have the same pore volume and number of grid blocks. Water intrusion to the reservoir has been modeled by attaching an aquifer to the lower end of the slab. This will be discussed in Section 3.1.4.

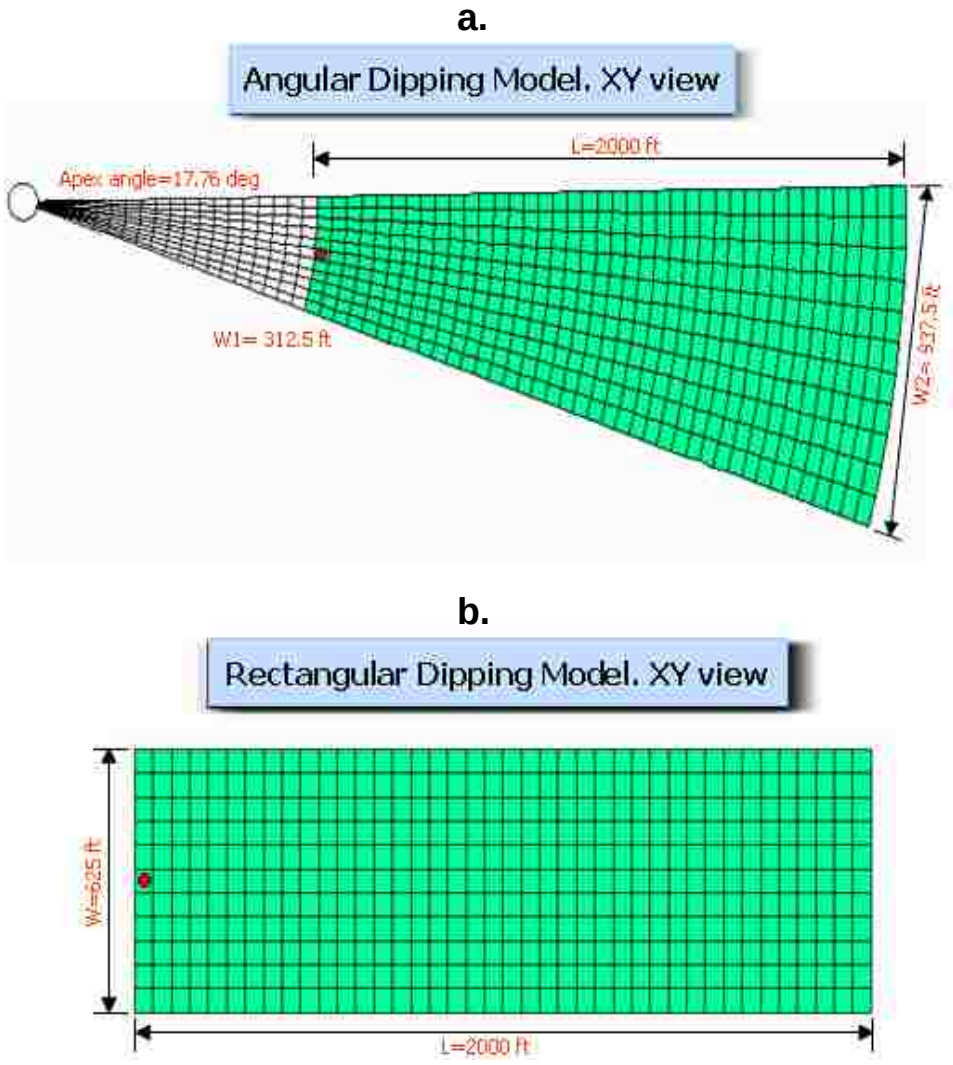

Figure 28: Angular and Rectangular Geometries for an Edge-Water Slab

Table 12 shows recovery at economic abandonment (defined in this study as 98% water cut) for the two different grid geometries tested. It is clear that the difference in recovery between both types of geometry is negligible - less than 0.2%. Because of its simplicity and ease of use, the rectangular dipping model geometry was selected as the approach to be employed.

Table 12: Recovery at Abandonment for Angular and Rectangular Geometries

Dip Angle (Degrees)	% Recovery Angular Geometry	% Recovery Rectangular Geometry	%Difference
5	78.5	78.6	0.17
15	79.5	79.6	0.14

Dip "Keyword" vs. Corner Point Geometry

The next step in selecting the grid geometry to be used in the simulation model for edge-water systems consisted in testing different methods to include the dip angle of the reservoir, α. Two methods were tested. First, the reservoir tilt was modeled using the "dip keyword" available in IMEX. This keyword allows a grid to tilt with respect to the gravity direction. Second, the reservoir tilt was obtained using corner point geometry, which consists in inputting depths for every corner in each grid-block. Using corner point geometry causes the reading of all depths ("Z"- coordinates) of the corner points required to define the grid. Therefore, this approach is more difficult to achieve than the "dip keyword" approach. Figure 29 shows 2D (XZ) cross sections of the slab obtained using these two methods.

Table 13 and Figure 30 summarize the effect on oil recovery of the method used to consider the tilt of the reservoir. A dip angle of 25 degrees was used in all cases presented in Figure 30. Such a high angle was used to magnify the effect of tilting. Two different end point

mobility ratios were considered: a favorable mobility ratio (M=0.4) and an unfavorable mobility ratio (M=10). It is clear that both approaches give similar results. The "dip keyword" approach, which is simpler and easier to use than the corner point method, will be employed in all other simulation studies in this dissertation.

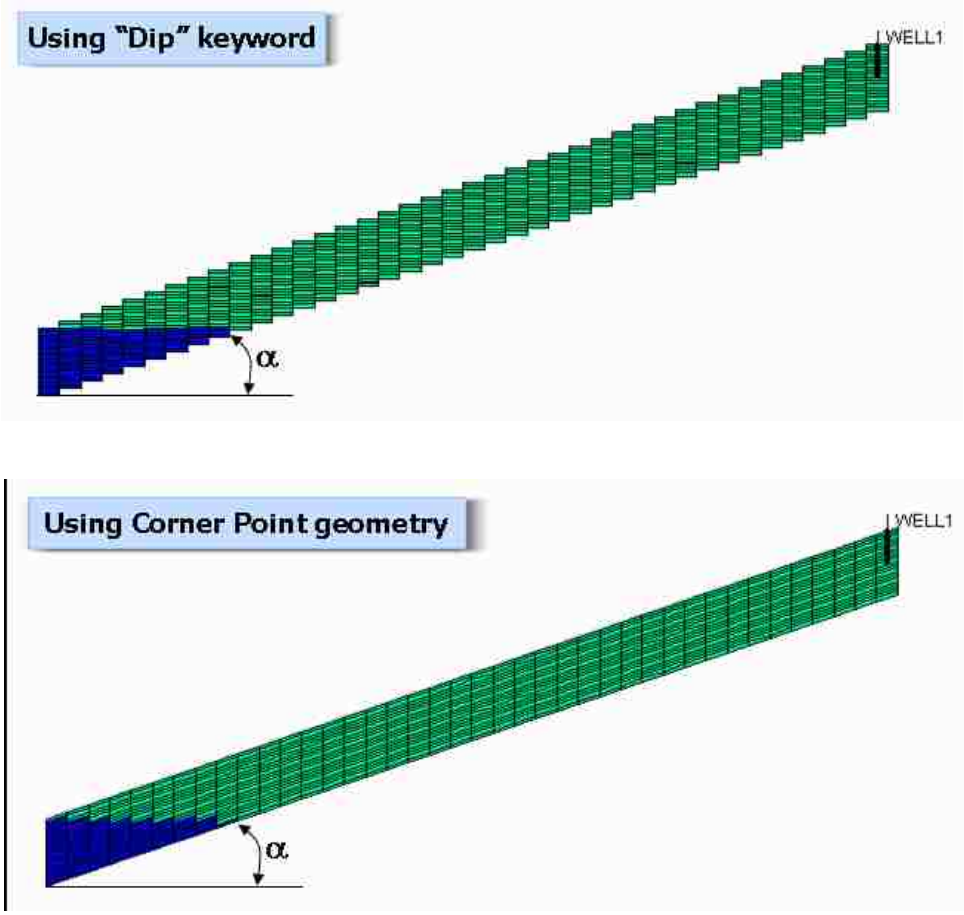

Figure 29: Dip and Corner Point Geometries for an Edge-Water Slab

Table 13: Recovery at Abandonment for Dip and Corner Point Geometries

Response	%Difference
Water Breakthrough Time (BT Time)	1.65
Recovery at Water Breakthrough	1.69
Recovery at Abandonment	0.38

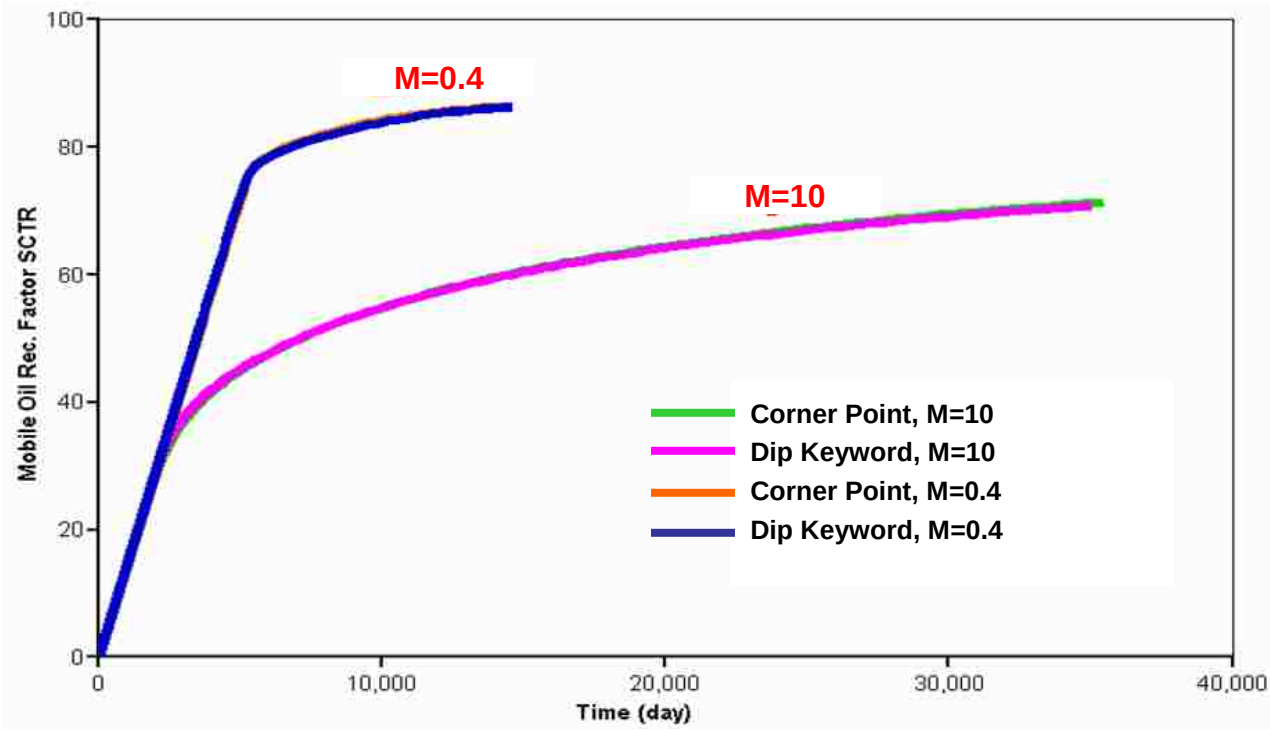

Figure 30: Oil Recovery for Dip and Corner Point Geometries

3.1.3 Grid Sensitivity Analysis

A grid sensitivity analysis has been carried out to find the best number of grid blocks in the simulation model. Table 14 shows the cases considered in the analysis. All cases were run with an end point mobility ratio (M) of 10. Three levels for the number of grid blocks were considered in the "X", "Y" and "Z" directions. The table also shows that Local Grid Refinement (LGR), was considered in one of the cases. The grid blocks containing the well (main or parent grid) were replaced by a refined grid made up of several small blocks that filled the space occupied previously by the parent fundamental block. This is shown in Figure 31. The type of refinement used was hybrid refinement, in which the refined grid is made up of stacked rings with optional angular subdivisions, much like a radial- angular cylindrical grid (IMEX Manual, 2005). Each grid block in the parent grid was subdivided into four refined blocks in the radial

and angular directions, and three refined blocks in the vertical direction. The following responses were analyzed: CPU time, water breakthrough time (BT time), oil recovery at water breakthrough (expressed as % of Movable Oil Volume, MOV) and oil recovery at abandonment (%MOV). Abandonment has been defined in this study as 98% water cut.

Table 14: Grid Sensitivity Analysis for Edge-Water Systems

Case #	DX	DY	DZ	Total	CPU time (days)	BT Time (days)	%Recovery at BT	%Recovery abandonment
1	20	11	10	2200	84.8	3600.0	16.8	72.7
2	20	11	20	4400	177.3	3327.0	15.3	74.8
3	20	21	10	4200	170.0	3559.0	16.6	72.7
4	20	21	20	8400	358.5	3265.0	15.1	74.8
5	40	11	10	4400	177.4	4276.0	19.5	73.3
6	40	11	20	8800	386.1	3729.0	17.0	75.3
6 with LGR	40	11	20	9760	486.1	3747.0	17.1	75.3
7	40	21	10	8400	359.4	4169.0	19.0	73.3
8	40	21	20	16800	787.5	3684.3	16.8	75.3
Maximum Difference (%)					828.3	31.0	29.3	3.6

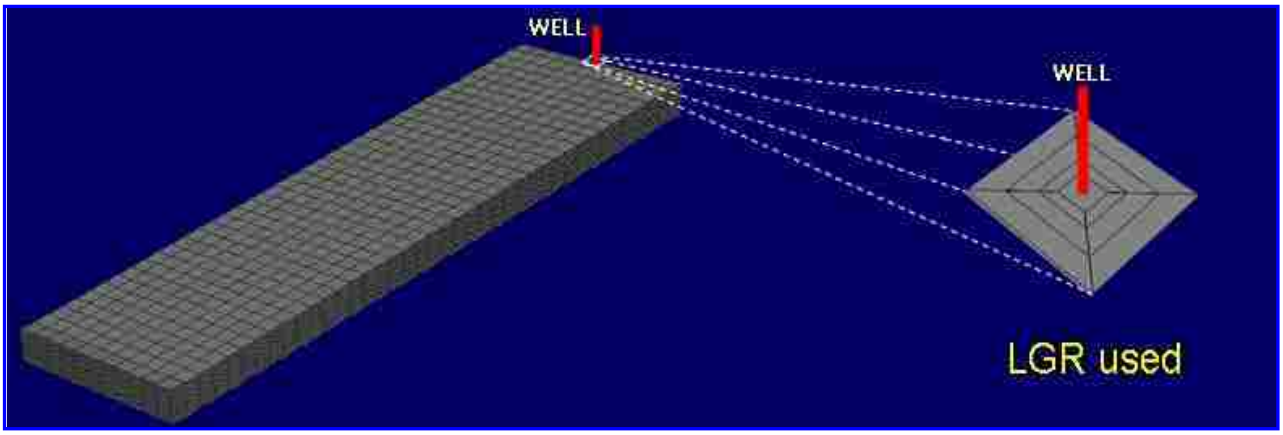

Figure 31: Hybrid Local Grid Refinement Considered

The results show that CPU time is significantly affected by changes in the number of grid blocks in each direction. Also important is the effect of the number of grid blocks on the water breakthrough time and recovery at breakthrough. Recovery at abandonment, however, is not

significantly affected by changes in the number of grid blocks. This can be confirmed by observing Figure 32, a plot of oil recovery vs. time for all nine cases. The results also indicate that there is no significant effect of using LGR around the well, other than an increase on the CPU time of about 21%. Because of these results, no refinement will be used in the simulation model to be employed to study oil bypassing in edge-water systems.

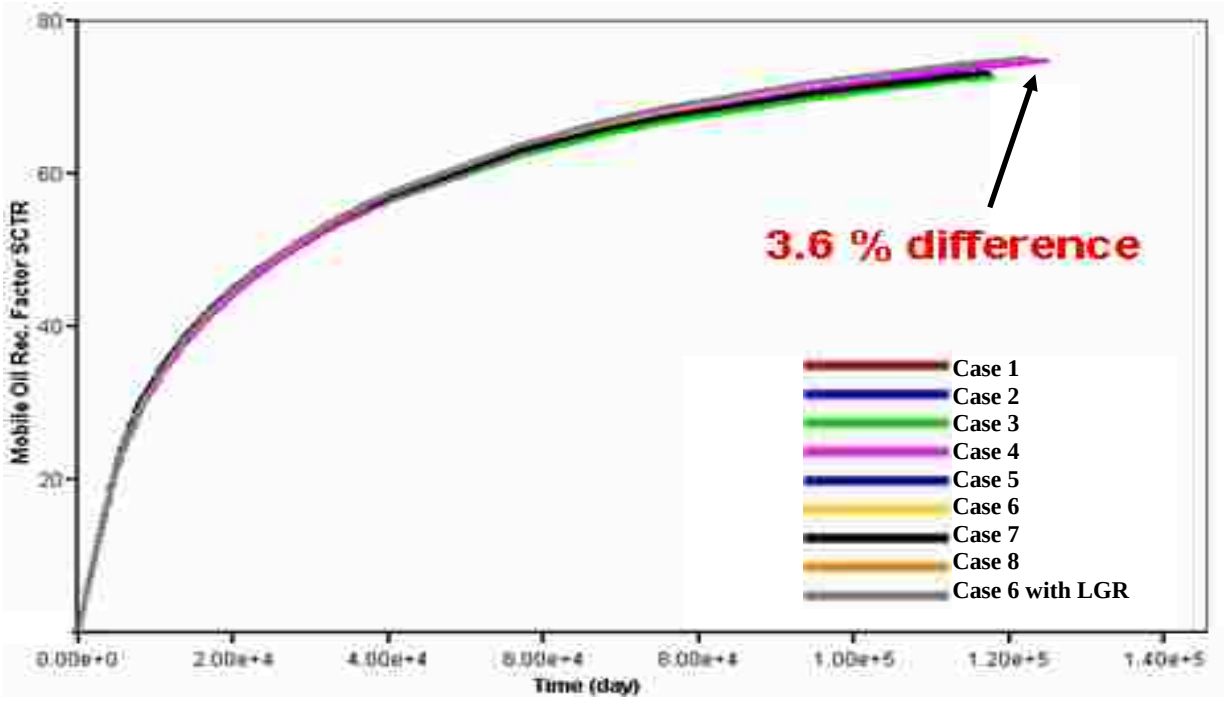

Figure 32: Grid Sensitivity Analysis (Edge-Water): Oil Recovery (%MOV) vs. Time

The relative contribution of the number of grid blocks in "X", "Y" and "Z" to each one of the responses was analyzed using the statistical package SAS (2003) and analysis of variance, ANOVA. Example results for three of the responses are shown in Figure 33. The results are summarized as follows:

- Increasing the number of grid blocks significantly increases the CPU time. However, no direction has a predominant effect.

- The larger the number of grid blocks in the "Z" direction is, the shorter the breakthrough time becomes. This may be because the thickness of the deepest layer of the model is smaller and, therefore, a thinner and longer water tongue forms along such layer. It was also observed that the water breakthrough time increases with increasing number of grid blocks in the "X" direction and that this effect is slightly more important for the water breakthrough time than the effect of increasing the number of grid blocks in "Z".
- Recovery at abandonment is slightly affected by the number of grid blocks in the "Z" direction. This could also be explained by the fact that thinner tongues are obtained for the cases with larger number of "Z" direction grid blocks.
- The number of blocks in the "Y" direction does not seem to have an important effect on the water breakthrough time and recovery at abandonment. The lower level of "Y" can be used without significant loss of accuracy.

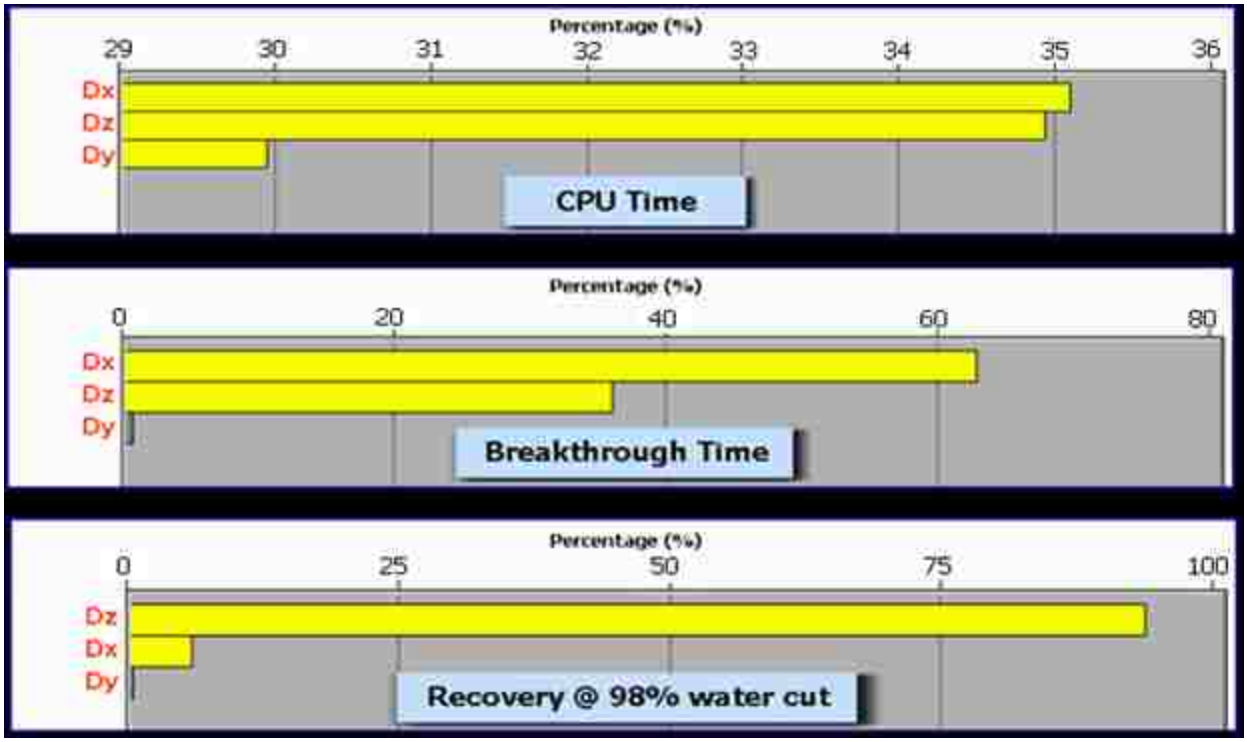

Figure 33: Grid Sensitivity Analysis: Example Pareto Plots Showing the Relative Importance of the Factors on the Responses (Edge-Water)

Case 6, which consists of 8800 grid blocks (40x11x20), was selected as the model to be used in the subsequent studies to be presented in this dissertation. This case combines the highest levels tested in "X" and "Z" with the lowest level in "Y" and, therefore, it combines accuracy with low CPU time. A schematic view of the slab model showing the proposed number of grid blocks in each direction is presented in Figure 34.

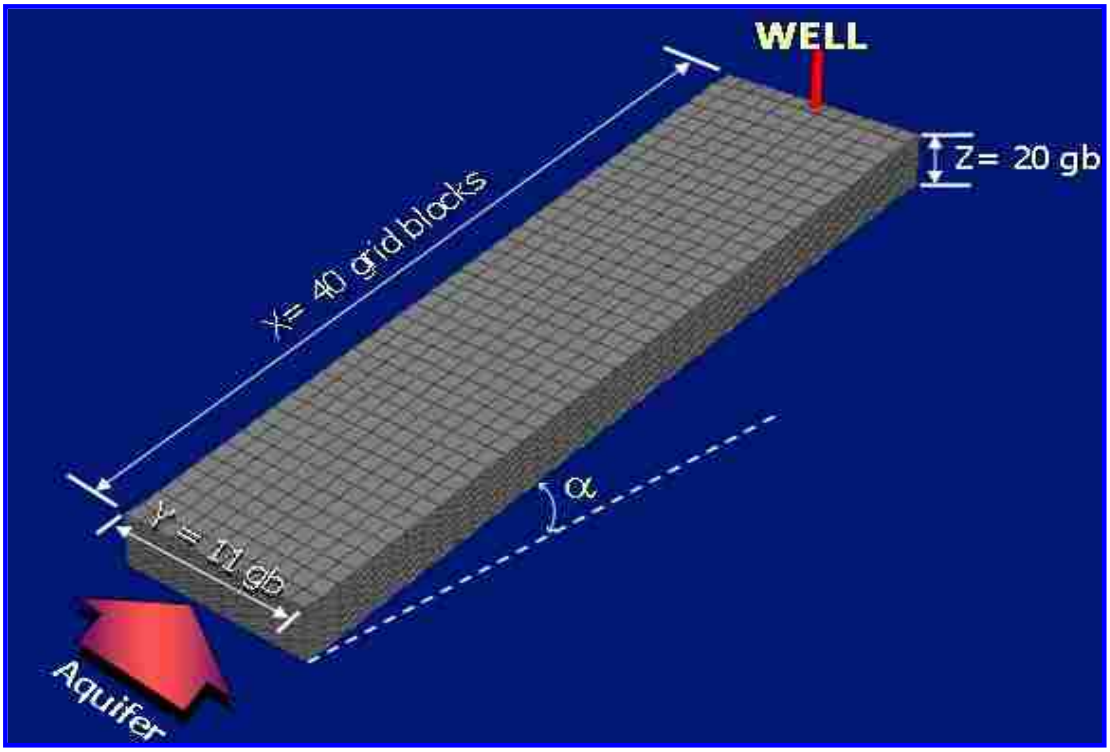

Figure 34: Schematic View of the Slab Model Showing the Proposed Number of Grid Blocks in Each Direction

3.1.4 Aquifer Modeling

Water intrusion to the reservoir was modeled analytically using a Fetkovich aquifer attached at the lower end of the slab. The Fetkovich approach is based on material balance. The flow of aquifer water into a hydrocarbon reservoir is modeled in a similar manner as the flow of oil from a reservoir into a well (IMEX Manual, 2005).

Figure 35 shows the interpretation given in this study to the geometry used in IMEX for Fetkovich aquifers in edge-water systems. The area of contact between the aquifer and the reservoir is calculated as the reservoir width, W, multiplied by the average reservoir thickness, H. The external radius of the reservoir, R_o, is calculated from the area of contact as $R_o = \sqrt{Area\ of\ contact\ /}$ [redacted]. The ratio between the external aquifer radius to the reservoir external radius (R_{aq}/R_o) is entered as input data.

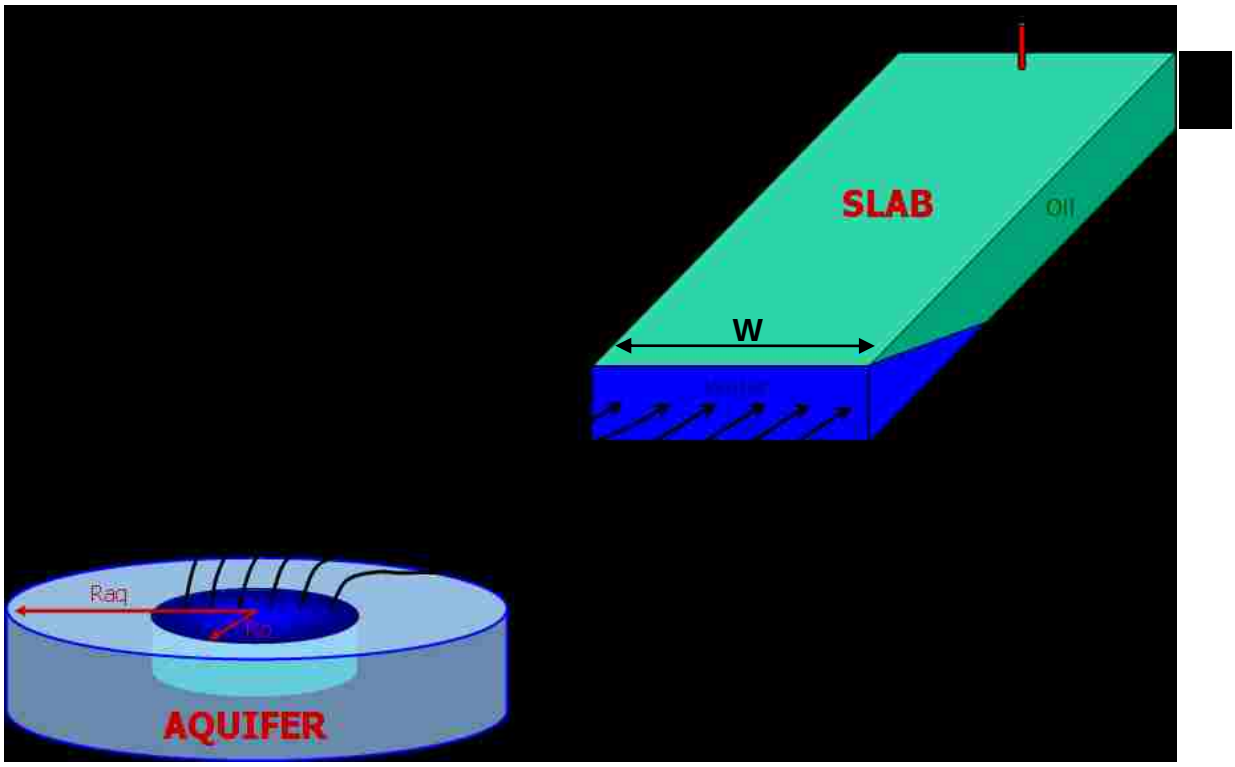

Figure 35: Interpretation of Geometry Used for Analytical Aquifer Model

The geometry shown in Figure 35 does not represent any real reservoir situation. However, it has shown to be an efficient method to model the flow of water into the slab (Hernandez, Wojtanowicz and White, 2006). Also, the selection of the type of aquifer model is not expected to have as much importance for edge-water systems as for bottom-water systems. This is because of the geometry of edge water systems – the original oil-water contact is

typically at a larger distance from the well than for bottom-water reservoirs. No attempt was made to consider the aquifer using actual grid blocks since this would significantly increase the size of the model and, therefore, CPU time and memory requirements.

3.1.5 Model Description

The numerical simulation model built to verify accuracy of the Dake's and Dietz' methods considers a reservoir slab with a linear drive pattern and has been created using the reservoir simulator "IMEX", developed by Computer Modeling Group (CMG). As indicated before (Section 3.1.3), the number of grid blocks has been determined with a grid sensitivity analysis. A regular orthogonal grid was used with 40 grid blocks in the "X" direction, 11 grid blocks in "Y" and 20 grid blocks in the "Z" direction, for a total of 8800 grid blocks. The grid blocks have a size of 50 ft in the "X" direction, 56.8 ft in the "Y" direction and 2 ft in the "Z" direction. Water intrusion was modeled using an analytical Fetkovich aquifer attached at the lower end of the slab (Section 3.1.4). A production well was partially completed (layers 1 and 2, 10% of well penetration) at the upper end of the model. This represents the real situation in which the fluids are produced through a single well and not through a "wall of wells" - equivalent to well inflow boundary conditions of the analytical models.

3.1.6 Cases Considered

Two different sets of data were employed in this validation study. The properties of the rock and the fluids used in these data sets were summarized in Table 15. The properties for data set B are the same used in the analytical calculations presented in Chapter 2 (see Table 1). The parameters related to the geometry of the reservoir are the same shown in Table 3 (Section 3.1.1). Oil viscosities ranging from 1.154 to 115.4 cp, dip angles of the reservoir of 5, 25 and 40 degrees and injection rates of 260, 300 and 3000 bls/day, were used in the validation.

Table 15: Rock and Fluid Properties

Property	Data A	Data B
B_o (rb/stb)	1.1336	1.3
B_w (rb/stb)	1.0423	1.0
μ_o (cp)	1.154, 11.54, 115.4,	0.67, 3 and 10
μ_w (cp)	0.35	0.5
γ_o	0.727	0.81
γ_w	1.013	1.04
K_{abs} (darcies)	2	2
ϕ (fraction)	0.18	0.18
S_{wc} (fraction)	0.2	0.2
S_{or} (fraction)	0.26	0.2

Tables 16 and 17 show the cases considered for analysis. The end-point mobility ratio, M, was calculated using Equation (2.12). The dimensionless gravity number, *G*, was estimated from Equation (2.13). The oil-water front stability was determined using the Dietz criterion and the expression for critical rate (Equation (2.16)). As previously indicated, the critical rate defines the maximum flow rate allowed to keep the oil-water front stable. Below the critical rate, the difference in specific gravity maintains the o/w interface of constant shape (stable displacement). Above the critical rate, equilibrium is not possible and a water tongue develops (unstable displacement).

Table 16: Matrix of Numerical Experiments for Data A

Cases	μ (cp)	M	G	q_t (b/d)	Dip Angle	Type of Displacement
1-A	11.54	4.95	4.23	300	25	Stable
2-A	1.154	0.49	4.23	300	25	Stable
3-A	1.154	0.49	0.87	300	5	Stable
4-A	1.154	0.49	0.42	3000	25	Stable
5-A	1.154	0.49	0.09	3000	5	Stable
6-A	11.54	4.95	0.87	300	5	Unstable
7-A	11.54	4.95	0.42	3000	25	Unstable
8-A	115.4	49.46	4.23	300	25	Unstable
9-A	11.54	4.95	0.09	3000	5	Unstable
10-A	115.4	49.46	0.87	300	5	Unstable

Table 17: Matrix of Numerical Experiments for Data B

Cases	μ (cp)	M	G	q_t (b/d)	Dip Angle	Type of Displacement
1-B	10	7.50	5.50	260.00	25	Unstable
2-B	3	2.25	0.72	3000.00	40	Unstable
3-B	10	7.50	1.13	260.00	5	Unstable
4-B	10	7.50	0.72	3000.00	40	Unstable
5-B	10	7.50	0.48	3000.00	25	Unstable
6-B	10	7.50	0.10	3000.00	5	Unstable

3.1.7 Results and Discussion

Modification of Dake's Analytical Method

As shown in Figure 27 (Section 3.1.1), Dake's model (1978) considers no original horizontal oil-water interface in the down dip portion of the system. This is because the model was designed for the prediction of water advancement under water flooding. Dietz' model; however, was created for the prediction of water advancement due to natural water drive and, therefore, it considers an original horizontal oil-water interface (also shown in Figure 27). In order to ensure consistency in the results presented in this section, Dake's model was modified to account for the original oil-water interface. This was done using simple geometrical considerations.

Calculations at Water Breakthrough Time

Figure 36 shows relative errors in the water breakthrough times obtained using Dake's model and numerical simulation for the "stable" displacement cases shown in Table 16. The percentage of relative error is defined in this dissertation as,

$$\text{Relative Error (\%)} = \left| \frac{\text{result of analytical model} - \text{result of simulation}}{\text{result of simulation}} \right| * 100 \quad \text{.....(3.1)}$$

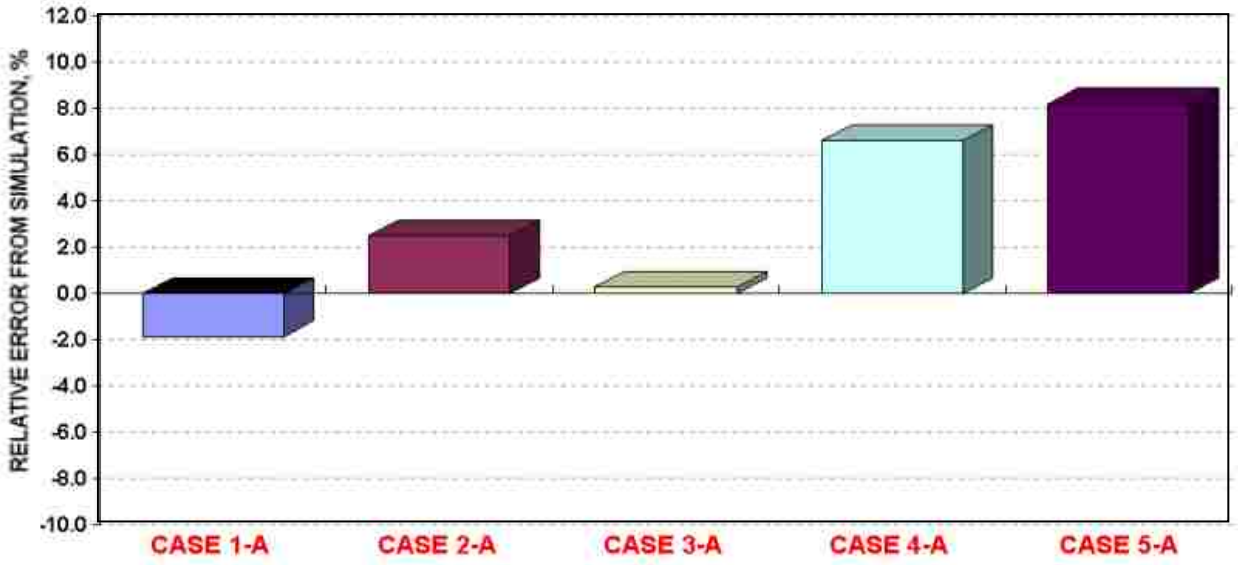

Figure 36: Comparison of Analytical (Dake) and Simulation Results: Water Breakthrough Time for Stable Displacement

Relative errors in the by-passed oil calculation at the water breakthrough using the Dake's model compared with numerical simulation are shown in Figure 37. Note that there are missing data from the Dietz model in Figures 36 and 37; the Dietz' model does not consider stable displacements.

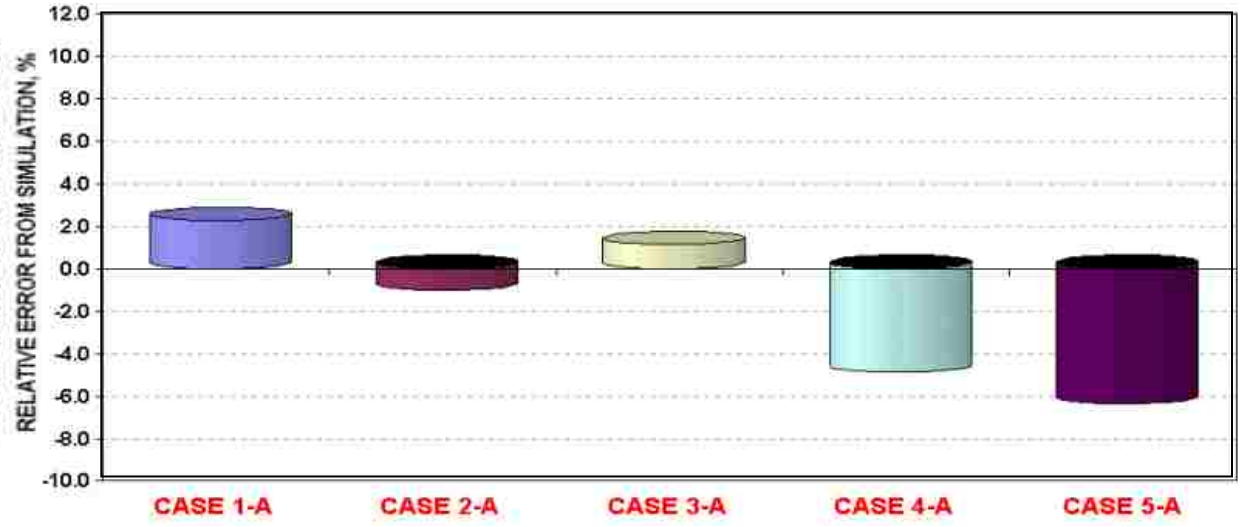

Figure 37: Comparison of Analytical (Dake) and Simulation Results- By-passed Oil at Water Breakthrough for Stable Displacement

From both Figures it is clear that the Dake's model is quite accurate in predicting both the breakthrough times and the amount of by-passed oil for the stable displacement cases. The average absolute deviation (%AAD) from the simulation was only 3.9% for the breakthrough time and 3.1% for the amount of by-passed oil at the water breakthrough.

Figure 38 shows relative errors in the water breakthrough time calculation using the Dietz' and Dake's models compared with numerical simulation for "unstable" displacements. The average absolute deviation (%AAD) from the simulation results was 45.75% for Dietz's model and 44.95% for Dake's model. Figure 39 shows the comparison between the volumes of by-passed oil at breakthrough obtained with the analytical models and the ones obtained using numerical simulation. For by-passed oil, the average absolute deviation (%AAD) from the simulation results was 9.16% for the Dietz's model and 8.82% for the Dake's model.

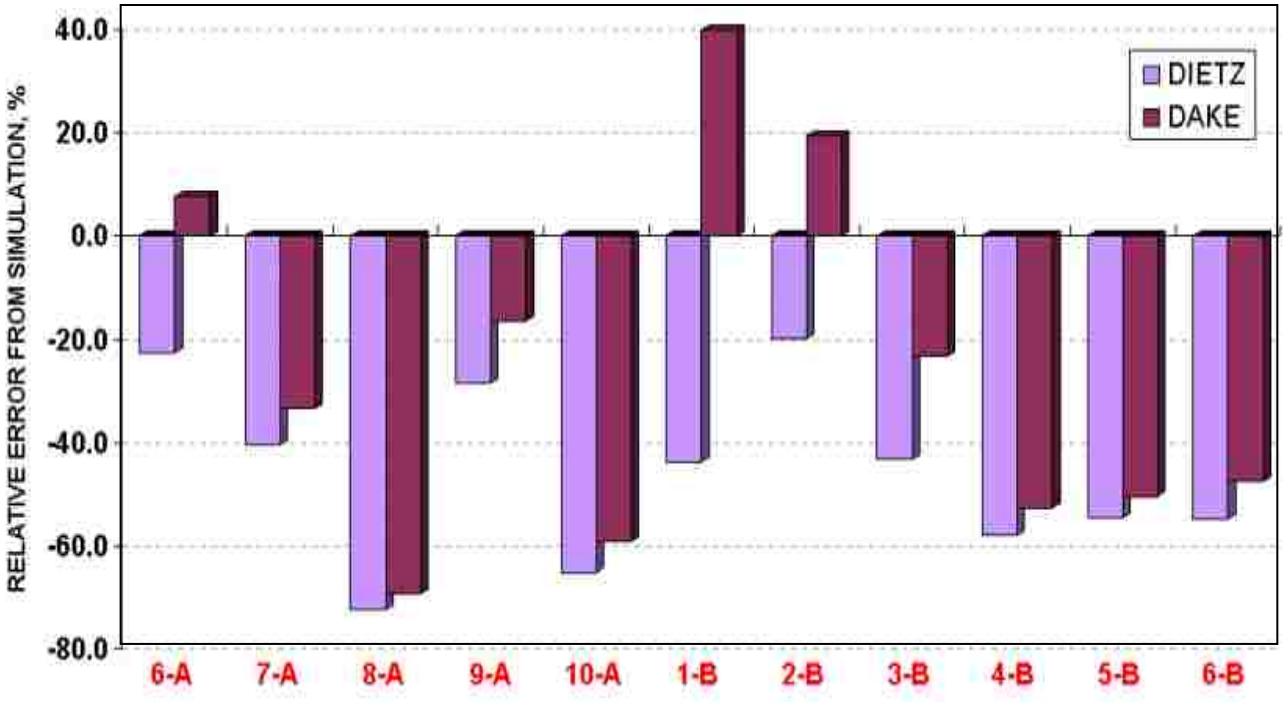

Figure 38: Comparison of Analytical (Dake) and Simulation Results:
Water Breakthrough Time for Unstable Displacement

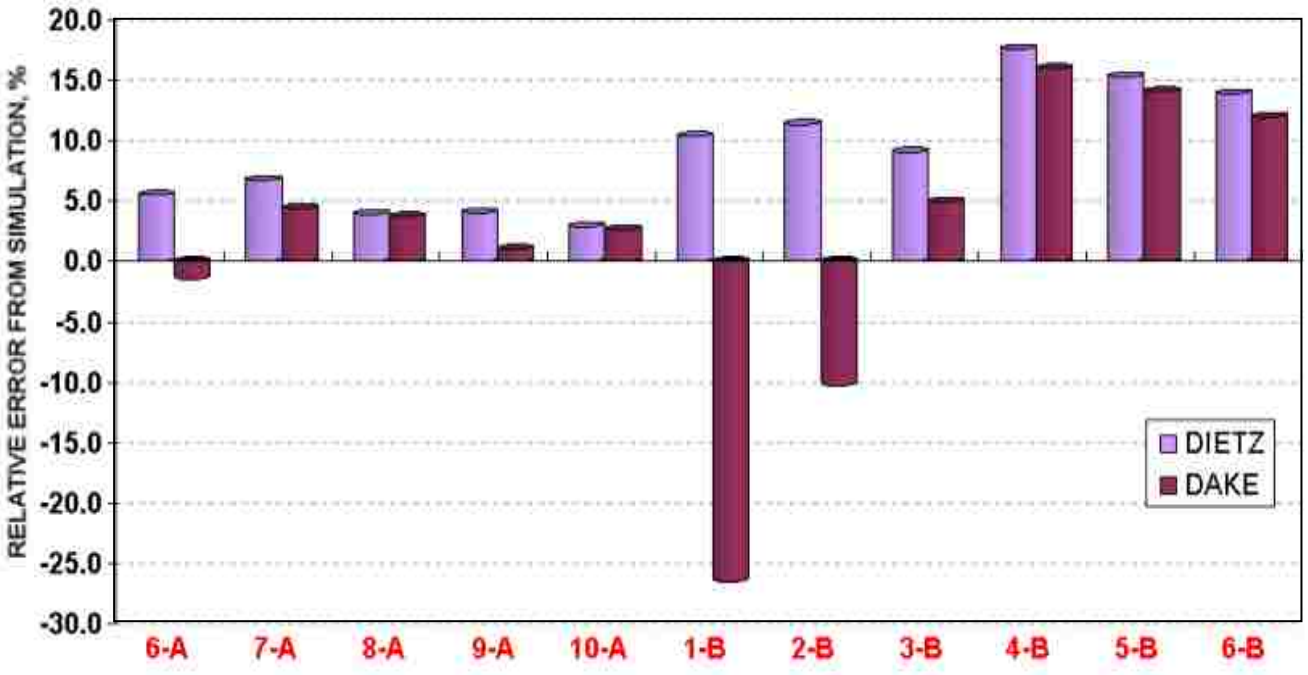

Figure 39: Comparison of Analytical (Dake) and Simulation Results:
By-passed Oil at Water Breakthrough for Unstable Displacement

When compared to numerical simulations, the analytical models have faster water breakthrough (under-estimated the water breakthrough time) and they over-estimated the volume of by-passed oil at breakthrough in most of the unstable displacement cases. This may be explained by the fact that the analytical models consider a sharp water-oil interface (they assume segregated flow), whereas some "diffusion" or dispersion of the water saturation fronts was observed in the simulations. According to Shaw and Dozzo (1990) no finite-difference method that relies on a fixed grid can claim to accurately model any sharp saturation front without degrading it into a smooth, uniform distribution. This is because the thickness of the interface is generally thin compared with the dimensions of the grid-blocks used in finite-differences schemes. The process of distributing or spreading saturation profiles is known as numerical dispersion (or diffusion), and it can render the simulation meaningless (Fleming and Mansoori, 1986).

Numerical dispersion may mask the real simulation results, which makes the comparison with the analytical results extremely difficult and misleading. Interestingly, there was virtually no dispersion in the stable displacement cases where, as indicated previously, the agreement between Dake's results and the simulation results was excellent. Additional sensitivities to the grid size were carried out to further understand the effect of diffusion on the simulations. Only the number of grid blocks in the "X" and "Z" directions was changed. The number of gridblocks in the "Y" direction was not changed since, as shown before, it does not have any significant effect on the simulation results. The results are summarized in the following paragraphs:

- It was found that dispersion/diffusion effects play an important role in the estimation of the water breakthrough time and on the characteristics of the waterfront in immiscible displacements of oil by water. Depending on number of grid blocks used in the X and Z directions, these effects may cause overestimations of the water breakthrough times of more than 37% or underestimations of more than 26%.
- A simulator-born numerical dispersion/diffusion generates smearing of the oil-water front (this smearing is not observed in the analytical models, where sharp saturation fronts are inherent). The smeared saturation fronts can significantly alter the calculated values of breakthrough times. Figure 40 demonstrates the smearing of saturation fronts. It also reveals that the diffusion/dispersion effects are more significant in the coarser grids.
- Figure 41 shows that numerical dispersion is larger for unstable displacements than for stable displacements (Cases 1-A to 5-A). In fact, for the stable displacement cases there was virtually no smearing of the saturation fronts. This is explained by the fact that some of the conditions needed for stable displacement, such as low production rates and low fluid viscosities, are the same conditions that promote vertical equilibrium and segregated

flow; whereas the conditions needed for unstable displacement are the same that promote diffuse flow. Moreover, Lantz (1970), showed that for immiscible displacements numerical dispersion increases for higher values of the derivative of the fractional flow curve, proportional to the end-point mobility ratio (high value of M is symptomatic for unstable displacement). This indicates that there are two types of dispersion implicit in the simulation results: numerical dispersion, caused by the need of using grid blocks and true physical dispersion, caused by fractional flow effects. Despite the fact that this last type is real (it may occur in real-life reservoirs), is not considered by the existing analytical models for oil bypassing in edge-water systems.

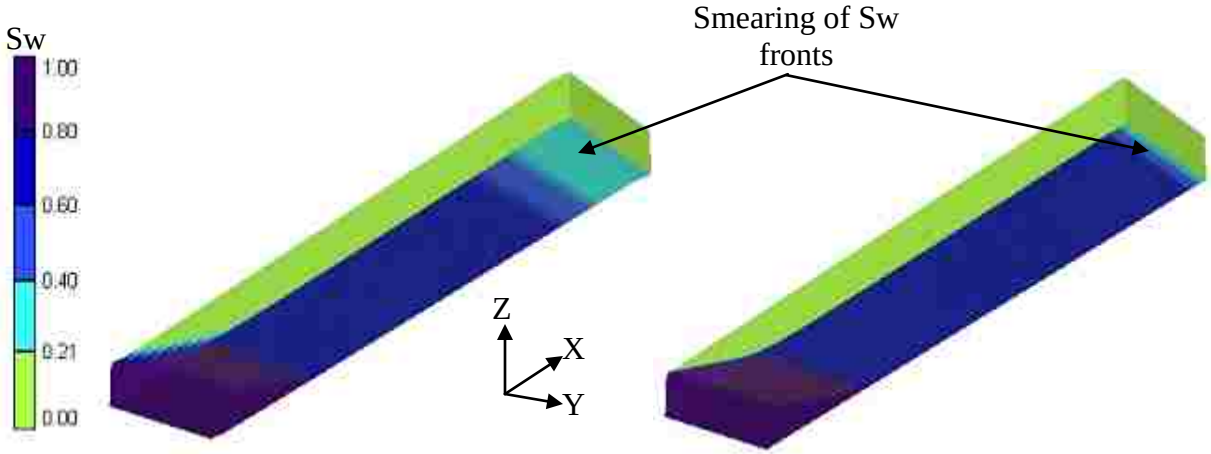

a) 30x1x400 model (coarse) b) 110x1x400 model (refined)

Figure 40: Smearing of Water Saturation Fronts for Case 10-A (Unstable Displacement).

- Water breakthrough times calculated using the Dietz' model were much closer to the ones obtained using numerical simulation when the effects of numerical dispersion/diffusion were minimized in the simulation model (by using the refined model). The agreement between the breakthrough times calculated using the Dake's model and the ones obtained using the simulation; however, was about the same.

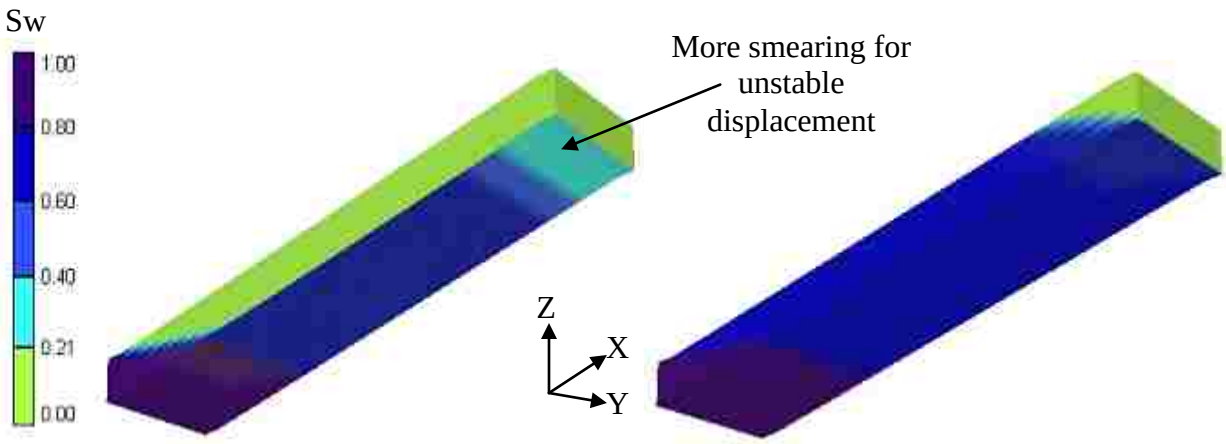

a) Case 10-A (unstable displacement) b) Case 3-A (stable displacement)

Figure 41: Smearing of Saturation Fronts for Stable and Unstable Displacements

- Because of the numerical dispersion/diffusion effects, large numbers of grid blocks are needed to accurately model unstable displacements than that for stable displacements. Unfortunately, resolving the sharp fronts merely by resorting to very fine meshes is impractical (Fleming and Mansoori, 1986). This is because very large models may be required, and they may take lot of CPU time to run. In fact, the runs presented in this dispersion study were finished at the water breakthrough time (it was impractical to run them for more time). As indicated in Section 3.1.3, a model consisting of 8800 grid blocks (40x11x20), was selected as the model to be used in this dissertation. This model combines low CPU time with accuracy, especially in the calculation of the amount of by-passed oil at abandonment - the main response analyzed in this study (as indicated in Section 3.1.3, oil bypassing or recovery at abandonment is slightly affected by the number of gridblocks used).

Calculations after Water Breakthrough Time

In this section, both water cut and oil by-passing plots obtained using the analytical

models are compared with the ones obtained using numerical simulation for some specific cases. Figure 42 shows the water cut and by-passed oil plots obtained for Case 3-A, which is a stable displacement case. As it was indicated before, Dietz' model does not apply to stable displacement and, therefore, it was not included in the figure. It is clear that the agreement between Dake's model and the simulation results is excellent. Excellent agreements between the analytical models and the simulation results were also obtained for all the other stable displacement cases.

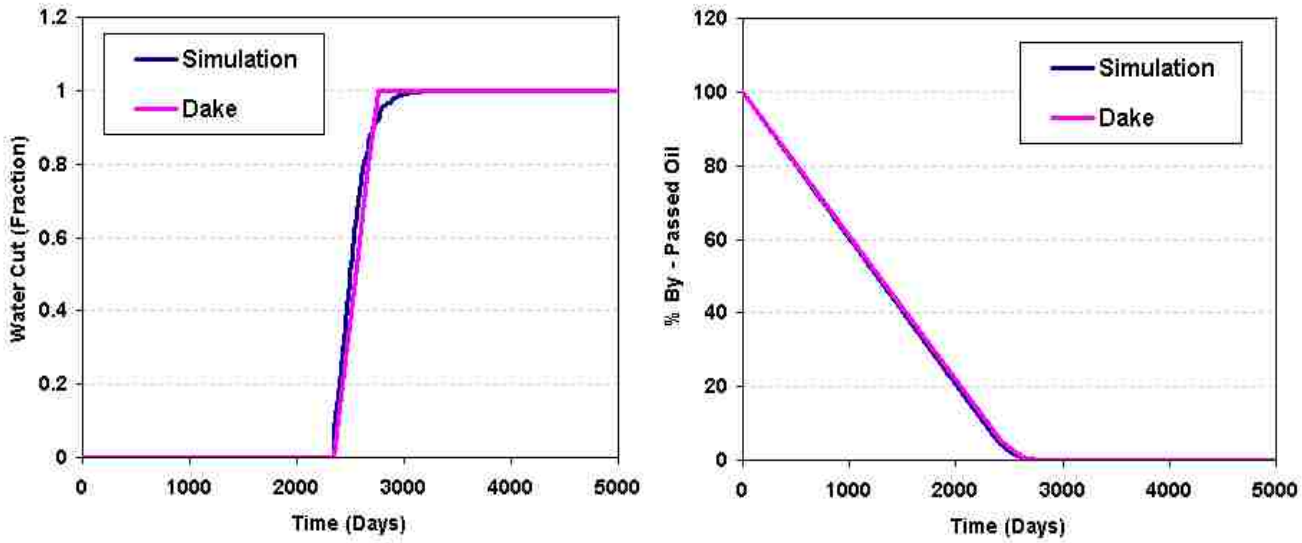

Figure 42: Comparison of Analytical and Simulation Results:
Water Cut and % of By-Passed Oil for Case 3-A (stable displacement)

Figure 43 shows the water cut and by-passed oil plots obtained for Case 9-A, the unstable displacement case for which the best agreement was obtained between the analytical and the numerical simulation results. Because of the numerical diffusion/dispersion effects, it is difficult to establish relationships among the different variables controlling the unstable displacement of oil by water. However, it was found that Dake's model is extremely sensitive to the gravity forces, G, and it gives inadequate results at small values of the M/G ratios. For example, Figure

44 shows the water cut and by-passed oil plots obtained for Case 1-A, the unstable displacement case with the lowest ratio of viscous to gravity forces, M/G, and the worst agreement between the Dake's and the numerical simulation results. Note also that the agreement between the Dietz' and the numerical simulation result is quite reasonable.

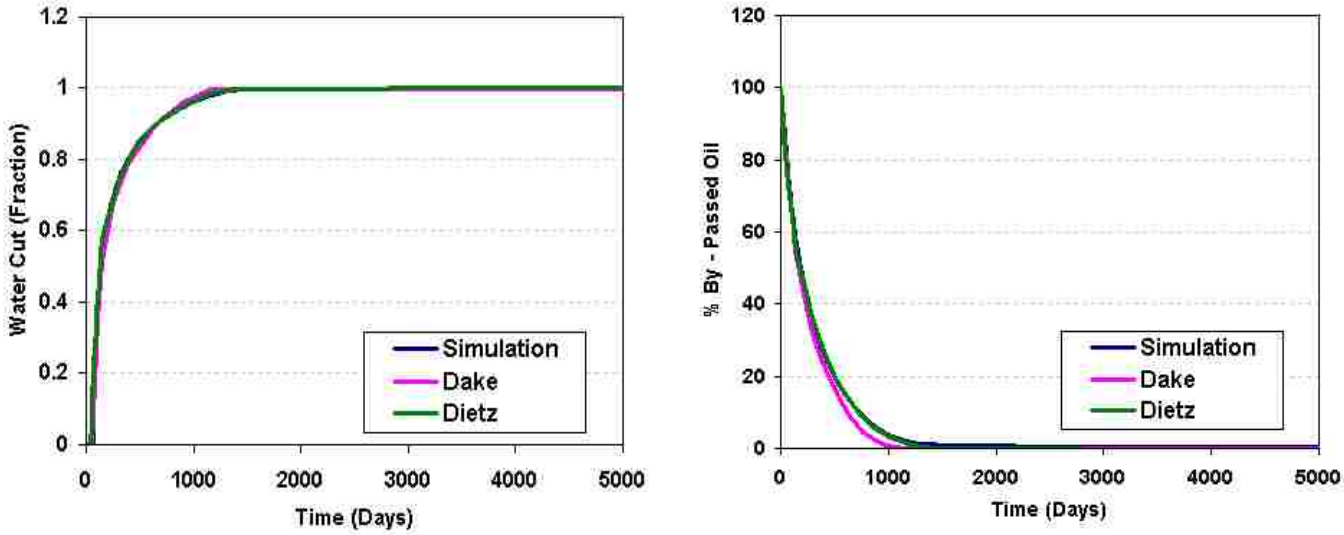

Figure 43: Comparison of Analytical and Simulation Results:
Water Cut and % of By-Passed Oil for Case 9-A (unstable displacement, best agreement)

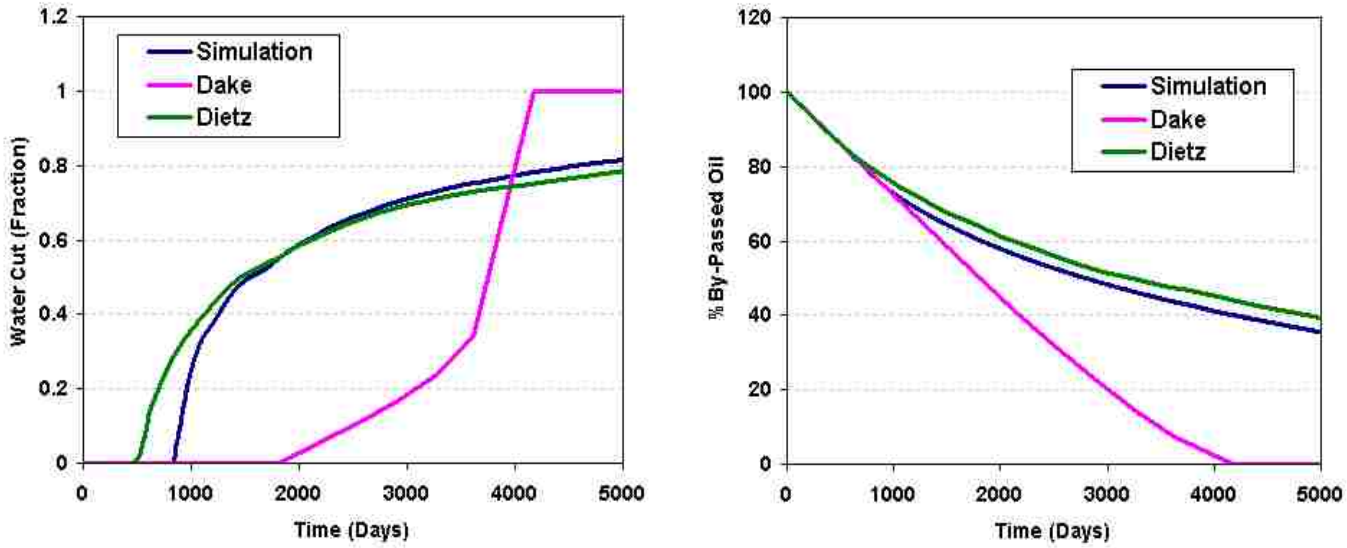

Figure 44: Comparison of Analytical and Simulation Results:
Water Cut and % of By-Passed Oil for Case 1-B (unstable displacement, worst agreement)

Summary: Insufficiencies of Analytical Models

Summarizing, the results presented in this section show that, for stable displacement, there is excellent agreement between the analytical (Dake's model) and the simulation results. For unstable displacement, most of the cases showed a very poor agreement between the breakthrough times obtained analytically and the simulation results. For example, both Dietz and Dake's models gave breakthrough times with an average absolute deviation (%AAD) of more than 44% from the times obtained using the simulator. It was also found; however, that the Dietz' model gives quite acceptable results for water cut and by-passed oil profiles when compared with numerical simulation.

A possible cause of the disparities between the analytical and the simulation results stems from the simplifying assumptions used in the analytical models. The assumptions may not represent the real physics of water displacement in dipping structures. For example, one of the assumptions used by Dake and Dietz is that the injection rate (or the rate of water influx into the reservoir) is equal to the production rate, i.e., steady-state displacement. When numerical simulation models are used; however, a steady-state condition is difficult to achieve in the presence of an aquifer.

In addition, the two analytical methods studied in this paper are two-dimensional in space, i.e., they assume that whatever arrives at the well is considered to be produced as if there is a wall of wells. This is equivalent to have a 2D water tongue, when in reality the immiscible displacement of oil by water in dipping system is a 3D process that involves the development of a water tongue, salient and coning (Arslan, 2005). Because of this assumption, the analytical methods are unable to predict the effect of well position and penetration on the displacement process. Also, no analytical model has been found in the literature to describe combined effects

of gravity underruning followed by water coning.

Finally, the numerical simulation models consider many rock and fluid properties that are not taken into account by the analytical methods, such as solution gas-oil ratio, rock, oil and water compressibilities, capillary pressures and relative permeability curvatures (analytical methods only consider the relative permeability end points).

3.2. Validation of Analytical Models for Bottom-Water Reservoirs

3.2.1. Analytical Calculations

In this section, the method proposed by Kuo and DesBrisay (1983) is used to calculate the development of unrecovered (by-passed) oil reserves over time. The procedure applies to oil reservoirs with bottom-water and water coning causing well's shut-in. A program was written in EXCEL to include the equations defining the method as shown in Section 2.2.2. The program was tested against the results published by Kuo and DesBrisay (1983). The results are shown in Figure 45. An excellent match of the published results was obtained with the program when Equation (2.40) was used for the calculation of the water breakthrough time. The match obtained when Equation (2.41) was employed, however, was not as adequate.

Input Data and Description of Cases

The properties of the rock and the fluids used in the calculations were shown in Table 15 (Data A). Other parameters used in the calculations are shown in Table 18. The cases considered are shown in Table 19. As can be noted, calculations include favorable and unfavorable mobility ratios, M. Table 19 also includes water breakthrough times (Equation (2.39)) calculated using Equations (2.40) and (2.41), which correspond to the Bournazel-Jeanson (1971) and the Sobocinski-Cornelius (1975) methods to estimate the dimensionless breakthrough time, respectively. As can be seen, both methods could give negative breakthrough times, which is

obviously unrealistic. A more detailed analysis on these methods showed that the problem is caused by the fact that Equations (2.40) and (2.41) present discontinuities for values of the dimensionless cone height, z (Equation 2.42), of 4.2857 and 3.5, respectively. This is shown in Figure 46. Therefore, breakthrough times calculated in the vicinity (or above, in the case of Equation (2.40)) of these values would be erroneous. The Bournazel-Jeanson (1971) method was used for the oil bypassing predictions for all the cases studied in this section except for Case 1, where the method gave negative results and, therefore, the Sobocinski-Cornelius (1975) method was used.

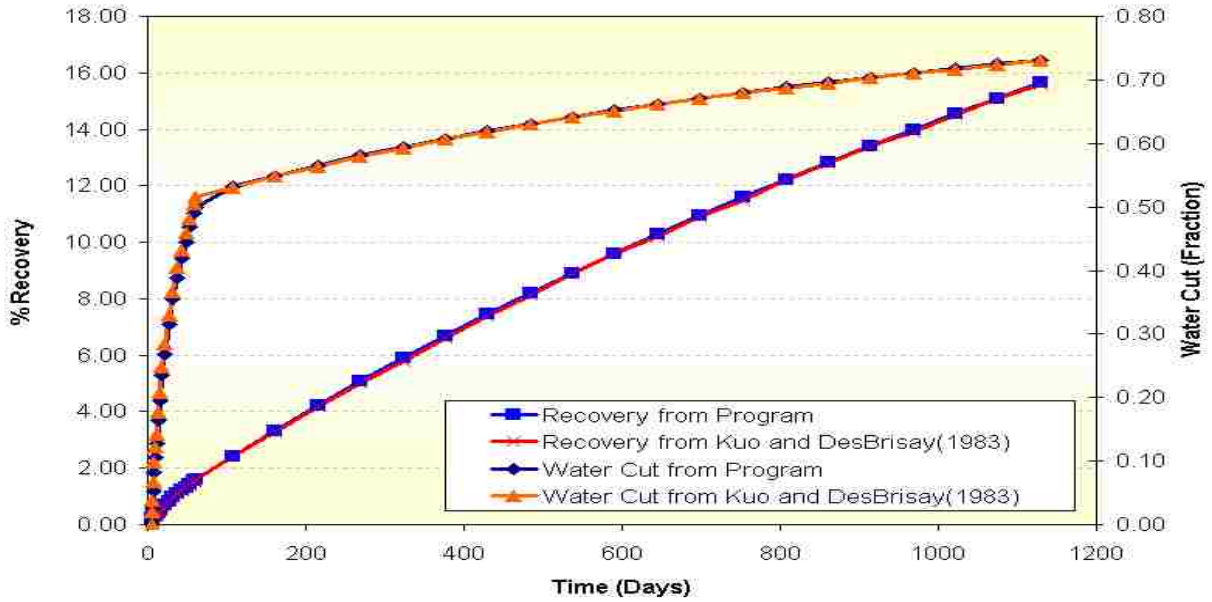

Figure 45: Comparison of Results Reported by Kuo and DesBrisay (1983) with Results of the Program

Table 18: Properties Used in Analytical Calculations for Bottom-Water Systems

Property	Value
Water Thickness, H_w (ft)	20
Oil Thickness, H_o (ft)	100
Well Penetration, H_p (ft)	20
Well Radius, r_w (ft)	0.35
Reservoir Radius, r_e (ft)	1000

Table 19: Description of Cases Used in Analytical Calculations for Bottom-Water Systems

Case	μ_o (cp)	M	q (b/d)	t_{BT} (eq.2.40) (days)	t_{BT} (eq.2.41) (days)
1	1.154	0.495	300.0	-25.3	7713.7
2	1.154	0.495	3000.0	112.7	-228.8
3	11.54	4.95	300.0	531.9	-1079.7
4	11.54	4.95	3000.0	9.6	19.0
5	115.4	49.50	300.0	30.3	60.1
6	115.4	49.50	3000.0	2.8	4.9

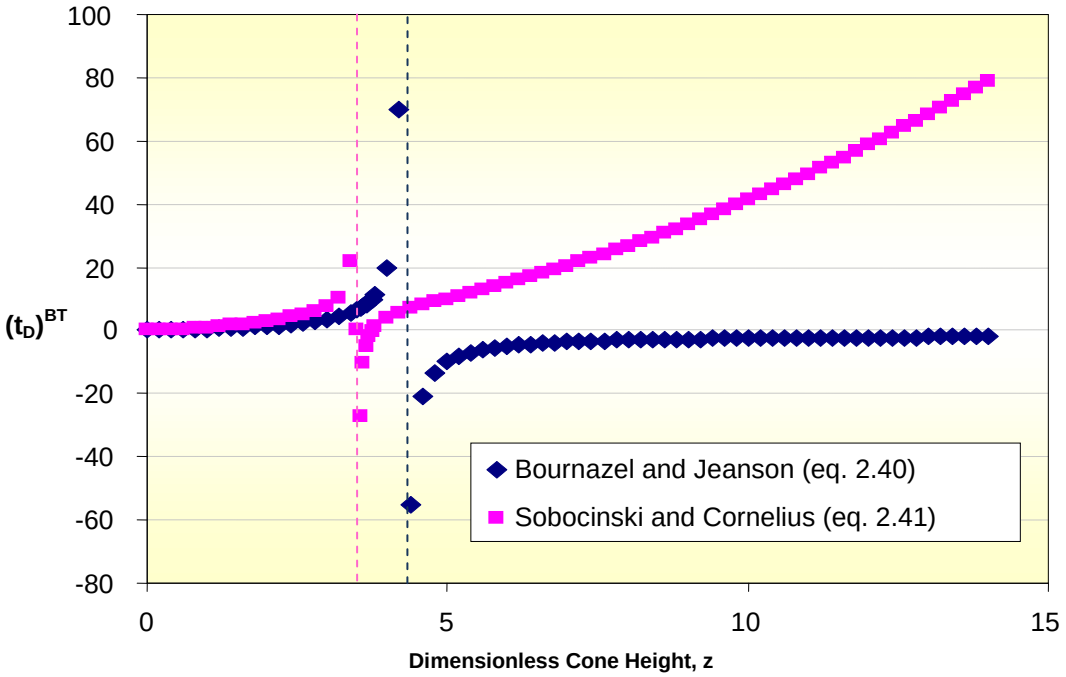

Figure 46: Problems with Equations (2.40) and (2.41) for Certain Values of the Dimensionless Cone Height, z (Equation 2.42)

Results of Analytical Calculations

Tables 20 and 21 show water cut and oil bypassing versus dimensionless time (defined as t/t_{BT}, Equation (2.37)); respectively, calculated using the Kuo and DesBrisay method for Cases 1 to 6. The concept of dimensionless time was used to make the comparison between the cases easier and more consistent (breakthrough in all cases occurs at a t_D =1). All calculations were

finished at a water cut of 0.98 (98%), which is the economic water cut limit considered in this study.

Table 20: Water Cut Calculated Using the Kuo and DesBrisay Method (1983)

Case 1 μ_o=1.154 cp q=300 b/d t_{BT} = 7713.7 days		**Case 2** μ_o=1.154 cp q=3000 b/d t_{BT} = 112.7 days		**Case 3** μ_o=11.54 cp q=300 b/d t_{BT} = 531.9 days		**Case 4** μ_o=11.54 cp q=3000 b/d t_{BT} = 9.6 days		**Case 5** μ_o=115.4 cp q=300 b/d t_{BT} = 30.3 days		**Case 6** μ_o=115.4 cp q=3000 b/d t_{BT} = 2.80 days	
t_D	Water Cut (Fraction)	t_D	Water Cut (Fraction)	t_D	Water Cut (Fraction)	t_D	Water Cut (Fraction)	t_D	Water Cut (Fraction)	t_D	Water Cut (Fraction)
0.00	0.000	0.01	0.000	0.00	0.000	0.10	0.000	0.03	0.000	0.36	0.000
0.00	0.000	0.04	0.000	0.19	0.000	**1.00**	**0.147**	**1.00**	**0.264**	**1.00**	**0.264**
0.00	0.000	0.09	0.000	0.94	0.143	1.05	0.156	1.65	0.450	1.79	0.479
0.01	0.000	0.44	0.000	**1.00**	**0.157**	2.09	0.303	3.30	0.707	3.57	0.737
0.01	0.000	0.89	0.029	1.88	0.312	4.18	0.458	16.50	0.912	17.85	0.912
0.06	0.000	**1.00**	**0.036**	4.70	0.579	6.28	0.533	33.00	0.914	35.71	0.913
0.13	0.000	1.77	0.080	9.40	0.682	8.37	0.540	164.99	0.922	178.53	0.922
0.26	0.000	2.66	0.127	14.10	0.720	10.46	0.548	247.49	0.927	357.05	0.930
0.39	0.000	3.55	0.175	18.80	0.749	26.15	0.597	329.99	0.930	714.10	0.942
0.52	0.005	4.44	0.223	28.20	0.793	52.29	0.657	494.98	0.937	1071.16	0.949
0.65	0.030	5.32	0.272	37.60	0.824	78.44	0.700	659.97	0.942	1428.21	0.955
0.97	0.104	6.21	0.310	47.00	0.847	104.59	0.734	824.96	0.946	1785.26	0.959
1.00	**0.111**	7.10	0.341	56.40	0.866	209.17	0.817	989.96	0.949	2142.31	0.963
1.30	0.194	7.99	0.372	65.81	0.881	313.76	0.862	1319.94	0.955	2499.37	0.965
1.43	0.233	8.87	0.403	75.21	0.893	418.35	0.891	1649.93	0.959	2856.42	0.968
1.56	0.274	13.31	0.552	84.61	0.904	522.93	0.911	1979.92	0.963	3213.47	0.970
1.69	0.317	17.74	0.683	94.01	0.913	627.52	0.926	2309.90	0.965	3570.52	0.972
1.81	0.361	22.18	0.787	112.81	0.927	732.11	0.938	2639.89	0.968	3927.58	0.973
1.94	0.407	26.62	0.864	131.61	0.939	836.69	0.947	2969.87	0.970	4284.63	0.975
2.27	0.522	31.05	0.916	150.41	0.948	941.28	0.954	3299.86	0.972	4641.68	0.976
2.59	0.634	35.49	0.949	188.01	0.961	1045.86	0.960	3959.83	0.975	4998.73	0.977
3.24	0.829	39.93	0.969	225.62	0.970	1255.04	0.970	4619.80	0.977	5355.78	0.978
3.89	0.961	41.70	0.975	244.42	0.974	1464.21	0.977	5279.77	0.979	5712.84	0.979
4.01	0.980	43.47	0.980	282.02	0.980	1568.80	0.980	5774.75	0.980	6069.89	0.980

Results show that both the production rate and the oil viscosity have an important effect on the water breakthrough time. For example, large rates and high viscosities give early breakthrough times. In general terms, however, multiplying the production rate by a factor of ten seems to have a larger effect on the breakthrough time than multiplying the oil viscosity by the same factor.

Table 21: Oil Bypassing Calculated Using the Kuo and DesBrisay Method (1983)

Case 1 μ_o=1.154 cp q=300 b/d t_{BT} = 7713.7 days		**Case 2** μ_o=1.154 cp q=3000 b/d t_{BT} = 112.7 days		**Case 3** μ_o=11.54 cp q=300 b/d t_{BT} = 531.9 days		**Case 4** μ_o=11.54 cp q=3000 b/d t_{BT} = 9.6 days		**Case 5** μ_o=115.4 cp q=300 b/d t_{BT} = 30.3 days		**Case 6** μ_o=115.4 cp q=3000 b/d t_{BT} = 2.80 days	
t_D	BPO (%MOV)	t_D	BPO (%MOV)	t_D	BPO (%MOV)	t_D	BPO (%MOV)	t_D	BPO (%MOV)	t_D	BPO (%MOV)
0.00	99.99	0.01	99.94	0.00	99.99	0.10	99.94	0.03	99.99	0.36	99.94
0.00	99.97	0.04	99.69	0.19	99.37	**1.00**	**99.44**	**1.00**	**99.83**	**1.00**	**99.84**
0.00	99.94	0.09	99.37	0.94	97.05	1.05	99.42	1.65	99.76	1.79	99.75
0.01	99.69	0.44	96.87	**1.00**	**96.88**	2.09	98.94	3.30	99.61	3.57	99.61
0.01	99.37	0.89	93.79	1.88	94.64	4.18	98.16	16.50	99.13	17.85	99.18
0.06	96.87	**1.00**	**93.02**	4.70	89.44	6.28	97.53	33.00	98.86	35.71	98.90
0.13	93.75	1.77	87.88	9.40	83.67	8.37	96.95	164.99	96.81	178.53	96.84
0.26	87.49	2.66	82.28	14.10	78.99	10.46	96.38	247.49	95.63	357.05	94.53
0.39	81.24	3.55	76.97	18.80	74.84	26.15	92.37	329.99	94.51	714.10	90.52
0.52	75.00	4.44	71.96	28.20	67.68	52.29	86.53	494.98	92.42	1071.16	87.11
0.65	68.86	5.32	67.25	37.60	61.68	78.44	81.50	659.97	90.52	1428.21	84.10
0.97	54.28	6.21	62.82	47.00	56.54	104.59	77.08	824.96	88.75	1785.26	81.41
1.00	**53.09**	7.10	58.61	56.40	52.06	209.17	63.03	989.96	87.11	2142.31	78.96
1.30	40.97	7.99	54.58	65.81	48.10	313.76	53.00	1319.94	84.11	2499.37	76.71
1.43	36.05	8.87	50.75	75.21	44.57	418.35	45.28	1649.93	81.41	2856.42	74.62
1.56	31.38	13.31	34.41	84.61	41.39	522.93	39.08	1979.92	78.96	3213.47	72.67
1.69	26.98	17.74	22.44	94.01	38.52	627.52	33.99	2309.90	76.71	3570.52	70.85
1.81	22.84	22.18	14.15	112.81	33.52	732.11	29.72	2639.89	74.62	3927.58	69.12
1.94	18.99	26.62	8.69	131.61	29.33	836.69	26.11	2969.87	72.67	4284.63	67.50
2.27	10.62	31.05	5.24	150.41	25.77	941.28	23.01	3299.86	70.85	4641.68	65.95
2.59	4.03	35.49	3.12	188.01	20.06	1045.86	20.34	3959.83	67.49	4998.73	64.48
3.24	-4.37	39.93	1.84	225.62	15.76	1255.04	15.98	4619.80	64.47	5355.78	63.08
3.89	-7.65	41.70	1.49	244.42	14.02	1464.21	12.64	5279.77	61.73	5712.84	61.74
4.01	-7.92	43.47	1.21	282.02	11.09	1568.80	11.23	5774.75	59.76	6069.89	60.45

For the cases with the lowest oil viscosity, there is a favorable endpoint mobility ratio (M<1) and, therefore, the amount of BPO at both breakthrough and abandonment is much smaller than for the cases with the highest oil viscosity. For example, it can be seen that oil bypassing at abandonment for the cases with the highest viscosity is about 60% of the movable oil volume – a significant amount. Thus, the formation of a water cone could lead to substantial water inflow and large amounts of by-passed oil to be abandoned in the reservoir for economical reasons. Results also suggest that the effect of changing the oil viscosity (or end-point mobility ratio) is much more significant to oil bypassing at abandonment than the effect of changing the

production rate. In other words, viscous forces appear to have a more pronounced effect than gravity forces.

It can also be seen that the development of water cut with time is much slower in the cases with high viscosities and production rates, which are the cases with the largest amount of by-passed oil. These cases show very premature water breakthrough (and beginning of water production) and the formation of a very thin and poorly defined water cone in the early years. Production is plagued with significant water cut for most of the life of the well. For example, Case 6 reached 48% water cut in just 5 days (t_D = 1.79). After this time, production continued at very high water cut until the economic water cut was reached at approximately 17,000 days ((t_D = 6069.89). Obviously, it would be very beneficial to accelerate oil production in reservoir/well systems with similar characteristics.

The next sections present the results of a simulation study completed with the objective of further validating the Kuo and DesBrisay method. As was done for edge-water systems, the study includes: first, the selection of the best geometry to be used in the simulator. Second, a grid sensitivity analysis designed to improve run times without compromising accuracy. Third, a brief description of the aquifer modeling method employed in the simulations. Fourth, a description of the simulation model used and the cases considered. Finally, a discussion of the results and summary of important findings.

3.2.2 Selection of Grid Geometry

A 2D (R, Z) radial-cylindrical geometry was used to represent an idealized one-well element of a bottom water-drive reservoir. Radial geometry is the most commonly used approach in studies of the behavior of wells in bottom water-drive systems (Mattax and Dalton, 1990). This is obviously because it is the best approximation to the true geometry of these systems.

Water intrusion to the reservoir has been modeled by attaching an aquifer underneath the oil zone. As it will be discussed later, two different aquifer modeling methods have been tested: an analytic approach and a numerical approach.

3.2.3 Grid Sensitivity Analysis

The number of grid blocks in the simulation model has been determined with a grid sensitivity analysis. Table 22 shows the cases considered. All cases were run with an end point mobility ratio of 1.8 and a percentage of well penetration of 10%. Three levels for the number of grid blocks were considered in each direction. Also shown in the table are the results for four different responses: CPU time, water breakthrough time, oil recovery at water breakthrough (expressed as % of Movable Oil Volume, MOV) and oil recovery at abandonment (%MOV). As indicated before, abandonment is being defined in this study as 98% water cut. It is clear that CPU time is significantly affected by the changes in the number of grid blocks in each direction. The effect of the number of grid blocks on the other responses, however, does not seem to be important. This can be confirmed by observing Figure 47, a plot of oil recovery in time for all nine cases.

The relative contribution of the number of grid blocks in the "Z" and "R" directions to each one of the responses was analyzed using the statistical package SAS (2003) and analysis of variance, ANOVA. Example results for three of the responses are shown in Figure 48. It can be seen that the number of grid blocks in the radial direction is slightly more important for the CPU time than the number of grid blocks in the vertical direction. For the water breakthrough time and recovery at abandonment, however, it can be seen that the effect of the number of grid blocks in the vertical direction is of substantially larger importance. Case 5, which consists of 3060 grid blocks, was selected as the model to be used in the subsequent simulations for bottom-

water reservoirs in this dissertation. This case combines accuracy with low CPU time. It is important to remember, however, that the results presented here suggest that the choice of the number of grid blocks used does not seem to have a substantial impact on the results at abandonment.

Table 22: Grid Sensitivity Analysis for Bottom-Water Systems

Case #	DR	DZ	Total	CPU time (days)	BT Time (days)	%Recovery at BT	%Recovery abandonment
1	26	30	780	32.91	4.00	0.23	89.56
2	26	60	1560	79.80	4.12	0.24	89.83
3	26	120	3120	220.80	4.21	0.24	89.96
4	51	30	1530	85.08	4.00	0.23	89.40
5	51	60	3060	218.55	4.09	0.23	89.74
6	51	120	6120	679.22	4.19	0.24	89.84
7	101	30	3030	252.62	4.01	0.23	89.34
8	101	60	6060	776.69	4.09	0.22	89.69
9	101	120	12120	2826.06	4.17	0.24	89.81
Maximum Difference (%)				8487.24	5.21	7.48	0.69

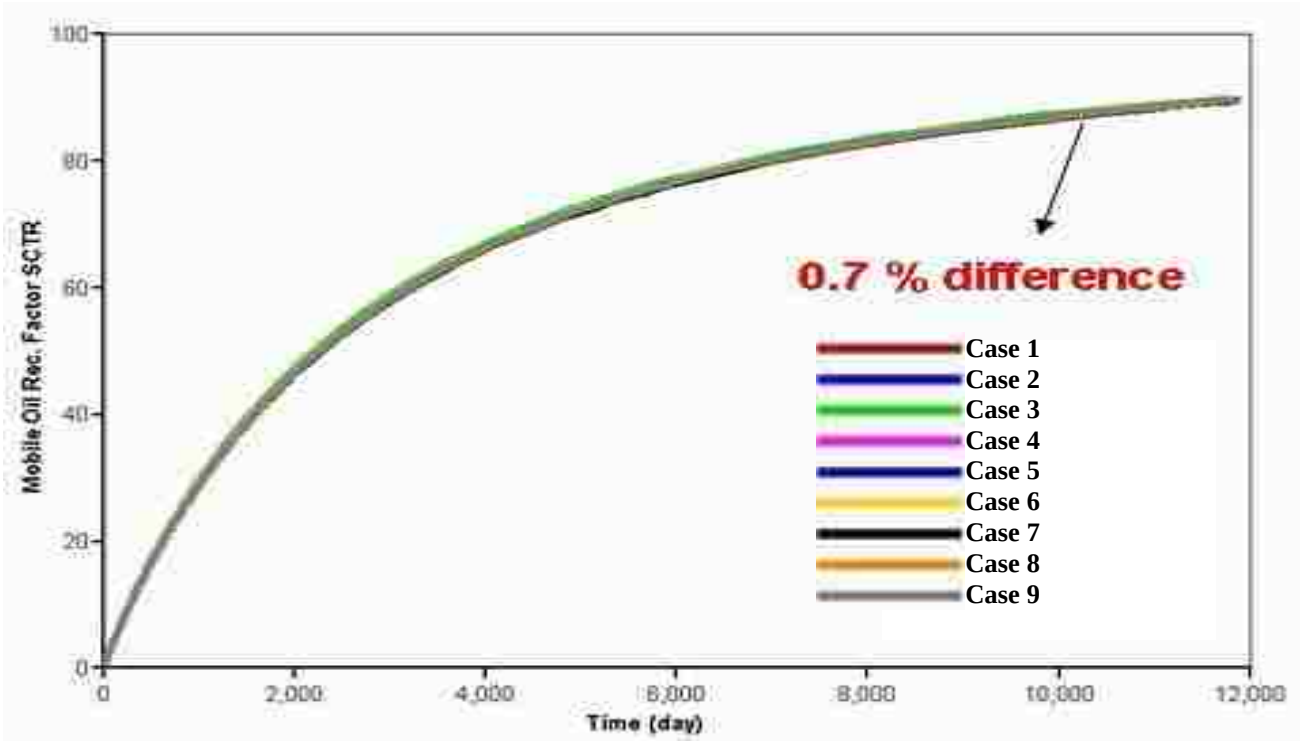

Figure 47: Grid Sensitivity Analysis (Bottom-Water): Oil Recovery (%MOV) vs. Time.

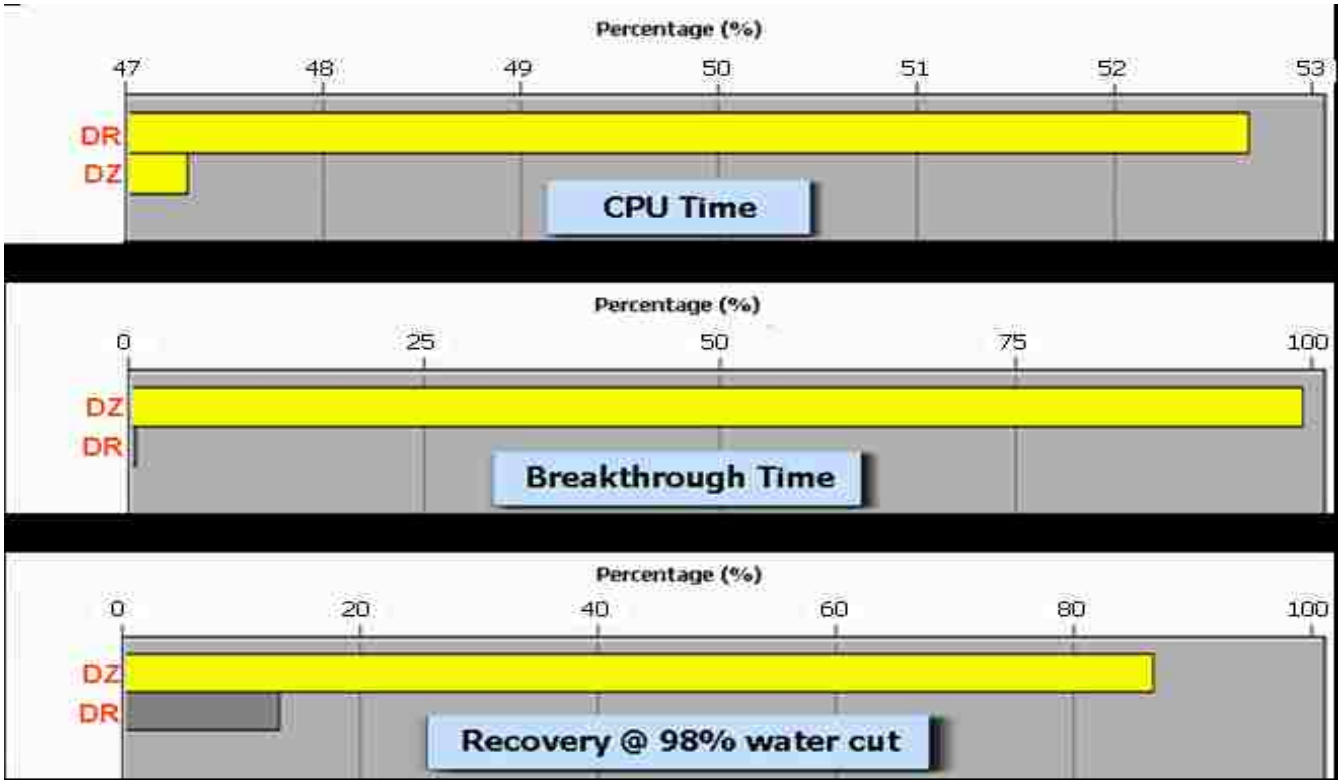

Figure 48: Grid Sensitivity Analysis: Example Pareto Plots Showing the Relative Importance of the Factors on the Responses (Bottom-Water)

3.2.4. Aquifer Modeling

Two different aquifer modeling methods have been tested in this study. First, water intrusion was modeled analytically using a Fetkovich aquifer attached to the bottom blocks of the radial model. Analytical methods have the advantage of reducing the computer resources needed. The Fetkovich approach is based on material balance and the flow of aquifer water into a hydrocarbon reservoir is modeled in a similar manner as the flow of oil from a reservoir into a well (IMEX Manual, 2005).

Figure 49 shows the interpretation given in this study to the geometry used in IMEX for Fetkovich aquifers in the bottom-water systems. The IMEX manual (2005) describes the geometry as a square contact area with a side dimension of L (L is equal to the square root of the

bottom contact area). The manual also indicates that an average reservoir thickness H is also used in the calculations and that the aquifer is assumed to be bounded by the edges of a wedge coming up to the bottom of the reservoir. Then, the theory for a concentric radial aquifer is applied, with the value for the angle taken as $2*\arctan\left[\frac{L/H}{360}\right]$, and the radius ($R_o$) taken as the square root of (L*H/pi). The ratio between the external aquifer radius to the reservoir external radius (R_{aq}/R_o), is entered as input data.

The second aquifer geometry tested in this study is a concentric cylinder underneath the oil zone. A schematic representation of this situation is shown in Figure 50. Water saturation in the lower cylinder was taken to be 100%. The concentric cylinders approach has been used by several researchers (Armenta, 2003, Kalla, 2005) to study water invasion due to coning. The radius of the aquifer in the model was significantly larger than the radius of the reservoir (infinite aquifer). This second approach has the disadvantage of requiring a higher number of grid blocks, which increases the required computer processing time and data storage.

Figure 51 shows a plot of water cut vs. time obtained using the simulator for an aquifer thickness of 12 ft. The aquifer volume was kept constant in all runs. The results for the two different aquifer models presented above were compared with results obtained using the analytical calculation method proposed by Kuo and DesBrisay (1983). It can be seen that the Fetkovich approach gives substantially lower water cut in the early days of production. This can be explained by the fact that Fetkovich gives a smaller area of contact between the aquifer and the reservoir (the approach calculates the area of contact using thickness of the aquifer (12 ft)). It is also clear that all methods give similar results later in the productive life of the reservoir. This is because late-time aquifer influx is mostly controlled by the volume of the aquifer, which is the same in all models. Finally, it can be seen that the water cut for the concentric cylinder approach

is in better agreement with the results given by Kuo and DesBrisay. Because of these results and the strange geometry associated with the analytical approach, we decided to use the concentric cylinders method in this dissertation.

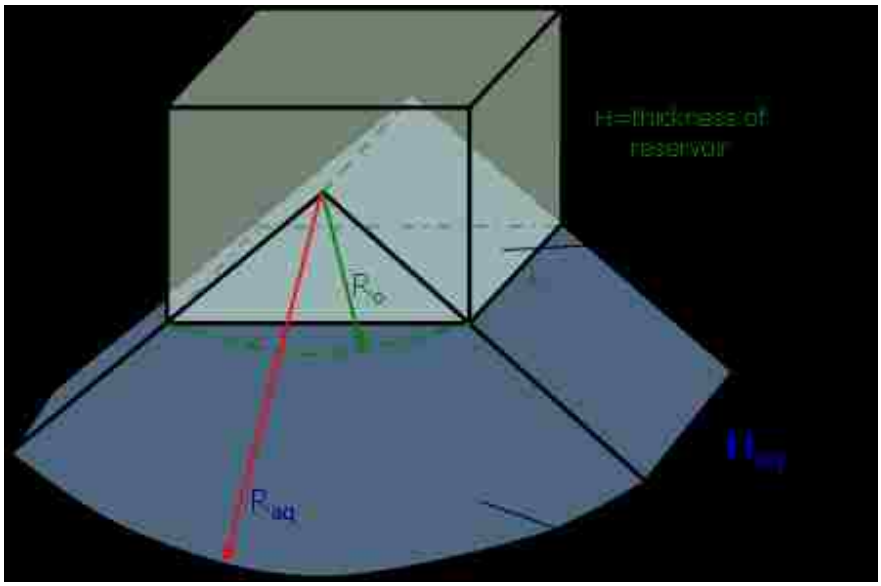

Figure 49: Interpretation of Geometry Used for Analytical Aquifer Model

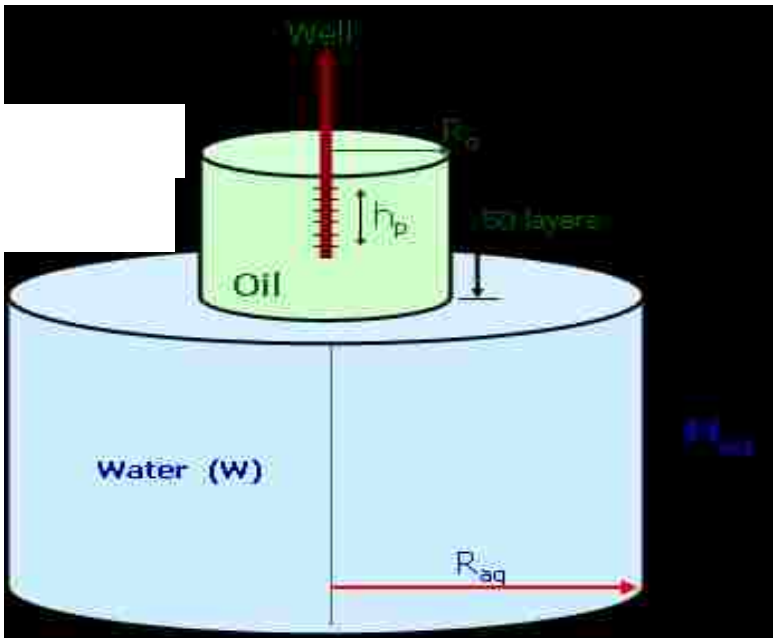

Figure 50: Aquifer Modeling Using Concentric Cylinders

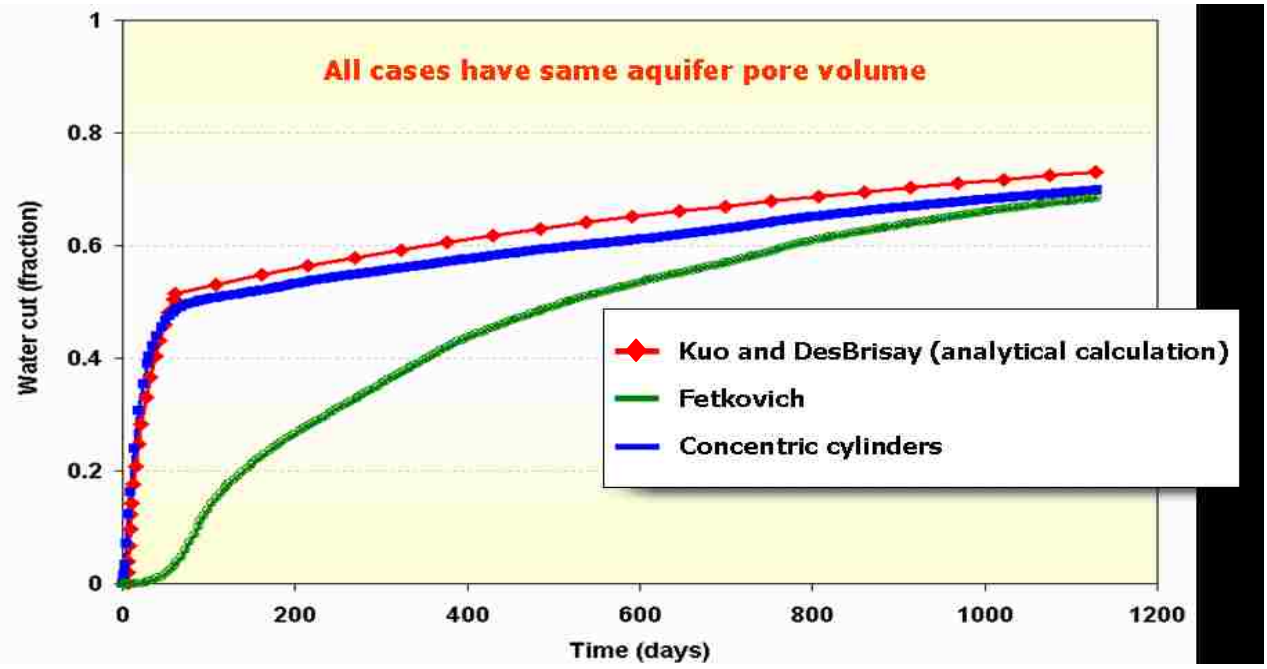

Figure 51: Water Cut vs. Time for Different Aquifer Modeling Approaches

3.2.5 Model Description

A 2D (R, Z) radial-cylindrical simulation model was used to verify accuracy of the Kuo and DesBrisay method. The model is shown in Figure 52 and it has been created using the reservoir simulator "IMEX", developed by Computer Modeling Group (CMG). No divisions were considered in the "angular" direction. As indicated before (Section 3.2.3), the number of grid blocks has been determined with a grid sensitivity analysis. The analysis suggested that accurate results can be obtained using 51grid blocks in the radial direction and 60 grid blocks in the vertical direction, for a total of 3060 grid blocks. The grid blocks in the radial direction were increased in size so that the radial locations of the block centers are roughly in geometric progression. The grid blocks in the vertical direction have a size of 2 ft. As shown before (Section 3.2.4), water intrusion was modeled by considering a concentric cylinder underneath the

oil zone. A production well was partially completed (layers 1 and 2, 10% of penetration) at the upper end of the model.

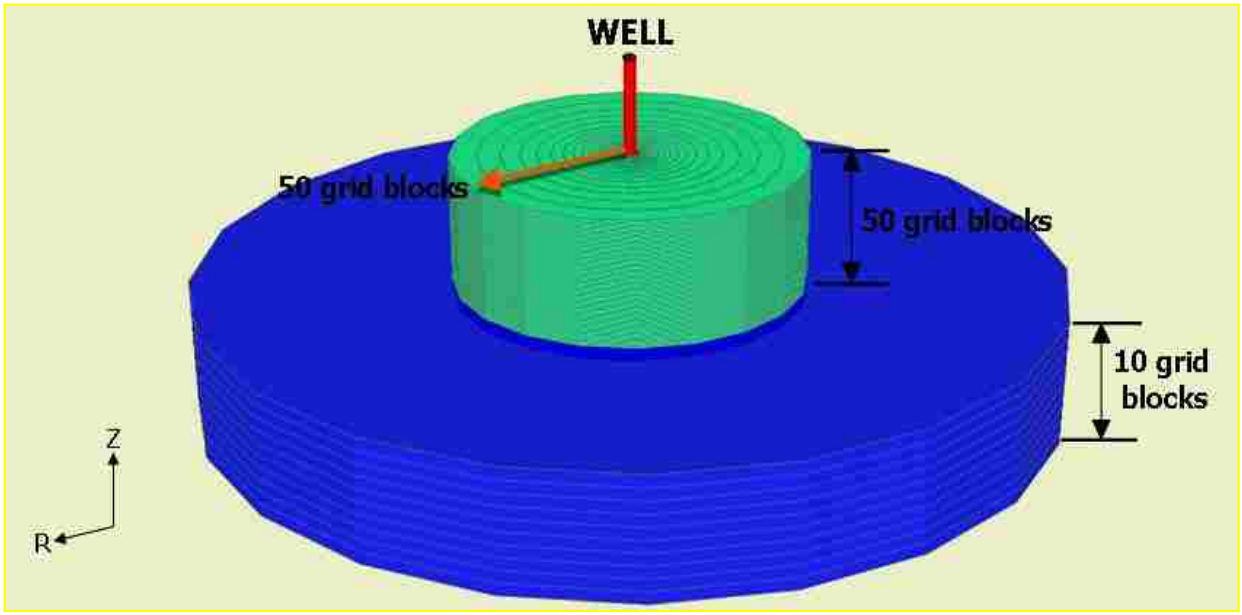

Figure 52: Simulation Model Used for Verification of Kuo and DesBrisay (1983) Method

3.2.6 Cases Considered

The same cases and properties considered for the analytical calculations completed in Section 3.2.1 are used in this validation study. These are shown in Tables 15, 18 and 19. As it can be seen, oil viscosities ranging from 1.154 to 115.4 cp and production rates from 300 to 3000 bls/day, were used in the validation.

3.2.7 Results and Discussion

Calculations at Water Breakthrough Time

Figure 53 shows the percentage of relative error (Equation 3.1) between water breakthrough times obtained analytically and using numerical simulation for the cases presented in Table 19. As previously explained, the Bournazel and Jeanson analytical method (Equation 2.40) was used to obtain the water breakthrough time for all cases except Case 1, where the

Sobocinski and Cornelius method (Equation 2.41) was used. The average absolute deviation (%AAD) from the simulation results was 91.9%. It can also be seen that the errors in the estimation of the breakthrough time are larger for the cases with larger oil viscosity, which are the cases where coning is more substantial. These results suggest that the analytical methods are quite poor estimators of the water breakthrough time in cases where coning is a predominant factor on the production behavior of the reservoir.

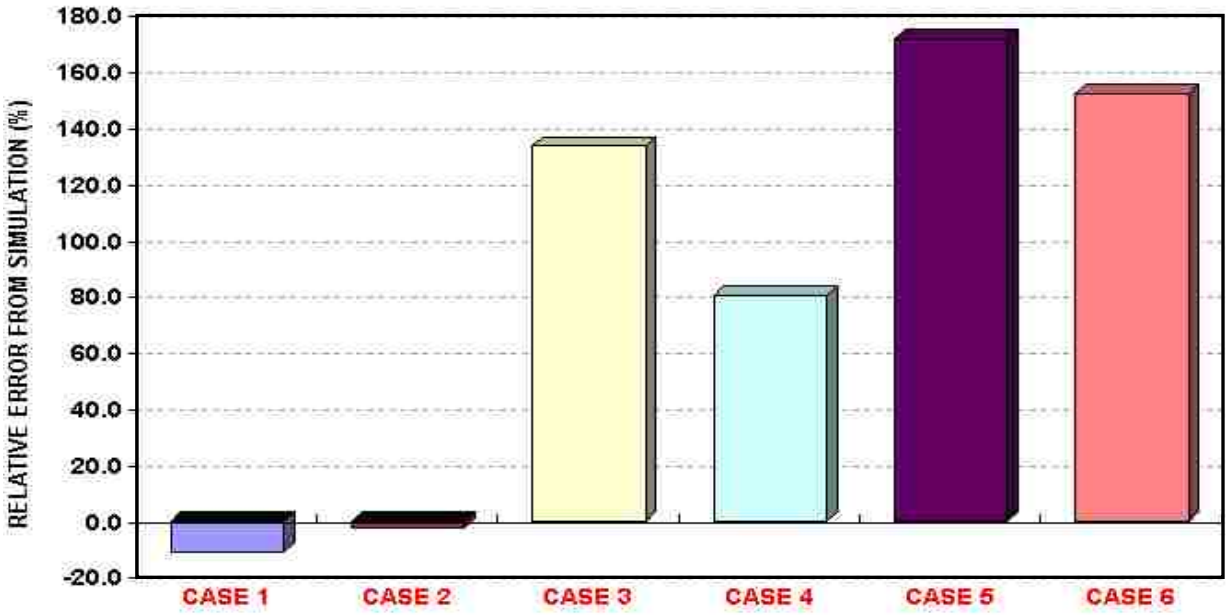

Figure 53: Analytical and Simulation Results for Bottom-Water Systems: Water Breakthrough Time

Relative errors in the by-passed oil calculation at the water breakthrough using the Kuo and DesBrisay Model compared with numerical simulation are shown in Figure 54. It can be seen that the agreement between the analytical and the simulation results is quite good for all the cases except Case 1. However, this is probably because Cases 2-6 showed very rapid water breakthrough times and, therefore, very little recovery (and very large oil bypassing) at breakthrough.

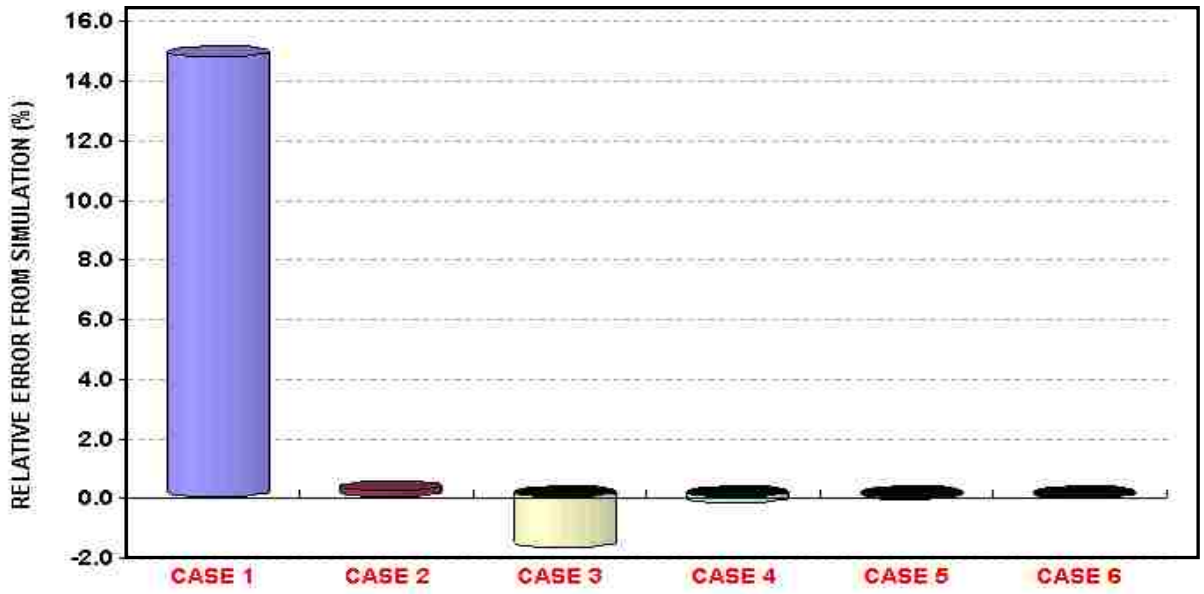

Figure 54: Comparison of Analytical and Simulation Results for Bottom-Water Systems: By-Passed Oil at Water Breakthrough

When compared to numerical simulations, the analytical models under-estimated the water breakthrough time and over-estimated the volume of by-passed oil at breakthrough in cases where significant coning occurs (Cases 3 to 6). This is similar to the results obtained in Section 3.1.7 for unstable displacement in edge-water system. As explained in Section 3.1.7, this may be caused by the fact that the analytical models consider a sharp water-oil interface (they assume segregated flow), whereas some "diffusion" or dispersion of the water saturation fronts is observed in the simulations, especially in the cases with the highest oil viscosities.

Calculations after Water Breakthrough Time

Figures 55 to 60 show a comparison of the water cut and amount of by-passed oil calculated using the Kuo and DesBrisay method with the ones obtained from numerical simulation for Cases 1 to 6 (Table 19), respectively. The results show that the agreement between the analytical and simulation results is, in general, quite poor. For example, the difference in oil bypassing at

abandonment between both methods for Case 5 is 57.5%. It can also be seen that for the cases with the highest viscosities (Cases 3 to 6), the Kuo and DesBrisay method tends to overestimate the water cut and underestimate the percentage of by-passed oil in time.

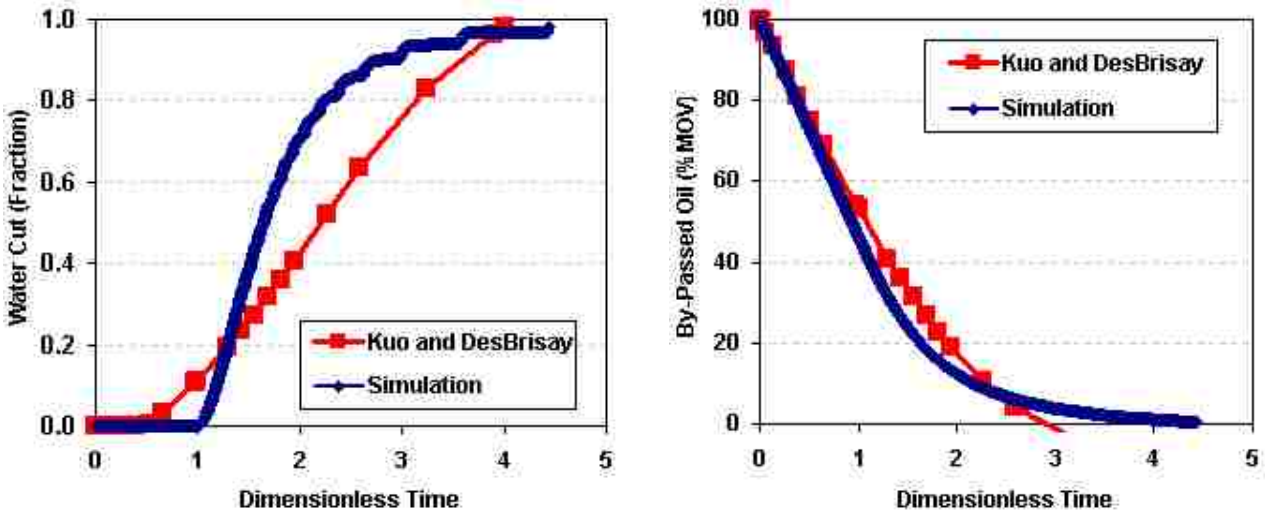

Figure 55: Comparison of Analytical and Simulation Results:
Water Cut and % of By-Passed Oil for Case 1

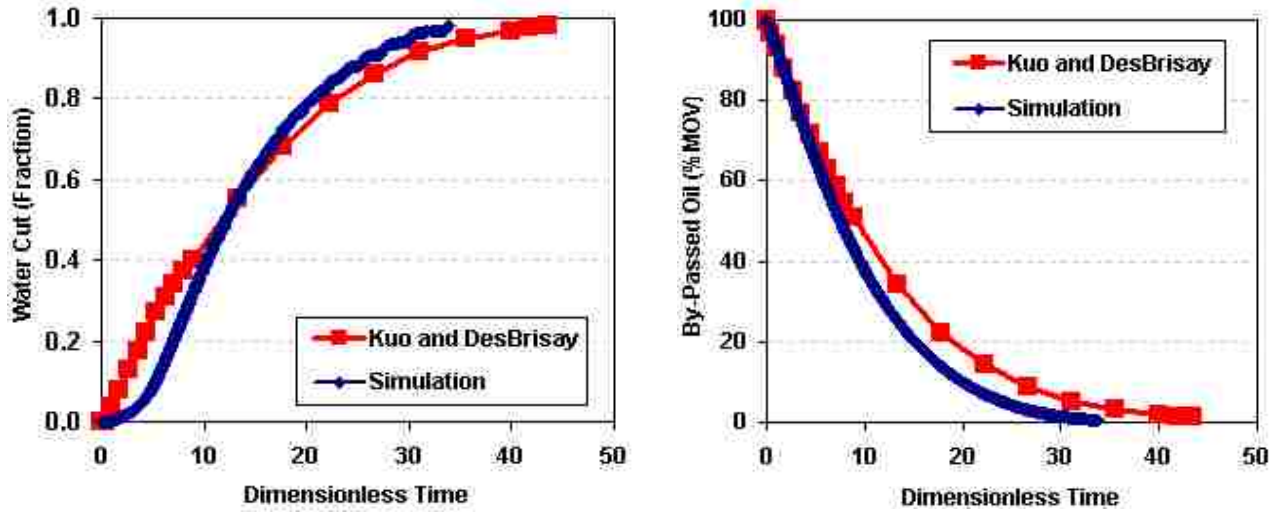

Figure 56: Comparison of Analytical and Simulation Results:
Water Cut and % of By-Passed Oil for Case 2

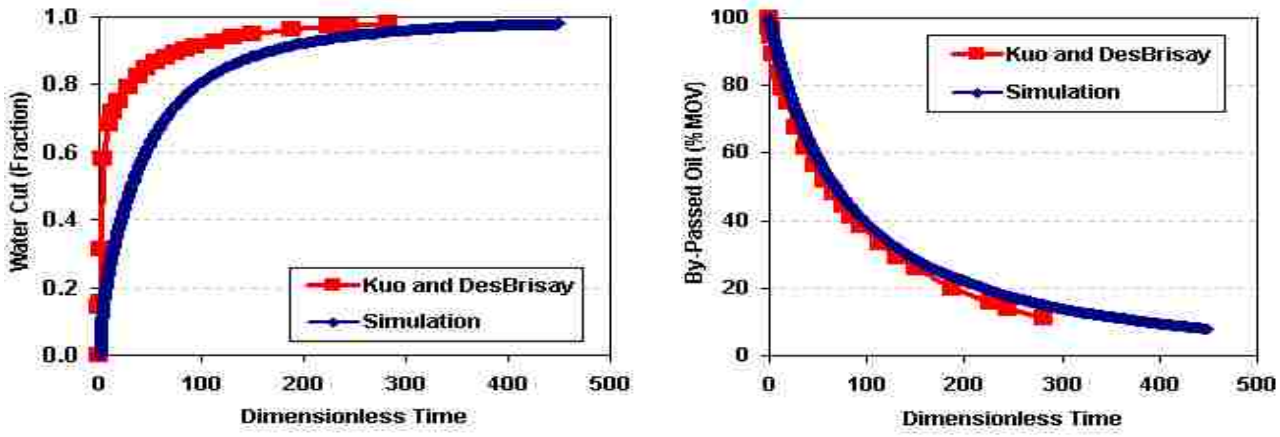

Figure 57: Comparison of Analytical and simulation Results:
Water Cut and % of By-Passed Oil for Case 3

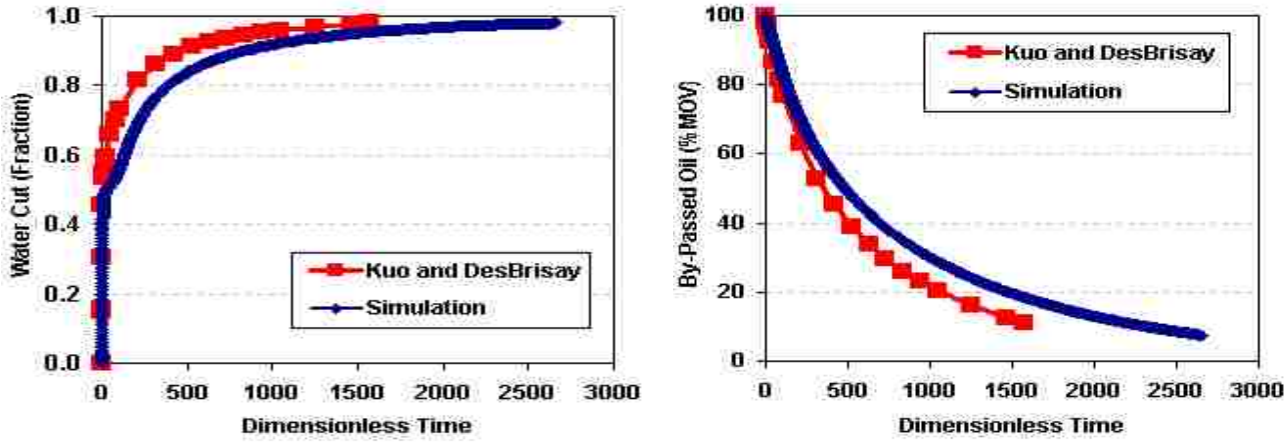

Figure 58: Comparison of Analytical and Simulation Results:
Water Cut and % of By-Passed Oil for Case 4

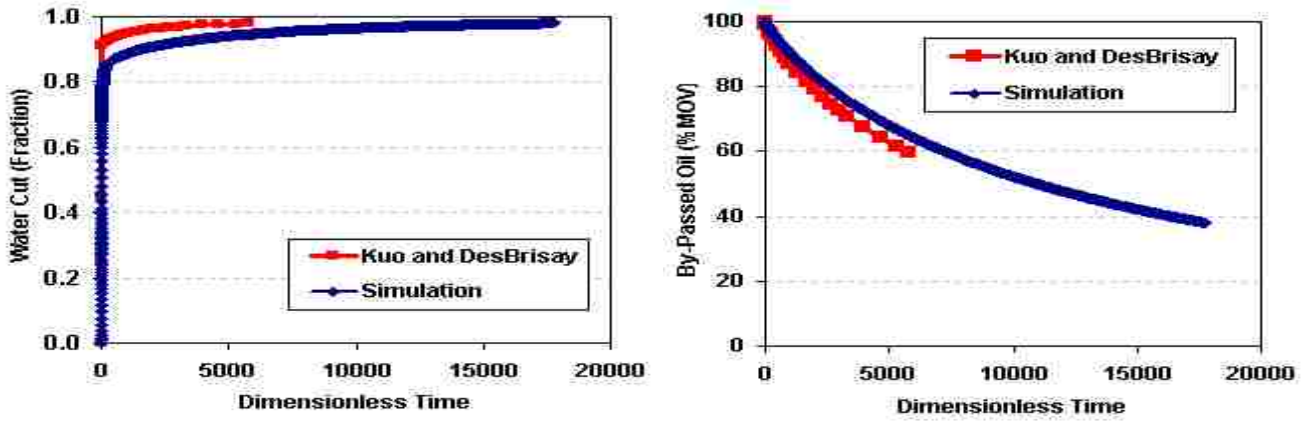

Figure 59: Comparison of Analytical and Simulation Results:
Water Cut and % of By-Passed Oil for Case 5

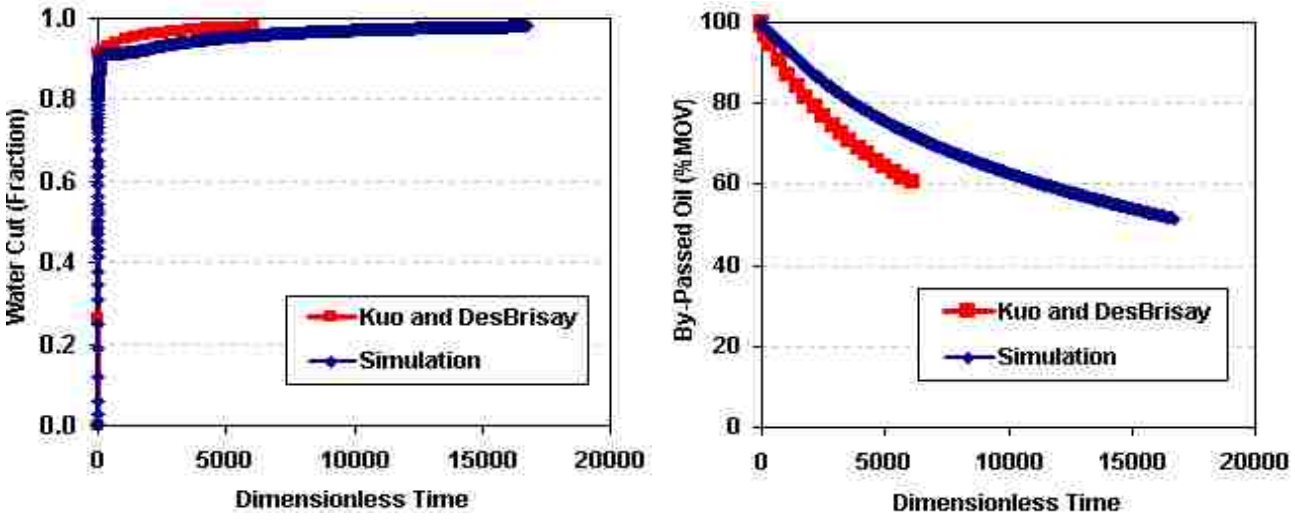

Figure 60: Comparison of Analytical and Simulation Results:
Water Cut and % of By-Passed Oil for Case 6

Summary: Insufficiencies of Kuo and DesBrisay (1983) Model

The Kuo and DesBrisay (1983) method is simple to use. However, the results of the method strongly depend upon the determination of the breakthrough time, which is very inaccurate and may give negative values (as shown in Figure 46 and Table 19). Other shortcomings of the method include:

- It assumes a constant production.
- There is lack of continuity in the mathematical model represented by Equations (2.44) to (2.46). These equations were obtained by pure curve fitting, so they do not have theoretical justification.
- A close observation of the Kuo and DesBrisay correlations shows that, even when dimensionless breakthrough time is lower than 1, a small amount of water may be produced. In other words, the model gives water production even before breakthrough (see Table 20). Obviously, this is because the correlations are based in pure curve fitting, and they lack physical meaning.

- Negative bypassed oil values can be obtained from the method (see Table 21, Case 1). As indicated above, this is because the method is based in pure curve fitting.
- It assumes a homogeneous strata; the method cannot be applied to reservoirs with local permeability barriers, high degree of stratification, or thick oil-water transition zone.
- Extreme care should be taken if the input data used is outside the ranges employed by Kuo and DesBrisay in their numerical experiments. Kuo and DesBrisay considered ratios of vertical to horizontal permeability from 0.01 to 1.0, completion penetrations from 20% to 80% of the oil column, production rates from 500 to 2000 rb/d and mobility ratios from 1.0 to 10. These conditions do not include the whole range of properties that can be obtained in petroleum reservoirs. Moreover, Kuo and DesBrisay based their correlations on a sensitivity study that included only 13 simulation cases defined by changing these properties.
- It over predicts water cut and under predict oil bypassing after breakthrough when used for cases with severe coning. One reason for the discrepancy seems to stem from the fact that the method does not consider a transition/diffusion zone. In the simulated flow (and in real reservoirs) a transition zone develops due to fractional flow effects and affects water delivery to the well. As was found for edge-water systems, the transition zone is more pronounced in the cases with largest oil viscosity (or largest end-point mobility ratio, M).

CHAPTER 4. OIL BYPASSING PREDICTION

In this chapter, a large statistical sample of possible reservoirs with edge and bottom-water drive has been created using a database of actual reservoir properties from throughout the world. Dimensional analysis allowed converting reservoir property distributions into dimension-less group distributions. Then, the amount of by-passed oil was correlated with dimensionless groups using designed experiments conducted with a reservoir simulator. The resulting dimensionless correlations determine the amount of oil that will be recovered by the end of the well's operation. The correlations are general as they cover a wide range of reservoir-well systems. The results also identify dimensionless groups that mostly control water invasion to wells. Finally, the new correlations are used to obtain statistics on the amount of oil that can be typically bypassed by water invasion to wells.

4.1 Edge-Water Systems

4.1.1 Inspectional Analysis: Groups Describing Water Invasion

Dimensional analysis can be defined as the process of determining the functional relationship between quantities by using the dimensions of each quantity. The basic axiom of dimensional reasoning is that the relative magnitude of two physical quantities of the same kind cannot be altered by any change of unit size. Bridgman (1969) explains it thus: "The principal use of dimensional analysis is to deduce from a study of the dimensions of the variables in any physical system certain limitations on the form of any possible relationship between those variables. The method is of great generality and mathematical simplicity".

The three primary purposes of dimensional analysis are:

- To generate nondimensional parameters that help in the design of experiments (physical and/or numerical) and in the reporting of experimental results.

- To obtain scaling laws so that prototype performance can be predicted from model performance.
- To predict trends in the relationship between parameters.

Groups from dimensional analysis can be joined to form global dimensionless groups, which can be more easily interpreted physically (e.g., the gravity number, G, reported by Dietz or the well known endpoint mobility ratio, M)(Novakovic, 2002).

In problems so well understood that one can write down in mathematical form all the governing laws and boundary conditions, the equations defining the problem, differential or otherwise, can be written so that all the variables are dimensionless. Simple "inspection" then shows how these dimensionless variables are related (Novakovic, 2002). This process is known as "Inspectional Analysis". Since inspectional analysis can take advantage of the problem's full mathematical specification, it may reveal a higher degree of information than a "blind" dimensional analysis and in that sense prove more powerful (Sonin, 1997). This is why inspectional analysis was the method selected in this dissertation. Dimensional analysis is, however, the only option in problems where the equations and boundary conditions are not completely articulated, and is always useful because it is simple to apply and quick to give insight (Sonin, 1997).

The workflow followed in this study to obtain dimensionless groups using inspectional analysis is essentially the same described by Novakovic (2002). The main difference is that in this dissertation capillary pressure, phase pressures and velocities were scaled in the "X" direction (following an approach by Shook et al. (1992)). In Novakovic's work; however, these properties were scaled in the "Z" direction. Table 23 shows the eight dimensionless groups used in this dissertation. The terms in the group's definitions are explained in the nomenclature. Some

comments follow:

- The groups described in Table 23 can be classified as aspect numbers (N_{RX}, N_{RY}), tilt numbers (N_{TX}) and physical numbers (N_g, N_ρ, N_c, M). The aspect numbers are just indicators of the reservoir geometry and heterogeneity. The dip angle group is a measure of the rotation of the system. The buoyancy number can be regarded as the ratio between viscous forces and gravity forces. The capillary number can be defined as a ratio between capillary forces and viscous forces.
- The capillary number group will be neglected in this study. This is mainly because some authors (Novakovic (2002), Shook (1992), Lake (1989)) suggest that that capillary numbers tend to be quite small in large-scale displacements of oil by water, such as the ones analyzed in this dissertation. The effect of capillary pressure on oil bypassing is studied in Section 4.1.10.
- The density number will also be omitted in this study. This is because both Shook et al (1992) and Novakovic (2002) suggest that such number is unimportant for the type of systems studied here and has no effect on oil recovery.
- The well penetration group, a contribution of this dissertation, was added to investigate the best well completion strategy in edge-water systems.

4.1.2 Data Base Construction

This section describes the procedure followed to find the levels of the six dimensionless groups (groups 1 to 6) selected for the analysis of their contribution to water invasion and oil bypassing. At first, a database of the reservoir parameters or properties forming the six dimensionless groups was created using actual reservoirs worldwide. No distinction was made regarding the type of reservoirs included in the database. The reservoir properties were mainly

taken from sources such as the National Petroleum Council (NPC), the Society of Petroleum Engineers (SPE) and the US Geological Survey (USGS). Next, probability distributions were plotted for each one of the properties. Table 24 shows statistics obtained from the probability distributions of each one of the properties. Then, Monte Carlo Simulations (10,000 passes) were run to randomly obtain probability distributions of each dimensionless group using the distributions of the individual parameters or properties. Finally, cross plots for each possible combination of groups were made and the percentiles to be used in the design were selected within the cloud of points representing the possible reservoirs.

Table 23: Dimensionless Groups Controlling Oil Bypassing in Edge-Water Systems

#	**Group Name**	**Symbol**	**Equation**
1	X-direction aspect ratio	N_{RX}	$\frac{L}{H}\sqrt{\frac{k_z}{k_x}}$
2	Y-direction aspect ratio	N_{RY}	$\frac{W}{H}\sqrt{\frac{k_z}{k_y}}$
3	Dip angle group	N_{TX}	$\frac{L}{H}\tan$ [redacted]
4	Well Penetration Group	H_p/H	$\frac{Well\ Penetration}{Reservoir\ Thickness}$
5	End point mobility ratio	M	$\frac{}{}$ [redacted] $_w$ / $_o$
6	Buoyancy number	N_g	$\frac{k_x}{u_T}$ [redacted] $_{ro}$ [redacted] $g\cos$ [redacted] $\frac{H}{L}$
7	Density number	N_ρ	[redacted]
8	Capillary Number	N_c	$\frac{}{Lu_T}$ [redacted] $_{ro}$ [redacted] $\sqrt{}$ [redacted] $_x$

The P(10%) and P(90%) of each distribution were recorded for each dimensionless group as the low and high levels to be used in the design, respectively. In some cases, however, these percentiles fell out of the cloud of points and, therefore, the P(20%) or P(30%) were selected as the low level and/or the P(80%) as the high level to be used in the design. An example cross plot for two of the groups showing the percentiles (levels) selected is shown in Figure 61. Table 25 presents the percentiles obtained for each group using Monte Carlo simulations. As can be seen, the range obtained for each group is quite wide and, hopefully, represents most possible reservoir situations.

Table 24: Statistics for Properties Forming the Dimensionless Groups

Property	**# points**	**P(10%)**	**P(50%)**	**P(90%)**	**Mean**
Oil viscosity (cp)	2043	0.4	4.0	310.0	374.2
Permeability (md)	3354	20	223.87	1737.8	697
k_v/k_h	126	0.01	0.238	0.94	0.352
Water viscosity (cp)	653	0.34	0.56	0.94	0.62
Thickness (ft)	1335	18	70.8	450.0	187.28
Inter-well distance (ft)	1258	552.0	1128.1	1867.0	1186.9
Total Rate (bpd)	708	53.8	155.6	1766.1	955.8
Density difference (g/cc)	2043	0.034	0.118	0.181	0.109
k_{ro} @ S_{wc}	113	0.656	0.942	1.00	0.871
k_{rw} @ S_{or}	113	0.063	0.238	0.557	0.288
Porosity (%)	3354	13.0	23.4	33.0	23.2

Table 25: Levels Used for the Dimensionless Groups: Edge-Water Systems

Levels	N_g	N_{RX}	N_{RY}	N_{TX}	M	H_p/H
Low	0.00039	2.49	1.24	1.58	0.25	0.1
High	0.20	29.23	14.61	18.14	101.72	1.0

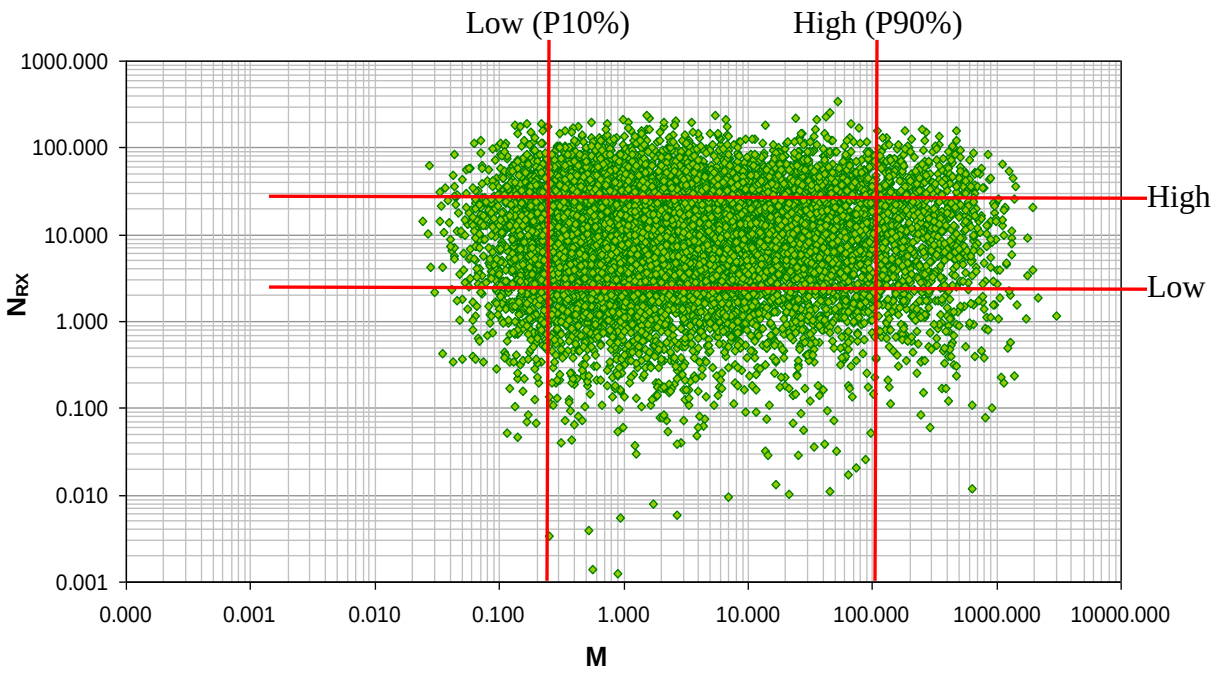

Figure 61: Example Cross Plot for Two of the Groups Showing the Levels Selected for Design

4.1.3 Matrix of Simulation Experiments

A two-level full factorial sensitivity analysis with a total of 64 runs (2^6 = 2 levels and 6 factors or groups) was designed to determine the influence of the dimensionless groups on oil bypassing. The levels shown in Table 25 were used in the analysis (each run is a combination of the levels shown in the table). They embrace a wide design space that represents as many different reservoirs as possible. Although the two-level designs are unable to explore fully the design space, they can reveal major trends and help to determine the future experimentation strategy. This study can be considered, therefore, a preliminary effort leading to more detailed sensitivity analysis of oil bypassing in the edge-water systems. Half of the runs satisfy the stability criteria given by Dietz (Equation (2.16)). The remaining cases depict unstable displacement.

The numerical simulation model used to study the effect of each group on oil bypassing was presented in Chapter 3. Summarizing, the model considers a reservoir slab with a linear drive pattern and has been created using the reservoir simulator "IMEX", developed by Computer Modeling Group (CMG). A regular orthogonal grid was used with 40 grid blocks in the "X" direction, 11 grid blocks in "Y" and 20 grid blocks in the "Z" direction, for a total of 8800 grid blocks. Water intrusion was modeled using an analytical Fetkovich aquifer attached at the lower end of the slab.

Validation of Dimensionless Groups

The six dimensionless groups were validated using the numerical simulation model previously described. The idea was to vary the parameters in the dimensionless groups but holding the values of the groups constant. The validation was done for all groups using the P(50%) level of each group. The study confirmed the validity of the six dimensionless groups. More details about the validation study can be found elsewhere (Hernandez, Wojtanowicz and White 2006).

4.1.4 Groups Controlling Oil Bypassing

The relative effect of the six dimensionless groups on oil bypassing at well abandonment was analyzed using the "Design of Experiments" option of the statistical package SAS, version 9.1.3, and the analysis of variance, ANOVA. Abandonment condition was defined by the water cut economic limit of 98%. This limit was estimated using an oil price of $35/bbl, an oil producing cost of $15/bbl and a water processing-disposal cost of $2/bbl. Figure 62 shows the contribution, expressed as percentage of the sum of squares, of the different groups to the by-passed oil. Only the main effects are shown for the sake of simplicity. Four groups were found to be significant based on ANOVA (a significance level of 5% was used in all ANOVA

calculations in this study).

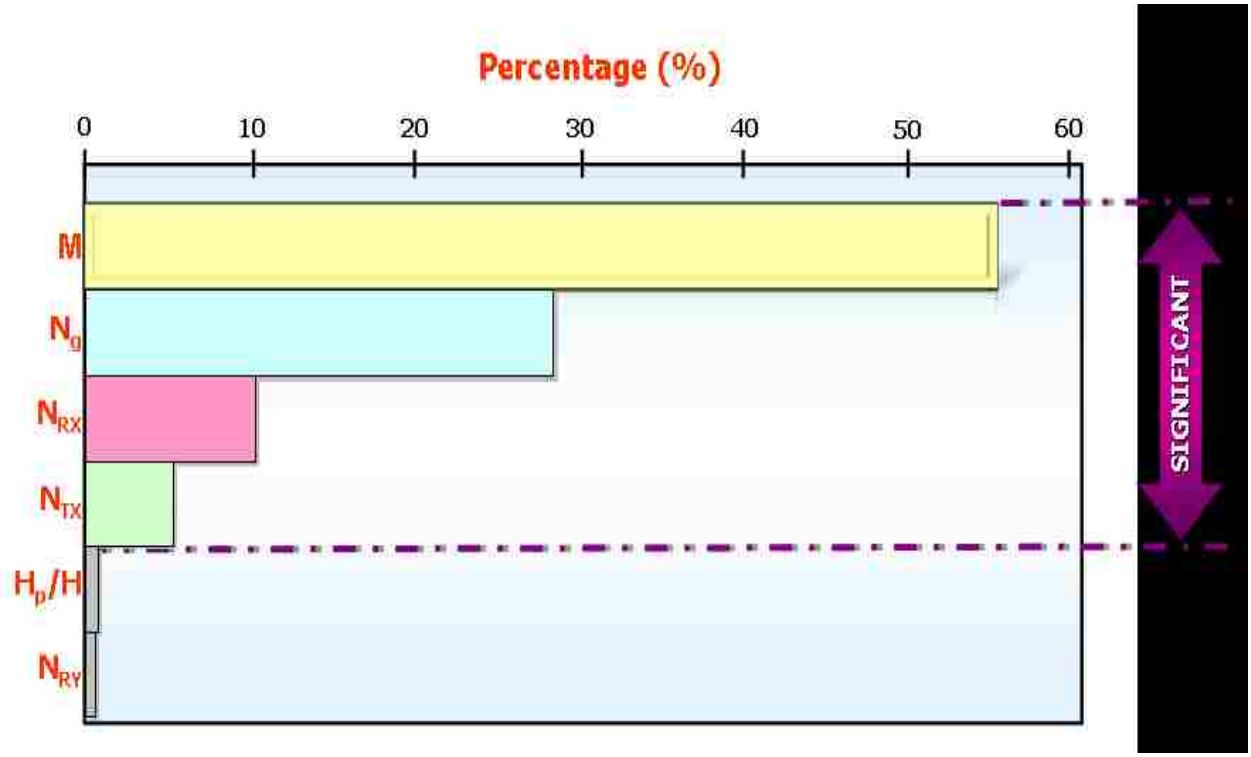

Figure 62: Effect of Dimensionless Groups on Oil Bypassing at Abandonment (Edge-Water)

It is clear that the end-point mobility ratio, which is a measure of the viscosity contrast between oil and water, is the main group affecting oil bypassing at abandonment conditions. The effect of the buoyancy number is also quite significant, which suggests that gravity forces may have an important impact on oil bypassing. Overall, it was found that oil bypassing is promoted by high end-point mobility ratios and Y-direction aspect ratios, as well as long well penetrations. Bypassing would be reduced with high X-direction aspect ratios, high values of the dip angle group and high gravity numbers. This is shown in Figure 63.

4.1.5 New Correlations for Oil Bypassing in Edge-Water Systems

The following regression formula was the best fit of the percentage of by-passed oil (%BPO) at abandonment as a function of the six dimensionless groups with their first-order interactions:

$$BPO\,(\%MOV) = 7.7027 + .2042 * N_g + .2237 * N_{RX} + .1350 * N_{RY} + .0876 * N_{TX} + 0.4373 * M + 2.6838 * H_p/H + .7607 * N_g * N_{RX} + .2405 * N_g * M + 0.0073 * N_{TX} * M \quad \text{.....(4.1)}$$

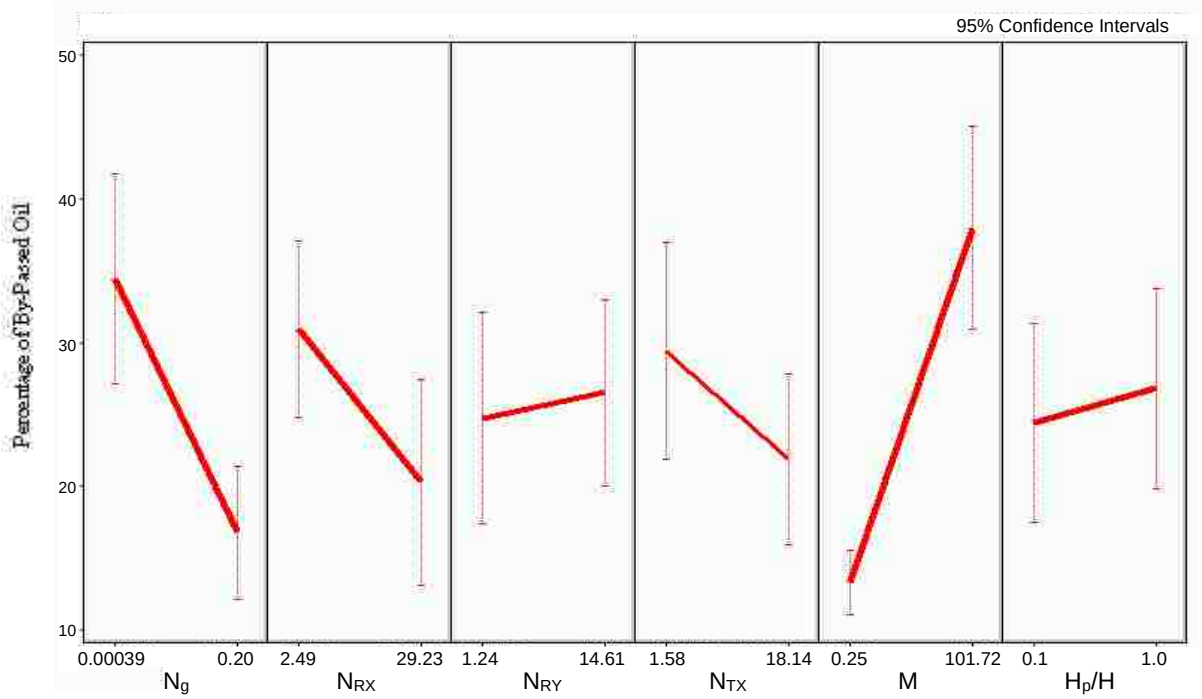

Figure 63: Conditions Promoting Oil Bypassing in Edge-Water Systems

Only significant terms were included in Equation (4.1). The correlation coefficient (r^2) for this formula was 90.2 %. This correlation removes some of the simplifying assumptions and problems with the existing analytical models for the prediction of oil by-passing (these problems were studied in Chapters 2 and 3).

4.1.6 Statistics of Oil Bypassing in Typical Edge-Water Systems

Equation (4.1) and the data base that was built for the purposes of this study have been used to create statistics for the amount of oil that can be typically bypassed by water invasion to wells. The procedure followed to create the statistics is described next:

- First, the 10,000 values obtained using Monte Carlo simulations for each one of the

groups were randomly combined to obtain 10,000 synthetic reservoirs.

- Second, reservoirs in which all the values of the groups were within the levels shown in Table 25 were selected. This resulted in a total of 2229 "typical" reservoirs.
- Third, Equation (4.1) was applied to the 2229 "typical" reservoirs.
- Finally, a plot of cumulative probability of oil bypassing at abandonment was built using the results. This plot is shown in Figure 64.

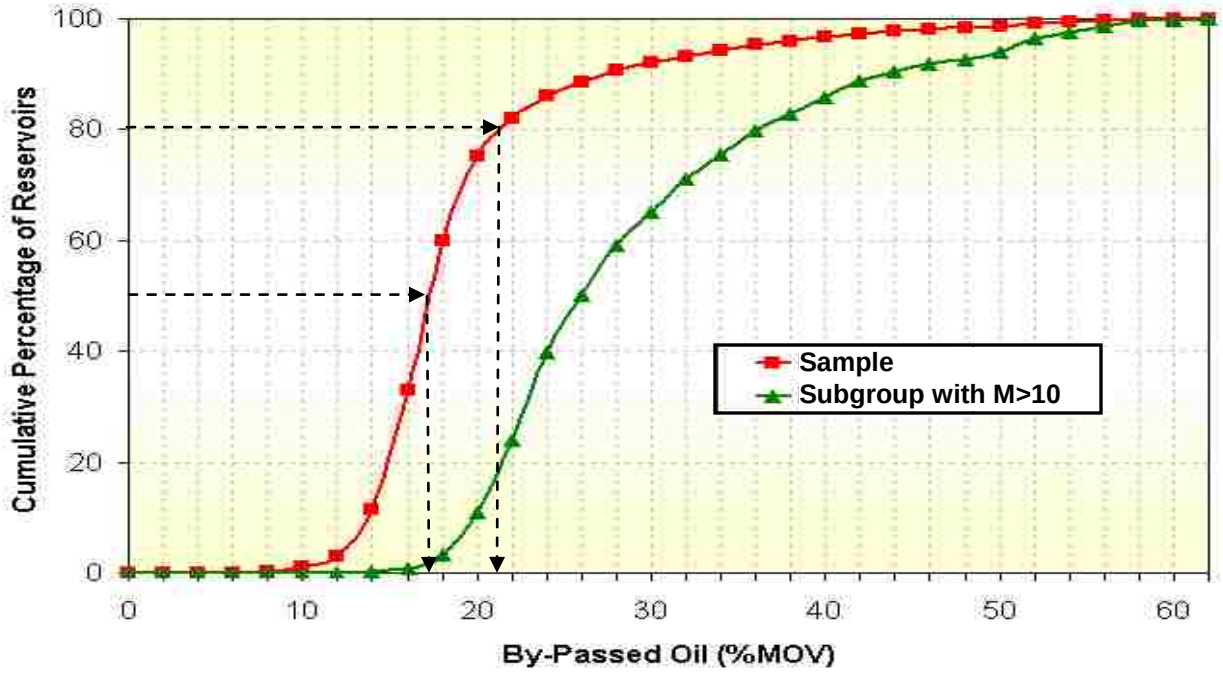

Figure 64: Cumulative Probability of Oil Bypassing at Abandonment for Edge-Water Systems

The figure shows that half of the reservoirs would bypass about 17% of the movable oil in place and one in five reservoirs (20%) would bypass 21% or more of the oil. It is also obvious that oil bypassing at abandonment could be very high – about 60% for the worst case scenario. This is quite significant because only homogeneous systems have been considered. Oil bypassing is expected to be much higher if the effect of heterogeneity is included. The effect of heterogeneity will be considered in Section 4.1.7.

In order to have an idea of the effect of the type of oil, expressed as a function of the end-point mobility ratio, on the statistics of oil bypassing, an additional curve is included on Figure 64 with results for a new subgroup of reservoirs with end-point mobility ratios larger than 10 (which roughly correspond to oil viscosities larger than 20 cp). It is obvious that oil bypassing is much more significant for systems with high mobility ratio (the curve is more flat than the one found for the entire sample of reservoirs). Half of this new group of reservoirs would bypass 26% or more of the movable oil volume and one in five would bypass 36% or more. These results suggest that the problem of oil bypassing in heavy oil reservoirs could be quite critical.

4.1.7 Effect of Heterogeneity on Oil Bypassing

Results presented in the previous section show that oil bypassing by water invasion could be a significant problem in homogeneous sands. It is well known, however, that one of the significant factors influencing recovery performance is the variation of reservoir permeability in the vertical direction. Water tends to move faster in zones of higher permeability, causing early breakthrough and more oil bypassing.

According to Poston and Gross (1986) sand bodies found in sandstones may be categorized as regressive, transgressive, serrated and homogeneous sequences. This section discusses the results of a cross-sectional simulation study aimed at analyzing the effect of water invasion on oil bypassing on these four basic depositional models. Poston and Gross (1986) described these sequences as follows:

Regressive Depositional Sequence

Regression can be defined as the seaward movement of the shoreline that occurs when the sedimentation rates outpace the rates of base-level rise at the shoreline (Catuneanu, 2002). A regressive depositional environment may be characterized by delta bar deposits, which reflect an

increasing-energy environment. The energy change is caused by the outward prograding of the delta into previously deeper-water environments. The higher energy environment (top) provides sediments with a greater grain size and better sorting. Figure 65a represents a typical example of the grain size distribution and log response for a delta bar deposit. Good examples of coarsening-upward sand sequences are the Lower Sparky formation of Alberta and Saskatchewan and the Ivishak sandstone in Prudhoe Bay Field (Begg et al., 1992).

Transgressive Depositional Sequence

Transgression can be defined as a landward movement of the shoreline indicated by a landward migration of the littoral facies in a given stratigraphic unit (Mitchum, 1972). A transgression occurs when the rate of sea level rise landward exceeds the rate of sediment input and causes an increase in accommodation, initiating the development of a transgressive surface.

A transgressive depositional sequence may be characterized by a channel-fill deposit. Channel fill deposits are the result of clastic sedimentation in river channels. Sedimentation occurs where the stream velocity is reduced by meanders in the stream bed or the occurrence of an obstruction. The coarsest grain sizes are located at the bottom of the section and there is a progressive decrease in grain size in the upward direction. Figure 65b shows a typical example of the grain size distribution and log response for a channel-fill deposit. A good example of a coarsening-downward sequence is the B sandstone of Tuscaloosa Formation at the Olive Field, Mississippi.

Serrated Sequence

A serrated sequence is normally composed of thin, alternating sand and shale beds. The sequence is formed by an environment undergoing a fairly rapid variation in depositional conditions. A typical log response for these systems is shown in Figure 65c. There is no vertical

gradation in the arrangement of the grain size. The K sands, in Mississippi Canyon 194 Field are good examples of serrated sequences.

Homogeneous Sequence

A homogeneous sequence can be represented by a beach sand deposit. Beach sand deposits are the result of a high-energy and geographically stable environment. The constant action of the waves causes beach sand deposits to be well sorted and nearly homogeneous. Figure 65d shows a typical log response of a homogeneous sequence. The S sand in Auger field in Gulf of Mexico is a good example of homogeneous sequences.

Figure 66 displays a conceptual geological model of a sand rich delta that includes coarsening-downward sequences (sands left upstream in channels, for example), relatively homogeneous sequences (sandy beaches near mouths of distributary channels) and corsening-upward sequenced (river mouth bars).

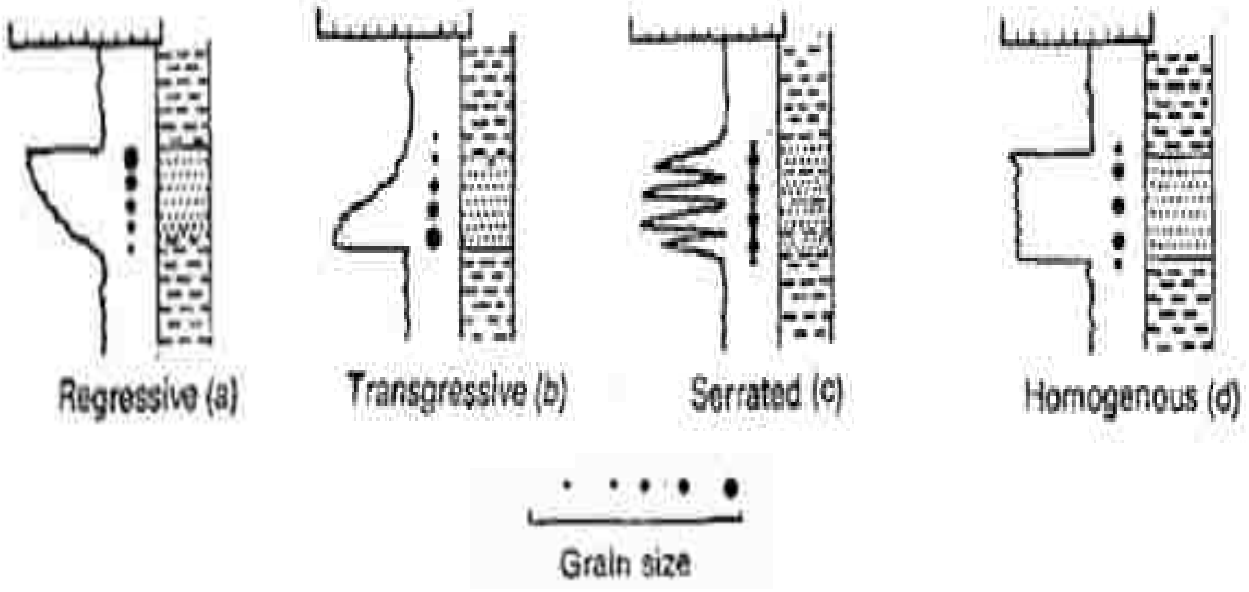

Figure 65: Typical Log Responses in Different Depositional Sequences
(after Poston and Gross, 1986)

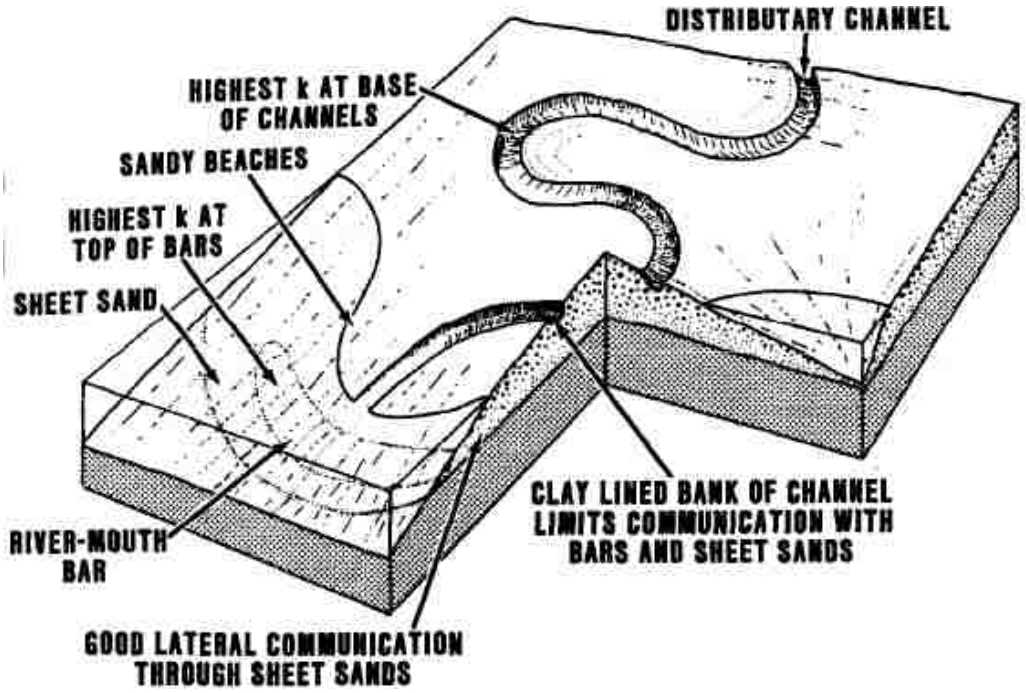

Figure 66: Conceptual Model of a Depositional Sequence in a Sand-Rich Delta (after Richardson et al., 1989)

Description of Model and Cases

The same simulation model employed in the previous sections of this Chapter has been used to study oil bypassing for the four different depositional sequences shown in Figure 65. The porosities and horizontal permeabilities used for each one of the sequences in the simulation model are shown in Table 26. Figure 67 displays the vertical distribution of permeability used for each sequence. The ratio of vertical to horizontal permeability of the original runs (homogeneous sequence) was maintained for all the other sequences. The model has been simplified by using constant connate water and residual oil saturations with depth. A total of 256 simulation cases, 64 for each type of depositional sequence, were completed in IMEX. The cases were defined by combining the low and high levels of the six dimensionless groups that characterize edge-water systems, as explained in Section 4.1.3.

Table 26: Vertical Arrangement of Layer Properties

Layer Number	Homogeneous		Transgressive		Regressive		Serrated	
	Porosity (%)	Permeability (md)	Porosity (%)	Permeability (md)	Porosity (%)	Permeability (md)	Porosity (%)	Permeability (md)
1	23.4	223.9	14.1	29.2	32.7	1697.7	18.3	56.0
2	23.4	223.9	15.1	36.1	31.7	1370.8	28.5	391.8
3	23.4	223.9	16.1	44.8	30.7	1106.9	18.3	56.0
4	23.4	223.9	17.0	55.4	29.8	893.8	28.5	391.8
5	23.4	223.9	18.0	68.7	28.8	721.7	18.3	56.0
6	23.4	223.9	19.0	85.0	27.8	582.7	28.5	391.8
7	23.4	223.9	20.0	105.3	26.8	470.5	18.3	56.0
8	23.4	223.9	21.0	130.4	25.8	379.9	28.5	391.8
9	23.4	223.9	21.9	161.5	24.9	306.8	18.3	56.0
10	23.4	223.9	22.9	200.0	23.9	247.7	28.5	391.8
11	23.4	223.9	23.9	247.7	22.9	200.0	18.3	56.0
12	23.4	223.9	24.9	306.8	21.9	161.5	28.5	391.8
13	23.4	223.9	25.8	379.9	21.0	130.4	18.3	56.0
14	23.4	223.9	26.8	470.5	20.0	105.3	28.5	391.8
15	23.4	223.9	27.8	582.7	19.0	85.0	18.3	56.0
16	23.4	223.9	28.8	721.7	18.0	68.7	28.5	391.8
17	23.4	223.9	29.8	893.8	17.0	55.4	18.3	56.0
18	23.4	223.9	30.7	1106.9	16.1	44.8	28.5	391.8
19	23.4	223.9	31.7	1370.8	15.1	36.1	18.3	56.0
20	23.4	223.9	32.7	1697.7	14.1	29.2	28.5	391.8
P50	**23.4**	**223.9**	**23.4**	**223.9**	**23.4**	**223.9**	**23.4**	**223.9**

The effect of reservoir heterogeneity was investigated in the transgressive and regressive sequences by creating log-normal distributions with a value of the Dykstra-Parsons coefficient of permeability variation (V_{DP}) of 0.75 (all the permeability distributions have the same median and standard deviation). The same coefficient of variation was used for the serrated sequence, where the even layers have permeability seven times larger than the odd layers. The Dykstra-Parsons coefficient is the most commonly used measure of permeability variation in the oil industry. It can be defined as the difference between the median permeability and the permeability at one standard deviation from the mean, divided by the median of permeability, or:

$$V_{DP} = \frac{K(P50\%) - K(P16\%)}{K(P50\%)} \quad \text{.....(4.2)}$$

Where *P50%* and *P16%* are the 50th and 16th percentiles, respectively. The possible values of Dykstra-Parsons coefficient range from zero to one. A coefficient of zero would have no variation (completely homogeneous system). Large variations would be described with a number closer to one. Dunn and Chukwu (2001) indicated that typical oil reservoirs have a Dykstra-Parson coefficients ranging from 0.5 to 0.9. A more specific range has been given by Lake (1989), who tabulated coefficients ranging from 0.65 to 0.89 for several producing formations. Perhaps the main disadvantage of the coefficient is that it does not consider the spatial distribution of permeability.

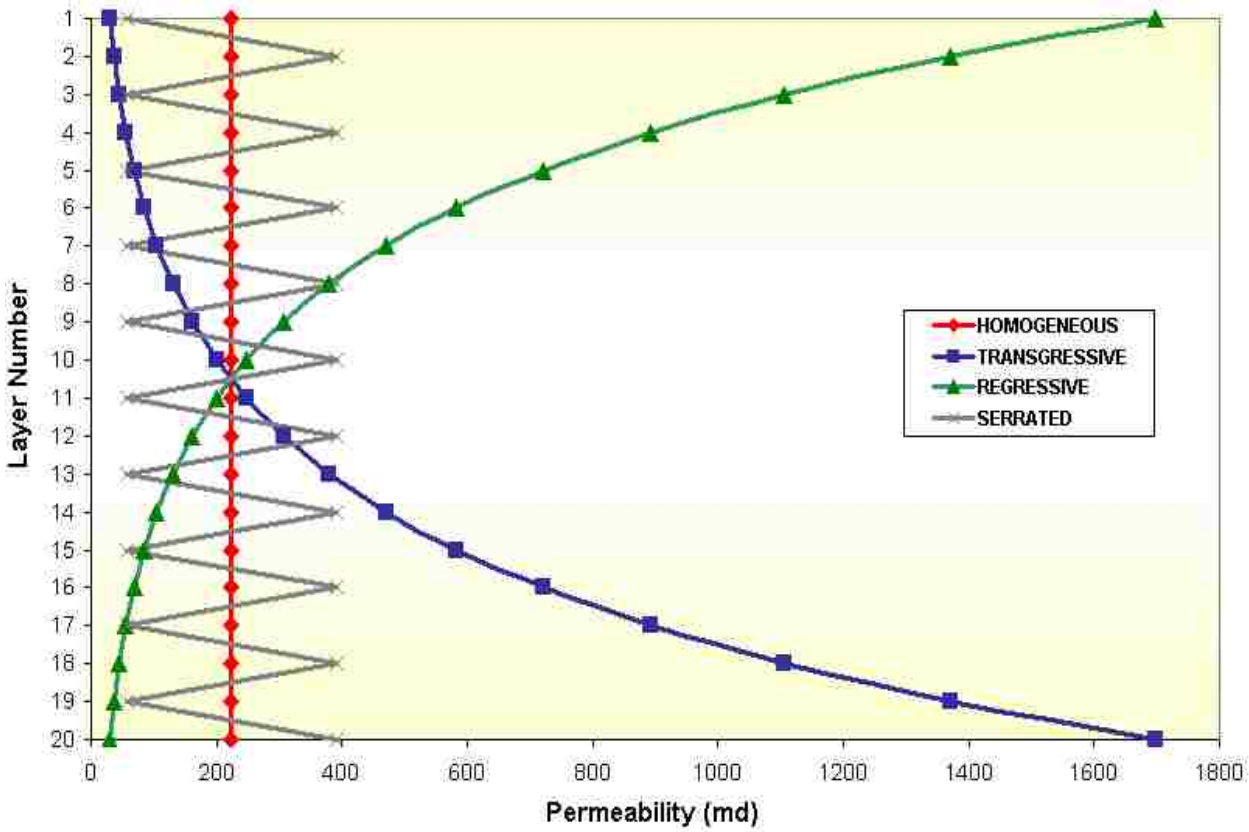

Figure 67: Vertical Distribution of Permeability for the Different Sequences Studied

Results

Figure 68 shows a plot of cumulative probability of oil bypassing at abandonment for the four different types of sequences. The plot was built following the procedure described in Section 4.1.6. New correlations for oil bypassing at abandonment as a function of the six dimensionless groups, similar to Equation (4.2), were created using SAS for each type of sequence:

Transgressive:

$$BPO\,(\%MOV) = 8.6390 - .8325 * N_g - .2025 * N_{RX} - .3129 * N_{RY} - .2904 * N_{TX} - 0.5304 * M - 4.3224 * (H_p/H) - .9589 * N_g * N_{RX} - .9312 * N_g * N_{RY} - 1.4202 * N_g * M - .0147 * N_{TX} * M - .5680 * N_{TX} * (H_p / H) - 0.0946 * M * (H_p / H) \quad (4.3)$$

Regressive:

$$BPO\,(\%MOV) = 20.7122 - 8.3954 * N_g - .3489 * N_{RX} - .0048 * N_{RY} - .0324 * N_{TX} - 0.3130 * M - 0.7276 * (H_p/H) - .6357 * N_g * N_{TX} - .8206 * N_g * M - 0.0021 * N_{RX} * M - .0231 * N_{RY} * N_{TX} - .0069 * N_{RY} * M \quad (4.4)$$

Serrated:

$$BPO\,(\%MOV) = 9.4420 - 2.5004 * N_g - .1464 * N_{RX} - .0662 * N_{RY} - .0987 * N_{TX} - 0.4380 * M - 2.5869 * (H_p/H) - .8641 * N_g * N_{RX} - .2363 * N_g * M - 0.0068 * N_{TX} * M \quad (4.5)$$

The correlation coefficients (r^2) for Equations (4.3), (4.4) and (4.5) are 0.95, 0.88 and 0.92, respectively.

The figure shows a quite wide variation in oil bypassing for the different sequences, which indicate the relevance of the permeability distribution of oil bypassing. Some comments follow:

- Transgressive depositional sequences produce the highest amount of bypassed oil at abandonment in water-drive reservoirs. High permeability zones at the bottom of the producing horizon stimulate the formation of a gravity water tongue (the water front advances faster in the bottom layers) and early water breakthrough.

- On the other hand, if permeability decreases with depth (regressive sequences), the effect of gravity will sharpen the displacement front and reduce oil bypassing.
- The serrated sequence displays oil bypassing midway between the transgressive and the homogeneous sequences.
- The amount of bypassed oil in the regressive and the homogeneous models is essentially the same at low-viscosities (low oil bypassing).
- The average amounts of by-passed oil for the homogeneous and transgressive sequences are 19.3% and 25.4%, respectively.
- The effect of permeability distribution is more important for heavy oils. This can be verified by observing Figure 69, which show the cumulative probability of oil bypassing at abandonment for reservoirs with end-point mobility ratios, M, larger than 10 (oil viscosities roughly larger than 20 cp). Note that the separation of the different curves is more pronounced than in Figure 68. The average amount of by-passed oil for the homogeneous and transgressive sequences when M>10 is 29.0% and 37.0%, respectively. This confirms that oil bypassing by water invasion can be a significant problem, especially in transgressive sequences with heavy oil.

Figure 70 displays 2D views of the simulation slab showing the position of two water saturation isosurfaces (S_w=20.5% and Sw=30%) at water breakthrough for the four sequences studied. The figure was created for one of the simulation cases that resulted in the largest oil bypassing at abandonment for all the sequences (65.6%, 83.4%, 58.5% and 66.9% for the homogeneous, transgressive, regressive and serrated sequences, respectively). The case is characterized by having the low levels for all groups (Table 25) except M, were it has the high level (M=101.72).

It is clear that for the transgressive sequence (Figure 70b), where high permeabilities are at the bottom, vertical communication exacerbates the creation of a water tongue and the oil bypassing problem. If the high permeability layers are at the top, which is characteristic of regressive sequences (Figure 70c), the influence of gravity will tend to mitigate the poor performance. Interestingly, Figure 70c shows water overriding, which was a quite unexpected result. The low permeability in the deepest layers reduced water migration towards the bottom of the slab and, therefore, stimulated its flow along the slab's top, where permeability is quite high. When the water front approached the well, pressure drawdown in the upper layers of the reservoir further induced flow of water along the top of the model. Figure 70 also shows that, similar to transgressive systems, both homogeneous (Figure 70a) and serrated (Figure 70d) sequences resulted in the formation of a pronounced water tongue.

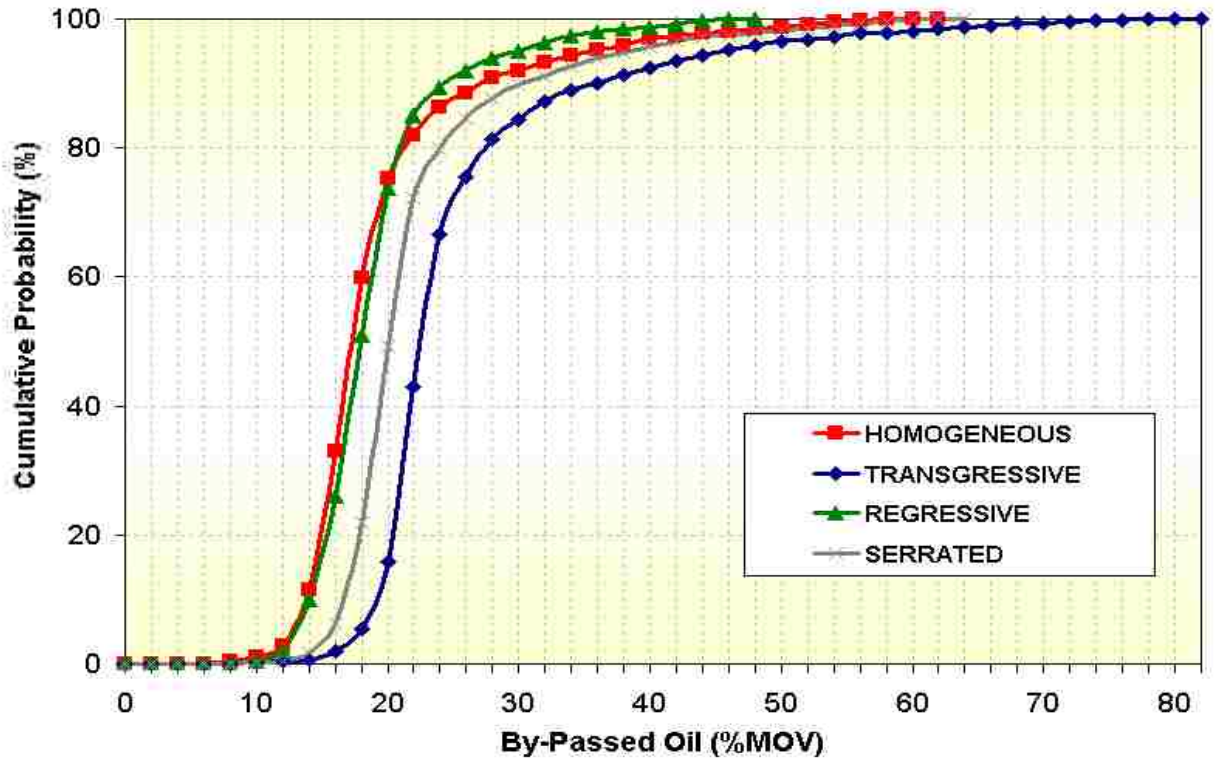

Figure 68: Cumulative Probability of Oil Bypassing at Abandonment for Edge-Water Systems Showing the Effect of Vertical Permeability Distribution

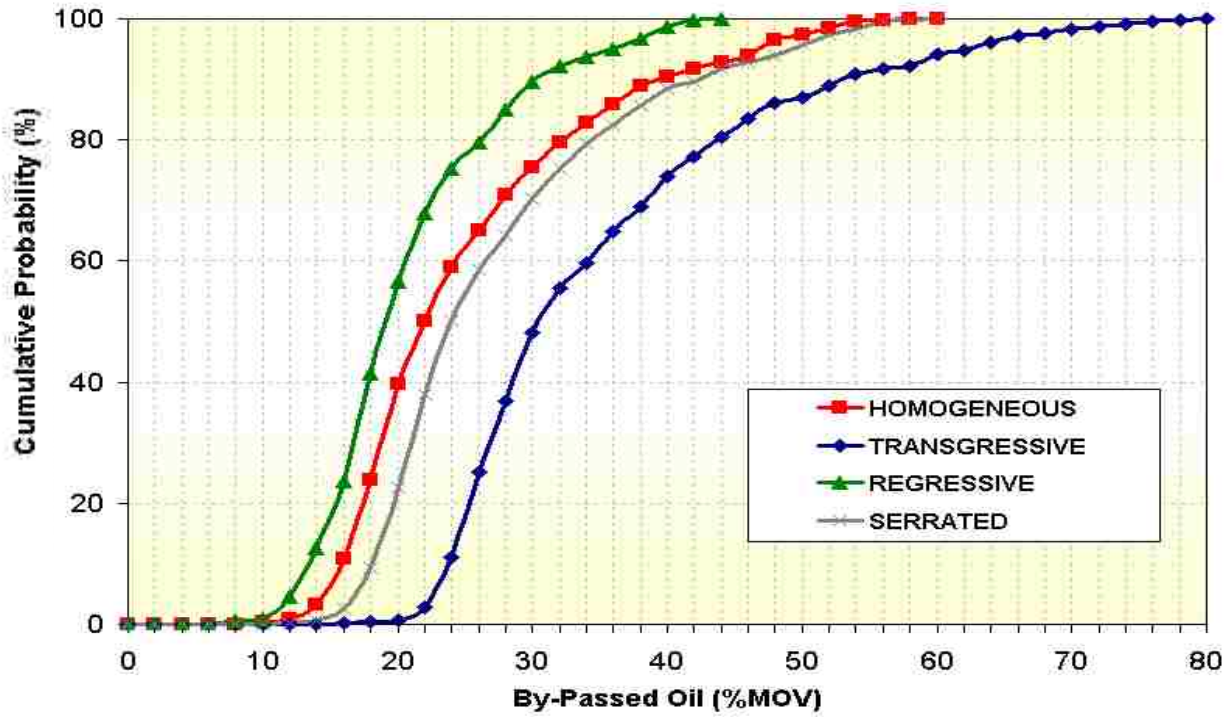

Figure 69: Cumulative Probability of Oil Bypassing at Abandonment for Edge-Water Systems Showing the Effect of Vertical Permeability Distribution for M>10

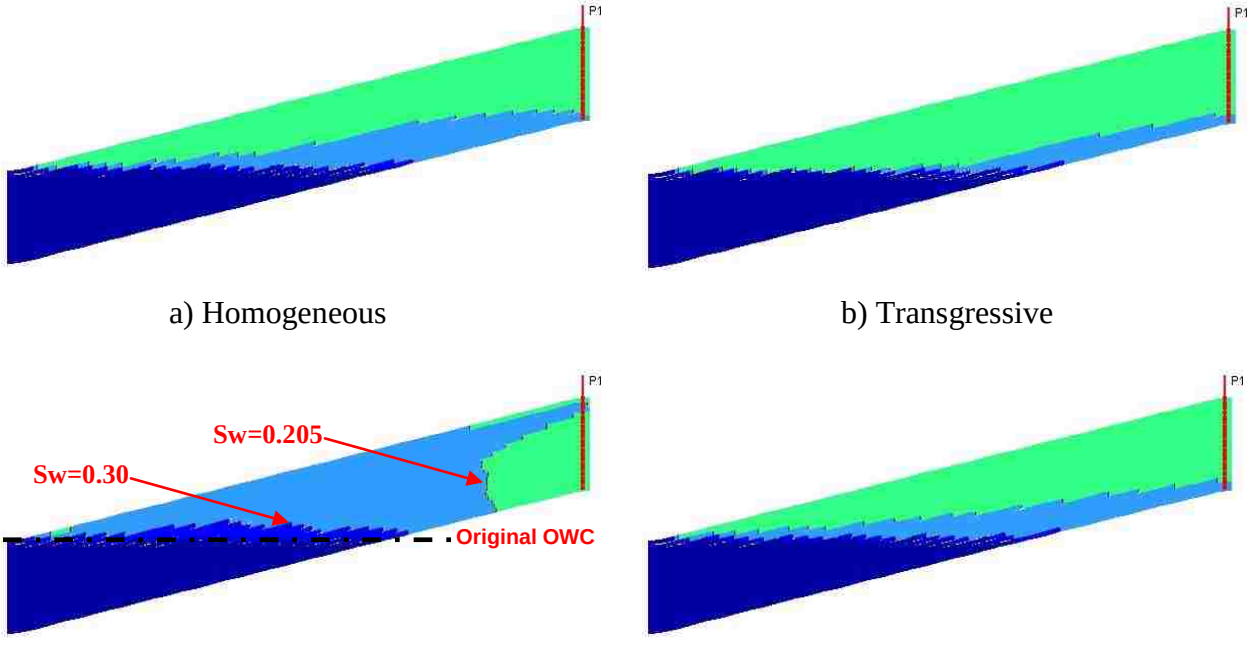

a) Homogeneous

b) Transgressive

c) Regressive

d) Serrated

Figure 70: Position of Water Saturation Isosurfaces at Water Breakthrough for the Different Sequences

4.1.8 Effect of Aquifer Strength

Petroleum reservoirs are often in contact with an aquifer that provides water influx. As the reservoir is produced, water encroaches into the producing reservoir and tends to support the reservoir pressure. Estimating the behavior of the associated aquifer is vital to proper reservoir management.

Reservoir/aquifer systems are typically classified on the basis of flow geometry as either bottom-water or edge-water drive. The rate of water influx is affected by the size, shape and flow properties of the aquifer. For optimal oil recovery in both systems, water must breakthrough at the wellbore after much oil has been displaced and produced. Too early breakthroughs will cause oil to be bypassed, thus reducing the oil recovery. Often, the strength of the water drive is not known initially because very few wells are drilled into the water zone.

This section assesses the effect of aquifer strength on oil recovery/bypassing for an edge-water drive system. As indicated before, the influx of water to the reservoir has been modeled using a "Fetkovich" analytical aquifer. Aquifer strength has been defined by changing the ratio of the external aquifer radius (R_{aq}) to the reservoir external radius (R_o). Three different aquifer strengths have been considered: infinite (R_{aq}/R_o = 100,000), moderately strong (R_{aq}/R_o = 100) and weak (R_{aq}/R_o = 10). Simulation sensitivities have been separated in two groups. First, sensitivities controlled by the liquid production rate. This is, the well is produced at a targeted liquid rate at all times (simulations stop if the maximum drawdown is reached). Second, sensitivities controlled by the minimum bottom hole pressure (BHP), in which the well is produced at its maximum drawdown at all times.

The following properties were used for the aquifer:

- Aquifer thickness = 40 ft (same as reservoir thickness)

- Aquifer porosity = 18% (same as reservoir porosity)
- Aquifer permeability = 500 md.
- Effective reservoir external radius (R_o) = $\sqrt{\text{area of contact aquifer - reservoir/}}$

  $= \sqrt{40 * 625/} = 89.21$ ft.
- Reservoir/aquifer contact angle (radians) = 1 (360 degrees).
- Ratio between the external aquifer radius to the external reservoir radius = $R_{aq}/R_o = 10$ (weak aquifer), 100 (moderately strong aquifer) and 100,000 (infinite aquifer).

Sensitivities Controlled by Maximum Liquid Rate:

Cases Considered

Table 27 shows the matrix of simulation sensitivities considered in this section. A three-level full factorial sensitivity analysis with a total of twenty-seven runs (3^3= 3 levels and 3 factors) was designed to assess the effect of aquifer strength on oil by-passing. The groups considered in the design are the end point mobility ratio (M), the gravity number (G) and the ratio between the external aquifer radius (R_{aq}) to the external reservoir radius (R_o). M and G were calculated using Equations (2.12) and (2.13), respectively. The gravity number (G) and the buoyancy number (N_g) (Table 23) are related as follows:

$$G = N_g \, x \, M \, x \, tan(\alpha) \, x(\, L / H) \quad \text{.....(4.6)}$$

Table 27: Matrix of Simulation Sensitivities: Runs Controlled by Maximum Liquid Rate

M	G	External Aquifer Radius(R_{aq})/External Reservoir Radius (R_o)
0.4	0.15	10
4.0	1.50	100
40.0	15.0	100,000

Results

The results of the experimental design runs are summarized in Table 28 and Figures 71 to 76. The table shows that most of the cases with infinite or moderately strong aquifer support, Cases 1-15, ended at 98% water cut. In other words, there was enough energy to keep the targeted liquid production rates for the entire simulation history. As will be explained later, for these cases water breakthrough, aquifer influx and oil bypassing are mainly a function of the endpoint mobility ratio, M, and the gravity number, G. This is, aquifer strength has little effect on the results. On the other hand, it can be seen that most of the cases with weak aquifer strength, Cases 19 to 25, did not reach water breakthrough by the end of the simulation. Because of their weak pressure support, these cases could not maintain the targeted production rates for long, which caused the simulations to stop before water breakthrough. Table 28 also shows that, in the cases with a gravity number (G) of 15, water breakthrough occurs very late into the production history of the well. This is because high gravity numbers are associated with low production rates (Equation 2.13) and, therefore, the displacement of oil by water is very slow.

Figure 71 shows cumulative water influx for each case. It seems that the development of water influx with time (water influx rate) is mainly a function of the gravity number, G (which is defined here by changes in the liquid rate): the cases with the lowest gravity numbers (highest rates) show faster influx of water with time. This is simply suggesting that the aquifer influx rate is mainly defined by the liquid production rate. It can also be seen that all the cases with G=0.15 fall on the same line. The same happens for G=1.5. For G=15; however, it can be noticed that there are three different lines defining the aquifer influx rate. There may be two explanations for this behavior. First, the effect of aquifer strength on the aquifer influx rate may only be important at high G's (low production rates). Second, there may be some impact of the end-point mobility

ratio on the aquifer influx rate for moderately strong and weak aquifers.

Table 28: Effect of Aquifer Strength: Runs Controlled by Maximum Liquid Rate

Case #	M	G	R_{aq}/R_o	Breakthrough Time (days)	Maximum Water Cut at Abandonment (%)	Total Aquifer Influx at Abandonment (bbls)	Bypassed oil at Abandonment (%)
1	0.40	0.15	100,000	2,248	98.00	769,584	0.20
2	0.40	1.5	100,000	21,038	98.00	778,513	0.00
3	0.40	15	100,000	207,822	98.00	811,749	0.00
4	4.0	0.15	100,000	520	98.00	2,717,000	1.62
5	4.0	1.5	100,000	6,078	98.00	1,893,780	1.19
6	4.0	15	100,000	170,910	98.00	1,362,490	0.01
7	40	0.15	100,000	129	98.00	8,069,030	25.72
8	40	1.5	100,000	1,162	98.00	8,416,460	14.59
9	40	15	100,000	15,004	98.00	4,271,250	6.94
10	0.40	0.15	100	2,248	98.00	766,462	0.21
11	0.40	1.5	100	20.972	98.00	771,316	0.00
12	0.40	15	100	207,457	98.00	1,222,590	0.00
13	4.0	0.15	100	520	98.00	2,704,650	1.50
14	4.0	1.5	100	6,078	98.00	1,887,920	1.09
15	4.0	15	100	170,291	98.00	2,161,410	0.16
16	40	0.15	100	129	97.34	6,046,030	32.36
17	40	1.5	100	1,164	97.12	6,339,110	24.01
18	40	15	100	15,009	96.14	6,370,080	11.00
19	0.40	0.15	10	not reached	0.00	62,468	89.64
20	0.40	1.5	10	not reached	0.00	63,057	90.92
21	0.40	15	10	not reached	0.00	62,745	91.26
22	4.0	0.15	10	not reached	0.00	57,518	92.41
23	4.0	1.5	10	not reached	0.00	62,704	91.43
24	4.0	15	10	not reached	0.00	62,868	91.13
25	40	0.15	10	not reached	0.00	9,329	98.10
26	40	1.5	10	1,184	47.74	60,702	92.99
27	40	15	10	8,100	18.96	62,328	91.75

On the other hand, Table 28 shows that the total aquifer influx volume for the cases that produced until 98% water cut seems to be a strong function of the end-point mobility ratio, M. For example, the largest aquifer influx volumes were found for the cases with the highest

mobility ratios. This suggests that total aquifer influx is directly related to the shape of the oil-water interface, which is mainly defined by M. Because of their weak aquifer support, Cases 16 to 27 were not able to produce until 98% water cut and, therefore, it is difficult to draw conclusions about the effect of the viscous and gravity forces on these cases.

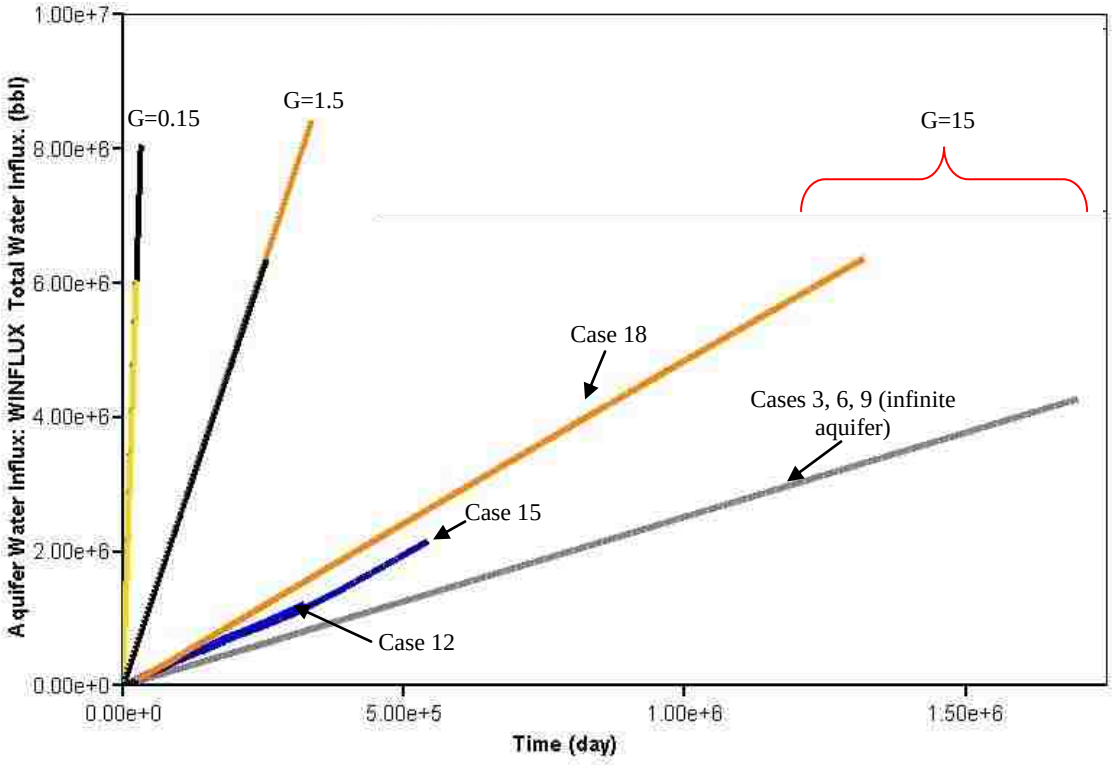

Figure 71: Aquifer Water Influx for Runs Controlled by Maximum Liquid Rate

Figure 72 shows the development of water cut in time for the cases considered in this section. A logarithmic scale was used for the X axis to improve the visualization of the results. As expected, water breakthrough time showed to be inversely proportional to the end-point mobility ratio (M) and directly proportional to the gravity number (G). This is obviously because high endpoint mobility ratios normally result in thin and long water tongues, whereas high

gravity numbers tend to stabilize the oil/water interface.

Figure 72 also shows that no water breakthrough was reached at the end of the simulation for Cases 19 to 25. Since aquifer support for these cases is weak, the reservoir pressure falls dramatically shortly after the beginning of production. This originates a small pressure drawdown and increasing difficulty to sustain the targeted liquid production rates (and keep the well open) for long enough to obtain water breakthrough. Cases 26 and 27 also have weak aquifer support. However, these cases have a high endpoint mobility ratio, which promotes unstable displacement and water invasion. This is why Cases 26 and 27 showed water breakthrough, contrary to Cases 19 to 25.

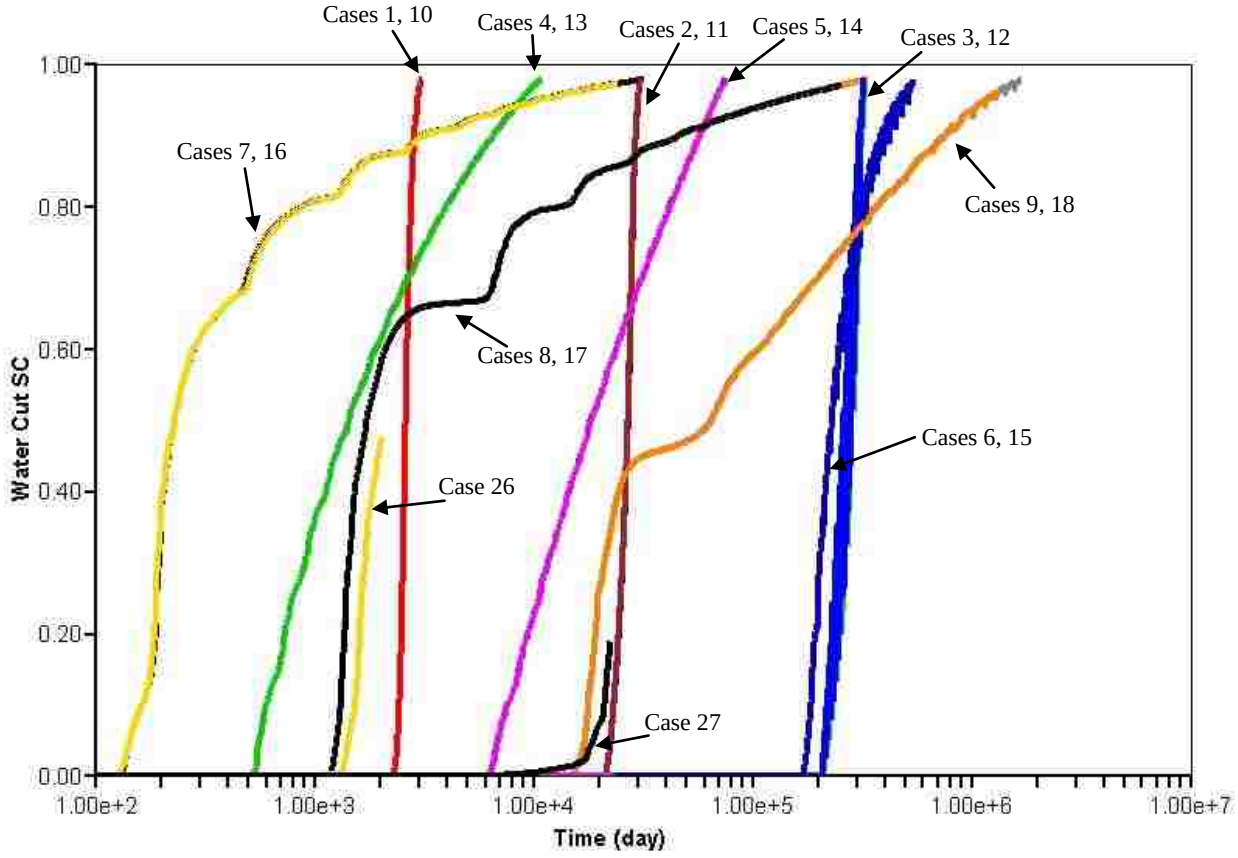

Figure 72: Water Cut vs. Time for Runs Controlled by Maximum Liquid Rate

For the cases that ended at 98% water cut (Cases 1 to 15), it can be seen that the shape of water cut development with time is mainly defined by the endpoint mobility ratio, M. For example, the cases with the highest M (M=40) show "lazier" development of water cut with time than the cases with the lowest M (M=0.4). This confirms the findings of previous studies (Hernandez and Wojtanowicz, 2006). These results also show that water cut is very much independent of the degree of aquifer strength. On the other hand, the development of water cut with time obtained in Cases 26 and 27 remains unexplained even though it is suspected that these two cases show some influence of aquifer strength on water cut development.

Figure 73 shows the recovery factor, expressed as a percentage of the movable oil volume (%MOV), for all 27 cases. It was found that, in the cases that ended at 98% water cut, recovery factor was very much a function of the endpoint mobility ratio, M and the gravity number, G. In other words, recovery is practically independent of the aquifer strength. For example, the cases with the highest M (M=40) and lowest G (G=0.15) resulted in lower recoveries and more oil bypassing than the cases with the lowest M (M=0.4) and highest G (G=15). The reason for this behavior has been explained in previous studies (Hernandez and Wojtanowicz, 2006) and is related to the stability of the oil-water interface. Regarding the cases with weak aquifer strength (Cases 19-27), it seems that each one of them follows the same recovery rate than the equivalent case (case with same M and G) with moderately strong or infinite aquifer strength. However, because the cases with weak aquifer strength cannot maintain the targeted production rates for long (low energy/pressure), they stopped before 98% water cut (and in many cases before breakthrough), which resulted in low recovery and substantial bypassing, up to 98.1% for Case 25, as can be seen in Table 28.

Oil recovery vs. cumulative liquid production for all 27 cases can be seen in Figure 74.

This type of plot gives an indication of the displacement efficiency. It can be seen that cases with the same end-point mobility ratio, M, and gravity number, G, fall within the same displacement efficiency line. This suggests that displacement efficiency is mainly a function of the shape of the water tongue and, therefore, it is independent of aquifer strength.

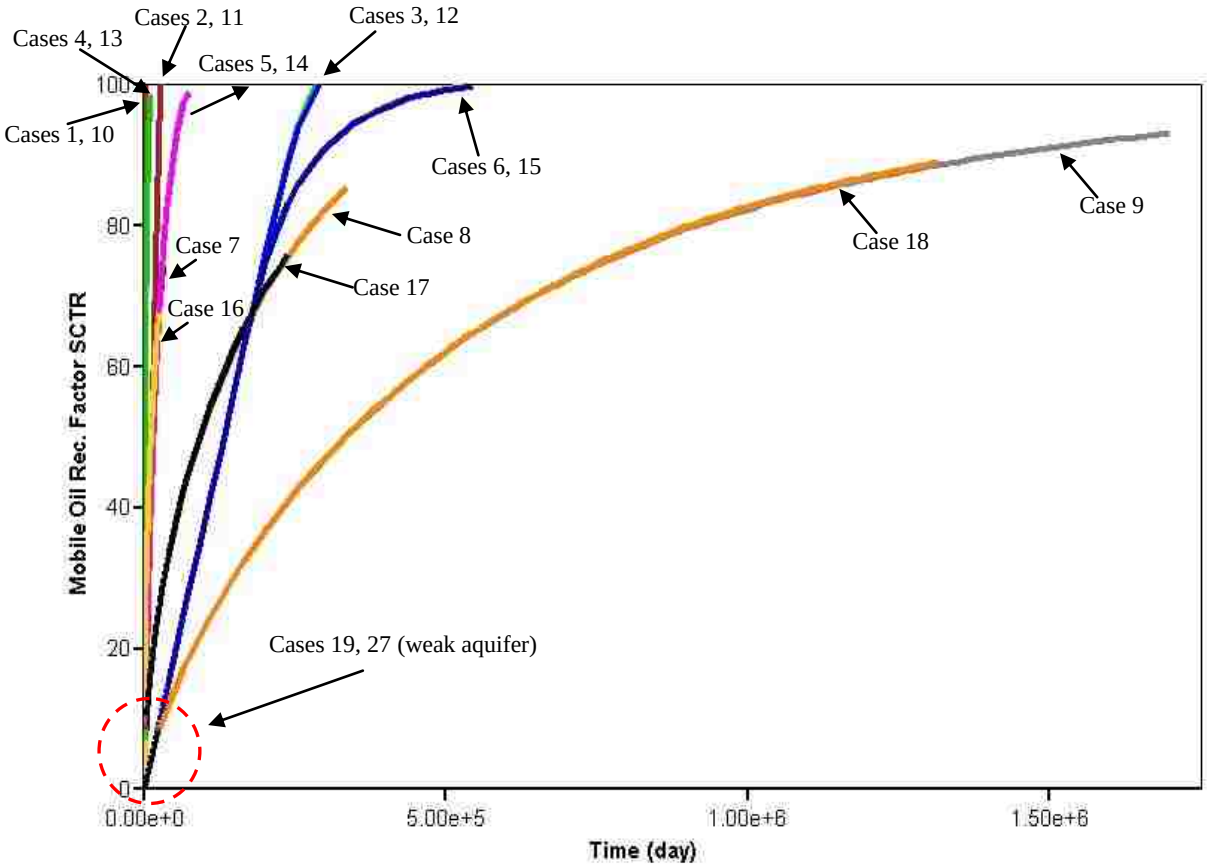

Figure 73: Oil Recovery vs. Time for Runs Controlled by Maximum Liquid Rate

Figure 74 also shows that the gravity number (G), which is defined in this study by changes in the liquid production rate, is not important for the cases with the lowest endpoint mobility ratio (M=0.4, Cases 1,2,3,10,11,12). In other words, for M=0.4 the displacement efficiency is independent of the liquid production rate. A possible explanation for this behavior may be the fact that all the cases with M=0.4 are stable displacement cases (see Equation (2.16)).

This is, the oil-water interface is approximately a straight line. On the other hand, there is a significant effect of the gravity number, G, for M=4 and M=40. Moreover, it can be seen that the best displacement efficiencies are obtained in the cases with the highest gravity numbers. This is because high gravity numbers tend to stabilize the oil-water interface. It can also be seen that the cases with the weak aquifer (Cases 19-27), ended at lower recoveries than the cases with the infinite aquifer. As explained before, this is because the weak aquifer is not able to sustain the targeted rates. Therefore, it is difficult to identify if Cases 19-27 fall within the same displacement efficiency curves than their equivalent cases (cases with same M and G) with stronger aquifer strength.

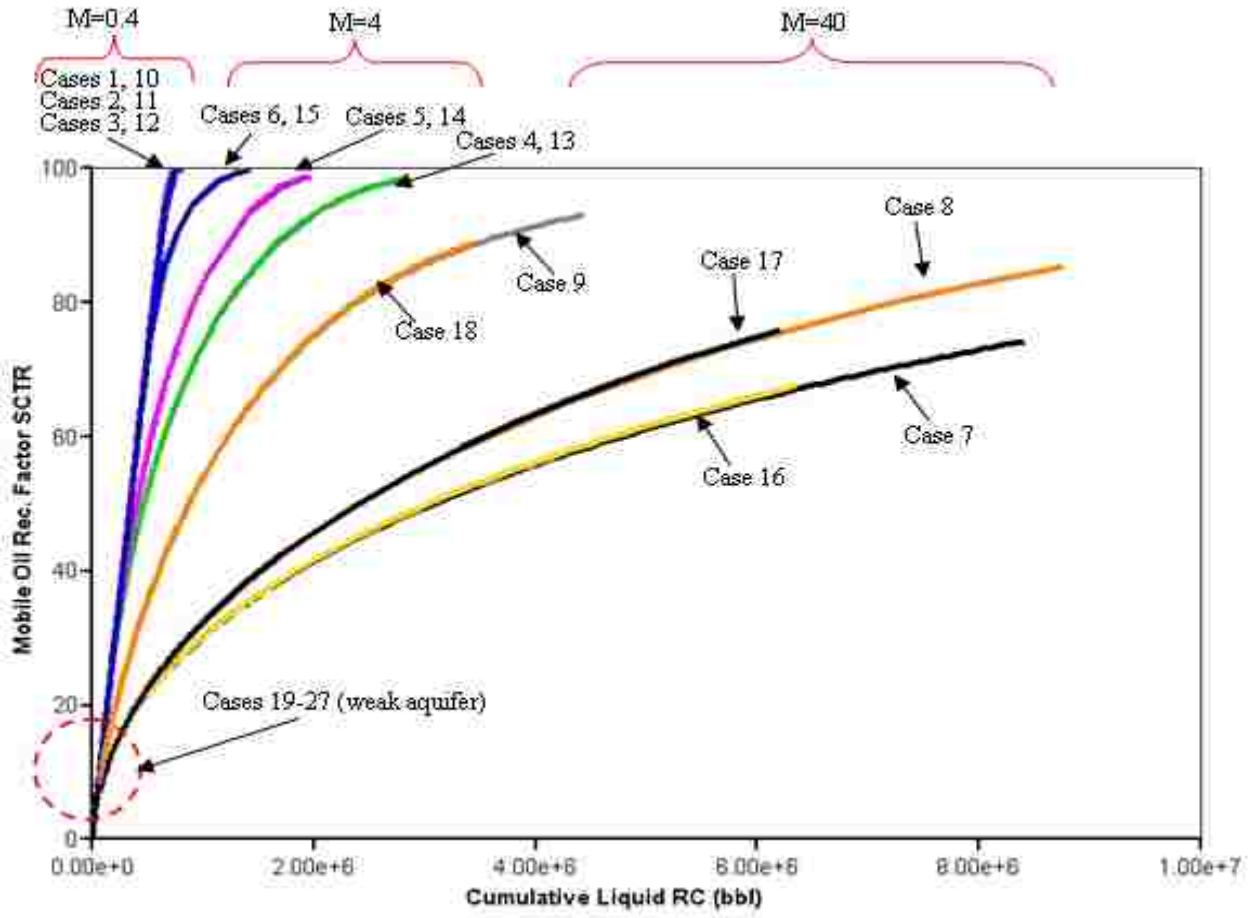

Figure 74: Oil Recovery vs. Cumulative Liquid for Runs Controlled by Maximum Liquid Rate

Figure 75 presents the average reservoir pressures for Cases 1-27. It can be seen that the average pressure is more or less sustained for the cases with infinite aquifer strength. For the cases with moderately strong and weak aquifer strength; however, it can be seen that the pressure depletion rate can be significant. In fact, in most of the cases with weak aquifer strength the average reservoir pressure fell below the minimum bottom-hole pressure after only a few years of production. Also, it was observed that the cases with weak and moderately strong aquifers show a pressure depletion rate that is a function of the liquid production rate: higher liquid production rates resulted in more pressure depletion.

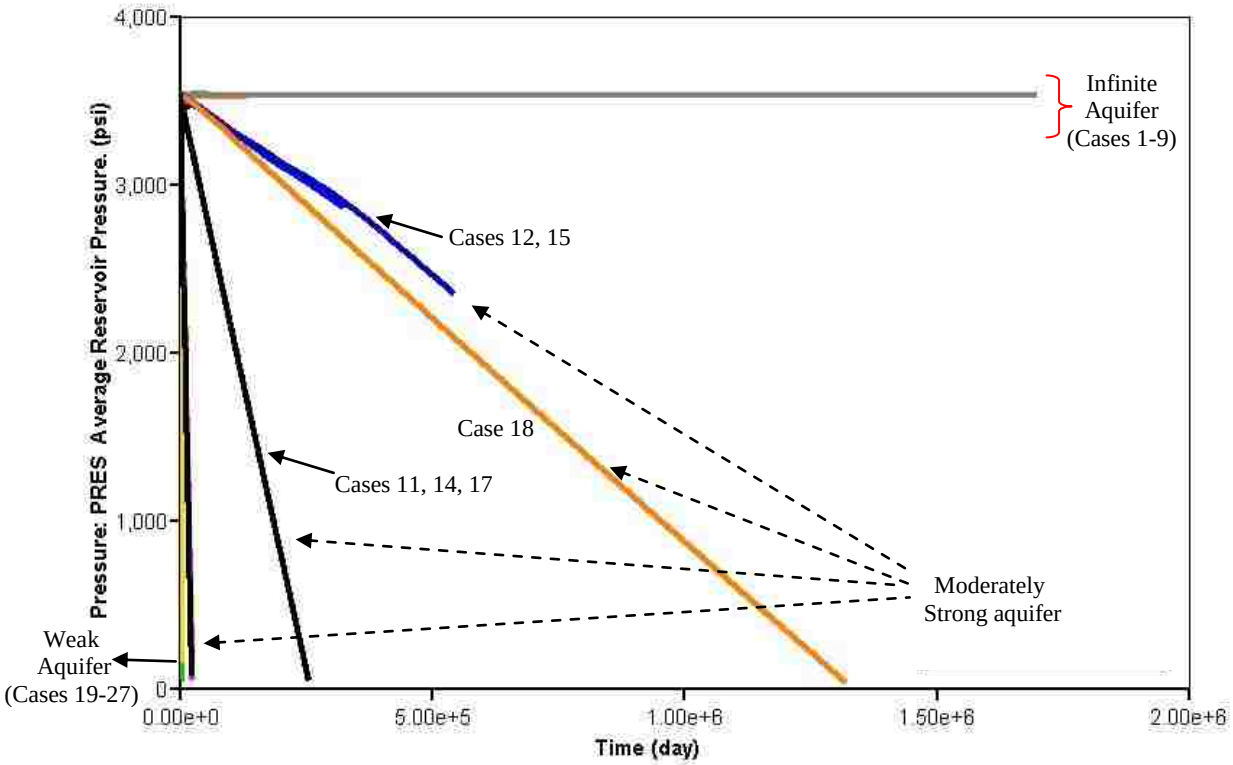

Figure 75: Average Reservoir Pressure vs. Time for Runs Controlled By Maximum Liquid Rate

Figure 76 displays average pressures vs. recovery factor for some selected cases (Cases 3, 4, 7, 12, 13, 16, 21, 22 and 25). It is clear that the cases with stronger aquifer support generally

give more recovery. However, as indicated before, this effect of aquifer strength on recovery is caused by the fact that the reservoir pressure is depleted and, therefore, the well does not have enough energy to continue producing. In other words, aquifer strength has very little effect of the shape of the oil-water interface and water invasion. To confirm this observation one more time, the reader may compare the recovery factor for Cases 3 and 12. These cases have different aquifer strength, but because the reservoir pressure is high enough to continue recovery until 98% water cut, they show about the same recovery. The same situation occurs for Cases 4 and 13. For Cases 7 and 16, however, the situation is different: Case 16 does not have enough pressure support to continue producing until 98% water cut and, therefore, it results in lower recovery than Case 7.

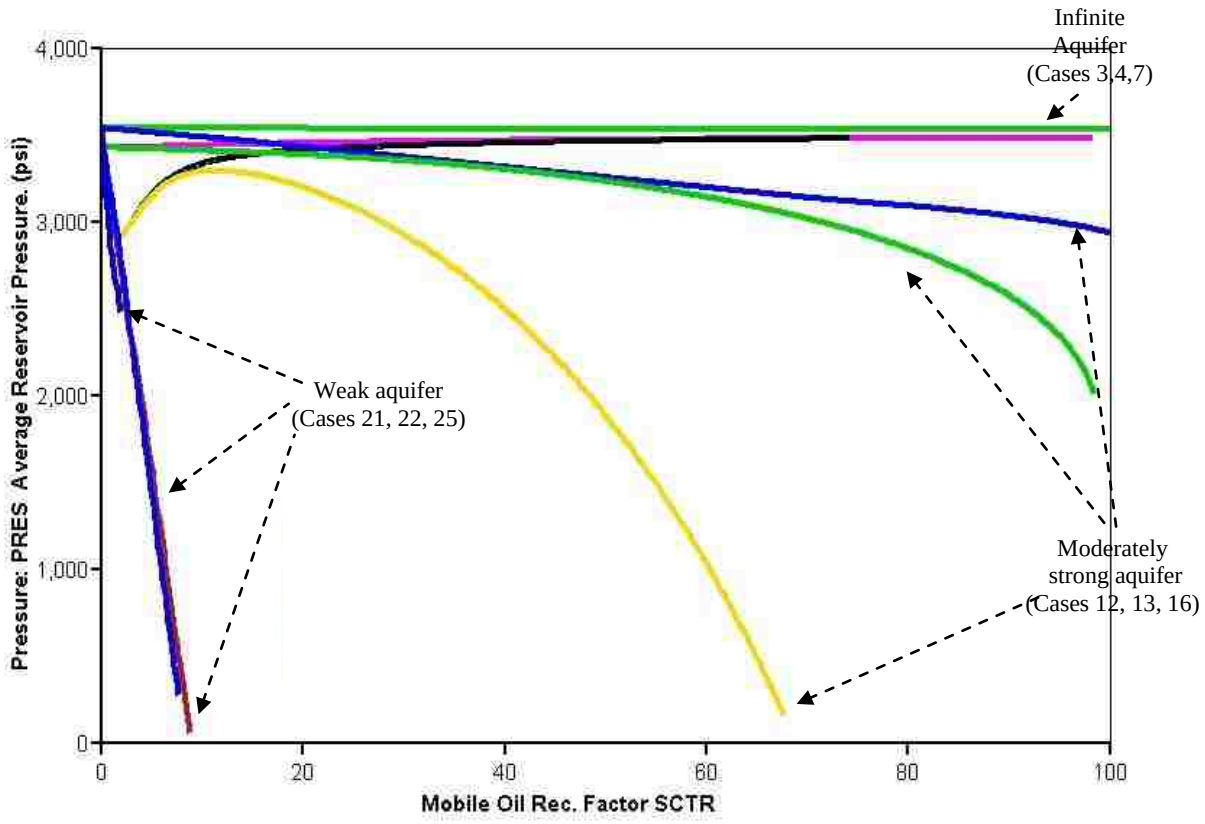

Figure 76: Average Reservoir Pressure vs. Recovery Factor for Runs Controlled By Maximum Liquid Rate

Sensitivities Controlled By Minimum Bottom Hole Pressure

Cases Considered

Table 29 shows the matrix of simulation sensitivities considered in this section. A three-level full factorial sensitivity analysis with a total of nine runs (3^2= 3 levels and 2 factors) was designed to assess the effect of aquifer strength on oil by-passing. Table 29 is equivalent to Table 28 but, since in this section the well is producing at the minimum bottom hole pressure (maximum drawdown), it will deliver at its maximum possible liquid rate. Therefore, no constraints on the liquid rate are needed in this section and no calculation of the dimensionless gravity number, G, is required (G assumes a constant liquid rate).

Table 29: Matrix of Simulation Sensitivities:
Runs Controlled by Minimum Bottom Hole Pressure

M	External Aquifer Radius(R_{aq})/External Reservoir Radius (R_o)
0.4	10
4.0	100
40.0	100,000

Results

Table 30 summarizes the results for the runs considered in this section. It can be seen that breakthrough time occurred in less than 106 days for all the cases except Cases 19-B and 22-B. This is because most of the cases started production at very high rates. It can also be seen that, except for the cases with weak aquifer, aquifer influx is very much a function of the endpoint mobility ratio, M. The higher the endpoint mobility ratio, the larger the cumulative amount of water that flows into the reservoir. Table 30 also shows that oil bypassing at the end of the simulation is also a function of the end-point mobility ratio, M: the higher the M the larger the amount of by-passed oil.

Table 30: Effect of Aquifer Strength: Runs Controlled by Minimum Bottom Hole Pressure

Case #	M	R_{aq}/R_o	Breakthrough Time (days)	Maximum Water Cut at Abandonment (%)	Total Aquifer Influx at Abandonment (bbls)	Bypassed oil at Abandonment (%)
1-B	0.40	100,000	54.62	98.00	827,273	0.74
4-B	4.00	100,000	62.07	98.00	2,719,780	2.67
7-B	40.00	100,000	100.08	98.00	7,635,680	26.84
10-B	0.40	100	54.53	98.00	833,270	0.69
13-B	4.00	100	62.07	98.00	2,715,490	2.55
16-B	40.00	100	105.82	97.45	6,362,410	31.04
19-B	0.40	10	not reached	0.00	63,262	87.44
22-B	4.00	10	not reached	0.00	63,255	88.43
25-B	40.00	10	155.00	53.85	63,202	91.63

Figure 77 shows the cumulative volume of water influx obtained for the cases considered in this section. As indicated before, it can be seen that for the infinite and moderately strong aquifers the total water influx is a strong function of M. The cases with the highest mobility ratio (Cases 7-B and 16-B, M=40), show the largest total aquifer influx volume. It can also be seen that cases with the same M show similar aquifer influx rates during the first years of the simulation. This suggests that the effect of aquifer strength, represented here as the ratio between the external aquifer radius (R_{aq}) to the reservoir external radius (R_o), is not important at early times, but it gains importance at late times. This is especially evident for the cases with high M (7-B and 16-B). Cases 19-B, 22-B and 25-B show very little water influx. This is because the aquifer in these cases is weak (these cases ended before 98% water cut).

Figure 78 shows the development of water cut in time for the cases shown in Table 30. In the previous section, in which the well was produced at a constant maximum liquid rate, the time of water breakthrough was inversely proportional to the endpoint mobility ratio, M. It is known that this is because high endpoint mobility ratios generally result in thin and long water tongues (Hernandez, Wojtanowicz and White, 2006). For the cases analyzed in this section; however,

water breakthrough showed to be directly proportional to M (at least for the cases with infinite and moderately strong aquifer strength). The cases with low M are able to produce at higher initial rates and, therefore, they are able to "pull" water from the aquifer at a higher rate in the early days of simulation. This can be confirmed by reviewing Figure 77.

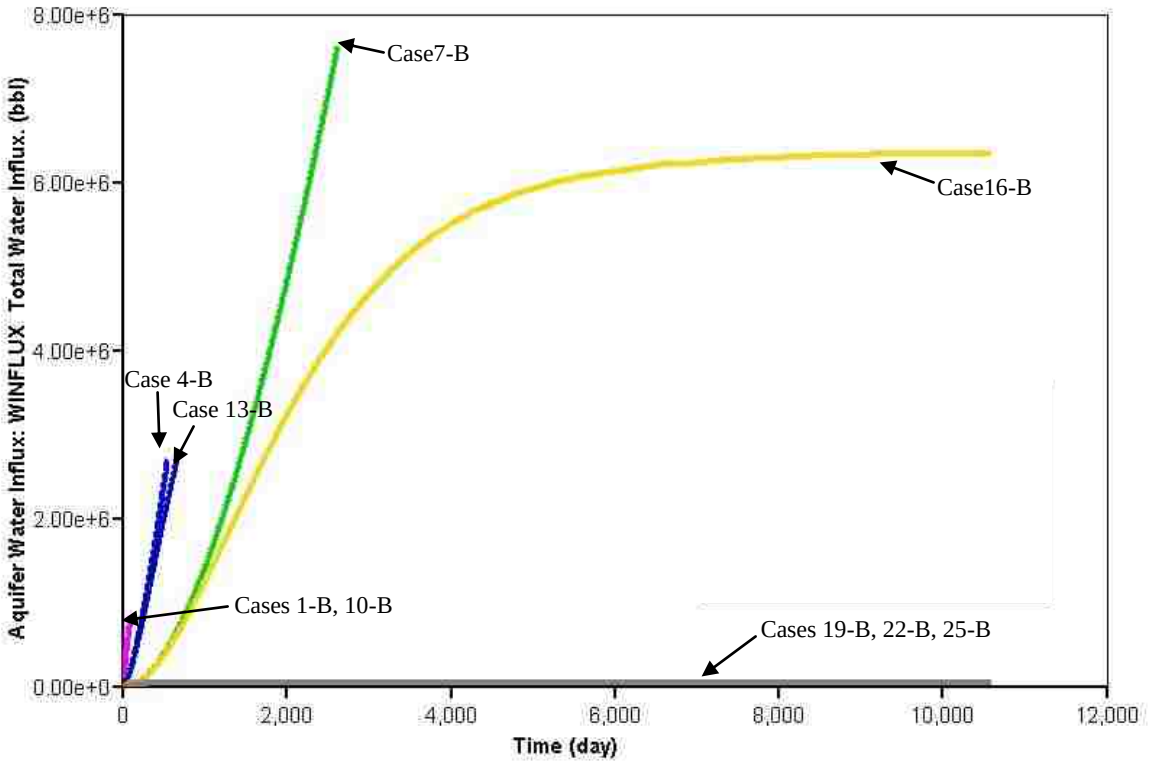

Figure 77: Aquifer Water Influx for Runs Controlled by Minimum BHP

Figure 78 also shows that no water breakthrough was reached at the end of the simulation (30 years) for Cases 19-B and 22-B. Because of their low mobility ratio, these two cases started producing at high liquid rates. However, since the aquifer support for these cases is weak, the reservoir pressure and liquid rates felt dramatically shortly after the beginning of production, which resulted in no water breakthrough at the end of the simulation. For Case 25-B, though, the initial liquid rate was not as high as for Cases 19-B and 22-B. Therefore, pressure did not decline as fast and the liquid rate was sustained for longer times, resulting in an earlier breakthrough.

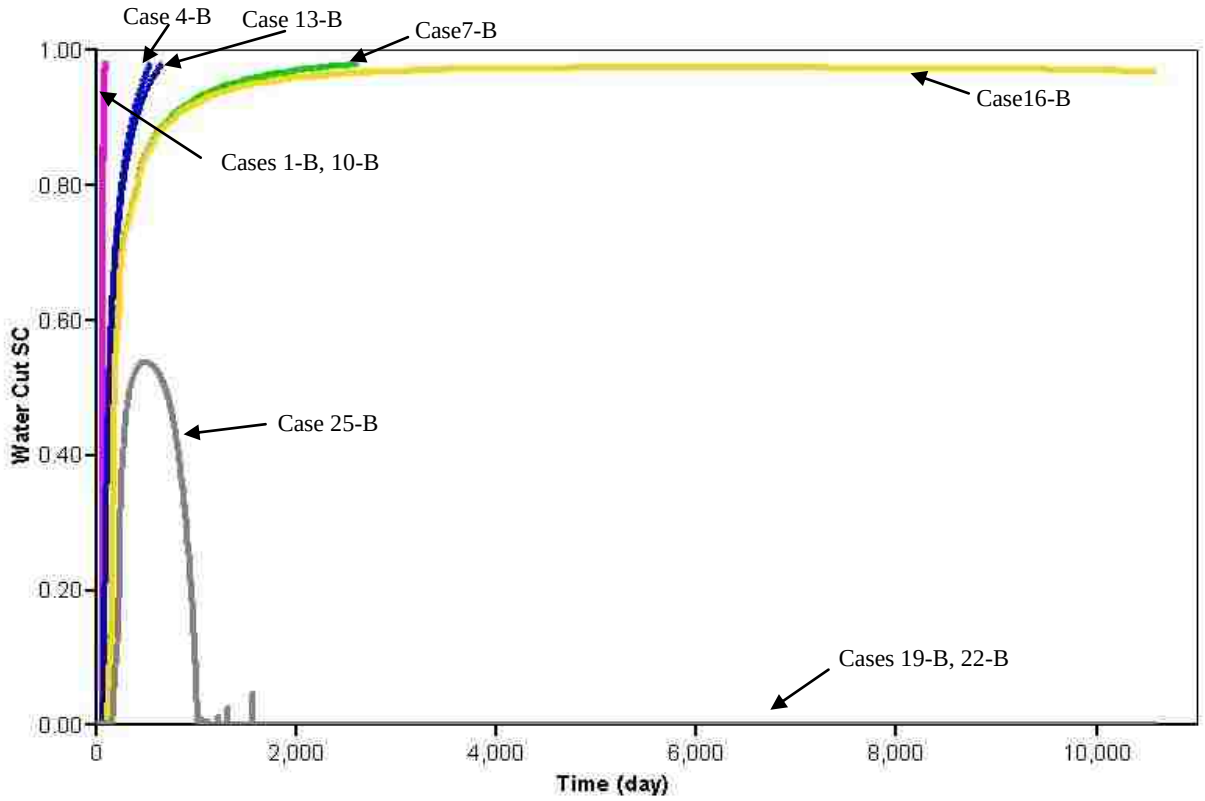

Figure 78: Water Cut vs. Time for Runs Controlled by Minimum BHP

Liquid rates for the nine cases considered in this section are presented in Figure 79. For visualization purposes, only the first 1000 days of production history are plotted. The first comment that can be made is that initial liquid rates are very much a function of the end-point mobility ratio: the smaller the ratio, the higher the initial rate. This also suggests that initial liquid rates are not affected by the degree of aquifer strength. It is also obvious; however, that aquifer strength can have a significant effect on liquid rates at later times. How late mainly depends on the end-point mobility ratio. For high mobility ratios, the aquifer takes more time to respond and its effect is felt at later times than for low mobility ratios.

Figure 80 shows the recovery factor, expressed as a percentage of the movable oil volume (%MOV), for the cases considered in this section. Similar to for the liquid rate, it was

found that recovery factor at very early times is very much a function of the endpoint mobility ratio, M: the cases with the smallest M (M=0.4) resulted in the fastest oil recovery rate. Table 30 and Figure 80 also show that, for the cases that finished at 98% water cut (Cases 1-B, 4-B, 7-B, 10-B and 13-B), the final amount of oil recovered is practically independent of the aquifer strength (final recovery is mainly a function of the endpoint mobility ratio, M). However, because of lack of reservoir energy (well block pressure equals bottomhole pressure shortly after the beginning of the simulation), Cases 16-B, 19-B, 22-B and 25-B stopped before 98% water cut. As it can be seen, this resulted in very little oil recovery and substantial oil bypassing for these four cases.

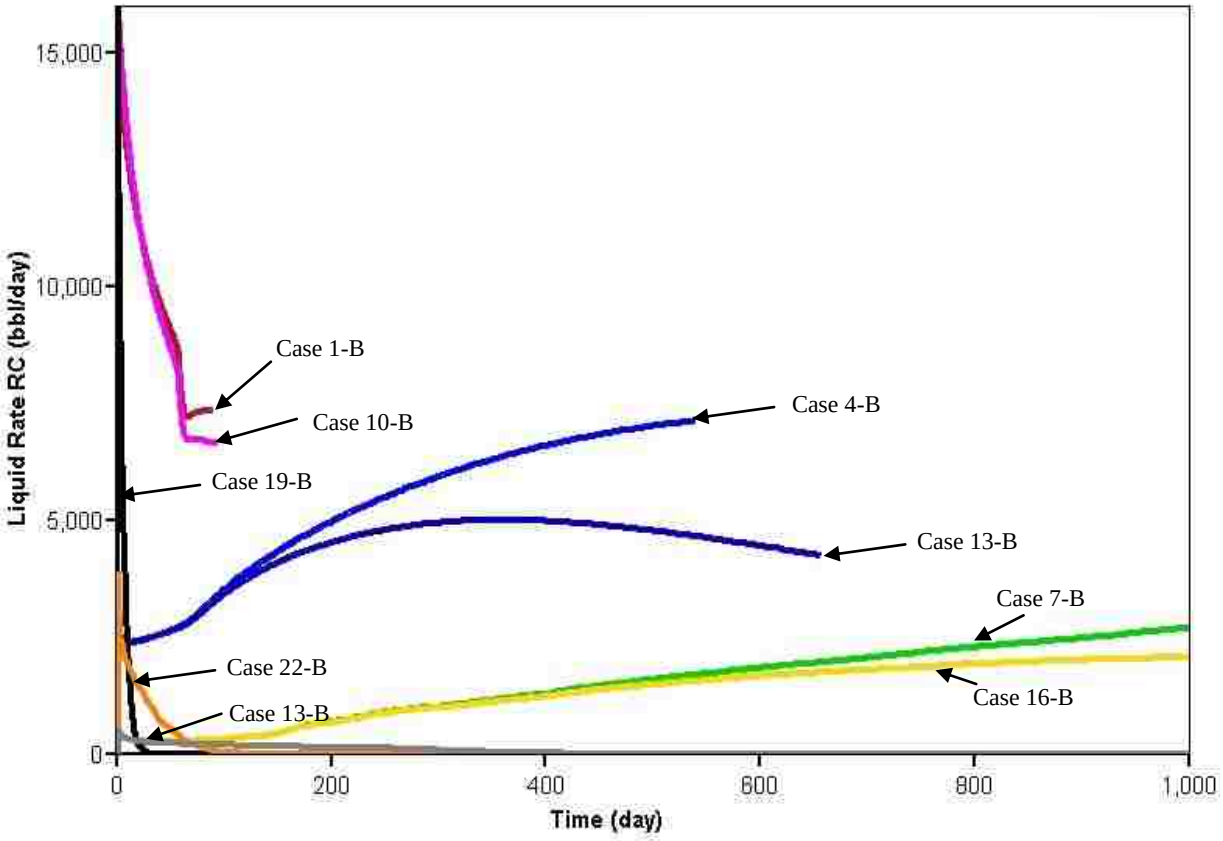

Figure 79: Liquid Rate vs. Time for Runs Controlled by Minimum BHP

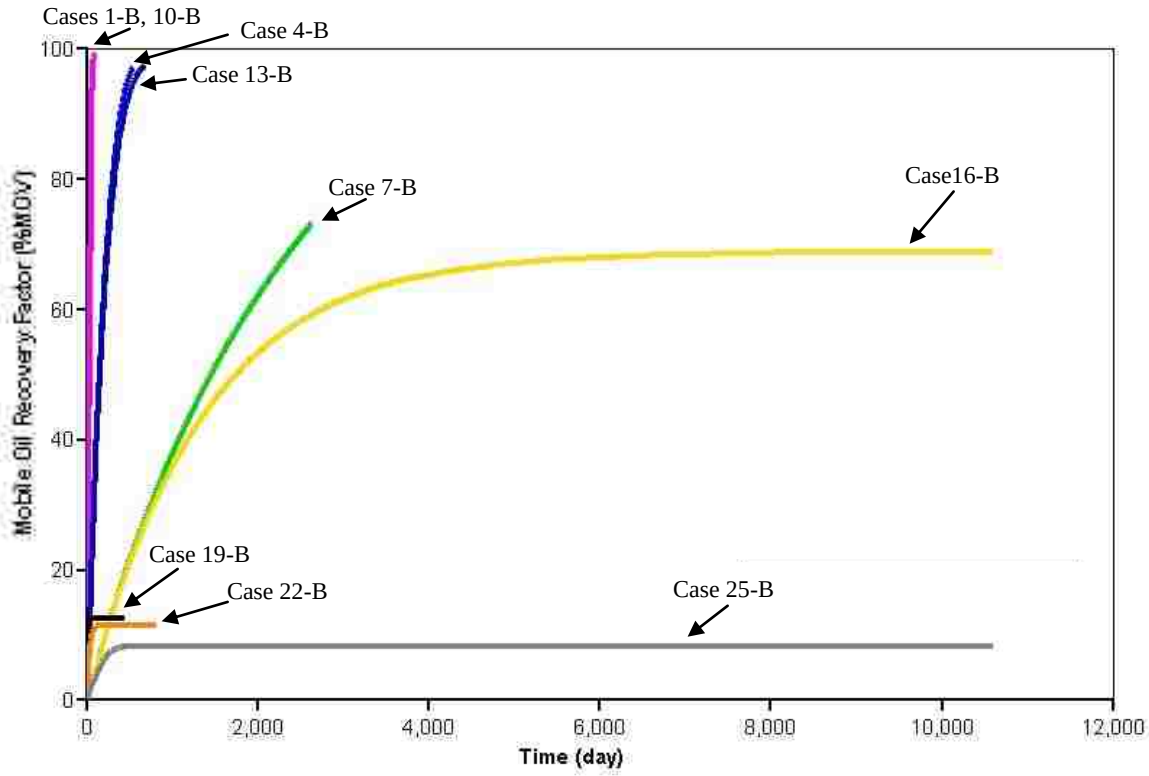

Figure 80: Oil Recovery vs. Time for Runs Controlled by Minimum BHP

Figure 81 shows oil recovery versus cumulative liquid production for all the cases considered in this section. As previously indicated, this plot can be regarded as a plot of displacement efficiency. It can be seen that cases with the same end-point mobility ratio fall within the same displacement efficiency line. These results suggest that displacement efficiency is mainly a function of the shape of the water tongue and, therefore, it is independent of aquifer strength. It can also be seen; however, that the cases with the weak aquifer ended at lower recoveries than the cases with the infinite aquifer. This is because for the weak aquifer the reservoir is not able to sustain the pressure, which results in the well block pressure being equal to the bottom-hole pressure and, therefore, no additional production of fluids.

Figures 82, 83 and 84 are cross sections of the slab model showing the distribution of different water saturation isosurfaces at or before water breakthrough. It can be seen that the

cases with the same end-point mobility ratio show similar shapes of the water tongue. This confirms that the shape of the water tongue is mainly a function of the mobility ratio and, therefore, it is independent of aquifer strength. The least pronounced tongues were obtained for the cases with the lowest mobility ratio, Cases 1-B, 10-B and 19-B. Because these three cases have an end-point mobility ratio smaller than 1, the oil-water interface becomes perpendicular to the bedding as time progresses, leading to low oil bypassing. This has been explained in previous studies (Hernandez and Wojtanowicz, 2006). Cases 19-B and 22-B show different behavior than other cases with their same mobility ratio. This is because water breakthrough was not reached during the simulation and the plotted oil-water interface is in the early stages of its development. Finally, Figures 82, 83 and 84 also show that the most pronounced tongues are obtained for the cases with the largest end-point mobility ratio (Cases 7-B, 16-B, 25-B).

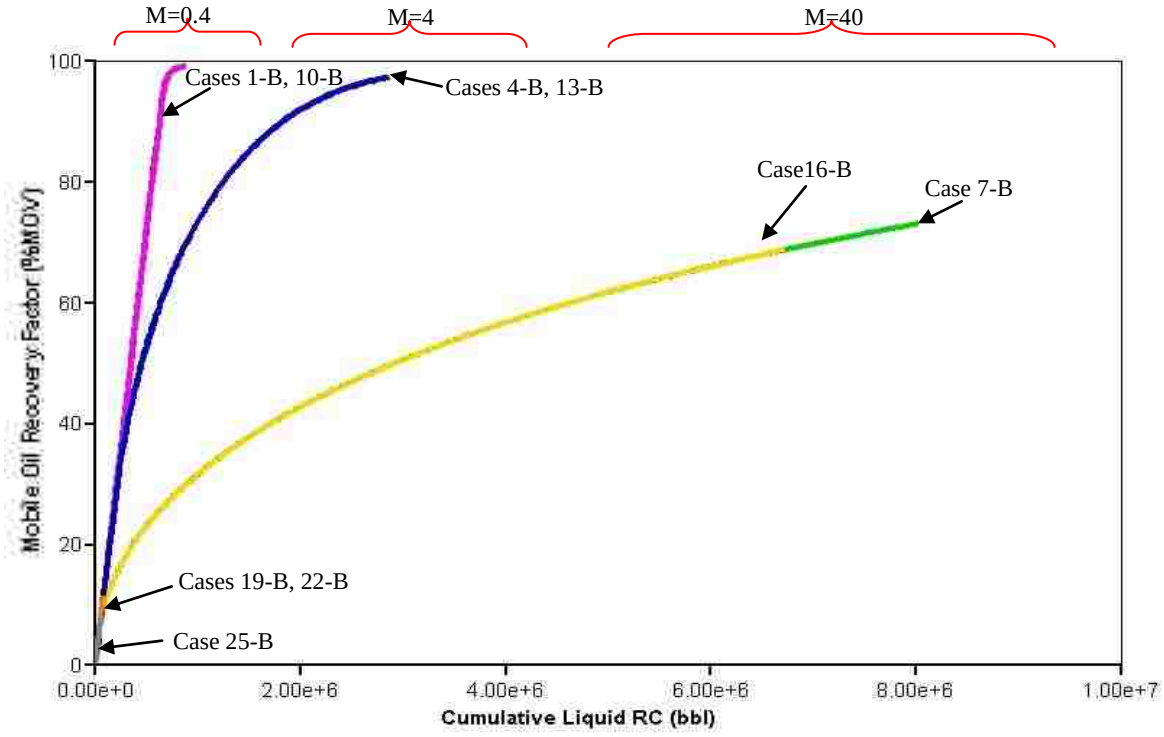

Figure 81: Oil Recovery vs. Cumulative Liquid for Runs Controlled by Minimum BHP

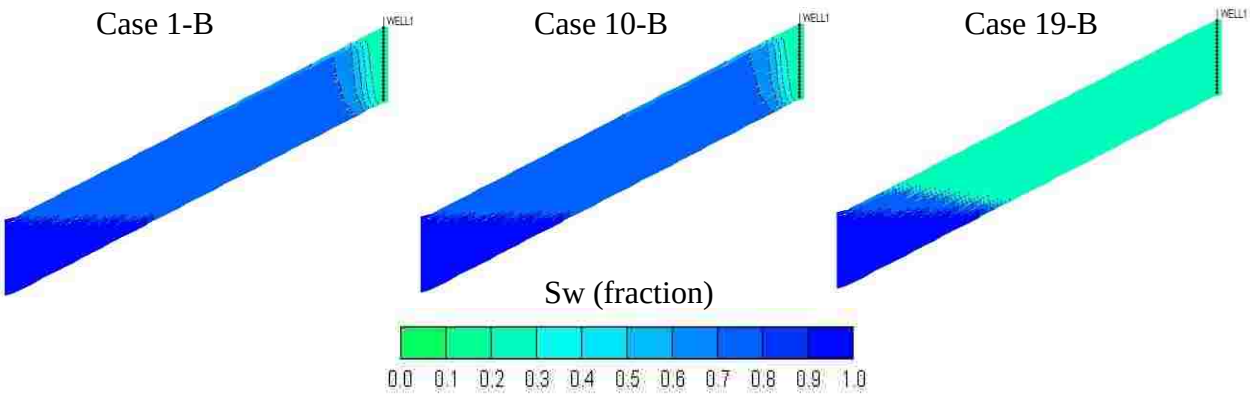

Figure 82: Water Saturation Isosurfaces for Cases 1-B, 10-B and 19-B (M=0.4)

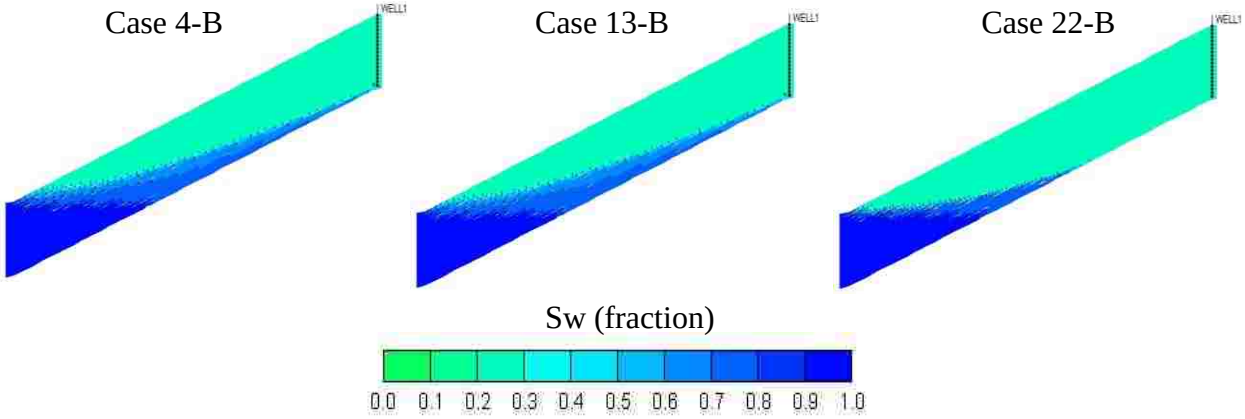

Figure 83: Water Saturation Isosurfaces for Cases 4-B, 13-B and 22-B (M=4)

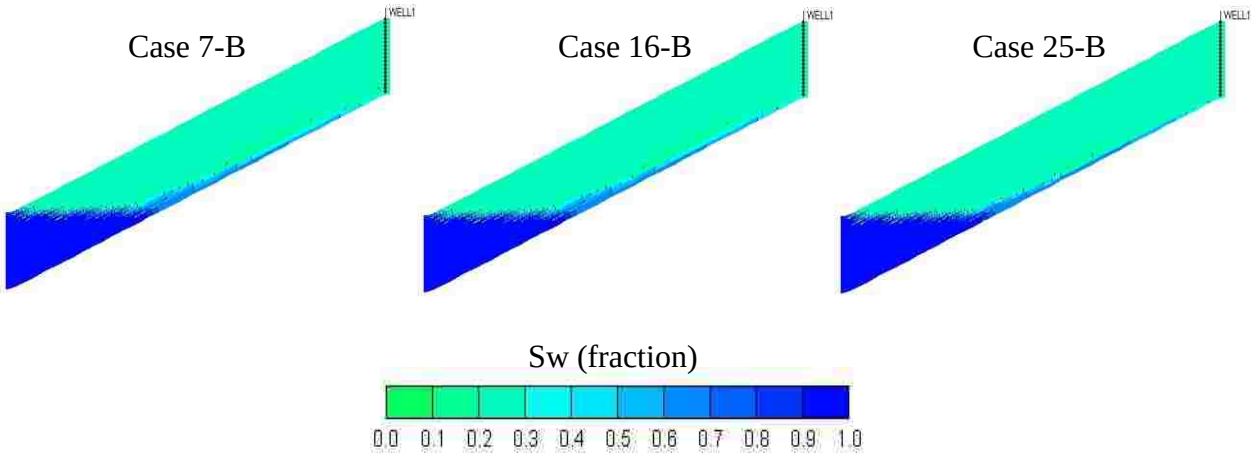

Figure 84: Water Saturation Isosurfaces for Cases 7-B, 16-B and 25-B (M=40)

Figures 85, 86 and 87 show the distribution of different water saturation isosurfaces at the end of the simulation for the cases analyzed in this section. The end of the simulation is defined here as 98% water cut, 30 years of simulation, or the time at which the well block pressure reaches the bottomhole pressure, whichever is first. Again, it can be seen that the shape of the oil-water interface is mainly a function of the end-point mobility ratio. The cases with weak aquifer strength (Cases 19-B, 22-B and 25-B), show different behavior because in these cases the simulation ended before 98% water cut.

In summary, the results presented in this section suggest that aquifer strength controls reservoir pressure and the time at which the simulations end, but it does not control the shape of the oil-water interface. The shape of the oil-water interface is mainly controlled by the end-point mobility ratio, M. The amount of bypassed oil at abandonment for the cases that ended at 98% water cut is a very strong function of the endpoint mobility ratio. Oil bypassing for the other cases is controlled by both aquifer strength and the end-point mobility ratio.

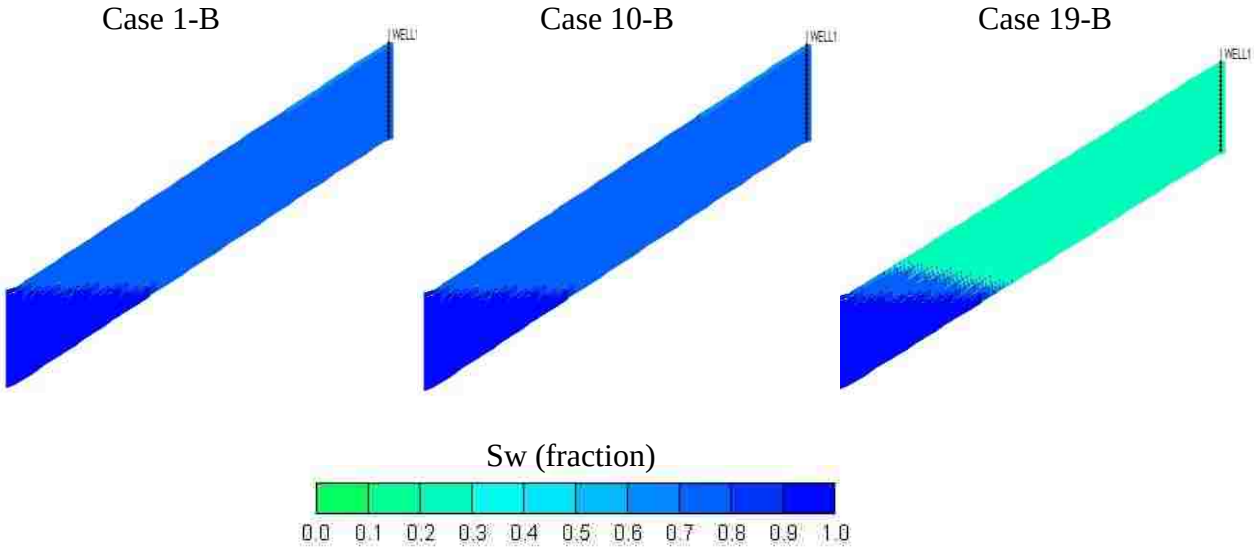

Figure 85: Water Saturation Isosurfaces at End of Simulation for Cases 1-B, 10-B and 19-B (M=0.4)

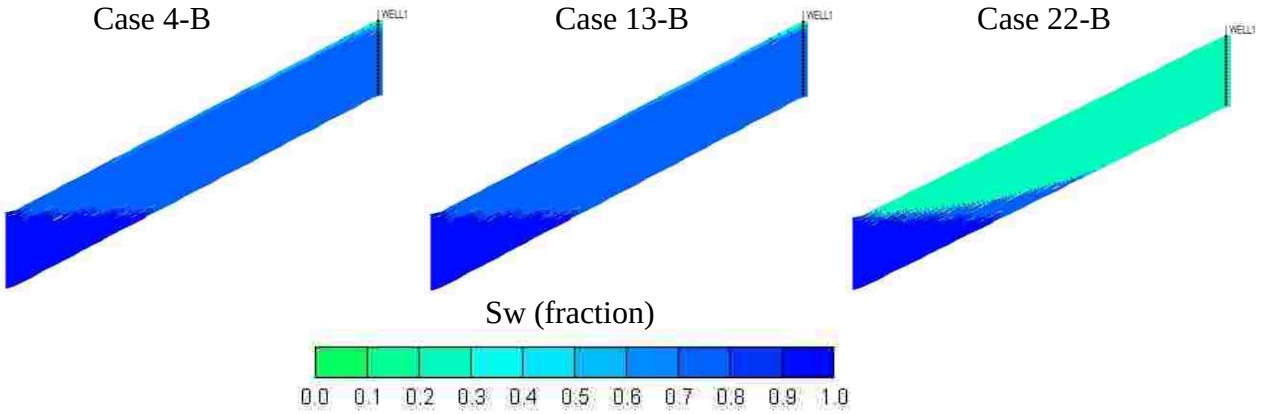

Figure 86: Water Saturation Isosurfaces at End of Simulation for Cases 4-B, 13-B and 22-B (M=4)

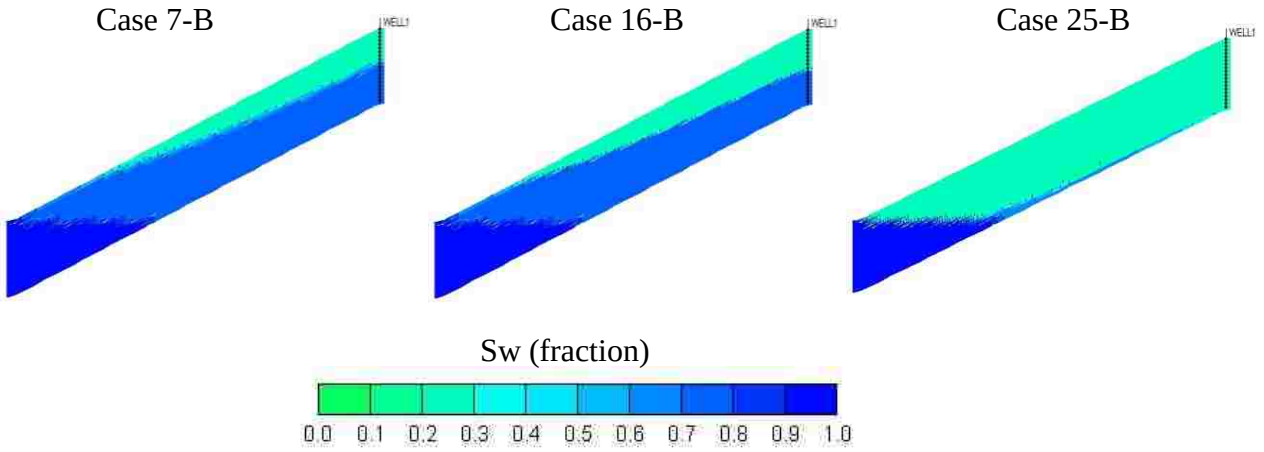

Figure 87: Water Saturation Isosurfaces at End of Simulation for Cases 7-B, 16-B and 25-B (M=40)

Summary

- For the cases that ended at 98% water cut, water breakthrough, aquifer influx and oil bypassing are mainly a function of the endpoint mobility ratio, M, and the gravity number, G. This is, they are almost not affected by the degree of aquifer strength.
- Aquifer strength controls reservoir pressure and the time at which the simulations end, but it does not control the shape of the oil-water interface. The shape of the oil-water

interface is mainly controlled by the end-point mobility factor, M, and also by the gravity number, G.

- The cases with weak aquifer strength exhibited poor pressure support and, therefore, they stopped before 98% water cut. This resulted in low recovery.

4.1.9 Effect of the Shape of the Relative Permeability Curves

The effect of relative permeability curvatures and end point saturations is generally neglected in studies involving dimensionless groups. This is because considering these parameters adds additional groups and complicates the analysis (Shook et al. 1992). Moreover, the Corey Exponents n_w and n_o, which describe the shape of the relative permeability curves, must normally be obtained experimentally. The objective of this section is to study the effect of changing the shape of the relative permeability curves on oil bypassing for edge-water systems. The following equations by Goda and Behrenbruch (2004) were used to obtain the relative permeability curves employed in the simulator:

Water curve equation:

$$k_{rw} = k_{rw}^{'} \left(\frac{S_w - S_{wi}}{1 - S_{wi} - S_{or}} \right)^{n_w} \quad \text{.....(4.7)}$$

Oil curve equation:

$$k_{ro} = k_{ro}^{'} \left(\frac{1 - S_w - S_{or}}{1 - S_{wi} - S_{or}} \right)^{n_o} \quad \text{……...(4.8)}$$

Table 31 shows the effect of the Corey exponents, n_o and $n_{w,}$ on the water breakthrough time and percentage of oil bypassing at breakthrough and at abandonment. The wettability conditions presented in the last column of Table 31 were obtained from Goda and Behrenbrush

(2006). Figure 88 shows the 2D shape of the oil water interface at water breakthrough for the cases presented in Table 31. The results can be summarized as follows:

Table 31: Effect of Relative Permeability Exponents on Oil Bypassing for Edge-Water Systems

Case #	n_w	n_o	BT time (days)	By-Passed Oil at Breakthrough (%MOV)	By-Passed Oil at Abandonment (%MOV)	Comments
1	2	4	9721.8	55.6	15.6	Slightly oil wet
2	4	4	13879.0	36.7	15.6	Intermediate
3	6	4	14924.5	31.9	15.6	Water wet
4	4	2	11371.9	48.1	3.2	Slightly oil wet
5	4	6	11762.0	46.3	30.3	Slightly water wet
6	3	3	11832.4	46.0	7.9	Slightly oil wet
7	2	2	8854.7	59.5	3.0	Slightly oil wet

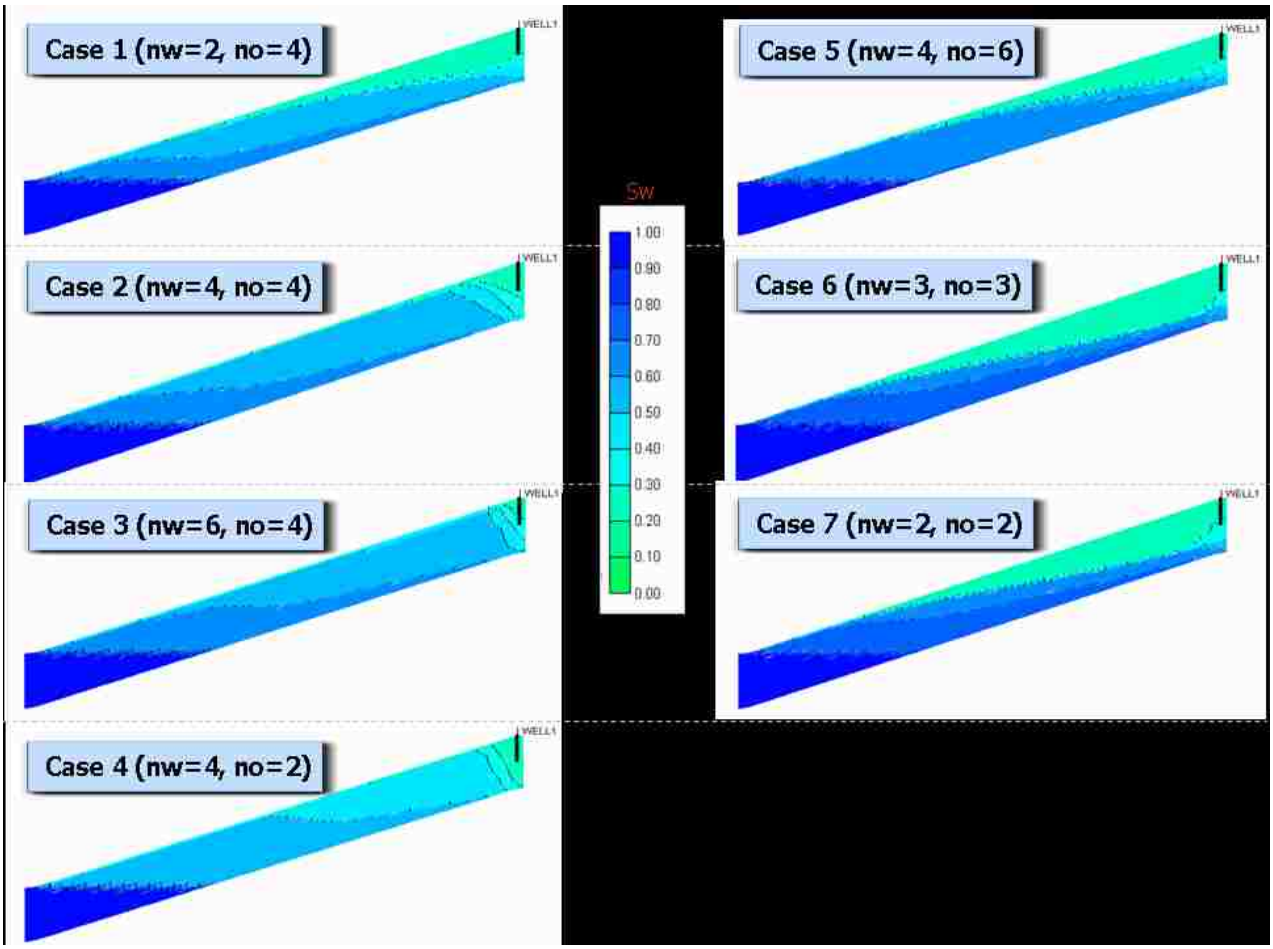

Figure 88: Effect of Relative Permeability Exponents on the Shape of 2D Water Tongue

- The effect of changes in the Corey exponents on water invasion and oil bypassing could be significant. The choice of these exponents not only affects the shape of the water tongue, but also the thickness of the transition zone (separation between water saturation isosurfaces). This important effect should be kept in mind for future sensitivity studies of oil bypassing in edge-water systems.
- High "n_o" and low "n_w" values result in more oil bypassing at abandonment. This is obviously because these conditions originate lower relative permeabilities to oil and higher relative permeabilities to water.
- Changes in the oil exponent "n_o" have a larger effect on oil bypassing at abandonment than changes in the water exponent "n_w".
- For a given n_o, there is more water tonguing for low n_w's (see Figure 88). This is because low n_w's promote fractional flow of water (water fractional flow curves are more shifted to the left, which results in little shock formation and a large mixing zone). A similar effect is obtained if n_o is increased keeping n_w constant.

4.1.10 Effect of Capillary Pressure

Two of the main sources of oil-water mixing in immiscible displacements are fractional flow effects and capillary pressure effects (see Figure 89). Other dissipative phenomena (cause mixing zones to grow faster than or differently from a dissipation free-flow) are fluid compressibility, dispersion, diffusion and thermal conductivity (Lake, 1989). The Buckley-Leverett (B-L) theory indicates that the movement of water in oil-water displacements is characterized by a steep saturation bank, front or shock, followed by additional gradual oil displacement. It is being shown that the shock portion of the displacement becomes more pronounced for low oil-water viscosity ratios (low M's), and less important for high oil-water

viscosity ratios (Lake, 1989). Lake (1989) has also indicated that "shocks are not present in nature since some dissipation (dispersion, diffusion, capillary pressure, compressibility, and thermal conductivity) is always present, which militates against their formation. When such effects are present, the shocks are smeared or spread around the shock front position, but the position of the shock is unaltered". In summary, fractional flow effects (which are a function of the oil-water viscosity ratios) define the size of the mixing zone behind the front or shock (if any), whereas dissipative effects explain the smearing of the shock front position. The Buckley and Leverett (B-L) theory neglects such dissipative effects and, therefore, there is no shock dissipation in B-L (only fractional flow effects are important).

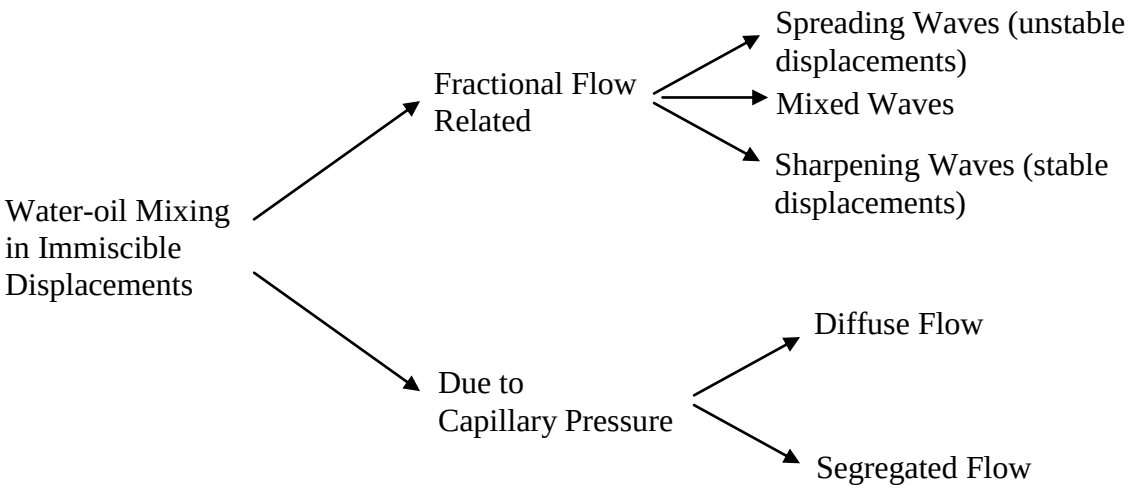

Figure 89: Water-Oil Mixing in Immiscible Displacements

The effect of capillary pressure on the recovery of oil in water floods has been studied by several researchers. In the book Enhanced Oil Recovery, Lake (1989) indicates that capillary pressure increases the water fractional flow at a given water saturation. He also indicated that at the shock, a local pressure gradient causes the oil and water to mix faster than under the

influence of viscous forces only. The resulting local mixing causes the shock to spread. Rapoport and Leas (1952) found that the effect of capillary pressure on recovery is more significant at low production rates, small lengths of reservoir and low water viscosity. Moreover, they found that the effect of capillary pressure on oil recovery is only important if the product velocity*length* water viscosity is smaller than a "critical" value. All floods corresponding to scaling coefficients larger than the "critical" value become similar to each other, regardless of rates, lengths or fluid viscosities. Above the critical value the effect of capillary pressure is minimal and, therefore, the saturation profiles will resemble those predicted by the B-L theory. The conditions under which stabilization is achieved (no effect of capillary pressure), vary from one core material to another and cannot be predicted on a theoretical basis. Finally, Rapoport and Leas (1952) also indicated that flooding behavior is usually stabilized (behavior independent of length and rate) under field conditions.

In their study on dimensionless groups controlling oil bypassing in dipping systems, Shook et al. (1962) indicated that "capillary numbers tend to be quite small in all the fields…this confirms another commonly held impression about the unimportance of capillary pressure in large-scale displacements". In a similar study, Wood et al. (2006) wrote: "the effect of capillary forces and dispersion were secondary effects in the model and were not included in the scaling" and "the global capillary number was dropped because of its negligible effect on recovery". These studies are the main reason why no effect of capillary forces was included in the simulation sensitivities previously presented in this dissertation.

The main objective of this section is to evaluate effect of capillary pressure on the 3D immiscible displacement of oil by water in dipping systems with side-water drive. Most of previous studies have considered the effect of capillary pressure on one-dimensional systems

subject to water flooding. Also, because of their one-dimensional nature, previous studies have not included the effect of having an original capillary transition zone. Moreover, most of previous studies have been carried out in horizontal reservoirs. This study is unique in the sense that it considers natural water drive with an initial transition zone, three dimensions and the effect of gravity forces. It also considers flow under three different conditions: first, a highly favorable mobility ratio. Second an unfavorable mobility ratio and, third, a highly unfavorable mobility ratio.

Figure 90 shows the capillary pressure values used in the simulation model. Capillary pressures were taken from a CMG IMEX example data set. Values considered range from 3 psi to 10 psi. Only drainage curves were defined in the simulator, which indicates that no hysteresis effects are included in the capillary pressures.

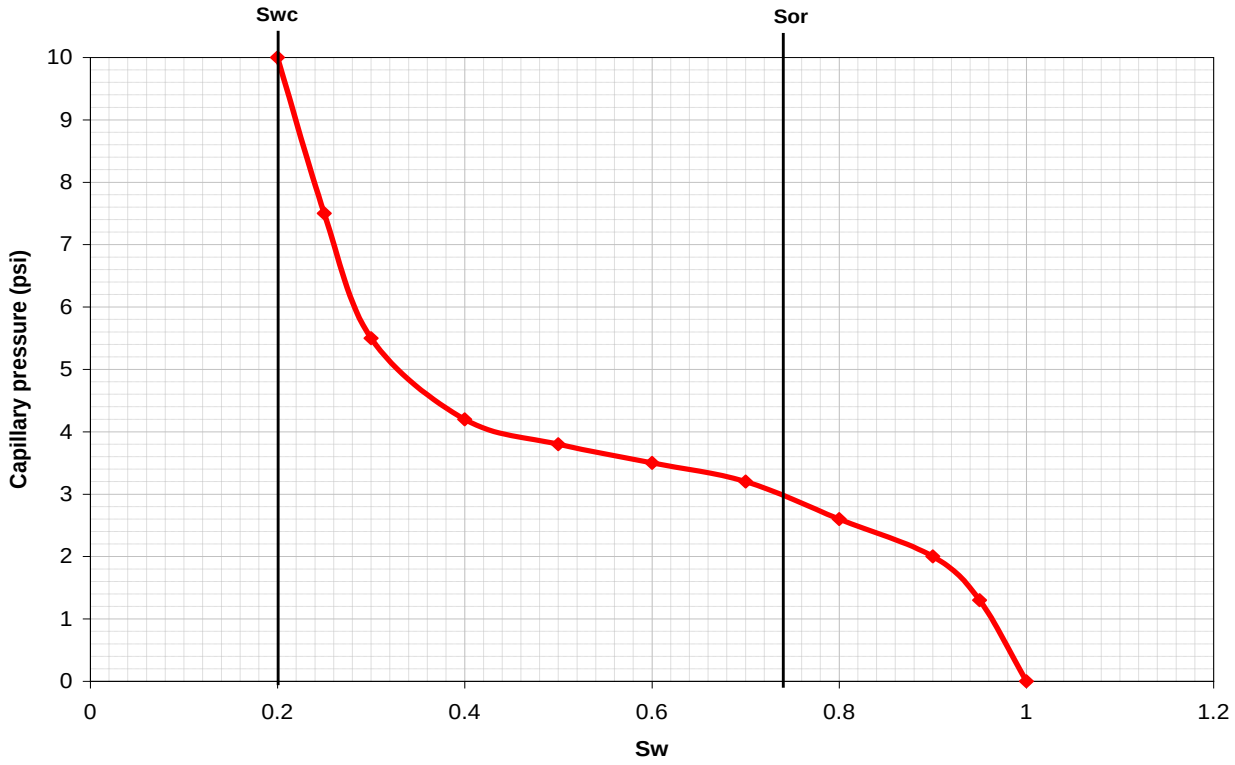

Figure 90: Capillary Pressures Used in the Simulation Model

Figure 91 shows the initial water saturation distribution of the slab with no capillary effects (left) and with capillary effects (right). In both cases, the 100% water saturation line is at a depth of approximately 8748 ft. With capillary pressure, the top of the transition zone is at a depth of approx. 8692 ft. This indicates that the thickness of the transition zone is approximately 56 ft, which has also been confirmed by analytical calculations. Three different water saturation iso-surfaces are shown. The first iso-surface corresponds to water saturation slightly above the connate water saturation. The second corresponds to a water saturation of 47%, which is the half-way point between the connate water saturation and 1-S_{or}. The third iso-surface corresponds to a water saturation slightly below 1-S_{or}.

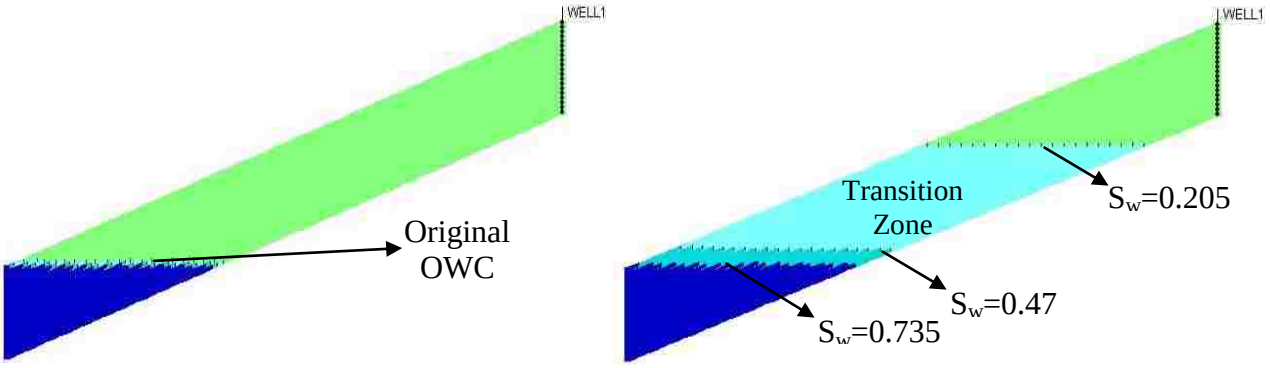

Figure 91: Initial Condition (Time=0) without Capillary Transition Zone (Left) and with Capillary Transition Zone (right)

Cases Considered

Table 32 shows the cases analyzed in this study. Each case was run with and without capillary pressure, for a total of 24 simulation runs. Mobility ratio was calculated using Equation (2.12). Dimensionless gravity number, G, was estimated using Equation (2.13). The oil-water front stability criteria used is based on Equation (2.16). The simulation cases can be separated

into three main categories or groups: first, cases with favorable end-point mobility ratio (M<1). Second, cases with slightly unfavorable end-point mobility ratio (M=4) and; third, cases with highly unfavorable mobility ratio (M=40).

Table 32: Cases Considered in the Study of the Effect of Capillary Pressure

Case #	M	q (b/d)	G	Condition
3-A	0.40	0.1	392.76	Stable
3-B	0.40	1	39.28	Stable
3-C	0.40	100	0.39	Stable
3-D	0.40	1000	0.04	Stable
6-A	4.00	0.1	392.76	Stable
6-B	4.00	1	39.28	Stable
6-C	4.00	10	3.93	Stable
6-D	4.00	100	0.39	Unstable
7-A	40.00	0.1	392.76	Stable
7-B	40.00	1	39.28	Stable
7-C	40.00	10	3.93	Unstable
7-D	40.00	100	0.39	Unstable

Results

<u>Analytical Results</u>

According to Lake (1989), capillary pressure will not affect a one-dimensional water oil displacement if the following condition is satisfied:

$$N_{RL} > 3$$

Where N_{RL} is the Rapoport and Leas Number, defined as (Lake, 1989):

N_{RL} [redacted] /2 [redacted] / k_{rw}' [redacted] os [redacted] ……………………………………………………………….(4.9)

The different terms in Equation (4.9) are defined in the nomenclature. Typically, for water wet media k_{rw}^{o} [redacted] os [redacted] ≈ 1 (mN/m) (Lake, 1989). Then, if we take ϕ =0.18, k=500 md and L=2000 ft (typical properties for the slab simulation model used in the dissertation), we will

obtain that [redacted] = 0.54 (cm^2* mPa-s/min) or 9.0 E-10 Newtons. In other words, our calculations suggest that for the conditions considered here, capillary pressure would only be significant if the production rate is smaller than 5.32 bpd. However, two questions arise: first, is the condition N_{RL}>3 applicable to all possible reservoirs? Second, can such condition be applied for 3D displacements with natural water drive and an original transition zone? The answer to these two questions remains unclear. However, Rapoport and Leas (1952) suggested that the conditions under which stabilization is achieved (no effect of capillary pressure), vary from one core material to another and, therefore, it seems that any proposed critical condition should be obtained for each system.

Simulation Results

Table 33 shows water breakthrough times (BT time) and oil recovery (%R, expressed as percentage of the movable oil volume) at breakthrough and at abandonment for the simulation runs completed. For the sake of simplicity, recovery is used here instead of oil bypassing (% Bypassed Oil=100-% Recovery). The percentage of difference, % Diff, has been calculated as follows:

$$\%Diff = \left| \frac{Value\ with\ No\ Pc - Value\ with\ Pc}{Value\ with\ No\ Pc} \right| * 100 \quad \text{.....(4.10)}$$

No results are reported for Cases 3-A, 6-A and 7-A. This is because water breakthrough for these cases was not obtained by the end of the simulation time (9999 years). These cases have a very high gravity number and, therefore, a small production rate (0.1 bpd). Results are summarized next and more detailed explanations are offered in the following sections:

- Water breakthrough time can substantially accelerated (up to 83%) by the presence of a capillary transition zone. It is obvious that the larger differences between the

breakthrough times obtained with and without capillary pressure occur at low production rates.

- Because of the acceleration of the water breakthrough time, oil recovery at breakthrough is substantially lower (up to 80% lower) when capillary pressure effects are considered.
- The effect of capillary pressure on oil recovery at 98% water cut is significantly lower than at water breakthrough.
- Oil recovery at 98% water cut can be promoted by the presence of a capillary transition zone. This is especially true at high end-point mobility ratios (lower influence of gravity forces).

Table 33: Water Breakthrough Times and Oil Recovery for the Cases Considered

Case #	BT time NO Pc (days)	BT time WITH Pc (days)	% Diff	% R at BT NO Pc	% R at BT With Pc	% Diff	% R at Abandonment NO Pc	% R at Abandonment WITH Pc	% Diff
3-A	>9,999 years								
3-B	556,999	186,221	66.6	80.1	31.3	60.9	97.6	100.0	-2.5
3-C	5,907	4,950	16.2	85.0	83.3	2.0	99.9	99.8	0.1
3-D	632	535	15.3	90.9	90.0	1.0	99.6	99.4	0.2
6-A	>9,999 years				20.0				
6-B	502,114	125,809	74.9	72.2	21.2	70.7	95.8	99.8	-4.2
6-C	26,802	16,314	39.1	38.6	27.5	28.8	99.4	98.8	0.6
6-D	1,480	1,986	-34.2	21.3	33.4	-57.0	98.5	97.3	1.2
7-A	>9,999 years								
7-B	123,519	21,364	82.7	17.8	3.6	79.8	91.3	98.7	-8.0
7-C	3,497	2,274	35.0	5.0	3.8	23.9	92.1	93.7	-1.8
7-D	343	221	35.6	4.9	3.7	24.6	77.6	83.4	-7.5

Summary of Results for M<1 (favorable mobility ratio)

Figures 92, 93 and 94 show the effect of capillary pressure on the shape of three different

water saturation isosurfaces for Cases 3-B, 3-C and 3-D, respectively. All the figures are cross sections of the slab model at the water breakthrough time. For the cases with no capillary pressure (left), it can be seen that the separation between the different water saturation isosurfaces increases with increasing rates (or gravity number). This is because for the higher rates the effect of the viscous pressure gradient becomes more significant, which results in increasing fractional flow effects and mixing. This can be confirmed by observing Figure 95, which shows the water saturation profiles in the last layer of the slab (Z=20) for all three cases and no capillary pressure. It can be seen that for the case with the lowest rate (q=1 bpd) the displacement in the last layer can be regarded as piston-like (no mixing zone). For the highest rates (lowest G's), however, the formation of a small mixing zone is clear. This can also be explained by observing Figure 96, which presents the fractional flow curves of Cases 3-C and 3-D. It is obvious that for the case with the highest rate (Case 3-D), the effect of the viscous forces is more important (fractional flow curve shifted more to the left), which results in more mixing.

For the cases with capillary pressure (at the right in Figures 92, 93 and 94), it can be clearly seen that the separation between the different water saturation isosurfaces decreases with increasing oil rates. This is characteristic of sharpening fronts and it suggests that there will be a rate at which there will be no separation between the different water saturation isosurfaces and, therefore, the displacement will be piston-like (no capillary pressure effects). As can be seen in Figure 97, which shows the water saturation profiles in the last layer of the slab Z=20 for the cases with capillary pressure, a perfect piston-like displacement may be achieved at rates above 1000 bpd. For rates at or below 1000 bpd but above 1 bpd the displacement approximates piston-like and, therefore, the effect of a capillary pressure on oil recovery is minimal. This seems to validate the results obtained analytically. Also, it can be seen that because the end-point mobility

ratio is less than 1, the water saturation isosurfaces tend to become perpendicular to the bedding, a process that is accelerated at high rates.

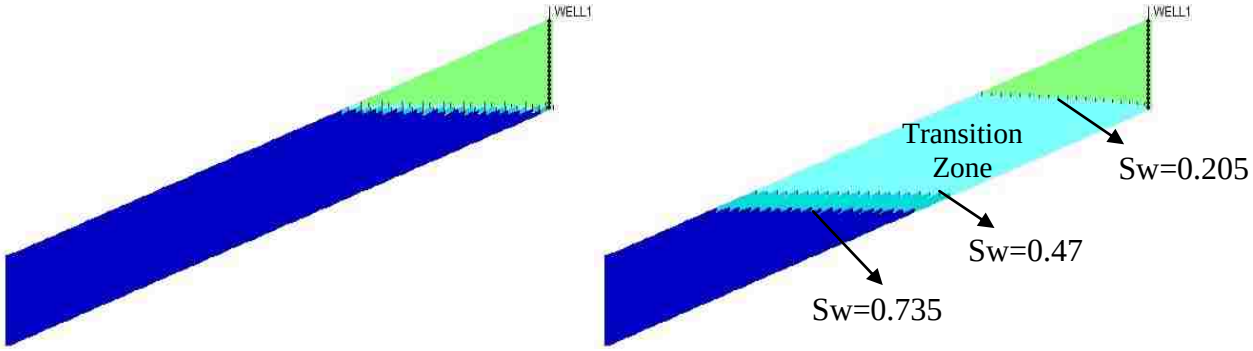

Figure 92: Shape of Sw Isosurfaces at Water Breakthrough for Case 3-B without (Left) and with (Right) Capillary Pressure

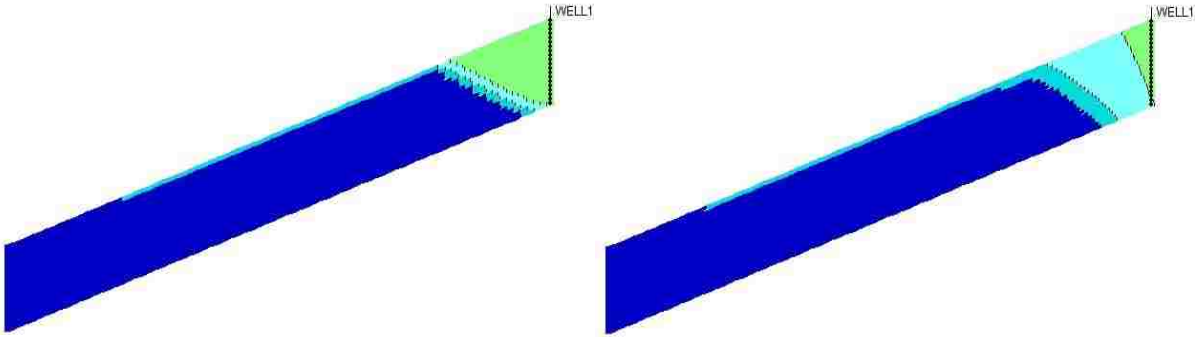

Figure 93: Shape of Sw Isosurfaces at Water Breakthrough for Case 3-C without (Left) and with (Right) Capillary Pressure

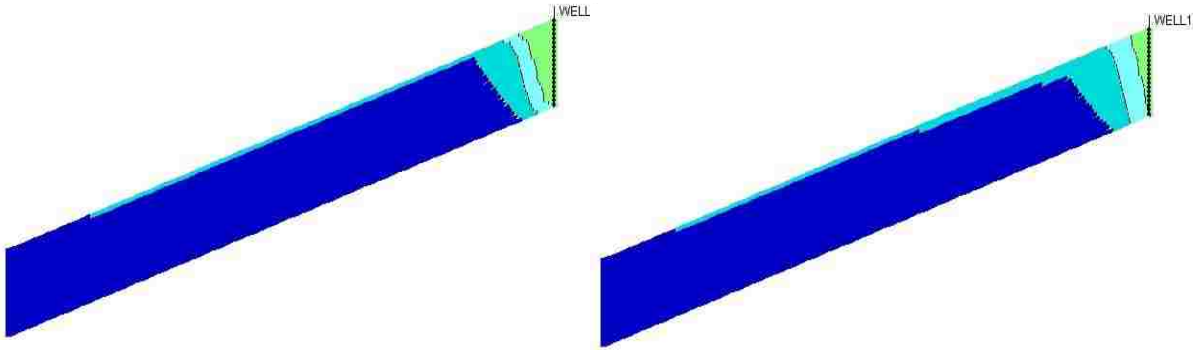

Figure 94: Shape of Sw Isosurfaces at Water Breakthrough for Case 3-D without (Left) and with (Right) Capillary Pressure

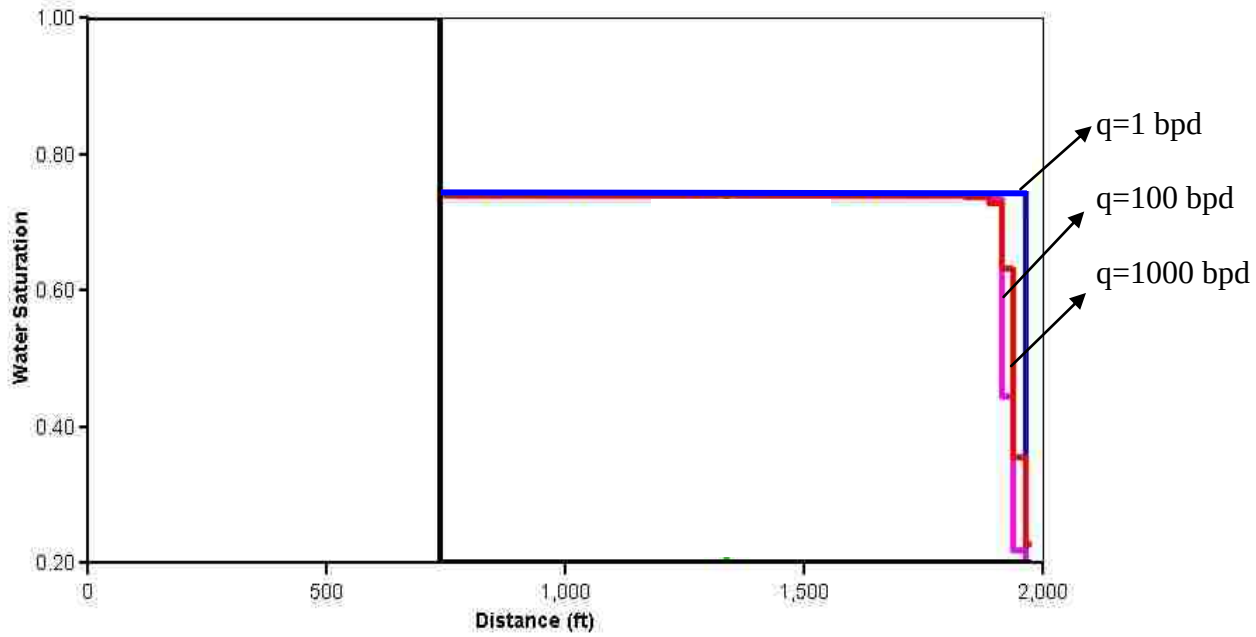

Figure 95: Water Saturation Profiles in the Last Layer of the Slab (Z=20) for Cases with M<1 and no Capillary Pressure

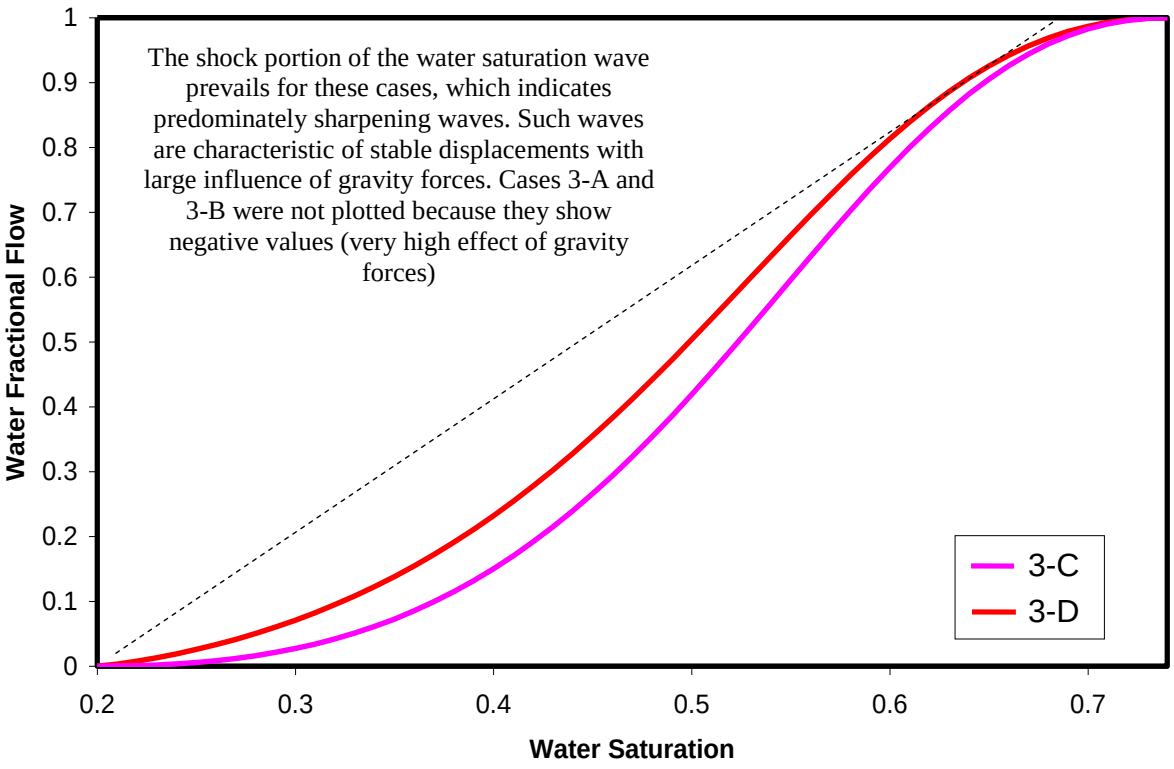

Figure 96: Fractional Flow Curves for Cases 3-C, 3-D.

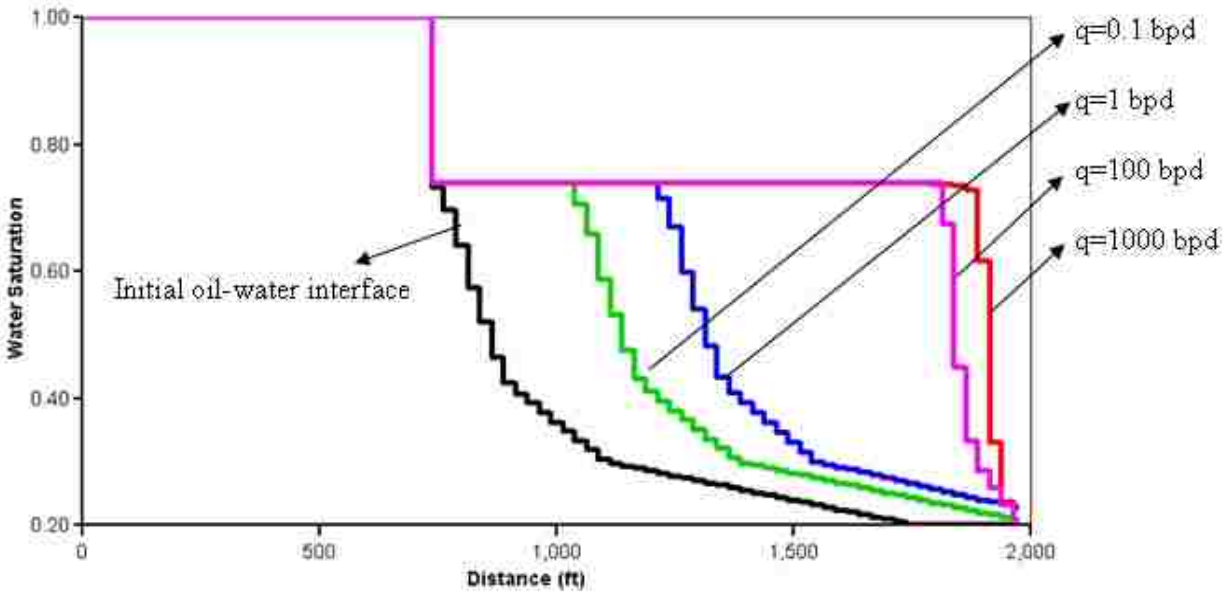

Figure 97: Water Saturation Profiles in the Last Layer of the Slab (Z=20) for Cases with M<1 and Capillary Pressure (Dispersed Initial Oil-Water Interface)

Figure 98 shows the effect of capillary pressure on oil production for Cases 3-B, 3-C and 3-D, respectively. Because of the highly favorable mobility ratio (which results in stable displacement), all 6 cases show large oil recovery at both breakthrough and 98% water cut (see Table 33). It can also be seen that capillary pressure has no effect on oil production before breakthrough. This is obviously because cumulative oil production before breakthrough is directly proportional to the oil rate (simulations were controlled using a maximum liquid rate). After breakthrough, water production starts and, therefore, oil production is not linearly proportional to the liquid rate. The lazier the cumulative oil production after breakthrough (smaller slope) the smaller the amount of oil produced with each barrel of liquid. In other words, the displacement efficiency decreases.

Figure 98 also shows that oil production at abandonment is higher for the cases with no capillary pressure. This is mainly because there is more oil originally available for such cases (there is no initial transition zone) and, therefore, more oil can be displaced. However, Table 33

shows that recovery factor at abandonment is about the same with and without capillary pressure. That is, capillary pressure has a negligible effect on oil recovery at abandonment. The maximum difference in oil recovery found was 2.5% for the case producing at 1 bpd. Finally, Figure 98 shows that the oil recovery development in the presence of capillary pressure is about the same for the cases producing at 100 and 1000 bpd. This confirms that the effect of capillary pressure decreases as production rate increases.

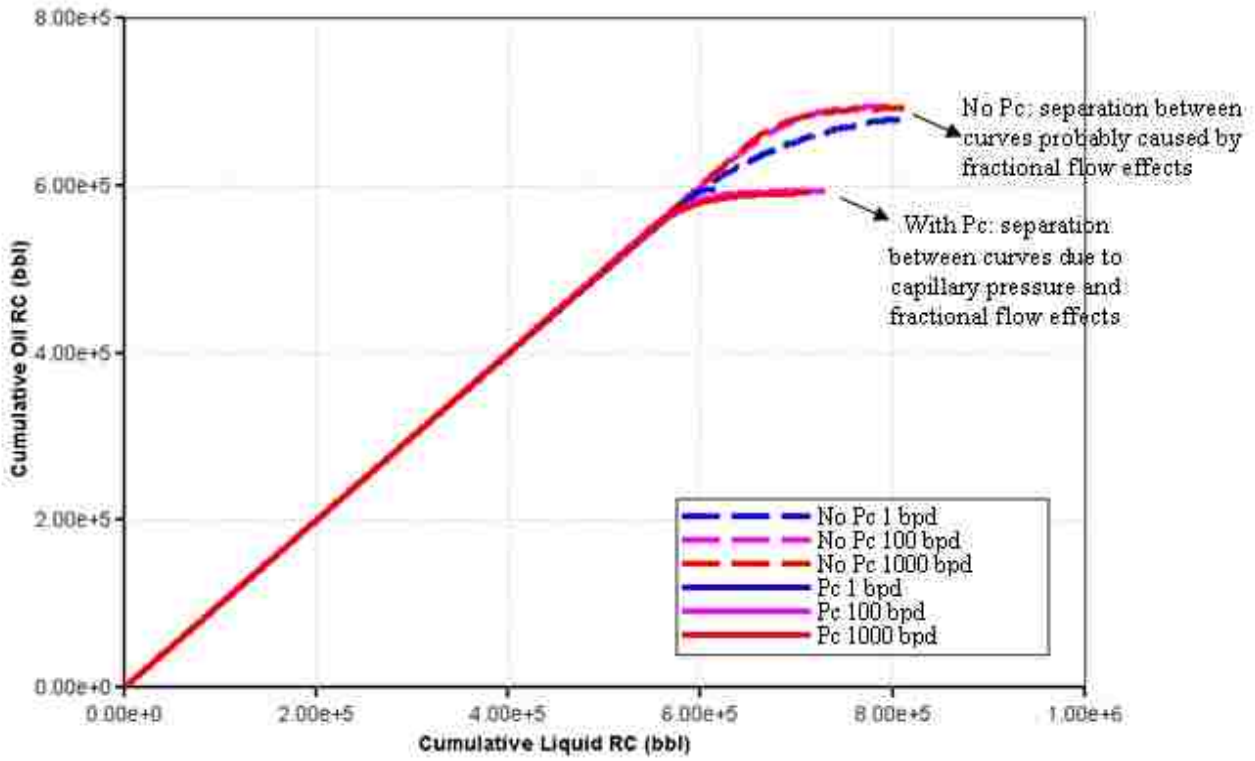

Figure 98: Cumulative Oil Production vs. Cumulative Liquid Production for Cases with M<1 (Highly Favorable Mobility Ratio)

Summary of Results for M>1 (unfavorable mobility ratio)

Figures 99, 100 and 101 show the effect of capillary pressure on the shape of three different water saturation isosurfaces for Cases 6-B, 6-C and 6-D, respectively. For the cases with no capillary pressure (left), it can be seen that the separation between the different water

saturation isosurfaces slightly increases with increasing rates. As explained before, this is because for the higher rates the effect of the viscous pressure gradient becomes more significant (effect of gravity becomes less important), which results in increasing fractional flow effects and mixing. This can be confirmed by observing Figure 102, which displays water saturation profiles in the last layer of the slab (Z=20) for four different production rates and with no capillary pressure. It can be seen that for the case with the lowest rate (q=0.1 bpd) the displacement in the last layer can be regarded as piston like. This is, there is no mixing zone. For the highest rates, however, the formation of a small mixing zone is clear. At a rate of 100 bpd, the viscous forces dominate over the gravity forces and the displacement becomes unstable (oil-water interface cannot remain as a straight line and it develops some curvature).

The behavior of the water saturation isosurfaces for the cases with capillary pressure (at the right in Figures 99, 100 and 101) is quite interesting. At low rates, the different water saturation isosurfaces remain at about the same distance during the displacement. This is because of the significant effect of the gravity forces (which are more important at low rates). The behavior at higher rates is quite intriguing. Figures 100, 101 and 103 show that high water saturation isosurfaces advanced more at the time of breakthrough than low water saturation isosurfaces. This behavior can be explained by analyzing Figure 104, which presents the fractional flow profiles for Cases 6-C and 6-D. Both cases show mixing waves: there is a shock portion at low water saturations (sharpening wave, which explains why the low water saturation values advance less) and a spreading portion at high water saturations (spreading wave, which explains why the high water saturations advance more). It can also be seen that the spreading portion is more significant for Case 6-D. This explains why there is more advancement of the high water saturation values for this case. These unique characteristics of Case 6-D (rate =100

bpd) may also explain why it is the only case in this study in which water breakthrough time was delayed by the presence of capillary pressure.

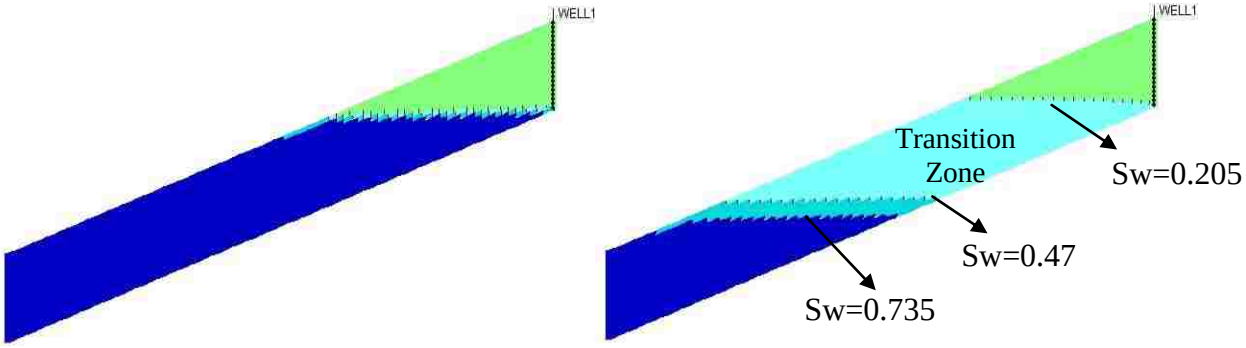

Figure 99: Shape of Sw Isosurfaces at Water Breakthrough for Case 6-B without (Left) and with (Right) Capillary Pressure

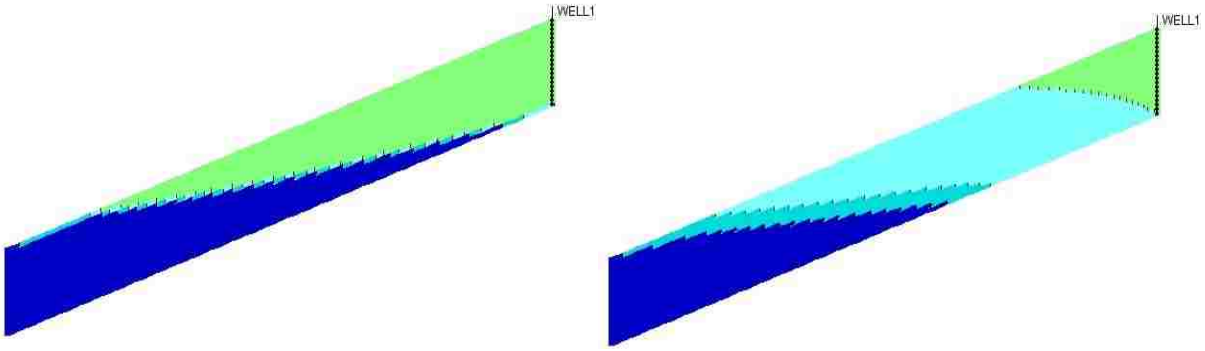

Figure 100: Shape of Sw Isosurfaces at Water Breakthrough for Case 6-C without (Left) and with (Right) Capillary Pressure

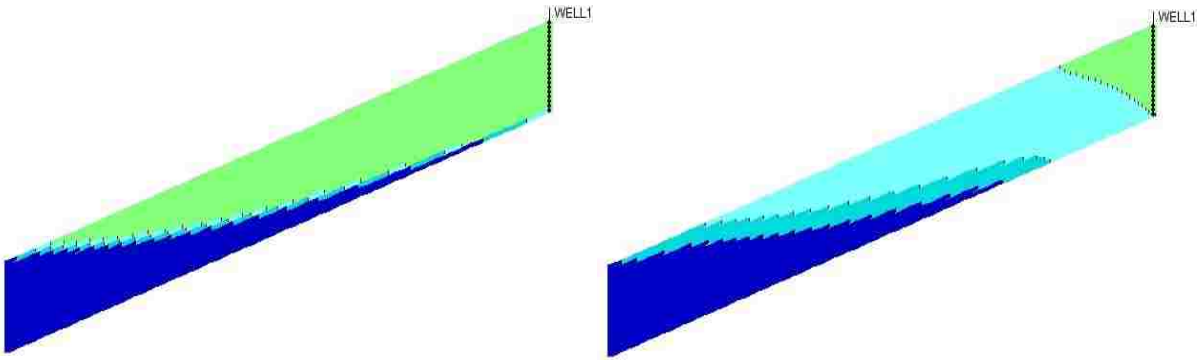

Figure 101: Shape of Sw Isosurfaces at Water Breakthrough for Case 6-D without (Left) and with (Right) Capillary Pressure

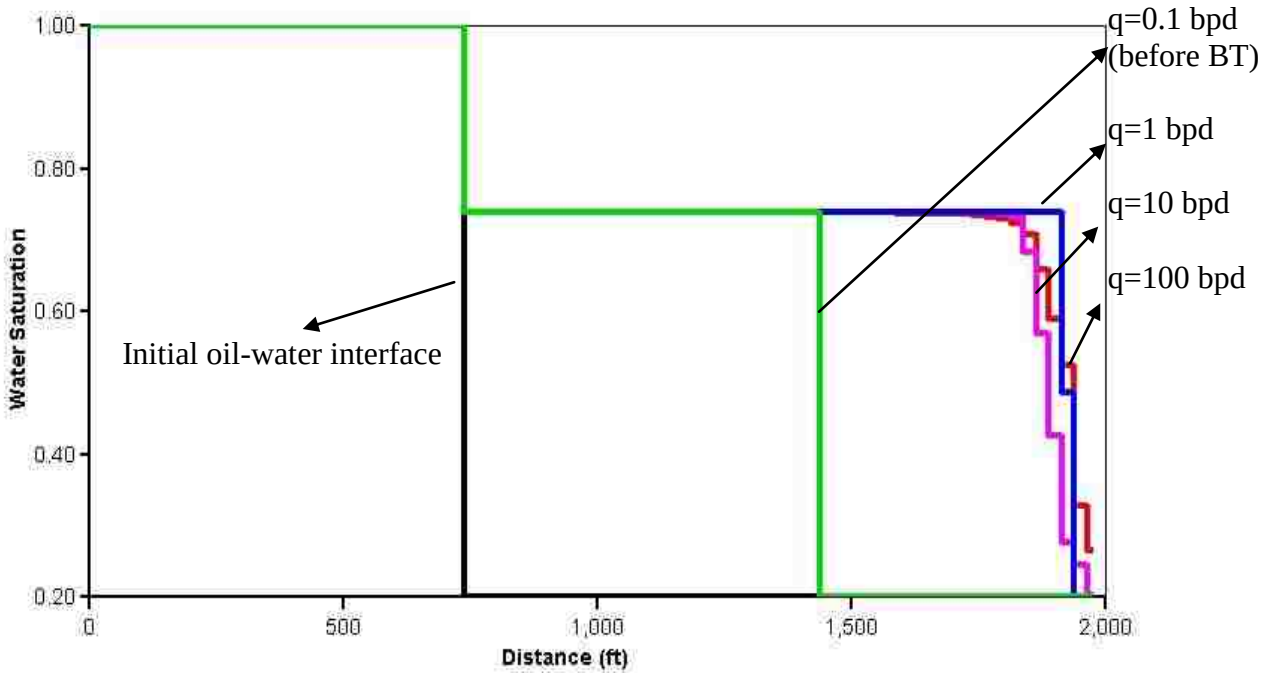

Figure 102: Water Saturation Profiles in the Last Layer of the Slab (Z=20) for Cases With Unfavorable Mobility Ratio (M=4) and No Capillary Pressure

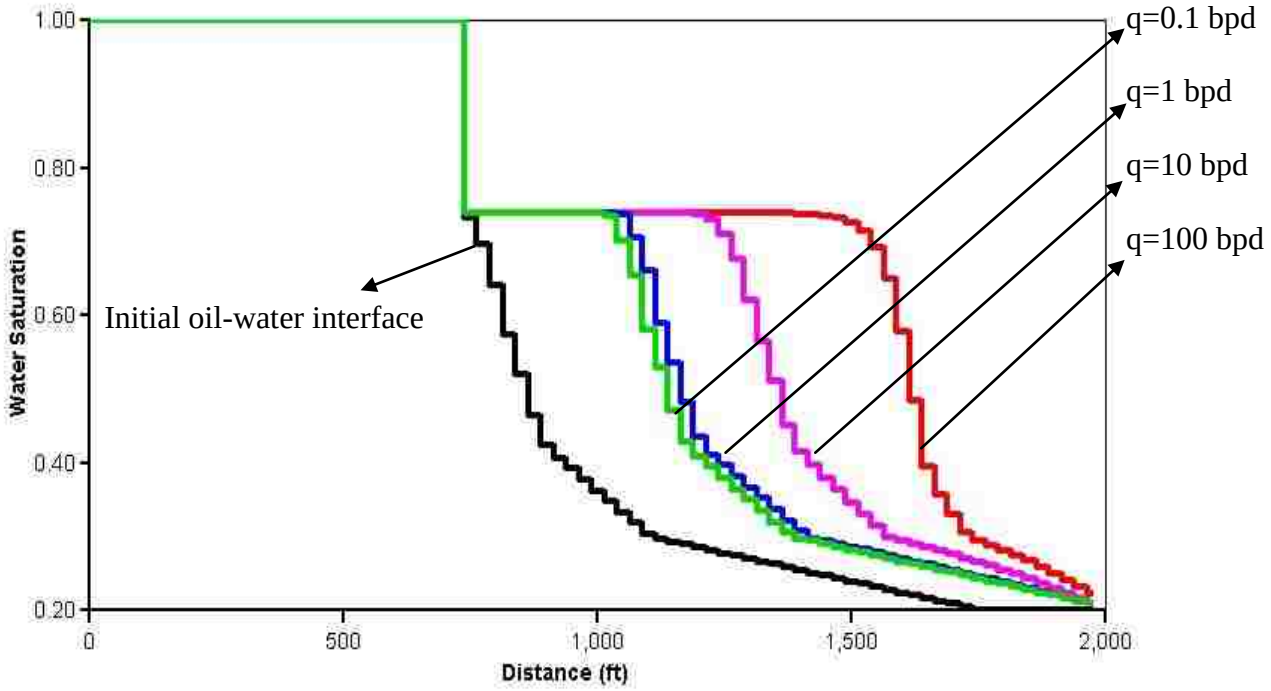

Figure 103: Water Saturation Profiles in the Last Layer of the Slab (Z=20) for Cases With Unfavorable Mobility Ratio (M=4) and Capillary Pressure

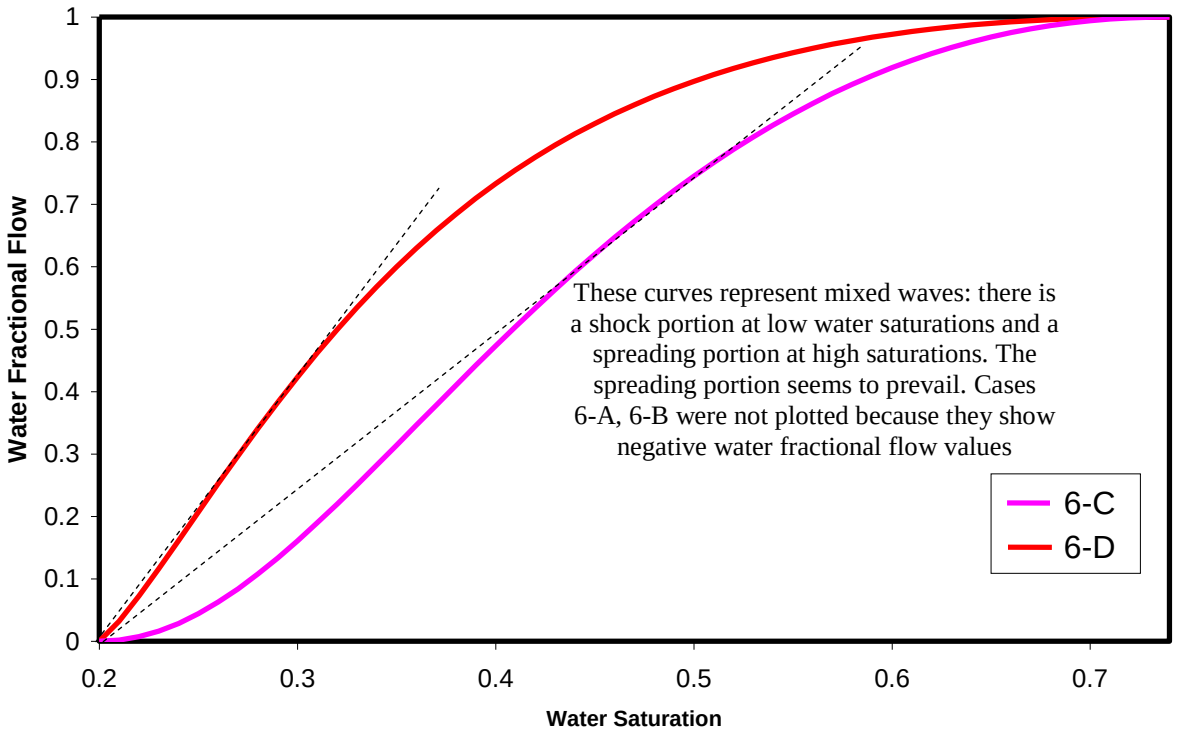

Figure 104: Fractional Flow Curves for Cases 6-C, 6-D.

Figure 105 shows the effect of capillary pressure on oil production for Cases 6-B, 6-C and 6-D. As explained before, oil production is linearly related to liquid production before breakthrough. After breakthrough, oil production is "lazier" for the cases with higher rates. This is because of the decreasing effect of the gravity forces and the increasing fractional flow of water at higher rates.

Figure 105 also shows that oil production at abandonment is much higher for the cases with no capillary pressure. As mentioned before, this is mainly because there is more oil originally available for such cases and, therefore, more oil can be displaced. Table 33 shows that recovery factor at abandonment is about the same with and without capillary pressure. It also shows that the effect of capillary pressure is relatively important at low production rates (4.2% of difference in oil recovery at 98% water cut), but almost inexistent at high rates.

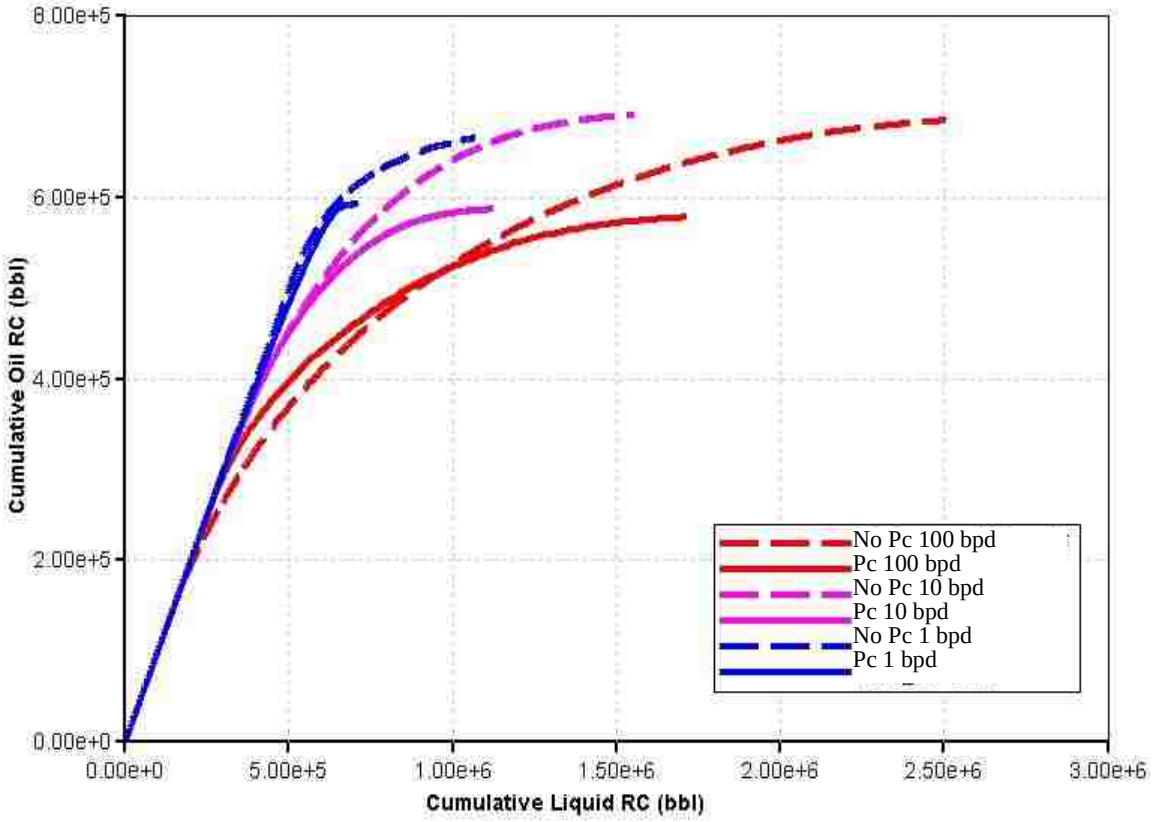

Figure 105: Cumulative Oil Production vs. Cumulative Liquid Production for Cases With M=4 (Unfavorable Mobility Ratio)

Summary of Results for M>>1 (highly unfavorable mobility ratio)

The effect of capillary pressure on the shape of the three different water saturation isosurfaces for Cases 7-B, 7-C and 7-D is shown in Figures 106, 107 and 108, respectively. For the cases with no capillary pressure (left), it can be seen that the separation between the different water saturation isosurfaces increases with increasing rates. As mentioned before, for the higher rates the effect of the viscous pressure gradient becomes more significant and the effect of gravity becomes less important, which results in increasing fractional flow effects, mixing, unstable displacement and the formation of a thin and elongated water tongue.

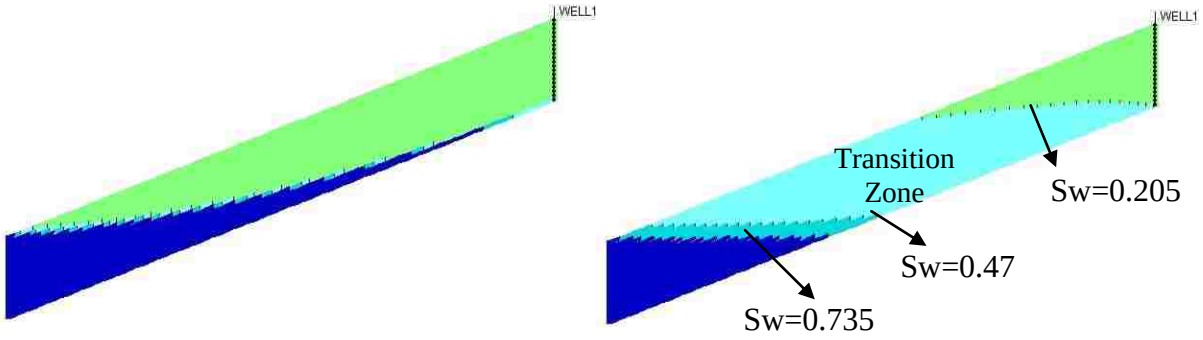

Figure 106: Shape of Sw Isosurfaces at Water Breakthrough for Case 7-B without (Left) and with (Right) Capillary Pressure

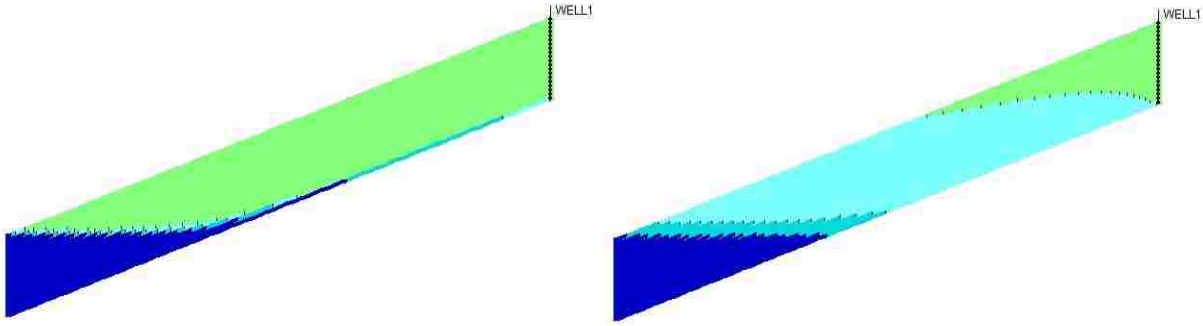

Figure 107: Shape of Sw Isosurfaces at Water Breakthrough for Case 7-C without (Left) and with (Right) Capillary Pressure

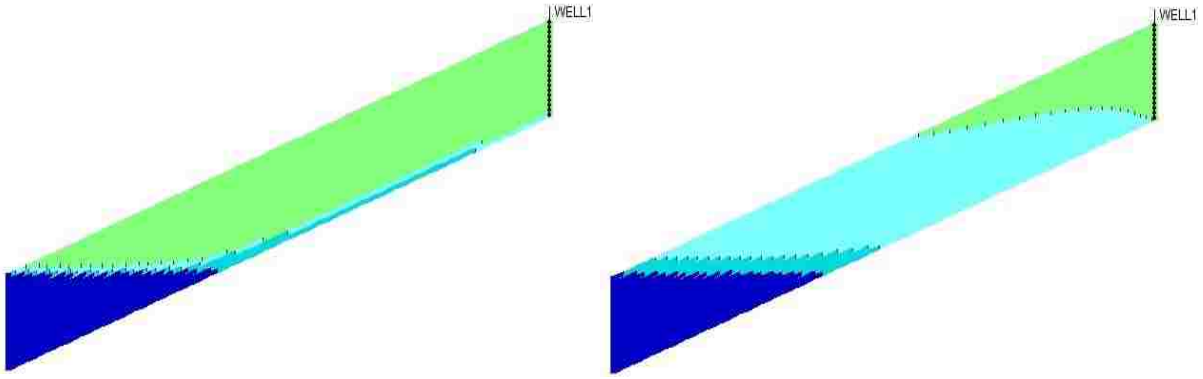

Figure 108: Shape of Sw Isosurfaces at Water Breakthrough for Case 7-D without (Left) and with (Right) Capillary Pressure

Figure 109 shows the water saturation profiles in the last layer of the slab (Z=20) for the three different production rates and no capillary pressure. It can be seen that the length of the

mixing zone is proportional to the oil rate. In fact, Figures 108 and 109 show that, for a rate of 100 bpd, the mixing zone length extends from the original oil-water contact to the well. This is obviously because the viscous forces substantially dominate over the gravity forces and the displacement is unstable. As can be noted in Figure 110, a high production rate causes the fractional flow curve to shift to the left, which leads to more fractional flow of water and mixing. Figure 110 also shows that there is no significant shock formation for Cases 7-B, 7-C and 7-D. This indicates that spreading waves are present (a wave in which neighboring saturation values become more distant upon propagation).

It can also be noted from Figures 106, 107 and 108 that there is almost no effect of production rate on the shape of the water saturation isosurfaces for the cases with capillary pressure. Moreover, Figure 111 shows that the shape of the water saturation profiles (at the last layer of the slab) is practically independent of the oil rate. This is because at highly unfavorable end-point mobility ratios the effect of the viscous forces is much larger than the effect of the gravity and/or capillary forces. Figures 106, 107, 108 and 111 also show that high-water saturations advance more slowly than the low water saturation isosurfaces, which is characteristic of spreading waves. However, the effect of this phenomenon on oil recovery is limited by the fact that water saturation isosurfaces are originally spread by the presence of a capillary transition zone. Because of this, spreading is more significant in the cases with no capillary pressure.

Figure 112 shows the effect of capillary pressure on oil production for Cases 7-B, 7-C and 7-D, respectively. Oil production at abandonment is much higher for the cases with no capillary pressure. Again, this is mainly because there is more oil originally available for such cases and, therefore, more oil can be displaced. Table 33 shows, however, that capillary pressure

can cause an increase in oil recovery at abandonment of up to 8% (for Case 7-B - a case with the lowest production rate).

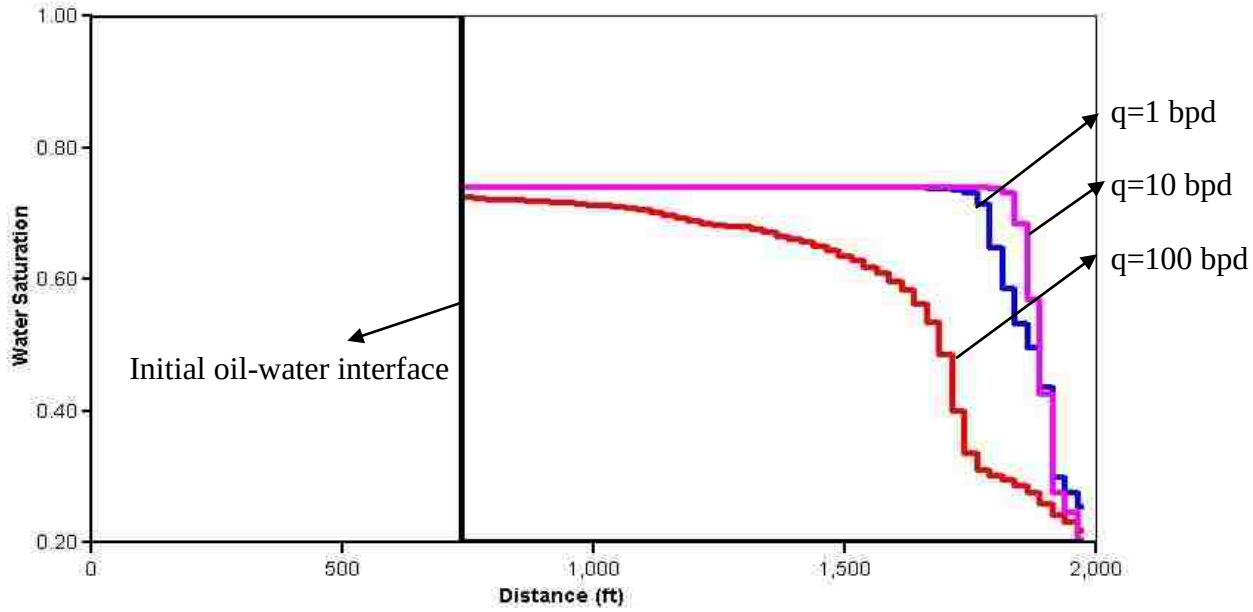

Figure 109: Water Saturation Profiles in the Last Layer of the Slab (Z=20) for Cases With Highly Unfavorable Mobility Ratio (M=40) and No Capillary Pressure

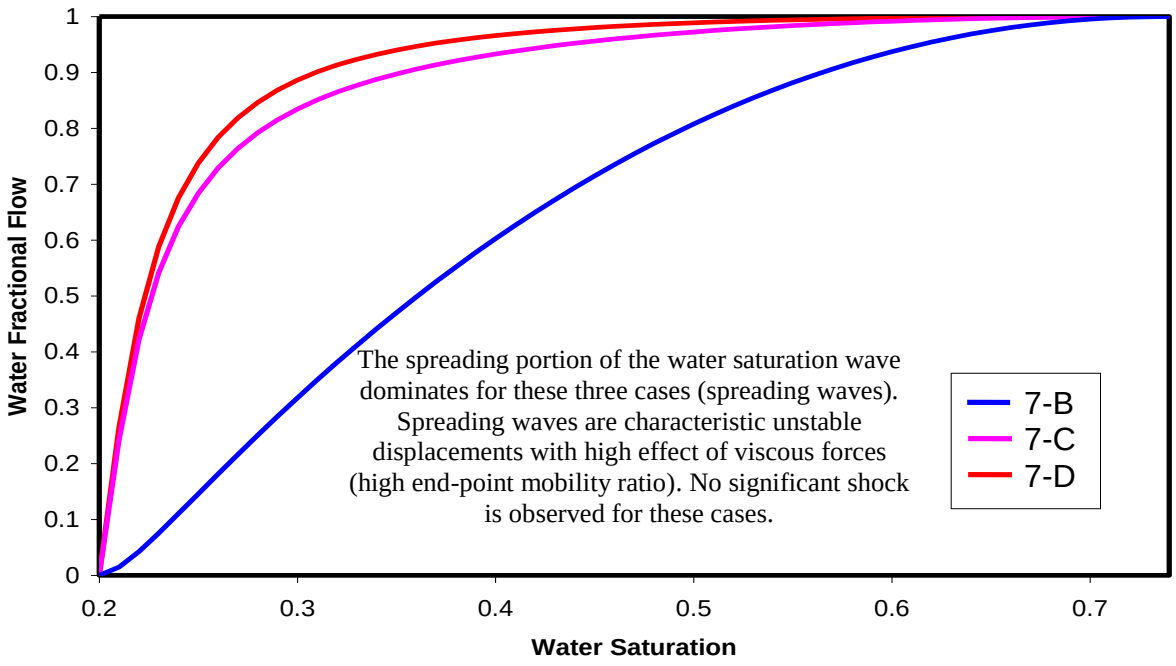

Figure 110: Fractional Flow Curves for Cases 7-B, 7-C, 7-D

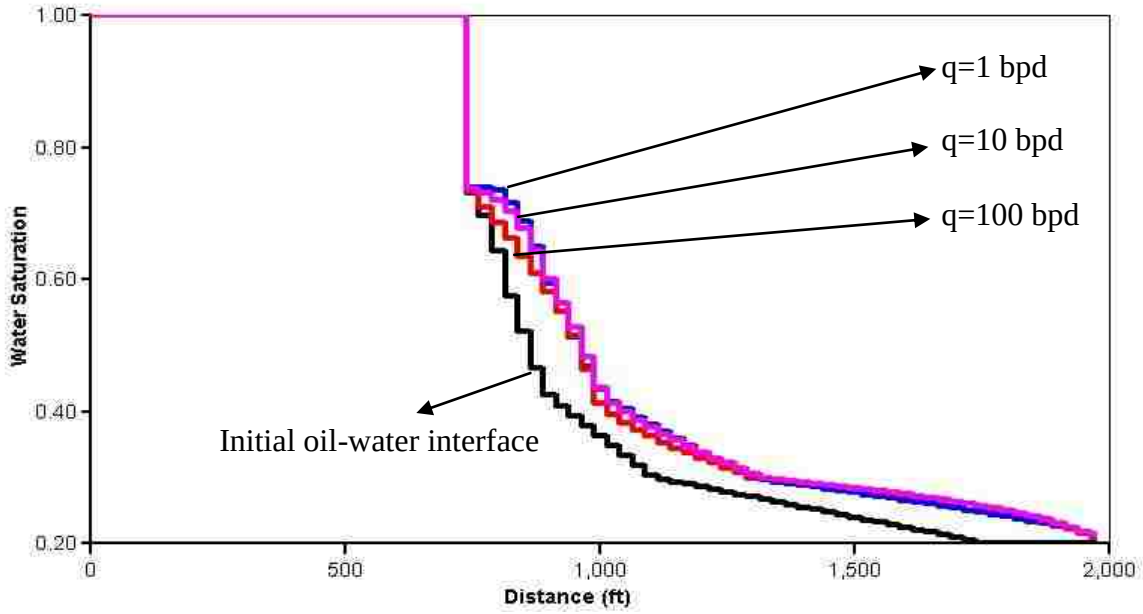

Figure 111: Water Saturation Profiles in the Last Layer of the Slab (Z=20) for Cases With Highly Unfavorable Mobility Ratio (M=40) and Capillary Pressure

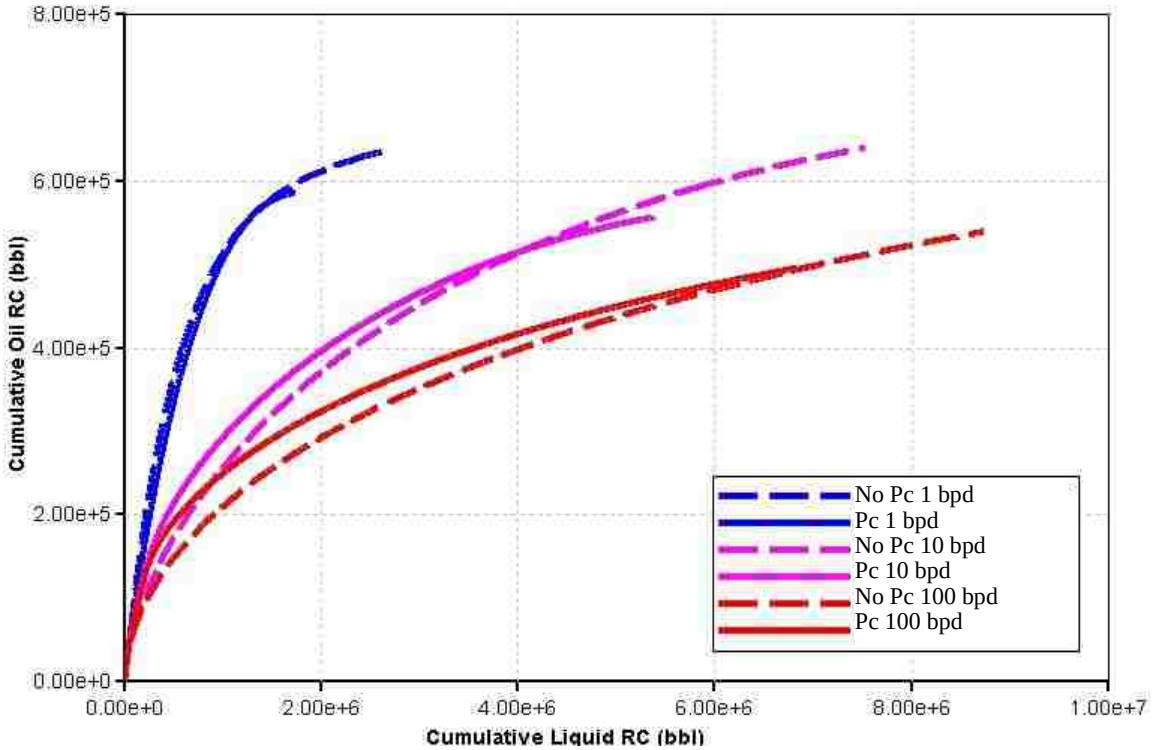

Figure 112: Cumulative Oil Production vs. Cumulative Liquid Production for Cases With M=40 (Highly Unfavorable Mobility Ratio)

All cases show decreasing displacement efficiency (less oil produced per barrel of liquid) with increasing oil rates. For high oil rates, the gravity number is smaller, which causes the fractional flow curve to shift to the left (see Figure 110). This results in more flow of water at the same water saturation and lower displacement efficiency. Figure 112 also shows that the cases with capillary pressure have better displacement efficiency immediately after breakthrough than the cases with no capillary pressure. It was found that this is because the cases with capillary pressure show slower water cut development immediately after water breakthrough. This suggests that capillary pressure has a stabilizing effect during the displacement of less mobile fluids (oil) by more mobile fluids (water). Because of the presence of an initial transition zone, the saturation fronts are already spread at the beginning of production. The resulting effect is less water underruning than in the cases with no capillary pressure as can be seen in Figures 106 to 108. This is especially true at high rates, where the predominance of viscous forces causes very significant underruning in the absence of an initial capillary pressure transition zone.

Summary-Additional Comments

- As previously indicated, water breakthrough time can be substantially accelerated (up to 83% in this study) by the presence of a capillary transition zone.
- The effect of capillary pressure is generally more significant at low production rates. This is because low production rates translate into higher gravity forces. These forces promote the stabilization of the different water saturation fronts - the transition zone remains almost unaltered during the displacement.
- At high production rates, the effect of capillary pressure at breakthrough depends on the type of oil-water displacements. For displacements with favorable end-point mobility ratio (stable displacements), the water saturation waves tend to sharpen. This and the fact

that the oil-water isosurfaces try to get perpendicular to the bedding (because M<1), leads to no effect of the capillary transition zone.

- For displacements with unfavorable mobility ratio (M>1), it was found that the presence of a capillary pressure transition zone may have a stabilizing effect during the displacement. Such stabilizing effect delays the formation of a water tongue and, therefore, is more significant at high rates and low gravity numbers (conditions promoting water underruning).
- The maximum effect of capillary pressure on oil recovery at abandonment found in this study was 8%. This suggests that the capillary pressure effects can be neglected.

4.2 Bottom-Water Systems

4.2.1 Inspectional Analysis: Groups Describing Water Invasion

Table 34 shows the dimensionless groups that control performance of bottom-water reservoirs. A description of each of the parameters forming the groups is presented in the nomenclature. Seven groups were obtained by Hanley et al. (1961) using Inspectional Analysis. As was indicated in Section 4.1.1, Inspectional Analysis is an extension of dimensional analysis that can be used in problems so well understood that all the governing laws and boundary conditions can be written down in mathematical form. The differential equations defining the problem can then be expressed so that all the variables are dimensionless. Simple "inspection" then shows how these dimensionless variables are related (Novakovic, 2002).

Only groups 1-4 will be considered in this dissertation. This is done to reduce the number of numerical experiments and because of the expected unimportance of the remaining groups. For example, the dimensionless well radius group is neglected since its possible practical range is quite small when compared to ranges for other groups. Also, the well radius is not expected to

have a large importance in the reservoir simulations completed here. The cumulative production parameter is not considered since its value is always one. This group is used to scale lab experiments to field level and vice versa, which is not an issue in this dissertation. Finally, the capillary to viscous forces ratio is ignored since Hanley at al. (1962) indicated that "capillary forces do not affect the sweep efficiency of bottom water drive reservoirs over the range of conditions normally encountered in the field". In fact, analysis of Hanley at al. (1962) work indicates that they also ignored groups 5 to 7.

Table 34: Dimensionless Groups Controlling Coning in Bottom-Water Systems

#	**Group Name**	**Symbol**	**Equation**
1	Gravity to Viscous Forces	G_v	$\frac{k\ A\ \Delta\rho\ g}{\mu_o\ q}$
2	Well Spacing	W_{sp}	$\frac{a}{H}\sqrt{\frac{k_v}{k_h}}$
3	End-Point Mobility Ratio	M	$\frac{k_{rw}}{k_{ro}}$
4	Well Penetration	H_p/H	$\frac{Well\ Penetration}{Reservoir\ Thickness}$
5	Dimensionless Well Ratio	R_{wd}	$\frac{r_w}{H}\sqrt{\frac{k_v}{k_h}}$
6	Cumulative Production Parameter	R_p	$\frac{H\ \phi\ (1-S_{or}-S_{wi})}{t\ q/A}$
7	Capillary to Viscous Force Ratio	R_{vc}	$\frac{\sigma\cos\theta}{\Delta\rho H\sqrt{k}\ g}$

4.2.2 Data Base Construction

The procedure described in Section 4.1.2 for edge-water systems, was also used to find the levels of the dimensionless groups needed for experimental design in bottom-water systems.

Furthermore, the same database of the reservoir parameters or properties presented in Section 4.1.2 was employed here to determine the values of the four dimensionless groups considered for analysis. Basic statistics obtained from the probability distributions of these properties were shown in Table 24. Similar to the edge-water systems, Monte Carlo Simulations (10,000 passes) were completed to randomly obtain probability distributions for each dimensionless group using the distributions of the individual parameters or properties. Cross plots for each possible combination of groups were made and the percentiles to be used in the design were selected from the cloud of points representing possible reservoirs.

The P(10%), P(50%) and P(90%) values for each distribution were recorded for each dimensionless group as the low, middle and high levels to be used in the design, respectively. The P(30%) and P(70%) values were also recorded for the end-point mobility ratio, M, the group with the largest influence on oil bypassing. Table 35 presents the percentiles obtained for each group using Monte Carlo simulations. The range obtained for each group is quite wide and, hopefully, represents most of the possible reservoir situations that could be encountered.

Table 35: Levels Used for the Dimensionless Groups: Bottom-Water Systems

Levels	G_v	W_{sp}	M	H_p/H
Low (P10%)	0.04	0.60	0.25	0.10
Mid-Low (P30%)	-	-	0.80	-
Mid (P50%)	3.76	4.74	2.60	0.50
Mid-High (P70%)	-	-	12.14	-
High (P90%)	20.21	24.05	101.72	1.00

4.2.3 Matrix of Simulation Experiments

A mixed full factorial sensitivity analysis with a total of 135 runs ($3^3 * 5^1$) was designed to determine the influence of the dimensionless groups on oil bypassing. Three levels were used for all the groups except M, for which five levels were employed. The reason behind this selection will be explained in the next sections. As it can be seen in Table 35, the levels were defined by taking the 10%, 30%, 50%, 70% and 90% percentiles of each group.

4.2.4 Validation of Dimensionless Groups

The four dimensionless groups were validated using the numerical simulation model previously described. The idea was to vary the parameters in the dimensionless groups but holding the values of the groups themselves constant. Agreement between cases where the parameters have changed would suggest that the dimensionless groups are appropriate (Shook, 1962).

The validation was done using the P(50%) level of each group (see Table 35). A total of six validation cases were run. The values of the parameters used for these runs are shown in Figure 113. As can be noticed, the individual parameters varied widely. Figure 113 also shows the water cut histories for the six validation cases. It is obvious that water cut is virtually identical for the six cases. Observed differences are insignificant and could be attributed to numerical dispersion effects (different grid block sizes were used in each case). In short, the results presented here confirm that the four dimensionless groups are appropriate. No additional validation was deemed necesary.

4.2.5 Groups Controlling Oil Bypassing

Similar to what was done for edge-water systems, the relative effect of the four dimensionless groups on the oil by-passed at well abandonment were analyzed using the “Design

of Experiments" option of the statistical package SAS, version 9.1.3 (2003), and analysis of variance, ANOVA. A significance level of 5% was used in all ANOVA calculations in this dissertation. The same abandonment criteria employed for edge-water systems was used here (abandonment is defined as 98% water cut – the economic water cut limit). Figure 114 displays the contribution, expressed as percentage of the sum of squares, of the different groups to oil bypassing.

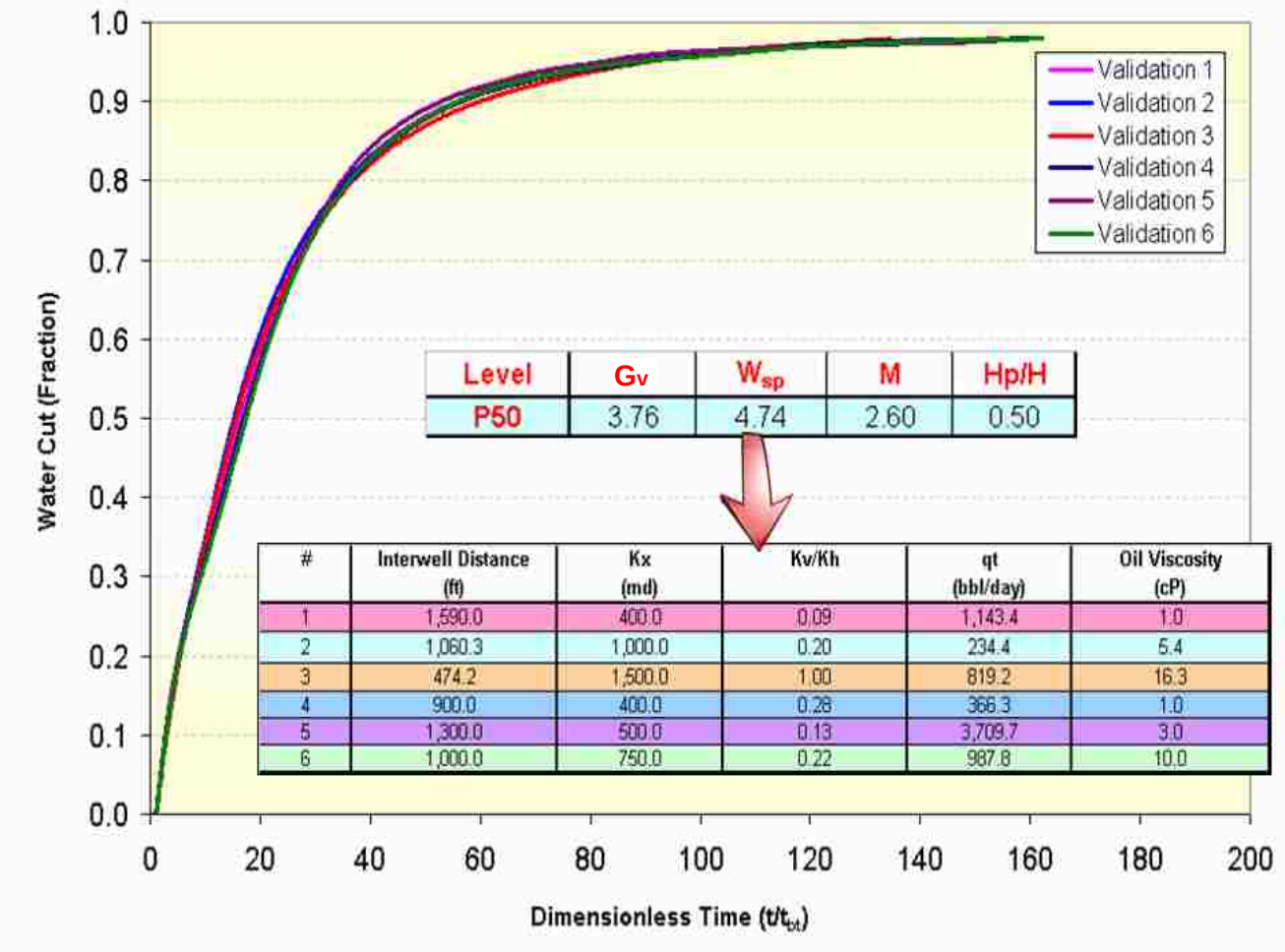

Figure 113: Validation of Dimensionless Groups: Bottom-Water Systems

It is clear that the end-point mobility ratio - a measure of the viscosity contrast between oil and water - is the main group affecting oil bypassing at abandonment conditions. Well

penetration also can be seen to be important, which obviously suggests that short well penetrations could be used for some specific reservoir conditions to delay water invasion in bottom-water systems. Overall, it was found that oil bypassing is promoted by high end-point mobility ratios, large well penetration, low gravity to viscous forces ratio (high rates) and large well spacing (large vertical to horizontal permeability ratios). It can also be seen that all the groups are statistically significant.

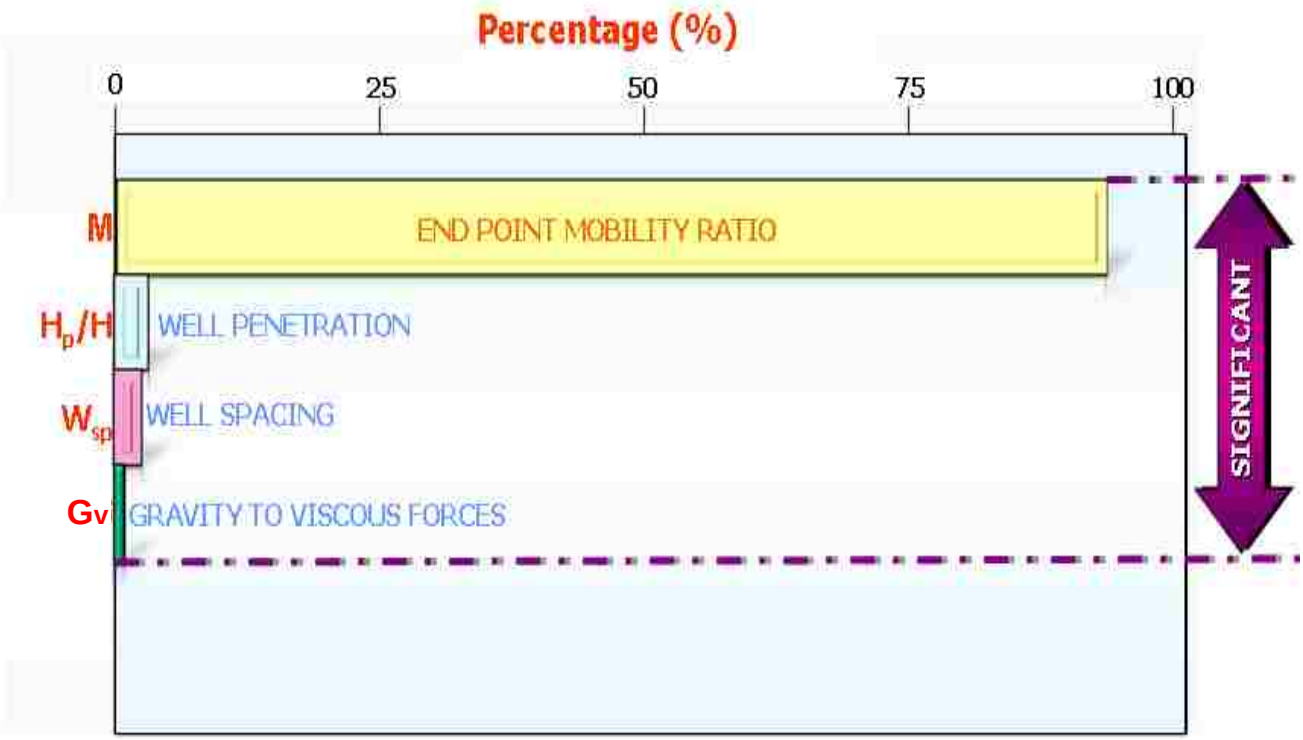

Figure 114: Effect of Dimensionless Groups on Oil Bypassing at Abandonment (Bottom-Water)

4.2.6 New Correlations for Oil Bypassing in Bottom-Water Systems

The following regression formula was the best fit of the percentage of by-passed oil (%BPO) at abandonment as a function of the four dimensionless groups with their first-order interactions:

$$BPO(\%) = 26.18 - 0.68 G_v - 1.04 V_{sp} - 0.87 M - 3.78 (H_p/H) - 0.0147 G_v^2 + 0.0044 G_v V_{sp} + 0.0017 G_v M + 0.2838 G_v (H_p/H) + 0.0278 V_{sp}^2 + 0.0095 * W_{sp} * M + 0.3950 V_{sp} (H_p/H) + 0.0066 M^2 + 0.2803 M (H_p/H) + 5.22 (H_p/H)^2 \quad (4.11)$$

The correlation coefficient (r^2) for this formula was 95.0%, which is quite high given the fact that only first order interactions were considered. The most popular existing method for the estimation of water cut and oil bypassing in bottom-water systems was developed by Kuo and DesBrisay (1983) using numerical simulation and dimensionless groups. This method was presented in Chapter 2 and validated in Chapter 3. As described in those Chapters, Kuo and DesBrisay (1983) only considered three dimensionless groups in their simulations. Moreover, the range of properties used by Kuo and DesBrisay to create their correlations was not obtained from a database of reservoirs and it is much narrower than the one employed in this study. In other words, the correlations provided here are more general as they cover a relatively wide range of reservoir-well systems. They also identify dimensionless groups that mostly control oil bypassing.

Equation (4.11) can be used to obtain surface plots as the one shown in Figure 115, which displays the effect of the two most influential groups, M and H_p/H on oil bypassing at abandonment. It can be seen that the effect of the end-point mobility ratio on oil bypassing is highly non-linear. This explains why five levels were used for M in the experimental design. When three levels were used, the correlation showed decreasing values of oil bypassing for increasing values of M, which is not realistic. As a recommendation, extreme caution needs to be exercised in the selection of the number of levels and their values for use in experimental

designs. Very erroneous results could be obtained if the results are not analyzed properly and/or if the researcher does not understand the physics of the process under consideration.

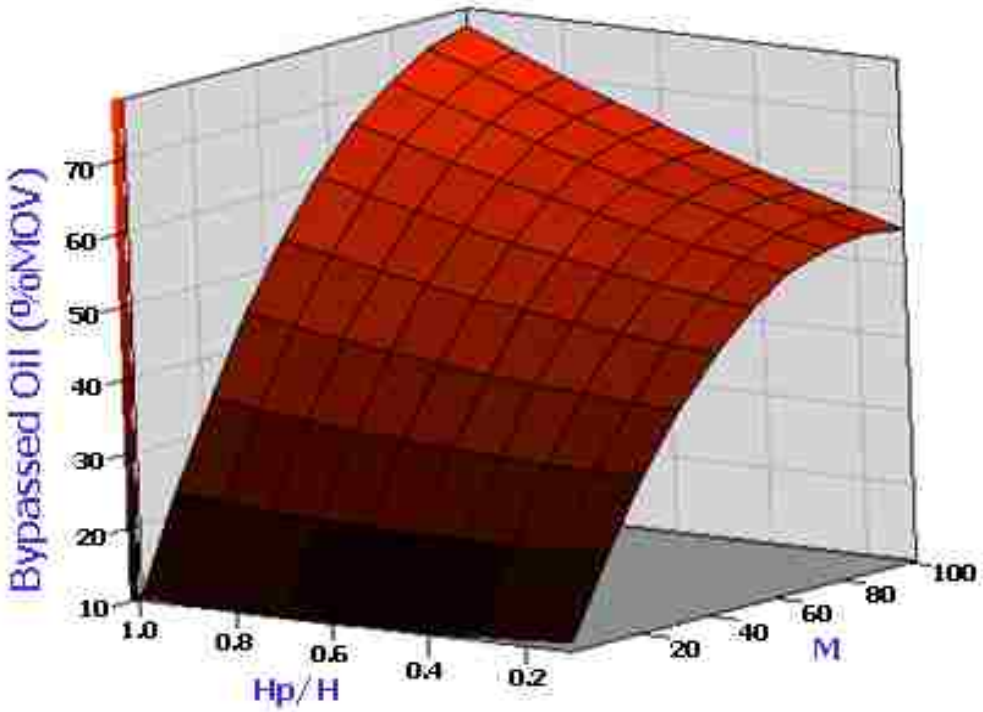

Figure 115: Surface Plot Showing the Effect of the Two Most Influential Groups on Oil Bypassing

4.2.7 Statistics of Oil Bypassing in Typical Bottom-Water Systems

Equation (4.11) and the data base that was built for the purposes of this study have been used to create statistics on the amount of oil that can be typically bypassed by water invasion to wells in bottom-water reservoirs. The procedure followed to create the statistics was described in Section 4.1.6. Figure 116 shows the results in form of a plot of cumulative probability of oil bypassing at abandonment.

The figure shows that half of the reservoirs would bypass about 25% of the movable oil in place and one in five reservoirs (20% of the reservoirs) would bypass 40% or more of the oil.

It is also obvious that oil bypassing at abandonment could be very high – almost 80% for the worst case scenario. These results suggest that oil bypassing in typical bottom-water reservoirs could be much more significant that in typical edge-water reservoirs. This is obviously because of the geometry associated with each of these systems – the initial oil-water contact in typical edge-water drive reservoirs is farther away from the well than in typical bottom-water systems.

In order to have an idea of the effect of the type of oil, expressed as a function of the end-point mobility ratio, on the statistics of oil bypassing, a new curve was added to Figure 116 with results from a new subgroup of reservoirs with end-point mobility ratios larger than 10 (which roughly correspond to oil viscosities larger than 20 cp). Half of this new subset of reservoirs bypasses 44% or more of the movable oil volume and one in five reservoirs in the subset bypasses 56% or more. These results confirm that the problem of oil bypassing in heavy oil reservoirs could be quite critical; thus solutions need to be identified and tested.

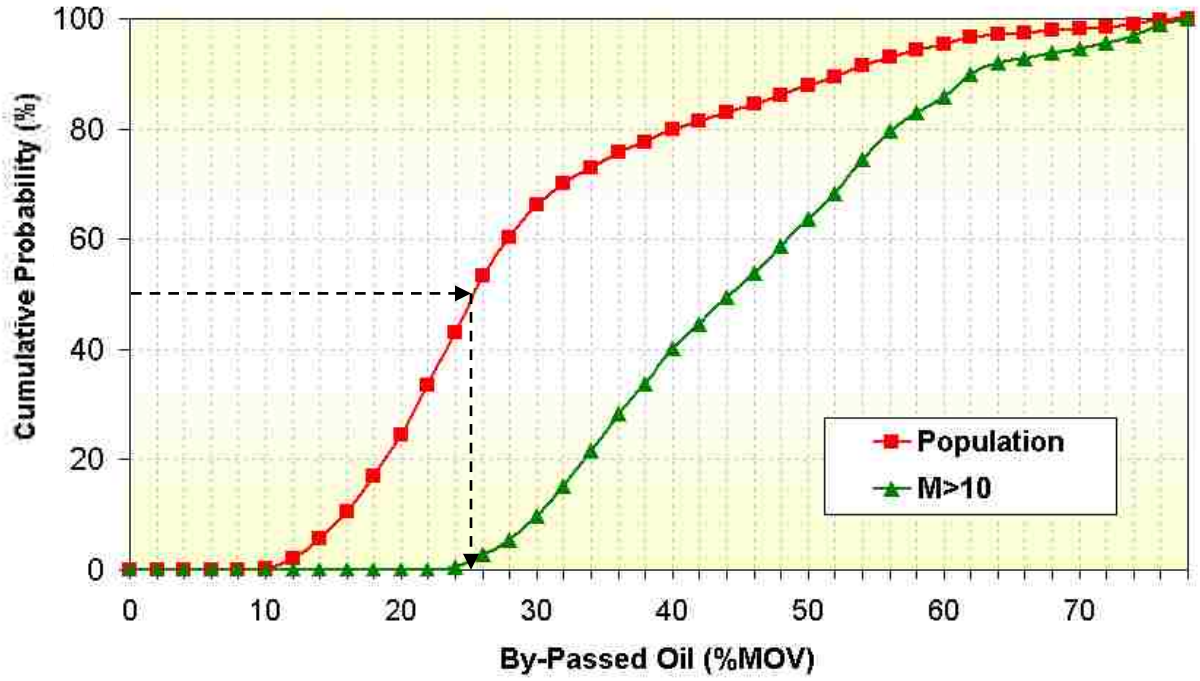

Figure 116: Cumulative Probability of Oil Bypassing at Abandonment for Bottom-Water Systems

4.2.8 Effect of Aquifer Strength

The effect of aquifer strength has been tested in this section by considering two different ratios of the pore volume of the aquifer to the pore volume of the reservoir (V_{aq}/V_o). Ratios of 10 and 6.2 MM were used to represent weak and infinite aquifers, respectively. These ratios were defined by changing the external radius of the aquifer only (aquifer thickness was the same in all sensitivities - 20 ft).

As was found in Section 4.1.8, many of the cases with weak aquifer strength exhibited poor pressure support and, therefore, ended before 98% water cut (the water cut abandonment criteria was not satisfied). This resulted in low recovery. The following error term was defined for each pair of runs - at the moment in which the runs with weak aquifer strength ended because of lack of reservoir energy - in order to have an idea of the effect of aquifer strength and the conditions promoting such effect:

$$\% \text{ Error} = \left| \frac{\%BPO\ strong - \%BPO\ weak}{\%BPO\ weak} \right| * 100 \quad \text{.....(4.12)}$$

Where *%BPO strong and %BPO weak* are the percentages of oil bypassing for the strong and the weak aquifers, respectively. As indicated above, for each set of reservoir conditions or dimensionless groups, these terms were defined at the time the runs for the weak aquifer stopped because of lack of pressure support. The overall average error was found to be quite low: 5.1%. This suggests that aquifer strength controls reservoir pressure and the time at which the simulations ended, but it did not significantly control the shape of the oil-water interface. The shape of the oil-water interface seems to be mainly controlled by the end-point mobility ratio, M. Similar results were obtained for edge-water systems.

4.2.9 Effect of the Shape of the Relative Permeability Curves

The effect of varying the exponents of the relative permeability curves on oil bypassing at

abandonment was studied using the same procedure described in Section 4.1.9. Table 36 shows the effect of the Corey exponents on water breakthrough time (BT time), percentage of oil recovery at breakthrough and percentage of recovery at abandonment. All simulation runs were completed using the P(50%) level for each one of the dimensionless groups. The wettability conditions presented in the last column of Table 36 were obtained from Goda and Behrenbrush (2006).

Table 36: Effect of Relative Permeability Exponents on Oil Bypassing for Bottom-Water Systems

Case #	n_w	n_o	BT time (days)	By-Passed Oil at Breakthrough (%MOV)	By-Passed Oil at Abandonment (%MOV)	Comments
1	2	4	494.0	95.2	19.3	Slightly oil wet
2	4	4	806.4	92.1	19.3	Intermediate
3	6	4	1083.0	89.4	19.0	Water wet
4	4	2	662.0	93.5	5.4	Slightly oil wet
5	4	6	956.0	90.6	32.2	Slightly water-wet
6	3	3	629.3	93.8	10.8	Slightly oil wet
7	2	2	514.0	95.0	5.5	Slightly oil wet

Figure 117 shows the 2D shape of the oil-water interface at water breakthrough for the cases presented in Table 36. Results show the same trends as for edge-water system. For example, it was found that the effect of the Corey exponents on water invasion and oil bypassing could be significant. It is shown that the choice of these exponents may not only affect the shape of the water cone, but also the thickness of the transition zone (separation between water saturation isosurfaces). This effect should be kept in mind for future studies of oil bypassing in bottom-water systems. It was also found that high "n_o" and low "n_w" values result in more oil bypassing at abandonment. This is obviously because these conditions originate low relative permeabilities to oil and high relative permeabilities to water, respectively.

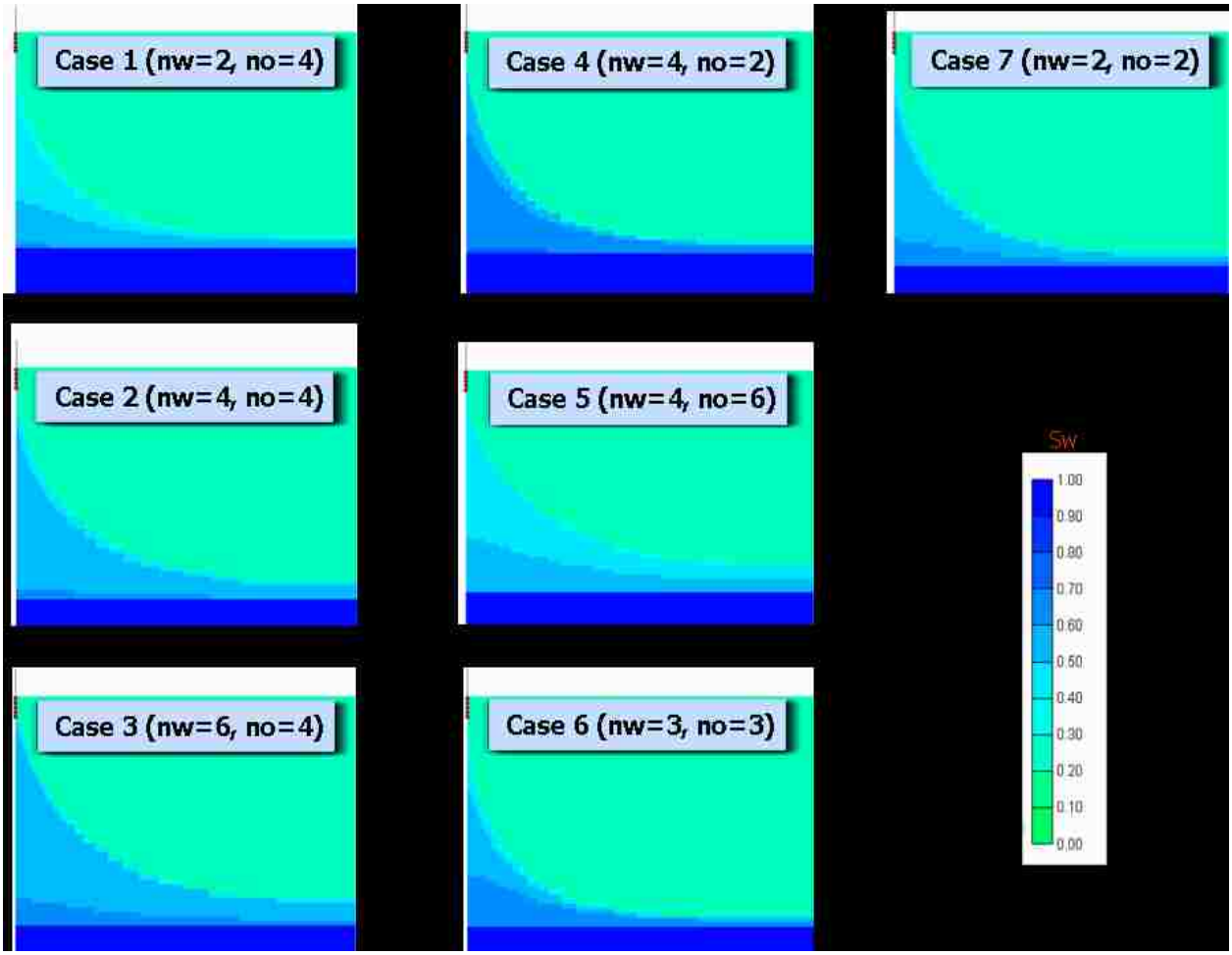

Figure 117: Effect of Relative Permeability Exponents on the Shape of Water Cone

4.3 Summary and Further Discussion

The reader should keep in mind that the reservoirs used in this research to obtain statistics on the amount of oil that may be typically bypassed in water-drive systems are "hypothetical". That is, they are formed using Monte Carlo simulations by randomly combining the values of each of the dimensionless groups. The values of the groups have been obtained by treating the individual parameters or properties contained in them as independent variables, which may be inappropriate. For example, correlations may exist between permeability and porosity. Perhaps a better approach to create statistics on oil bypassing may be to obtain oil bypassing values for

"real" reservoirs. However, generating a representative sample of reservoirs may require substantial data collection efforts. All 14 properties forming the dimensionless groups need to be found for each single reservoir in the sample.

As previously mentioned, all the dimensionless groups used in this dissertation have been obtained using Inspectional Analysis. According to Shook et al (1992), one of the steps in the analysis is the use of the method of elementary row operations to determine the number of "linearly" independent groups. By plotting each possible combination of groups (as was done in Figure 61), however, it was found that some of the groups are "correlated" or "dependent". The following explanation by Robert Nau (2007) may clarify the difference between these different terms: "the term "independent" can be used in at least three different ways in regression jargon: any *single* variable may be called an *independent variable* if it is being used as a predictor, rather than as the predictee. A *group* of variables is *linearly independent* if no one of them can be expressed exactly as a linear combination of the others. A *pair* of variables is said to be *statistically* independent if they are not only linearly independent but also utterly uninformative with respect to each other. In a regression model, you want your *dependent* variable to be *statistically dependent* on the *independent* variables, which *must* be *linearly* (but not necessarily *statistically*) independent among themselves". In other words, this explanation seems to suggest that the different dimensionless groups considered in this research are "linearly" but not "statistically" independent.

The correlations (response surface polynomial) for the prediction of the amount of bypassed oil at abandonment for edge-water systems (Equations (4.1), (4.3), (4.4) and (4.5) were created using a two-level design. As previously indicated, two-level designs are unable to explore fully the design space, which compromises the accuracy of these correlations. For

example, results obtained in Section 4.2.6 show that the effect of the endpoint mobility ratio on oil bypassing for bottom water systems is quite non linear. A similar result may be expected for edge-water system if more levels are considered in the experimental design. Oil bypassing could be substantially underestimated by using two-levels if the effect of endpoint mobility ratio on oil bypassing for edge-water systems takes a convex shape - as it did for bottom water systems (Figure 115). This study can be considered, therefore, a preliminary effort leading to improved correlations for oil bypassing in the edge-water systems. The accuracy of all the correlations presented in this chapter should be independently tested.

As can be observed in Tables 23 and 34, no group containing the petrophysical relations n_w, n_o (Corey Exponents) and $J(S_w)$ (Leverett J-function) has been included in this research. As explained by Shook et al. (1992), these relations are usually obtained experimentally, which can be difficult and uncertain. Simulation results presented in this chapter showed, however, that the effect of these relationships on the process of water invasion and oil bypassing could be significant. Additional effort is needed to find dimensionless groups that include these petrophysical relations.

The main response considered in this chapter was oil bypassing (or ultimate recovery) at the economic water cut for a well and its area of drainage (defined in this research as well-reservoir system). A water cut economic limit of 98% has been estimated using an oil price of $35/bbl, oil producing cost of $15/bbl and a water processing-disposal cost of $2/bbl. In other words, a well will not make any profit after its water cut exceeds 98%. Obviously, the water cut economic limit is very sensitive to the oil price, which has proven to be quite volatile in the last years. Ultimate recovery could also be defined as the time at which the Net Present Value of a project reaches its maximum. However, this definition is mostly used for large companies to

define the time of duration of a given project and it may not be adequate for small operators. After the maximum NPV the water cut may still be below the economic and, therefore, the well may still make money.

The problems associated with the use of the Dykstra-Parsons coefficient as an estimate of permeability variation are widely recognized in the literature. For example, Jensen and Lake (1988) showed that, because the Dykstra-Parsons coefficient is a one-parameter measure of permeability variability, permeability distributions exhibiting different reservoir performance can have the same Dykstra-Parsons coefficient. Jensen and Lake also studied the dependability of the coefficient on the sample size. They mention that large errors could be expected in the determination of the coefficient for a small number of data and that accuracy should increase as the number of data increases. They also mention, however, that there is no clear agreement on how many data are needed to obtain a sufficiently accurate estimate.

Despite all these problems, the Dykstra-Parsons coefficient seems to remain as the most commonly used measurement of permeability variation in the oil industry today. This is obviously because of its simplicity, which is also the main reason why the coefficient was selected as the measurement of permeability variation in this research. The fact that the coefficient is a one-parameter measurement of permeability is ideal for this research since the type of vertical distribution of permeability has been artificially imposed by considering different depositional sequences (transgressive, regressive and serrated). Also, the problems associated with the dependability of the coefficient on the number of data are not an issue in this research since a single value of the coefficient is used to study water invasion in these different depositional sequences.

CHAPTER 5. PERFORMANCE OF WELLS WITH MODIFIED COMPLETIONS

Results presented in Chapter 4 demonstrated that oil bypassing due to water invasion can be a significant problem in both edge and bottom-water reservoirs. Many different methods have been used to attack oil bypassing because of water invasion. Typically, they are classified as mechanical and chemical methods, as shown in Figure 118. Mechanical methods involve the use of packers, bridge plugs, well abandonment, infill drilling, pattern flow control and horizontal wells (Seright et al., 2003). Among the most commonly used chemical methods are cement, sand, calcium carbonate, gels, resins, foams, emulsions, particulates, precipitates, microorganisms and polymers. An effective strategy for selecting a proper method should involve a careful diagnosis of the excessive water problem. Seright et al. (2003) proposed a methodology to attack the various types of water problems by categorizing them from the least to most difficult. Water coning and underruning were considered the most difficult with no easy, low-cost solution. The authors maintained that gel treatments will almost never work for coning and underruning problems. Their observation was based on extensive reservoir and completion engineering studies and analyses of many field applications.

Gel treatments target the reduction of water inflow to wells implicitly assuming that oil inflow would increase. In the case of water coning and underruning the flow of water is an integral part of flow deliverability and, as such, cannot be stopped or reduced without reducing the oil flow. Thus, strategies studied in this chapter address the increased/accelerated oil recovery, instead of reduced water production. Two different methods for recovery increase/acceleration are studied using numerical simulation: changes in well penetration and dual completion installation featuring downhole water sink (DWS). The effect of a well

penetration is studied first, and then compared with downhole water sink (DWS). The two types of well completions are compared for new wells in edge and bottom-water systems.

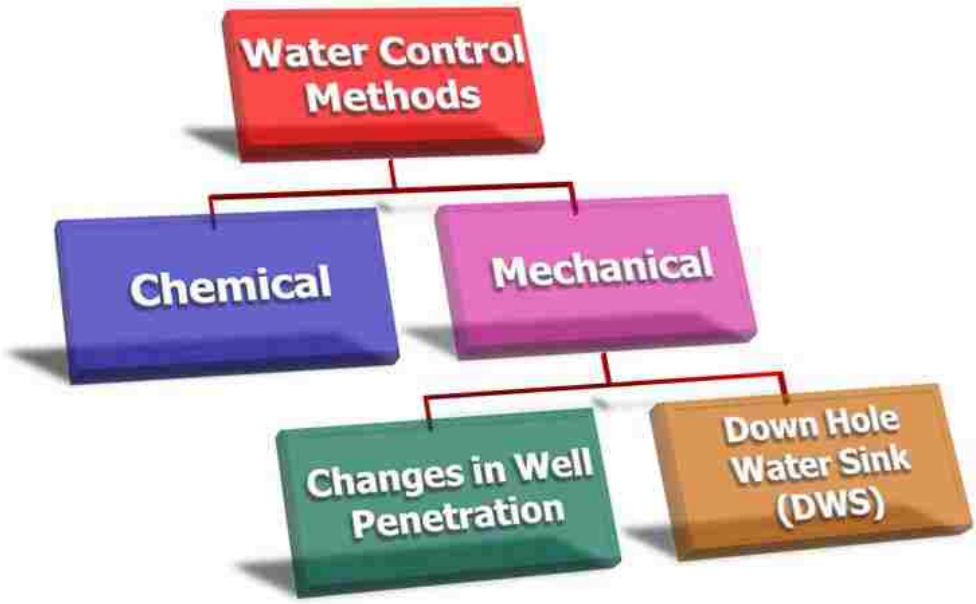

Figure 118: Classification of Methods Used to Control Water Invasion

5.1. Edge-Water Systems

5.1.1 Effect of Well Penetration on Oil Bypassing

5.1.1.1 Production Controlled by Maximum Total Rate

Figure 119 is an interaction plot showing the effect of well penetration for homogeneous edge-water systems. The plot was obtained using the results from the experimental design described in Chapter 4. It is shown that oil bypassing in edge-water systems is promoted by long well completions (fully penetrating wells), which can also be seen in Figure 63, Chapter 4. It is clear; however, that the effect of well penetration in edge-water systems in which production is controlled by maintaining a total (oil+water) production rate is - overall - **not statistically significant** (see Figure 62, Chapter 4). There are two explanations for this finding. First, if there is enough reservoir energy, the production would be maintained at the "targeted" (constant)

liquid rate during the production history, whether the formation is partially or fully penetrated. Second, because of the typical dimensions of edge-water systems - large length to thickness ratios - recovery is mainly controlled by water underruning and not by coning. The shape of the water tongue (and displacement efficiency) is mainly affected by the total production rate, not by the percentage of well penetration. For example it was found that, for most cases, the water breakthrough time in edge-water reservoirs produced at constant rate is not significantly affected by the percentage of well penetration.

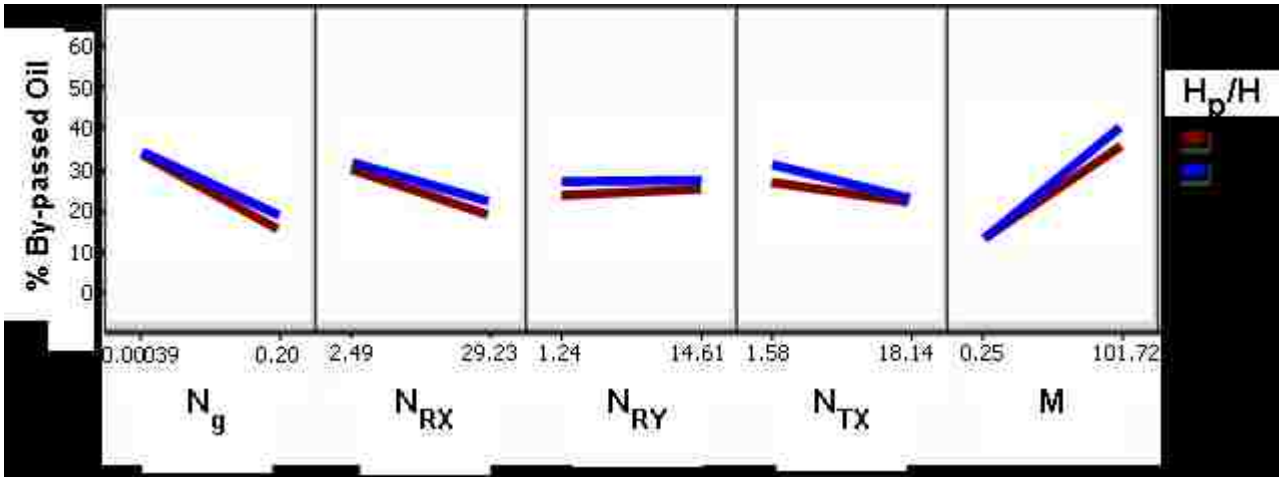

Figure 119: Interactions Plot Showing the Effect of Well Penetration for Homogeneous Edge-Water Systems

Despite the small overall effect of well penetration on oil bypassing, a case by case revision of the results of the experimental design presented in Chapter 4 shows that, under some specific conditions, oil bypassing could be largely influenced by the effect of well penetration. Figure 119 shows that the conditions that could promote the effect of well penetration in homogeneous edge-water systems are large N_g's (e.g., low production rates), N_{RX}'s (e.g., large k_z/k_x) and M's (e.g., large oil viscosity) and small N_{RY}'s (e.g., large k_y/k_x and/or thickness) and

N_{TX}'s (e.g., small dip angles). Analysis of the results showed that the first three conditions seem to be the most important ones. Similar results were found for transgressive, regressive and serrated sequences.

Figure 120 shows the effect of well penetration on oil bypassing (or oil recovery) for case 51 of the design, a case defined by using the highest levels for N_g, N_{RX} and M and the lowest levels for N_{RY} and N_{TX} (as shown in Table 25). The effect of penetration on oil bypassing for these conditions is of large importance: the 10% penetration scenario recovered about 60% more oil than the full penetration scenario. Oil bypassing for these conditions could be substantially reduced by using short penetrating wells. Figure 120 also shows; however, that oil recovery is quite slow, which may hamper the overall economic performance of the well.

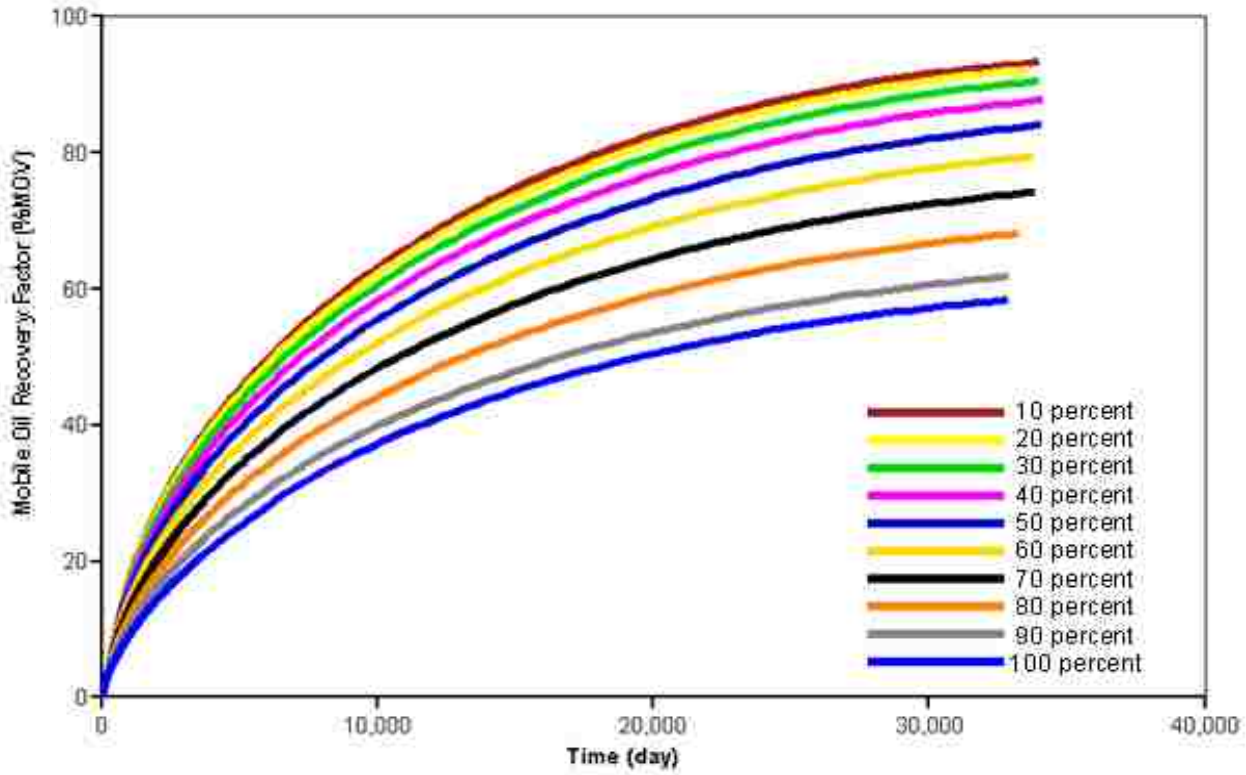

Figure 120: Effect of Well Penetration on Oil Recovery/Bypassing for Case 51 (N_g=0.20, N_{RX}=29.23, N_{RY}=1.24, N_{TX}=1.58 and M=101.72)

Figure 121 displays the shape of the oil-water interface at breakthrough for Case 51. Note the formation of a very thin and long water tongue that gets to the bottom of the well very quickly. Water breakthrough time for the full penetration case is only 165 days, whereas water breakthrough for the 10% penetration case occurs in 775 days. This delay in water breakthrough time is obviously beneficial for the recovery of oil.

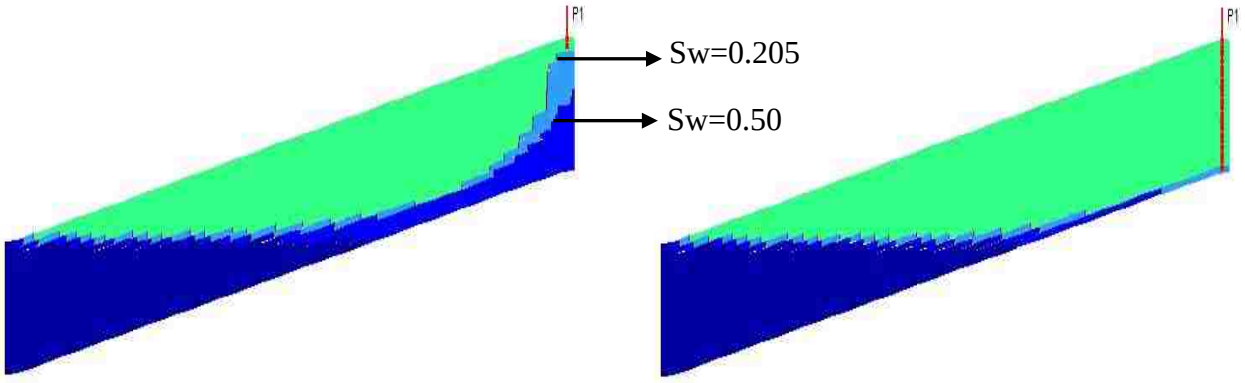

Figure 121: 2D Shape of Oil-Water Interface at Water Breakthrough for Case 51 at 10% Penetration (Left) and 100% Penetration (Right)

Oil recovery vs. cumulative liquid production for Case 51 can be seen in Figure 122. As indicated in Chapter 4, this type of plot gives an indication of the displacement efficiency (defined in this research as oil recovered per barrel of fluid produced). It is obvious that displacement efficiency is significantly better for the cases with short well penetrations. Since displacement efficiency is defined by the characteristics of the oil-water interface, these results suggest that shape of the oil-water interface can be substantially affected by the degree of well penetration for cases with the characteristics of Case 51.

Figure 123 shows recovery vs. time for Case 27 (N_g=0.00039, N_{RX}=29.23, N_{RY}=14.61, N_{TX}=1.58 and M=101.72), a case in which the degree of well penetration has a very minimal

effect on oil bypassing at abandonment. Since the effect of well penetration was found not to be statistically significant for typical reservoirs (see Figure 62 (Chapter 4) and Figure 119), this is perhaps the most common situation. Figure 123 also show, thus, that oil bypassing for Case 27 is quite large – about 60%. As was suggested before, the small effect of well penetration on oil bypassing for most of the edge-water reservoirs can be explained by their typical dimensions (large length to thickness ratio). Recovery is mainly controlled by water underruning and not by coning. The time of development of the cone in typical edge-water systems is quite short compared with the total time water takes to get from the original oil-water interface to below the well. Because of this, the effect of well penetration on water breakthrough time is commonly very small. For example, water breakthrough times for Case 27 were 15.3 and 18.1 days for the full and 10% penetration scenarios, respectively.

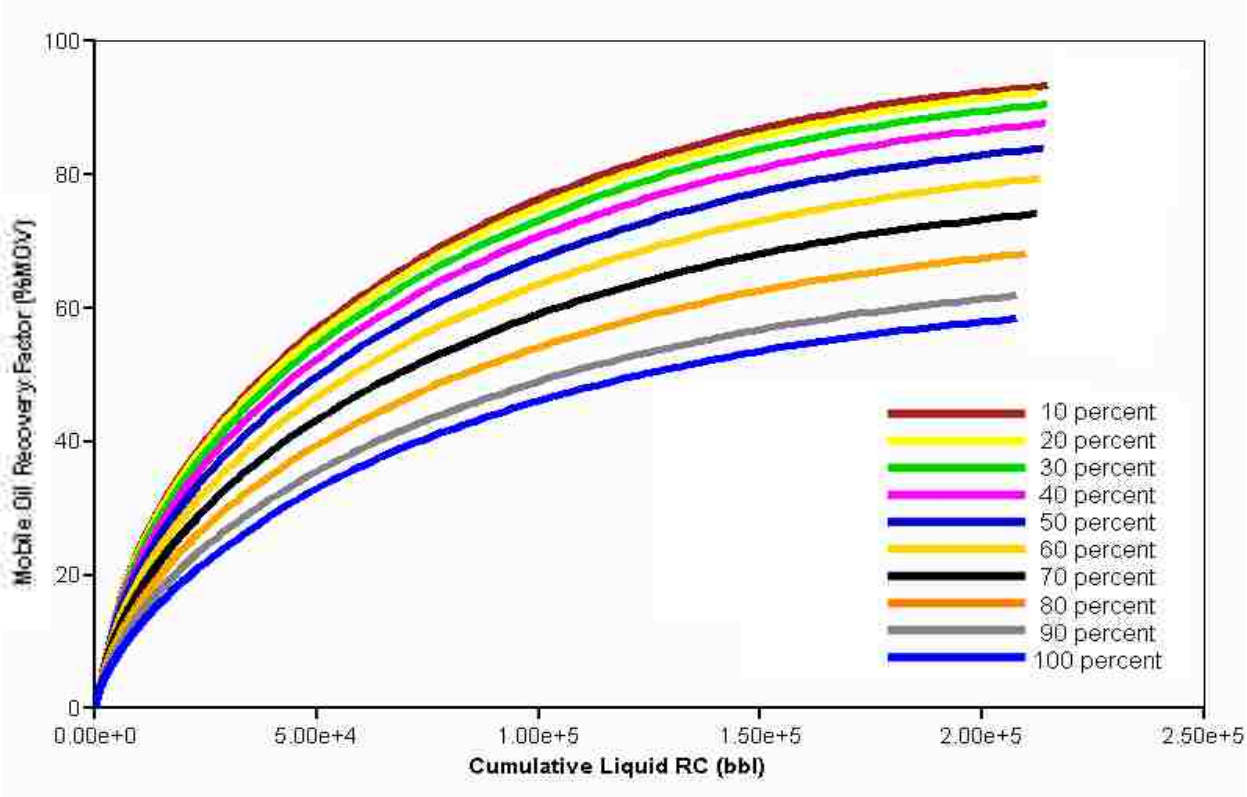

Figure 122: Recovery vs. Cumulative Liquid Production for Case 51 (N_g=0.20, N_{RX}=29.23, N_{RY}=1.24, N_{TX}=1.58 and M=101.72)

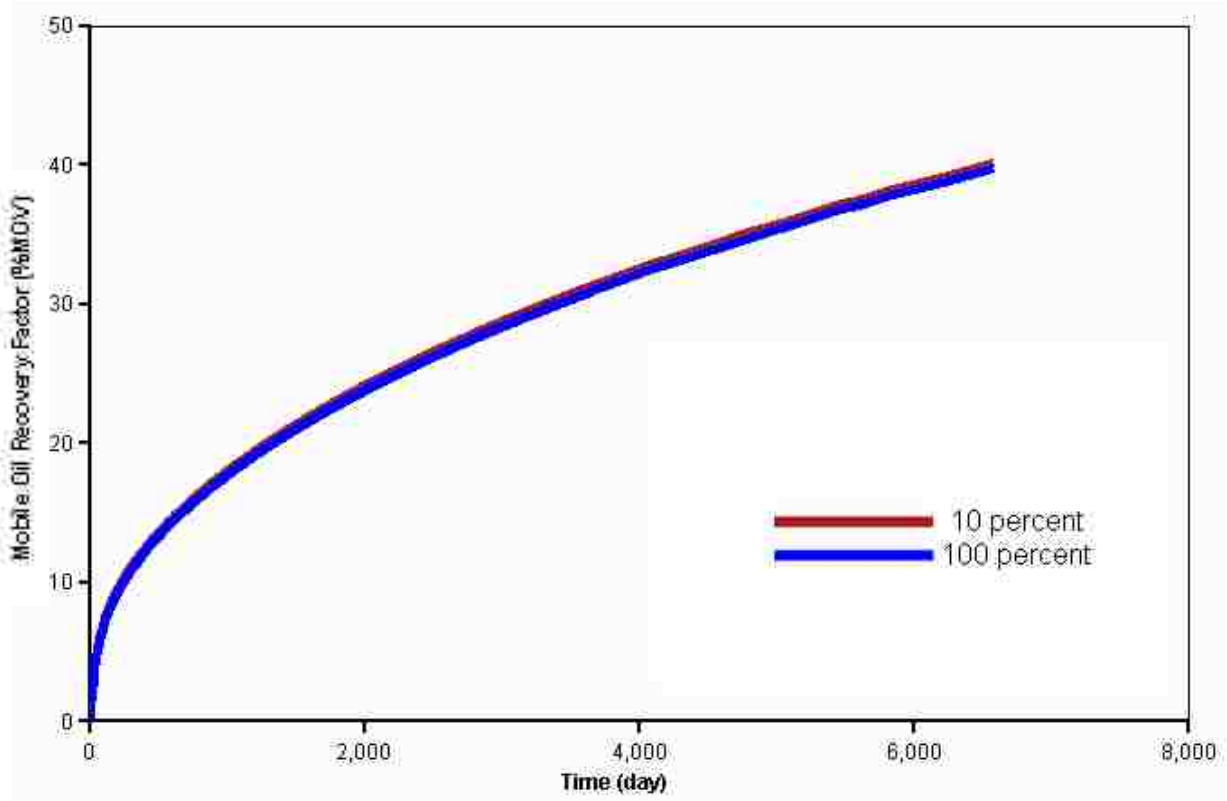

Figure 123: Effect of Well Penetration on Oil Recovery/Bypassing for Case 27 (N_g=0.00039, N_{RX}=29.23, N_{RY}=14.61, N_{TX}=1.58 and M=101.72)

Figure 124 shows oil recovery vs. liquid production for Case 27. It is obvious that the degree of well penetration does not have a significant effect on the displacement efficiency for the conditions of Case 27. As previously suggested, this is because the displacement is controlled by water underruning and not by coning.

5.1.1.2 Production Controlled by Minimum Bottom Hole Pressure

This section shows the effect of well penetration on oil bypassing when the system is produced at the maximum possible drawdown. No constant production rate target is defined in the simulations. Therefore, it is not possible to calculate a unique value for the buoyancy number group, N_g. The maximum drawdown is defined in this dissertation by setting a minimum bottom-hole pressure, which is taken to be slightly above the bubble point pressure.

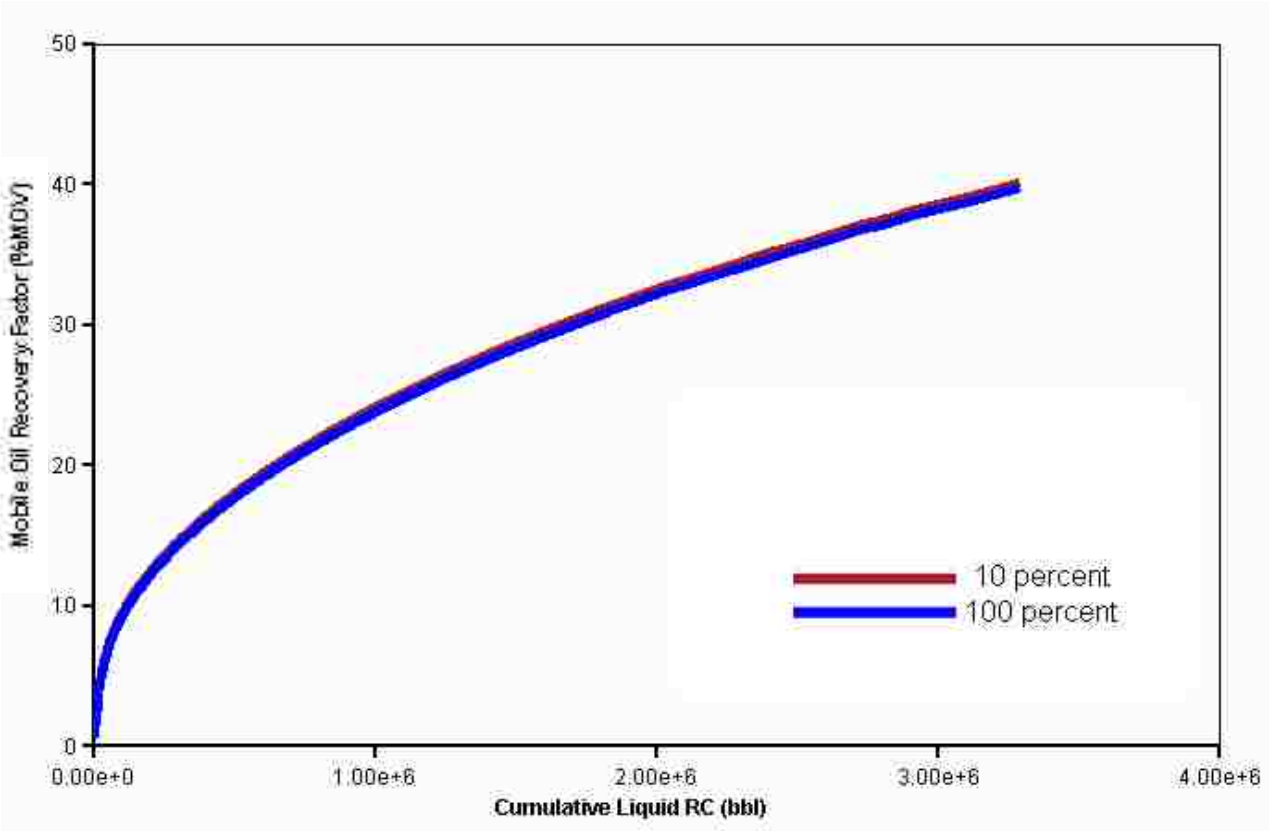

Figure 124: Oil Recovery vs. Cumulative Liquid Production for Case 27 (N_g=0.00039, N_{RX}=29.23, N_{RY}=14.61, N_{TX}=1.58 and M=101.72)

Figure 125 shows the effect of well penetration on oil recovery for Case 51 of the experimental design presented in Chapter 4. This case showed an important effect of well penetration on oil bypassing in the previous section (constant-rate production). It can be seen that recovery for the deep penetrating wells is faster than for the short penetration scenarios. This is because long completions allow larger area of contact between the well and the reservoir. It can also be seen, however, that overall recovery is smaller for the deep penetrating scenarios. This is because using deep penetrating wells would accelerate water breakthrough and promote the formation of thin and long water tongues. For example, water breakthrough time for the full penetration and 10% penetration scenarios occurred at 55 and 304 days, respectively.

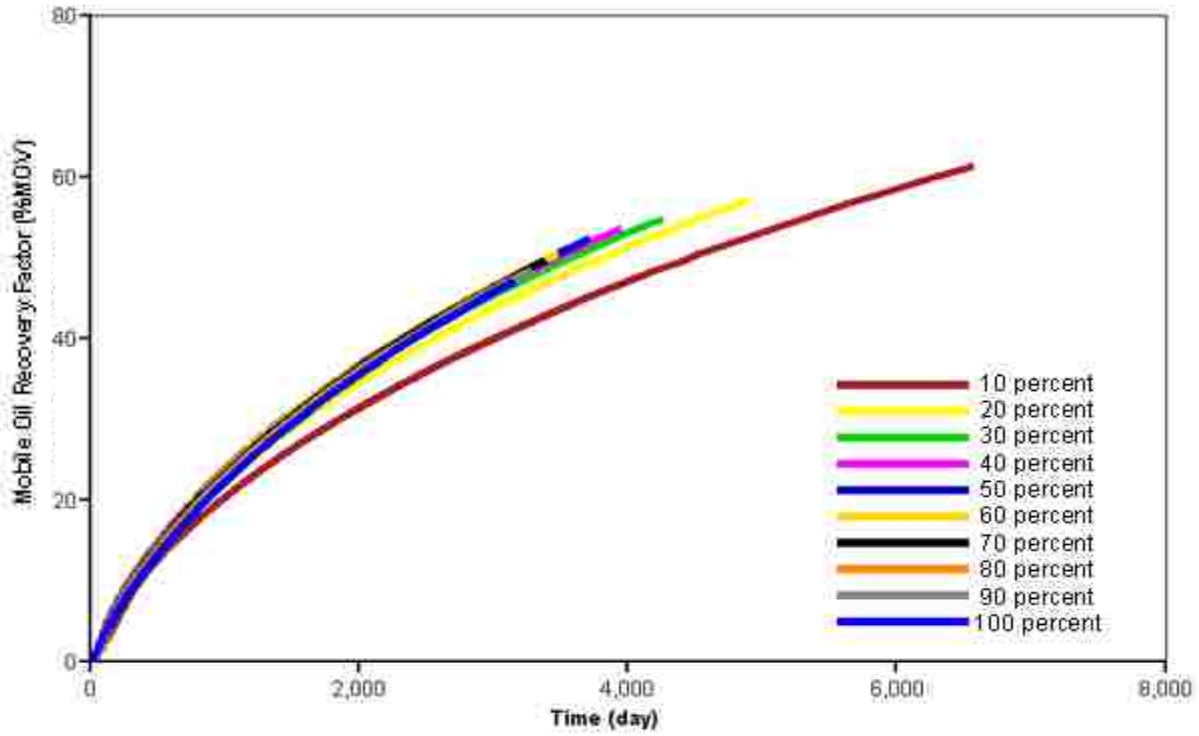

Figure 125: Effect of Well Penetration on Oil Recovery/Bypassing for Case 51 (N_{RX}=29.23, N_{RY}=1.24, N_{TX}=1.58 and M=101.72)

Oil recovery vs. cumulative liquid production for Case 51 can be seen in Figure 126. As was found for the cases controlled using a constant liquid rate (previous section), it is obvious that displacement efficiency is significantly better for the cases with short well penetrations. This confirms that the shape of the oil-water interface can be substantially affected by the degree of well penetration for cases with the characteristics of Case 51.

Figure 127 displays the effect of well penetration on oil recovery for Case 27 of the experimental design. This case showed almost no effect of well penetration on oil bypassing in the previous section (constant-rate production). It can be seen that total recovery for the full penetration scenario (%R=32.6) is similar to that with 10% well penetration (%R=35.7). However, recovery for the full penetration scenario takes less than a fourth of the time (75% shorter). As explained before, this is because long completions allow larger area of contact

between the well and the reservoir. These results also demonstrate the effect of the unique geometry of edge-water systems. Typically, the length of the reservoir is much larger than its thickness. This causes the displacement to be mainly controlled by the formation of a water tongue (water underruning), and not by coning. As a consequence, using long well penetrations would not result in substantial acceleration of the water breakthrough time when compared with short penetrations.

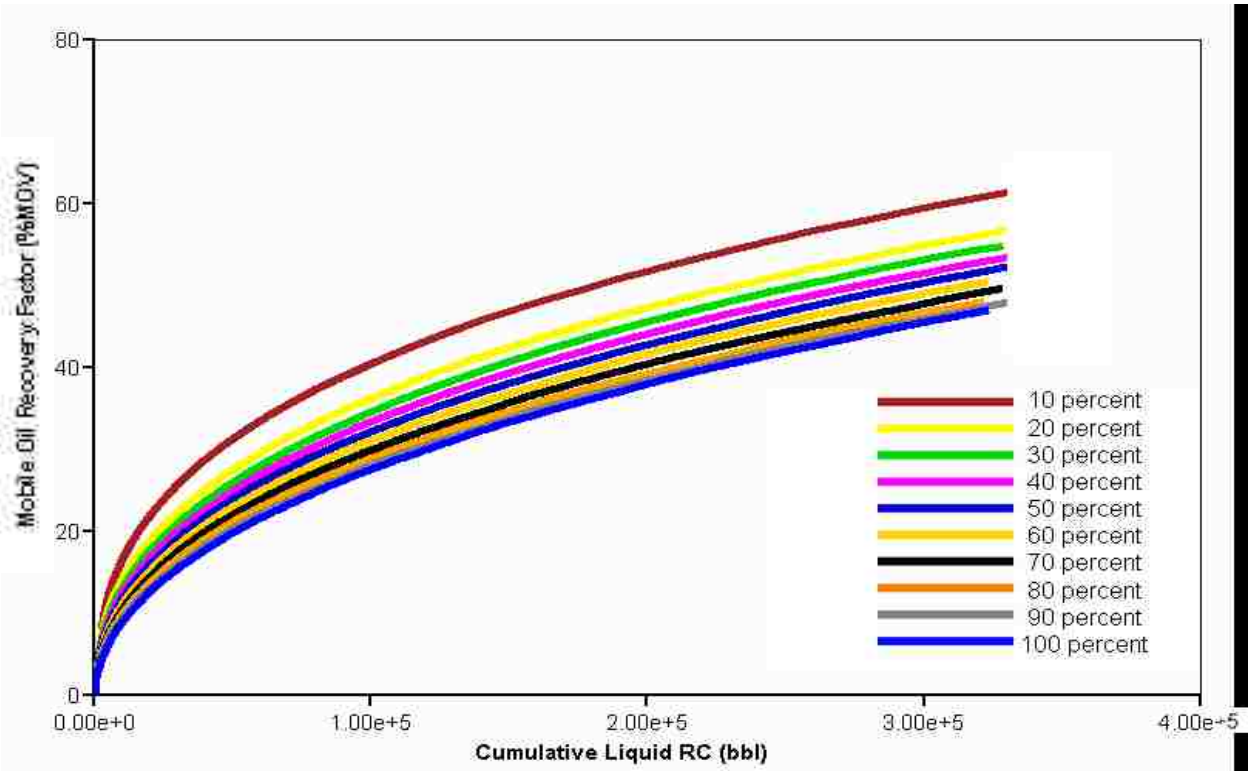

Figure 126: Oil Recovery vs. Cumulative Liquid Production for Case 51 (N_{RX}=29.23, N_{RY}=1.24, N_{TX}=1.58 and M=101.72)

Figure 128 shows oil recovery vs. liquid production for Case 27. Similar to what was obtained for this case in the previous section (constant-rate production), it is clear that the degree of well penetration does not have any significant effect on the displacement efficiency for the conditions of Case 27.

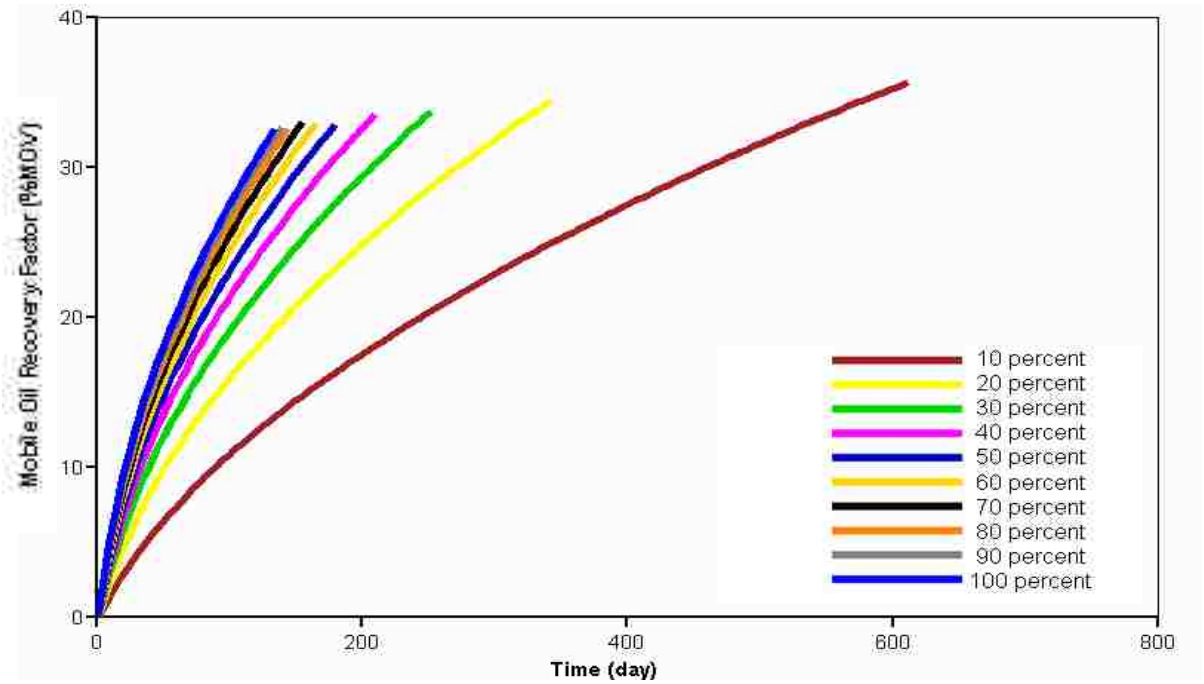

Figure 127: Effect of Well Penetration on Oil Recovery/Bypassing for Case 27 (N_{RX}=29.23, N_{RY}=14.61, N_{TX}=1.58 and M=101.72)

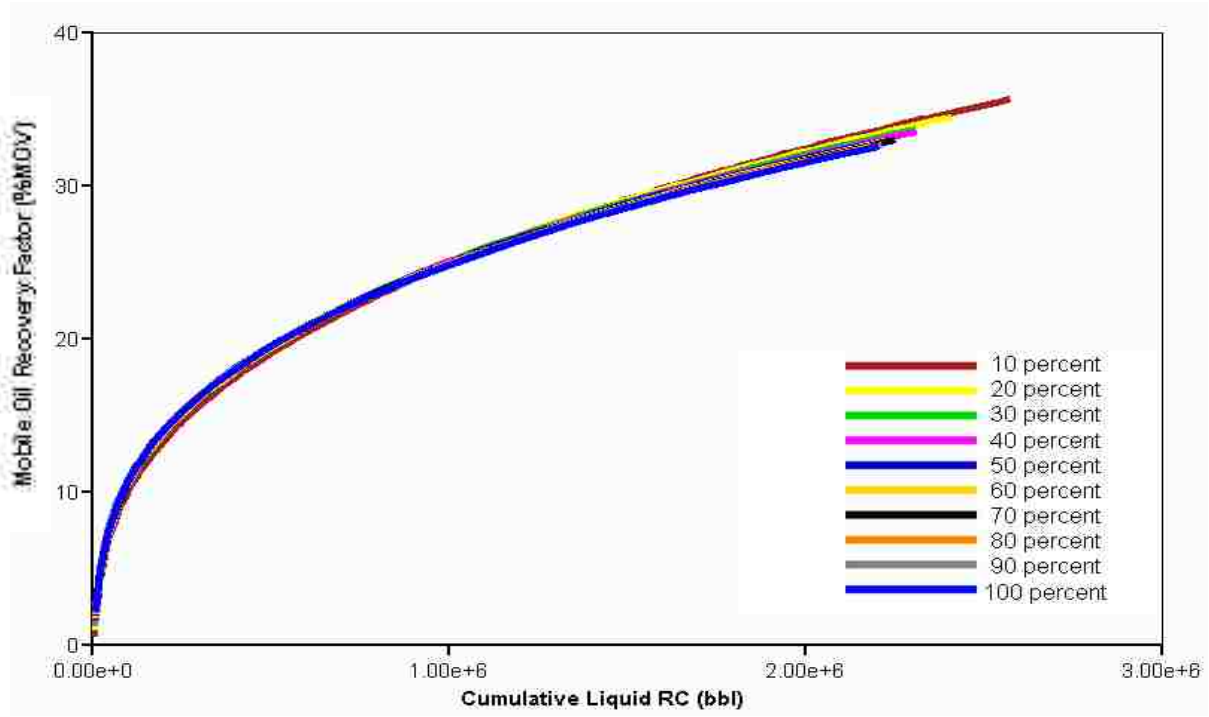

Figure 128: Oil Recovery vs. Cumulative Liquid Production for Case 27 (N_{RX}=29.23, N_{RY}=14.61, N_{TX}=1.58 and M=101.72)

5.1.1.3 Summary on the Effect of Well Penetration

Results presented in the previous section suggest the following:

- For reservoirs with large N_g's (e.g. small production rates), N_{RX}'s (e.g., large k_z/k_x) and M's (e.g., large oil viscosity), the effect of well penetration on oil recovery/bypassing could be important. The results suggest that reservoir with these conditions should be operated using short penetrating wells, since this may improve displacement efficiency (defined as oil recovered per barrel of fluid produced) and delay water breakthrough.
- For reservoirs with most of the other possible combinations of dimensionless groups, (most typical situation), having different degrees of well penetration would not substantially affect displacement efficiency. Reservoirs in this category could be produced using deep penetrating wells, since this could accelerate recovery.
- Changing the degree of well penetration may not improve recovery in typical edge-water systems affected by the formation of thin and elongated water tongues. Then, it is obvious that a method is needed to reduce oil bypassing in these systems.

5.1.2 Dual Completions with Water Sink (DWS) for Edge-Water Systems

This section shows a comparison between single (partial and full penetrations) and Down Hole Water Sink (DWS) completions for newly completed wells. Wojtanowicz (2004) describes DWS as a technique for producing water-free hydrocarbons from reservoirs with water drive and strong tendency to water coning. Conventional wells in these reservoirs produce increasing volumes of water with decreasing amounts of oil, which ultimately leads to early shut down of these wells without sufficient oil recovery. According to Inikori et al. (2002) "the basic idea is to perforate both the oil zone and the water zone and produce each fluid with a separate completion string. The production of water from the water zone creates a "pressure sink" and counters the

development or progression of the water cone toward the oil completion".

Produced water in conventional wells is contaminated with hydrocarbons and, therefore, requires costly treatment prior to offshore discharges or subsurface injections. DWS technology eliminates water cutting the hydrocarbon production by employing hydrodynamic mechanism of coning control in-situ at the oil-water contact (Wojtanowicz, 2004).

Figures 129 and 130 show the two basic variants of the DWS systems. These variants are described by Wojtanowicz (2004) as follows: in the drainage-production variant (Figure 129), water is co-produced to the surface with oil. The wells can be operated such that the drained water is free of oil and readily discharged. The systems can also be designed for maximum oil production with the upper completion producing water-free oil and the water sink completion producing water with some oil cut. In the latter case the design involves inversing the water cone to create oil breakthrough into the water sink. In the drainage-injection variant (Figure 130) the drained water, free from oil contamination, is either re-injected downhole into the same aquifer (downhole water loop) or into a deep injection zone (split drainage-injection). This could result in economic advantages since there are no lifting, treatment and/or surface disposal costs associated with water.

Optimization of well-reservoir systems with DWS can be a difficult process. Historically, DWS systems in numerical simulation studies and field trials have been operated by setting constant production rates at both the top and the bottom completion. Examples of this practice can be found in Shirman and Wojtanowicz (1998), Wojtanowicz et al. (1999), Inikori and Wojtanowicz (2001), Siddiqi and Wojtanowicz (2002), Inikori et al. (2002) and Ju et al. (2005). Generally, the top and bottom rates have been "guessed" rather than obtained using a systematic approach.

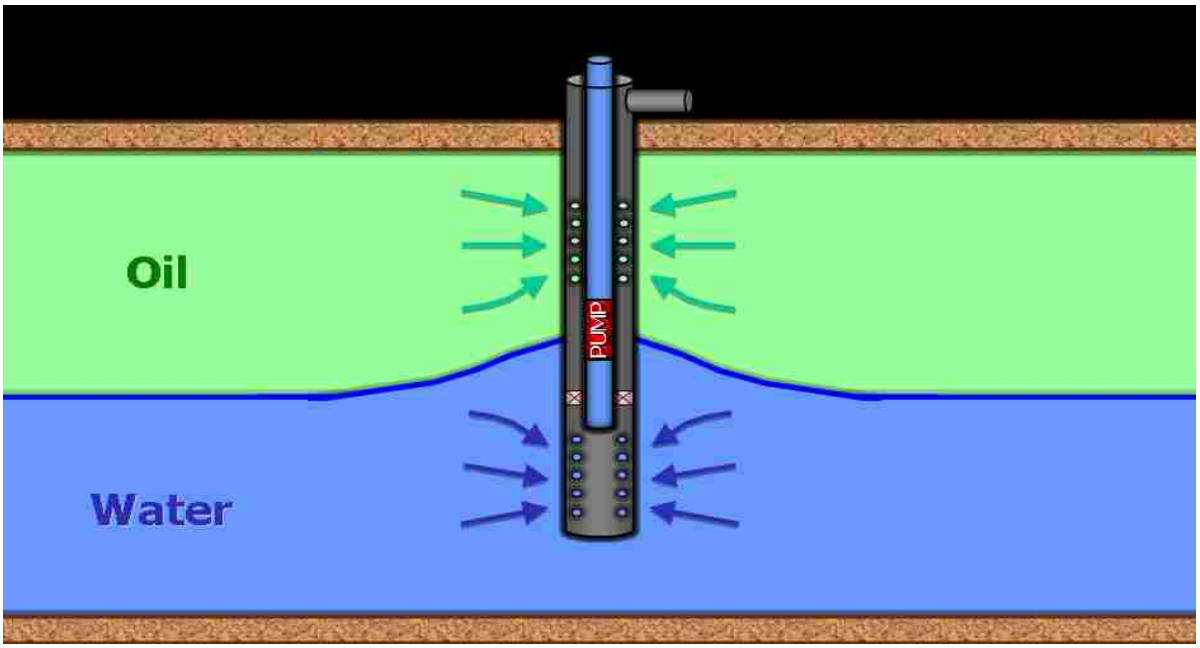

Figure 129: Water Drainage-Production Variant of DWS Completion

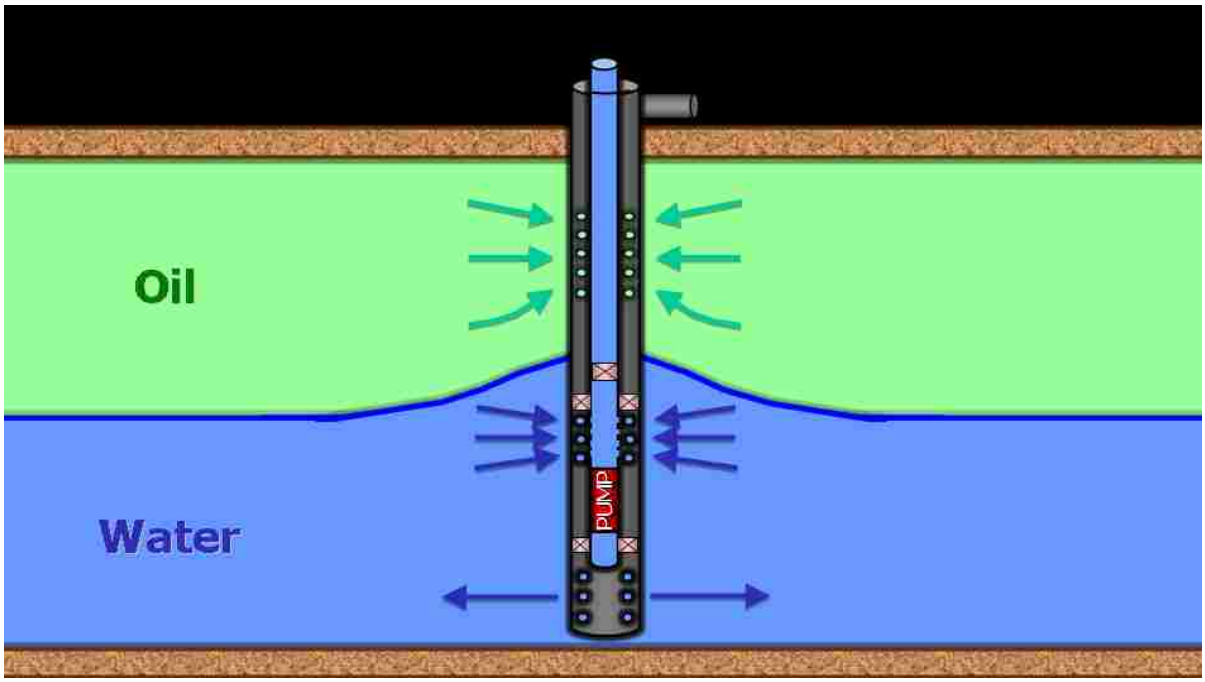

Figure 130: Water Drainage-Injection Variant of DWS Completion

Arslan (2005) provided what can be considered as the first consistent method to select the production and water drainage rates needed to optimize DWS well performance via numerical simulation. Arslan suggested that the best operating condition for DWS should be constrained by the inflow performance relationship (IPR), the tubing performance relationship (TPR) and the limiting drainage rate. Arslan also indicated that DWS systems should be operated at the maximum allowable pressure drawdown at top and drainage completions to ensure completion stability and that the drainage completions (sink) should be kept oil-free for environmental reasons.

Arslan related all these operating limitations in a single plot called a DWS characteristic plot (Figure 131). The plot shows a reverse coning region, where oil cones into the bottom completions, and a water coning region, where water is produced at the top completions. These two regions are separated by a "flip-flop line" under which the top completion flow rate dominates over the drainage rate and water coning occurs. Above the flip-flop line, the drainage rate overcomes the top completion rate and reverse coning occurs.

Arslan (2005) demonstrated that, for bottom-water reservoirs, the slope of flip-flop line can be approximated by the ultimate water cut value as presented by Kuo and DesBrisay (Equation (2.43), Chapter 2). For edge-water systems, the ultimate water cut can be obtained using Equation (2.15) proposed by Dake (1978):

$$WC_{ul} \approx \frac{M b_e \rho_e (1-\rho_e) G}{1 - M \rho_e b_e} \quad \text{.....(2.15)}$$

Where G can be calculated using Equation (2.13) and b_e is the fractional thickness of water ($b_e=H_w/(H_o+H_w)$) at the producing end of the reservoir. If G is neglected (for example, for horizontal reservoirs), the resulting equation is:

$$WC_{ul} \approx \frac{M\, b_e}{1 - M - b_e} \quad \text{.....(5.1)}$$

Equation (5.1) is equivalent to the equation for bottom-water systems (Equation (2.43)).

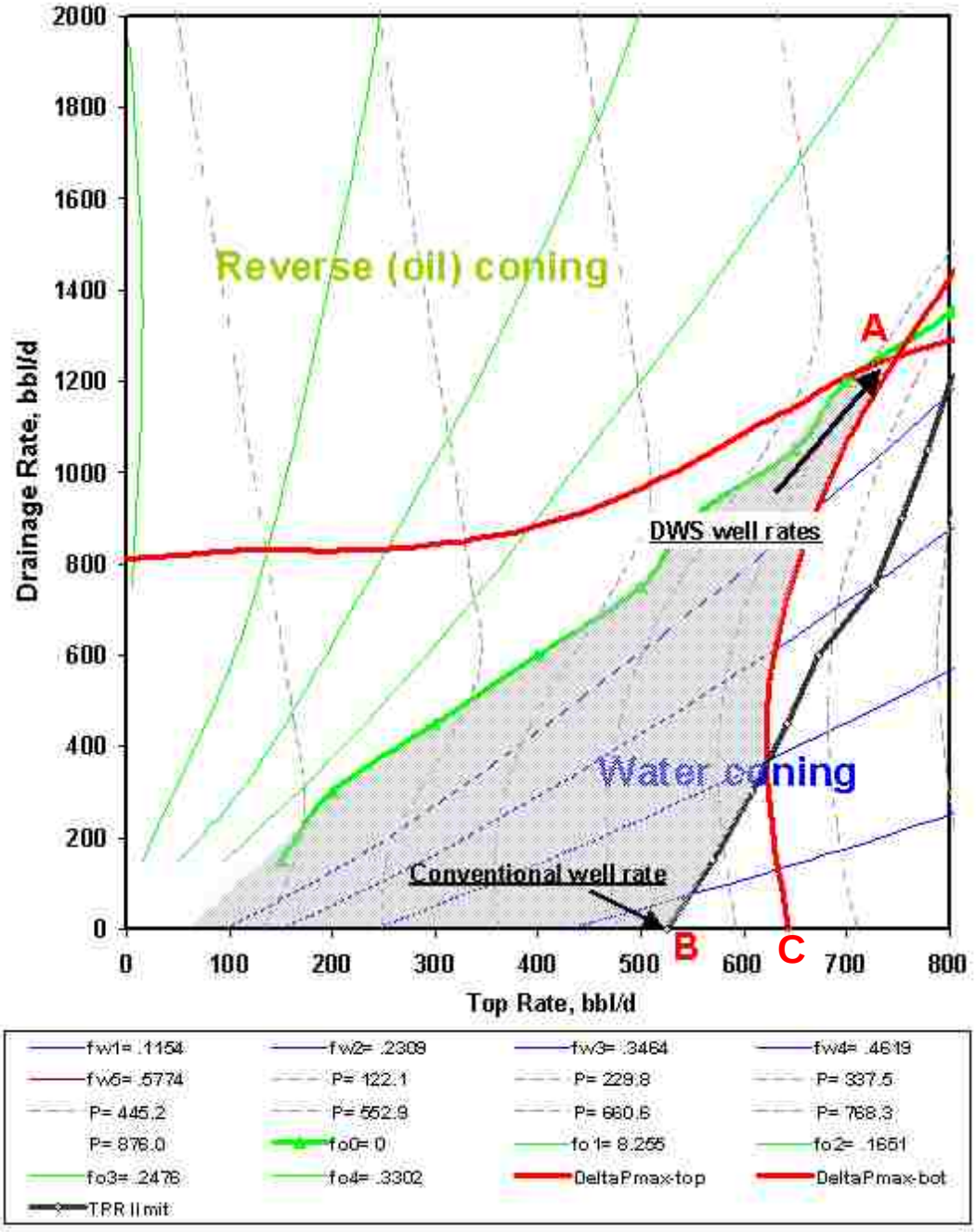

Figure 131: DWS Characteristic Plot (Arslan, 2005)

Equations (2.15) and (2.43) assume stabilized flow conditions, fully penetrating wells and equal pressure drop in the oil and water zones. These equations give an approximate estimation for the flip-flop line slope and can be used to understand DWS well operations. Some factors - not included in Equations (2.15) and (2.43) - that can affect the slope of the flip-flop line are distributed or "diffused" saturation effects around the wellbore and partial penetration effects.

Arslan (2005) also indicated that, at the maximum allowable pressure drawdown for the top completion (thick red line at the bottom-right of Figure 131), the top completion rate can be improved by draining water from the bottom completion to the point of the flip-flop line where the top completion has no water coning (point A in Figure 131). This asseveration will be tested later in the Chapter. As the depletion of the oil zone continues, the water-oil interface moves upward. As the water thickness increases, the drainage rate required to maintain a low water cut at the top completion also increases, as well as the slope of the flip-flop line (see Equations (2.15) and (2.43)). In other words, the optimum top and bottom completion rates will change with time.

Arslan (2005) included all the operation principles presented in Figure 131 in a successive nodal analysis approach. He wrote a computer code with interface to a numerical simulator to estimate the optimum top and bottom rates. The main problems associated with Arslan's approach are:

- Because the DWS characteristic plot (Figure 131) changes with time, it requires countless simulation runs to define the optimum top and bottom rates at each time step (all possible combinations of top-bottom rate need to be run at each time). This may be impractical, especially if a large number of grid blocks is used in the simulations and/or if sensitivity to other parameters - other than the top and bottom rates - is required.

- User interaction is required to define new ranges for the rates and a new set of runs at each time. Tuning the ranges of top and water drainage rates at each stage is not an efficient process.
- Because Equations (2.15) and (2.43) assume stabilized flow conditions, all the simulations have to be run until steady-state. This may be time consuming and it requires the use of oil and water injectors.

Arslan proposed a stepwise optimization method to remove the need for user intervention and improve the number of simulator runs. However, the optimization method also requires a large number of simulations and, because of its inherent complications; it is not practical for common field operations where rapid assessment of the best operational conditions is required.

5.1.2.1 A New Method for DWS Operation by Varying the Bottom Completion Rates

A new simplified version of the successive nodal analysis approach developed by Arslan (2005) is proposed here to determine appropriate production rates for a DWS system. The method involves using variable water production rates at the bottom completion in a single simulation run. Variable rates are justified since the dynamics of water coning and the position of the horizontal oil-water contact change with time. This new way of utilizing DWS is possible due to advances in the numerical simulation package used in this dissertation.

The new method is based in the ultimate water cut equations previously presented (Equations (2.15) and (2.43)). It calculates the bottom completion rates required for defined water cuts at the top completion. In addition to the parameters needed for Equations (2.15) and (2.43), the only input data required are the maximum allowable rate at the top completion ($q_{total\ top}$= rate at maximum pressure drawdown), and the desired initial and final water cuts at the top

completion. The procedure to calculate the bottom completion rates can be summarized as follows:

1. Calculate the ultimate water cut using Equation (2.43) for bottom-water systems or Equation (2.15) for edge-water systems. This has to be done from $h_w = H_w$ to $h_w = H_w + H_o$ (i.e., from the initial OWC to the point where the entire oil zone is being displaced by water).
2. Assume initial and final water cuts at the top completion. Assign the initial water cut at the top to $h_w=0$ and the final to $h_w= H_w + H_o$. Distribute the top water cut values uniformly between these two limits.
3. For each h_w, calculate the water rate at the top ($q_{water\ top} = WCut_{top} * q_{total\ top}$).
4. For each h_w, estimate the oil rate at the top ($q_{oil\ top} = q_{total\ top} - q_{water\ top}$).
5. Calculate the total water production (top+bottom) using the ultimate water cut concept. For example, for bottom water systems or nearly horizontal edge-water systems ($G \approx 0$), the total water production is calculated as:

$$q_{water\ total} \frac{WC_{ul}}{1 - WC_{ul}} q_{oil\ top} \quad \text{.....(5.2)}$$

6. Calculate the water rate at the bottom ($q_{water\ bottom} = q_{water\ total} - q_{water\ top}$)
7. Run the simulator with the new calculated (variable) bottom rates, if the final bottom completion rate is too high (i.e., if the minimum bottom hole pressure is reached), assume a larger final water cut in step 2. This will give smaller final water rates in the bottom completion.

Some comments on the new method are:

- The rate at the bottom completion is defined/controlled by the water cut from the top completion. This allows a dynamic control of the water cone and, therefore,

improvement on the displacement efficiency. For example, if the water cut in the top completion is kept at zero - an ideal situation - the method would calculate the bottom completion water rates that would give water-free production in the top zone. In other words, the method calculates the bottom completion rates that would result from the intersection of a given top completion rate with the corresponding flip-flop line.

- The water cut from the top completion is defined by the maximum bottom completion rate that can be achieved according to the maximum allowable pressure of the system. Calculations with the method have shown that maintaining production at the flip-flop line (water cut at the top=0) could require very high rates from the bottom, which may be unachievable. Analysis of Equations (2.15) and (2.43) shows that this is especially true for systems with high endpoint mobility ratios. This indicates that in many situations the best practice would be to operate below the flip-flop line.
- Only one simulation run is needed since, due to advances in the simulation package used, the bottom completion water rates can be dynamically changed in the simulator by using multipliers. This provides a substantial advantage over Arslan (2005) method, which may require thousands of simulation runs.
- Since the method calculates the water rates in the bottom completion needed to produce at or below the flip-flop line, it ensures oil-free production from the bottom completion.
- Another advantage of the method is that it calculates the initial drainage production rates needed for desired initial rates and water cuts from the top completion. The "guessing" of rates required by previous studies (Shirman and Wojtanowicz (1998),

Wojtanowicz et al. (1999) Inikori and Wojtanowicz (2001), Siddiqi and Wojtanowicz (2002), Inikori et al. (2002) and Ju et al. (2005)) has been eliminated.

The new method was tested under different conditions for both edge and bottom-water systems. Figure 132 depicts rates from the bottom completion vs. water cuts from the top completion obtained with the new method and with the simulator for a bottom-water case with G_v=0.044 (i.e., high production rate), W_{sp}=24.05 (i.e., large well spacing and/or large ratio k_v/k_h) and M=10. The initial top rate for this case was 2614 bpd and the initial water and oil thicknesses were 20 ft and 100 ft, respectively. It can be seen that the agreement is excellent. This was expected since the simulator was provided the bottom completion rates as constraints which were obtained from the new method.

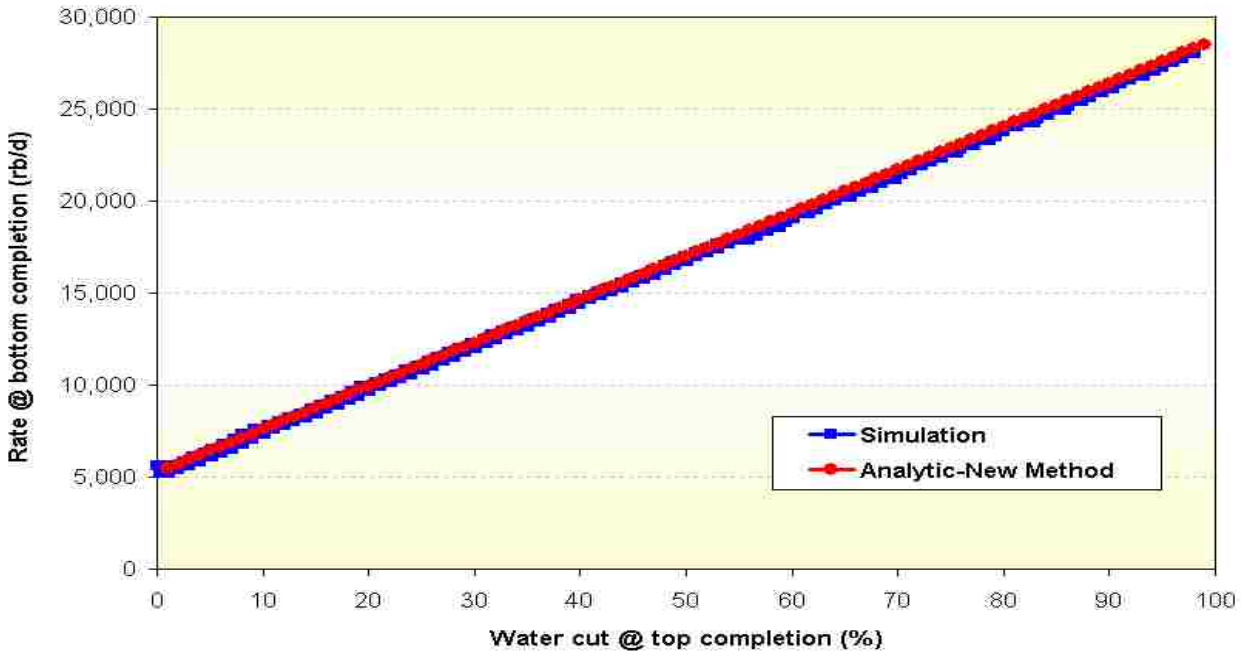

Figure 132: Comparison of Rates Obtained with the Simulator and the New Method

Material balance calculations were included in the new method for more detailed comparison with simulation results. Figure 133 displays the total (top+bottom) water cut obtained from both approaches. It can be seen that the agreement is quite good both when the

cone grows laterally (zone at the left of the curves where there is no increase in water cut) and when there is vertical movement of the oil-water contact (zone at the right of the curve). These results suggest that the ultimate water cut equations (Equations (2.15) and (2.43)) can be used with reasonable confidence to predict oil bypassing and calculate the bottom rates needed for DWS operation. Differences between the simulation and analytical results can be explained by the inherent assumptions of the ultimate water cut equations. For example, the equations assume full well penetration and segregated flow. Therefore, they may not work well in cases where the penetration effects are important or where there is substantial smearing of the oil-water interface. It is outside the scope of this dissertation to determine the conditions for which Equations (2.15) and (2.43) would give the most accurate results. However, it has been found that they work particularly well in systems with large well spacing and low water thickness.

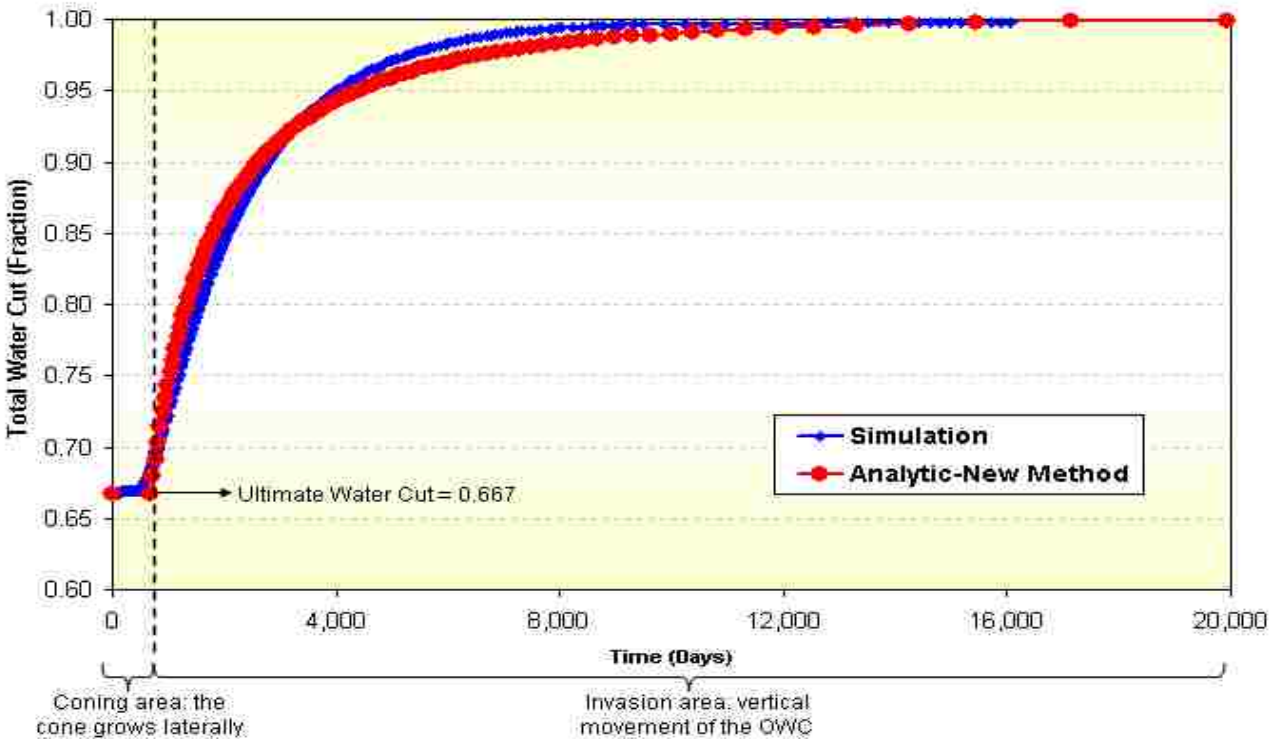

Figure 133: Comparison of Total Water Cut vs. Time Obtained with the Simulator and with the New Method

5.1.2.2 DWS with Variable Bottom (Drainage) Rate vs. Conventional DWS

In this section, two different approaches to model the bottom completion rates in wells with DWS are compared. The first approach, called here conventional DWS, consists of maintaining a constant water production rate at the bottom completion during the entire production history. This approach has been used in most of the existing numerical simulation studies and field tests featuring DWS (Shirman and Wojtanowicz (1998), Wojtanowicz et al. (1999), Inikori and Wojtanowicz (2001), Siddiqi and Wojtanowicz (2002), Inikori et al. (2002) and Ju et al. (2005)). The second approach, DWS with variable bottom rate, uses the method to calculate the sink rates introduced in the previous section. Final water cut from the top completion for the second approach was taken to be 100%. As previously indicated, using lower final water cuts from the top zone requires larger rates from the bottom completion, which may not be possible because of pressure drawdown constraints.

Figure 134 shows recovery vs. time for Case 27 (N_g=0.00039, N_{RX}=29.23, N_{RY}=14.61, N_{TX}=1.58 and M=101.72), a case in which the degree of well penetration had a very minimal effect on oil bypassing at abandonment (the effect of penetration for this case was discussed in Section 5.1.1). Single completion scenarios are included for comparison purposes. The bottom completion for the DWS scenarios is started once water arrives at the well. It is clear that using a water sink not only accelerates production, but also causes an increase in oil recovery of up to 80% (for variable rate DWS) when compared with the scenarios with a single completion. This may result in substantial improvements on the field's economics. It is important to mention, however, that cumulative water production for the scenario with variable rate DWS was found to be about sixteen times larger than for the scenarios with a single completion. The figure also shows the advantage of using DWS with variable bottom rates over the conventional approach –

the variable rate approach resulted in about 29% more oil recovered in less than one third of the time.

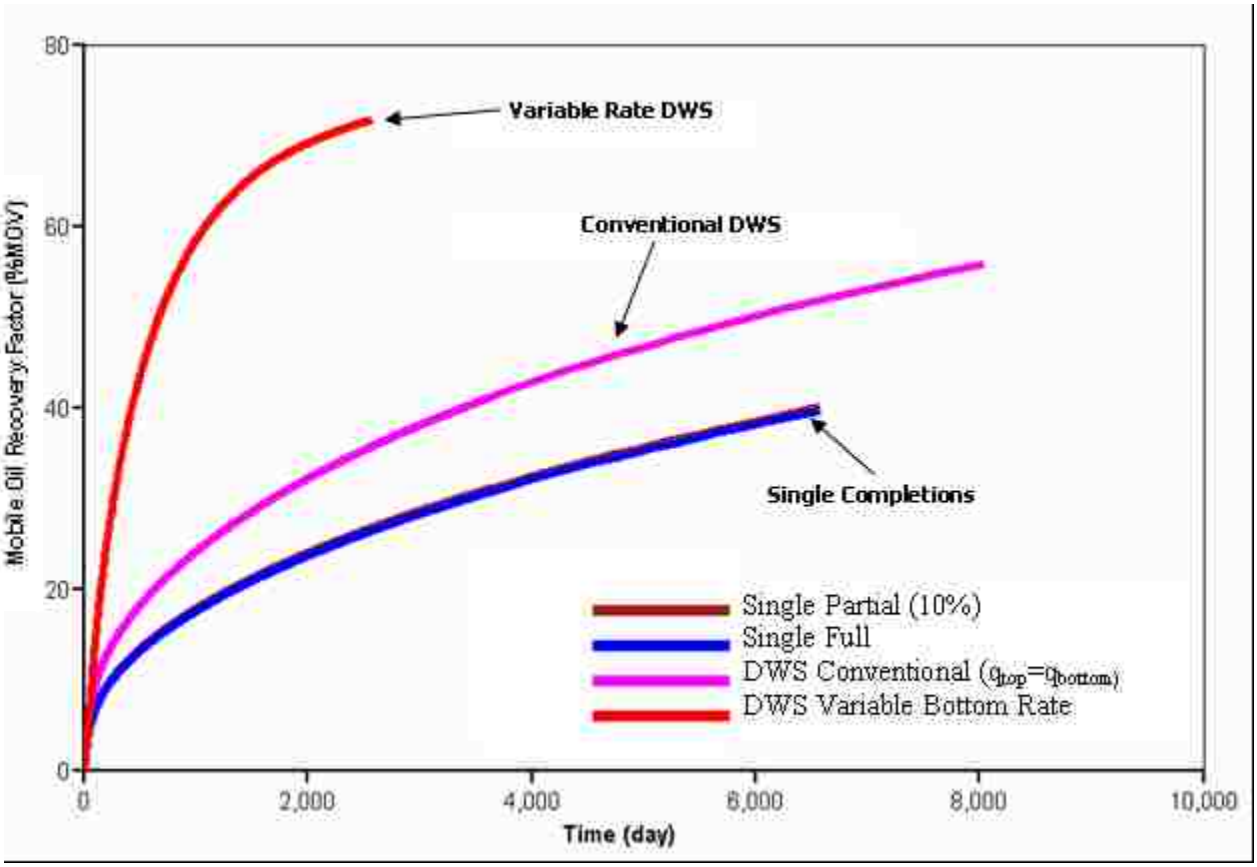

Figure 134: Oil Recovery vs. Time for Conventional (Constant Rate) and Variable Bottom (Drainage) Rate DWS for Case 27 (N_g=0.00039, N_{RX}=29.23, N_{RY}=14.61, N_{TX}=1.58 and M=101.72)

Figure 135 displays oil recovery vs. time for Case 51 (N_g=0.20, N_{RX}=29.23, N_{RY}=1.24, N_{TX}=1.58 and M=101.72) – a case in which the effect of penetration showed to be important. Case 51 shows a quite favorable effect of the gravity forces on oil recovery that can be exploited by using partial penetrations. Similar to Case 27, the variable bottom rate scenario shows acceleration of oil recovery. However, the advantage of using DWS for these conditions is not as substantial as for the conditions of Case 27. The single-short completion scenario gave a quite high recovery to start with and, therefore, improvement using the variable rate DWS concept was

not as significant. Also, it seems that the bottom water rates for the conventional DWS scenario are not high enough to cause any significant increase in recovery when compared with the 10% penetration case.

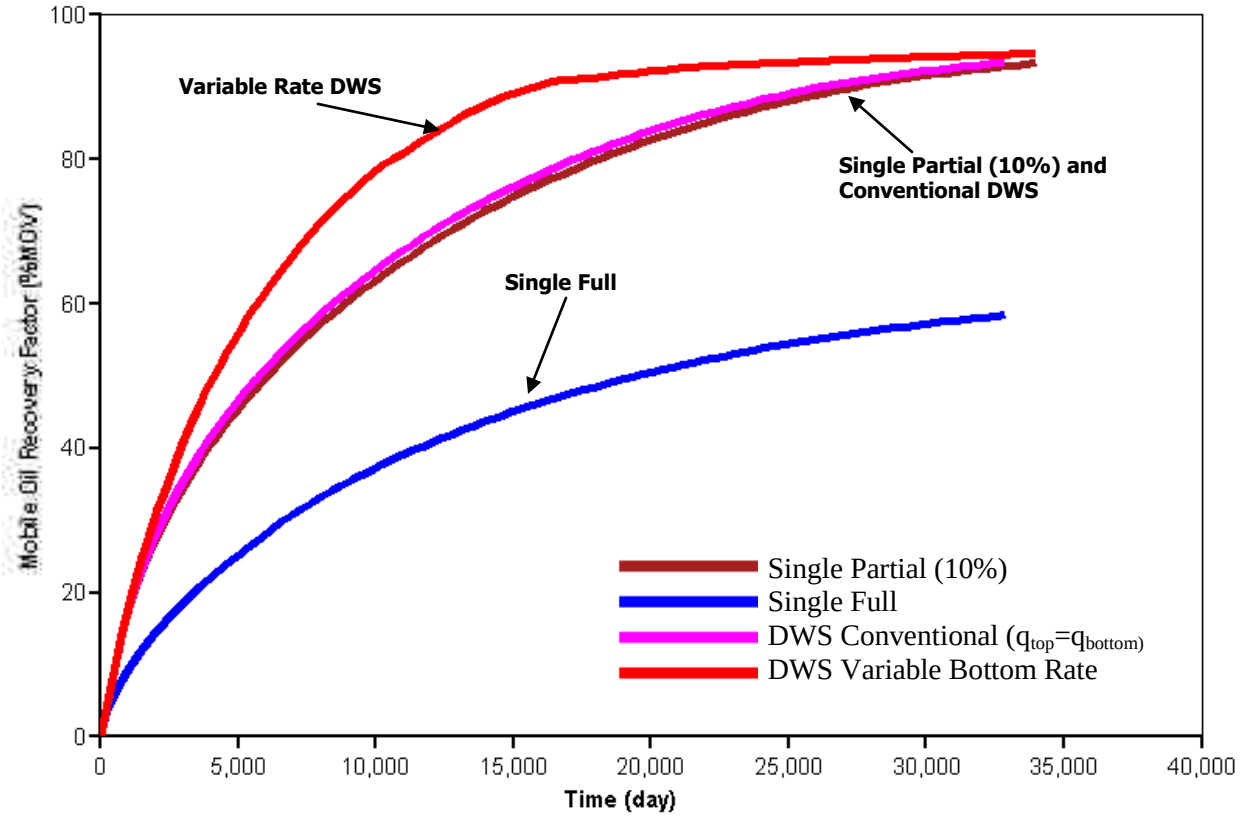

Figure 135: Oil Recovery vs. Time for Conventional (Constant Rate) and Variable Bottom (drainage) Rate DWS for Case 51(N_g=0.20, N_{RX}=29.23, N_{RY}=1.24, N_{TX}=1.58 and M=101.72)

In summary, results presented in this section show that the new method for DWS rate selection results in higher recoveries than the conventional approach. The advantages of the new approach result from the physics of the displacement of oil by water in water drive reservoirs. Variable bottom zone water rates are needed because, for a given mobility ratio, the ultimate water cut (and, therefore, the slope of the flip-flop line) will increase with time (h_w increases

with time, h_o decreases with time, see Equation (2.43)). This indicates that increasing bottom zone rates in time are needed for a specific top completion rate in order to maintain production at a certain water cut from the top zone.

5.1.2.3 Comparison between Single and Dual Completions (DWS) Using the Same Total Rate

Many previous studies have shown that DWS performance is superior to conventional single-completion performance (Shirman and Wojtanowicz (1998), Wojtanowicz et al. (1999), Inikori and Wojtanowicz (2001), Siddiqi and Wojtanowicz (2002), Inikori et al. (2002) and Ju et al. (2005)). In most of these studies; however, both types of completions have been compared using different conditions; for example, different total production rates. This section presents a comparison between single and dual completions (DWS) in which all scenarios are produced at the same total rate at all times, and production is finished at the same overall water cut. Also, all scenarios are operated at a bottomhole pressure just above the bubble point (to prevent gas liberation in the oil zone, which would reduce oil productivity and complicate the analysis). The DWS scenario is operated at a top rate of 500 bpd (constant) and at variable bottom production rates estimated using the method introduced in the previous sections. In order to evaluate all scenarios at exactly the same total-variable production rates, these rates were taken from DWS runs in the simulator and applied to the single completion scenarios. The upper and lower completions in the DWS scenario penetrate 10% of the formation thickness at the top and bottom of the reservoir, respectively.

Figure 136 display recovery vs. time for Case 27 (N_{RX}=29.23, N_{RY}=14.61, N_{TX}=1.58 and M=101.72). As indicated before, this case showed a very minimal effect of well penetration on oil bypassing at abandonment in Section 5.1.1. Since the rates are varied with time, the calculation of a single buoyancy number group value is not possible. The figure suggests that, if

systems are produced at the same total rates, there is no advantage of using DWS over using single-full completions. A possible explanation for this will be given in the next section and it is related to the overall mobility of the production stream. It is also obvious that both the DWS scenario and the full penetration scenario resulted in faster recovery than the 10% penetration scenario. Because the 10% penetration scenario has a lower area of contact between the well and the reservoir, it could not achieve the total variable liquid production rate targets and, therefore, it switched to the minimum bottomhole pressure constraint shortly after the beginning of production. This resulted in a lower total liquid production and lower recovery.

Similar to the 10% penetration scenario, the upper completion for the DWS scenario only penetrates 10% of the formation thickness. This completion started producing at a constant rate of 500 bpd and, once water arrived at the well, the bottom completion was started at approximately the same rate. In other words, the total production rate for the DWS scenario once water arrived at the well was approximately 1000 bpd. Since production from the bottom completion was mostly water, it required less pressure drawdown to achieve the targeted rate than what would have been required for oil. For the 10% penetration scenario, the total liquid rate was applied to a single completion, which indicates that a larger pressure drawdown was needed at such completion to achieve the targeted rates. For the conditions presented here a larger drawdown was not possible if production was to be maintained above the bubble point. This is why the targeted production rate could not be achieved and recovery was delayed. These results give an obvious advantage of DWS over single completions: **because of the separation of production streams, DWS systems can produce the same total rate with a lower pressure drawdown than systems with single-short penetrations.**

Figure 137 displays oil recovery vs. time for Case 51 (N_{RX}=29.23, N_{RY}=1.24, N_{TX}=1.58

and M=101.72). It can be seen that recovery for the DWS scenario is not significantly larger than for the single completion scenarios when the same total production rate is considered. Curiously, it can also be noted that, contrary to what was obtained in Section 5.1.1, there is not a significant difference in recovery between the 10% penetration scenario and the full penetration scenario; thus, there is not substantial effect of well penetration. One possible explanation for this stems from the fact that production rates considered here, obtained using the variable-rate concept, are much higher than the ones considered in Section 5.1.1 (constant-rates). The higher production rates result is a lower effect of the gravity forces (well penetration effects are stimulated by high G's) and more dispersion of the water fractional flow fronts.

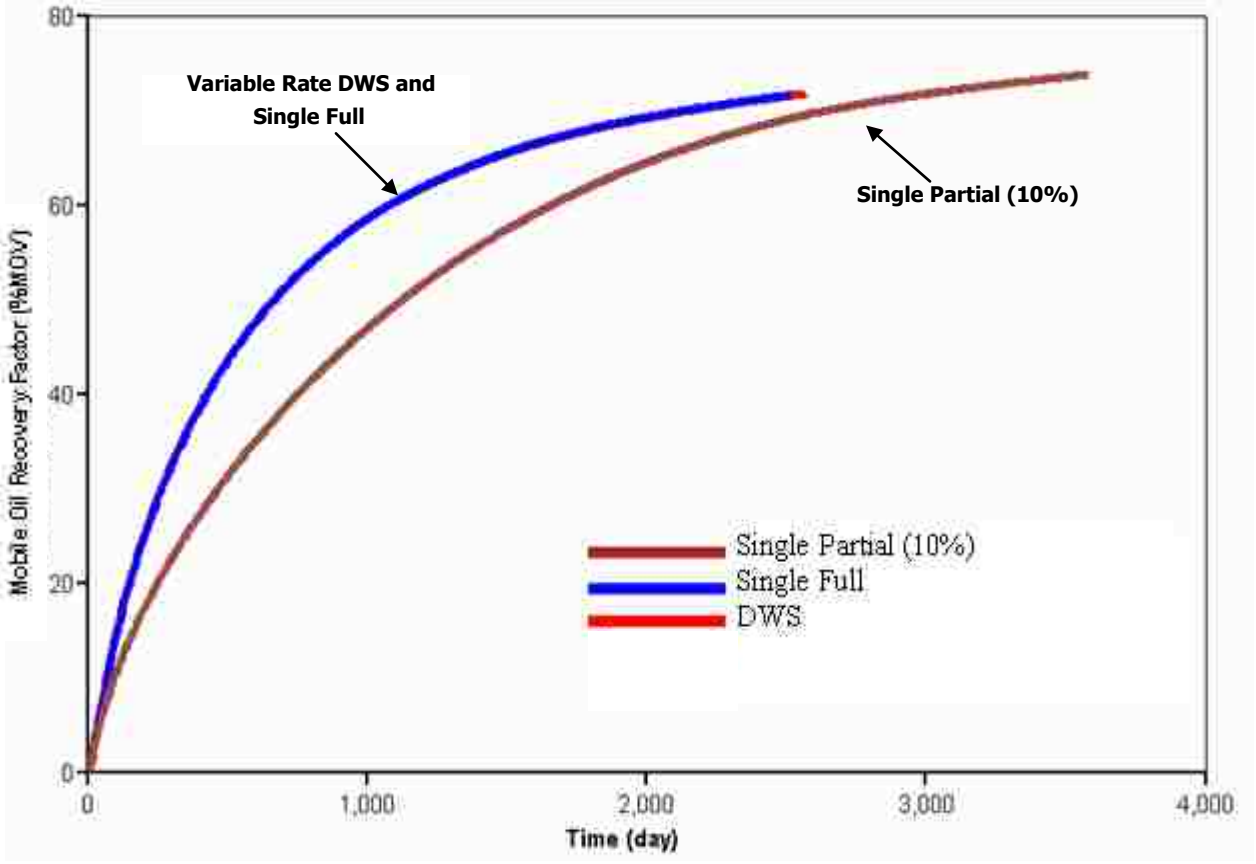

Figure 136: Oil Recovery vs. Time: Comparison of Single and Dual Completions (DWS) for Case 27 (N_{RX}=29.23, N_{RY}=14.61, N_{TX}=1.58 and M=101.72)

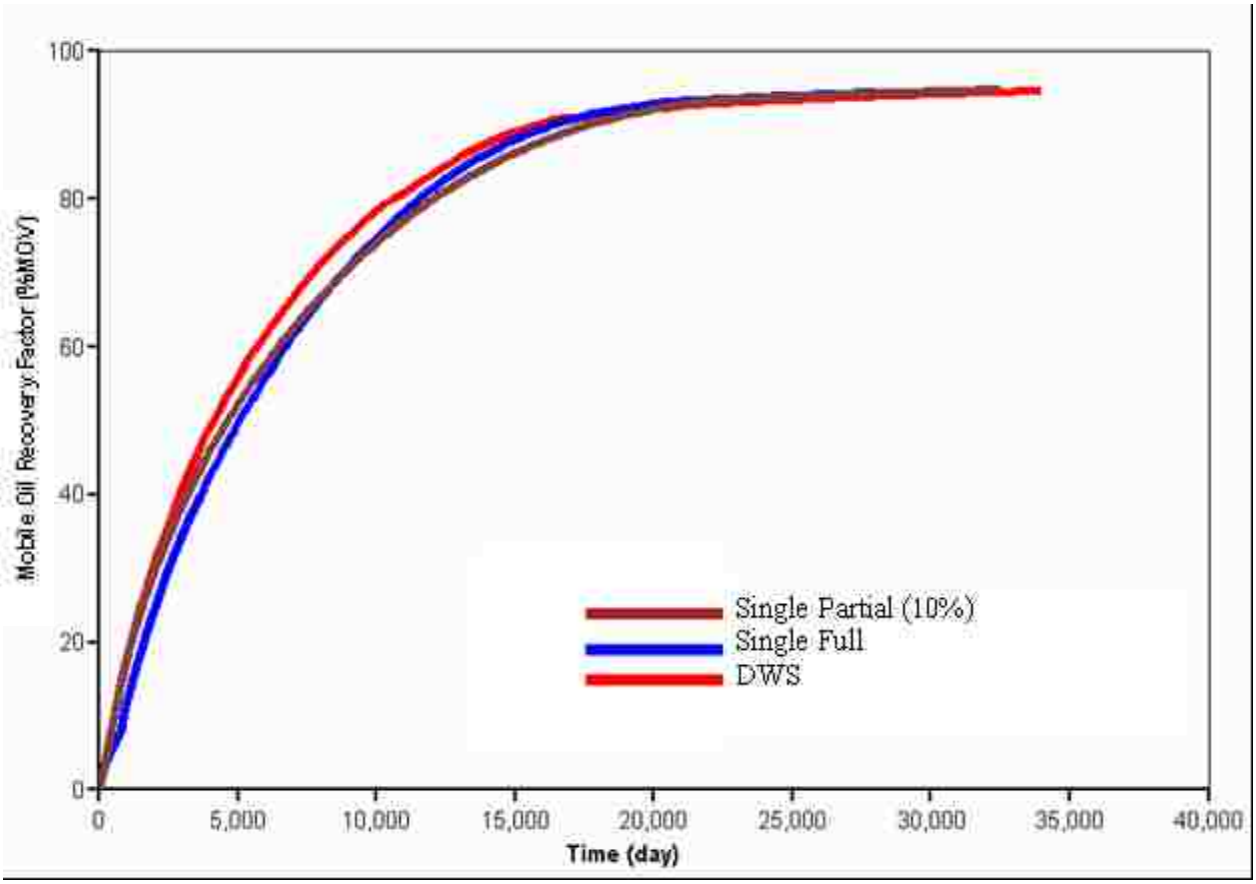

Figure 137: Oil Recovery vs. Time: Comparison of Single and Dual Completions (DWS) for Case 51 (N_{RX}=29.23, N_{RY}=1.24, N_{TX}=1.58 and M=101.72)

5.1.2.4 Effect of Total Mobility on DWS Performance

In general, well productivity is strongly related to the total mobility of the produced fluid. Since oil and water are interacting in a DWS well, the total mobility is expected to change as the fractional amount of water changes. Figure 138 shows the total mobility for Cases 27 and 51 of the experimental design. These cases have an end-point mobility ratio, M, of 101.72. The total mobility is defined as (J. Lee, 2002):

$$\lambda_t = \frac{k_o}{\mu_o} + \frac{k_w}{\mu_w} \quad \text{.....(5.3)}$$

According to Equation (5.3), the presence of water in the production stream has two

effects: first, an increase in the total mobility caused by a reduction of the overall viscosity of the produced fluid. Second, a reduction in the total mobility due to reduction of the overall effective permeability (effective permeability to oil decreases as water saturation increases). Figure 138 shows that, as the water fraction increases around the well, there is a substantial increase in the total mobility for Cases 27 and 51. This indicates that the effect of viscosity reduction caused by the presence of water is larger than the effect of reduction of the effective permeability. Obviously, this effect is caused by the fact that the endpoint mobility ratio (and, therefore, the viscosity ratio) for Cases 27 and 51 is very large.

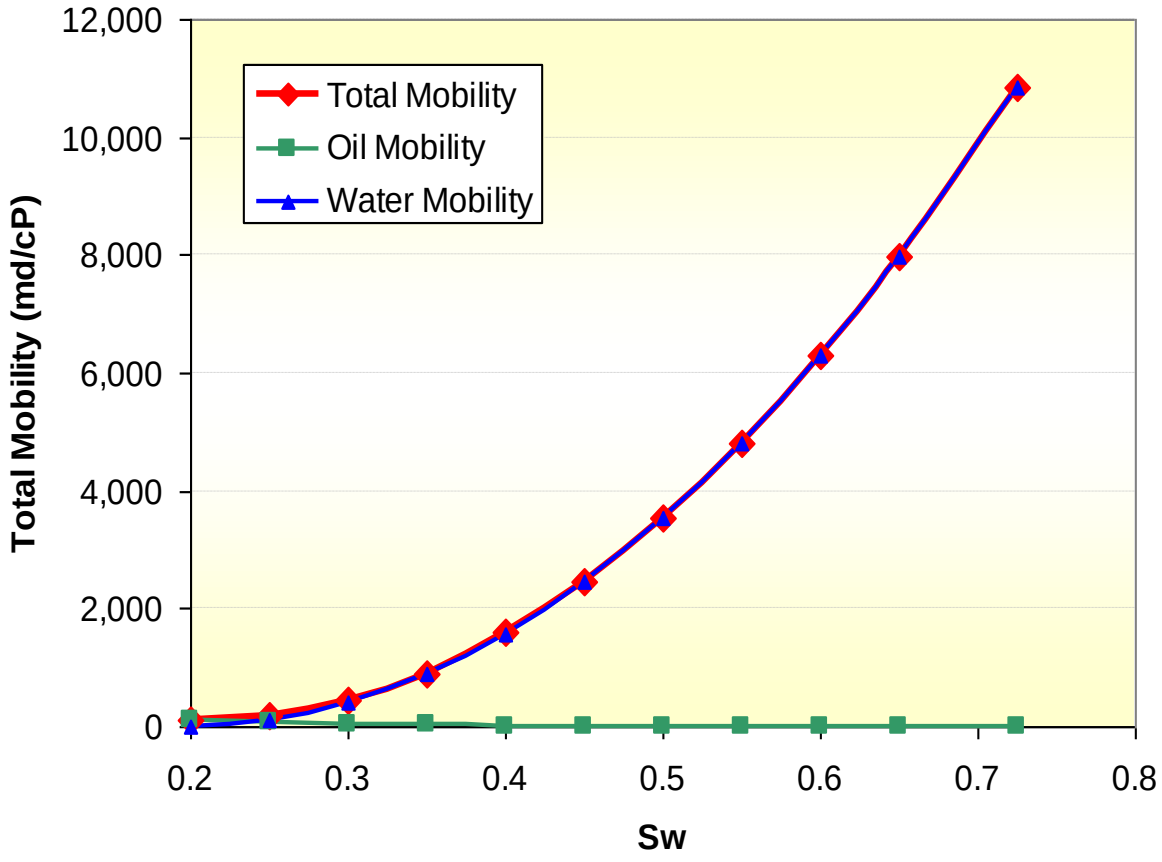

Figure 138: Total Mobilities for Cases 27 and 51 (M=101.72)

Because the total mobility of the produced fluid increases as the water saturation

increases, there is no advantage in using dual completions (DWS) other than the fact that, as explained in previous section, DWS systems can produce the same total rate with a lower pressure drawdown than systems with single-short penetrations. Results presented previously suggest, however, that such effect may not be significant. In summary, it can be said that there is no substantial advantage of DWS over single completions when the total mobility of the produced fluid increases due to the presence of water.

Results presented by Arslan (2005) in Figure 131 showed that, however, at a maximum pressure drawdown (red line at right of figure), the top completion rate for a DWS well (point A) could be larger than the maximum achievable rate for a conventional well (point C). This is only possible if the total mobility of the mixture decreases in the presence of water – contrary to what was obtained for Cases 27 and 51 (Figure 138). A decreasing total mobility for increasing water saturation values may be obtained only if the reduction of the overall effective permeability due to the presence of water is larger than the increase in the mobility caused by the reduction of the overall viscosity. According to Equation (5.3) this may happen, for example, for low end-point mobility ratios (i.e., low oil viscosities) and/or when the effective permeability to oil, as described by the relative permeability curves, has a substantial reduction with increasing water saturations.

Figure 139 presents total mobilities for the 10%, 50% and 90% percentiles values of the endpoint mobility ratio (M) obtained from the database used for this dissertation. It is clear that low M values may result in decreasing mobilities as water saturation increases. However, the reader should keep in mind that low endpoint mobility ratios would also result in less “smearing” of the water saturation fronts (the displacement is more piston-like). Therefore, the flow behavior within the relative permeability endpoints becomes less important.

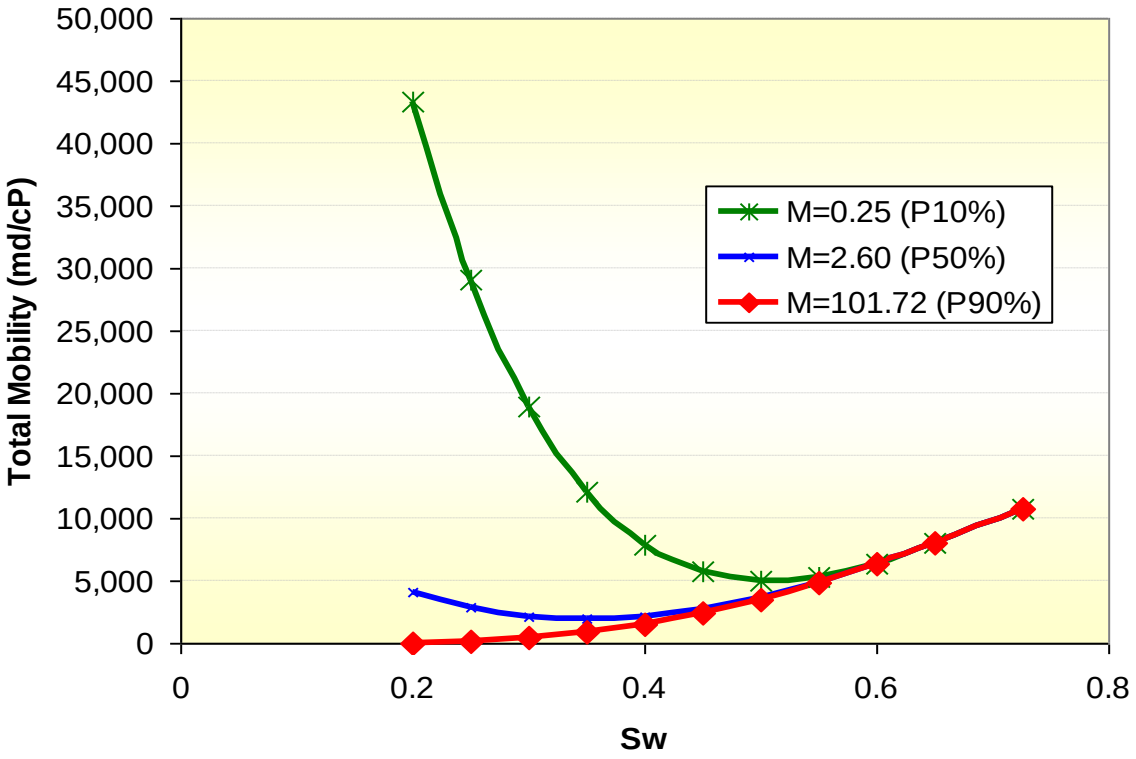

Figure 139: Effect of the End Point Mobility Ratio on the Total Mobility of the Mixture

Contrary to the results obtained for cases where the total mobility of the production stream increases with increasing water saturations, simple logic suggests that DWS may be an efficient remediation technique for scenarios in which the total mobility decreases in the presence of water. By having a "sink", the top completion could be maintained water free for longer and, therefore, oil productivity may be better than for a single completion well, where oil and water would be produced simultaneously. A new set of simulation runs was prepared to test this hypothesis. Simulations were run using the P50% values of all the groups from the original data set developed for this dissertation except for M, where the P60% (M=5.28) was used. This was done to promote water tonguing and oil bypassing. It can be said then that the conditions considered here represent an average reservoir. Variable bottom water rates, calculated using the new method described in previous section, were used in all scenarios.

Figure 140 shows recovery in time for the "average" reservoir obtained with the different completion scenarios. All cases give approximately the same recovery. However, it can be seen that recovery for the full and DWS scenarios is much faster. For example, at 2195 days of simulation recovery for the full and DWS scenarios was about 11% higher than for the partial penetration scenario. Because of its smaller area of contact with the reservoir, the partial penetration case produces at a lower rate for the same pressure drawdown. This case could not achieve the assigned variable production rates (calculated using the method previously introduced). This caused slower recovery in time.

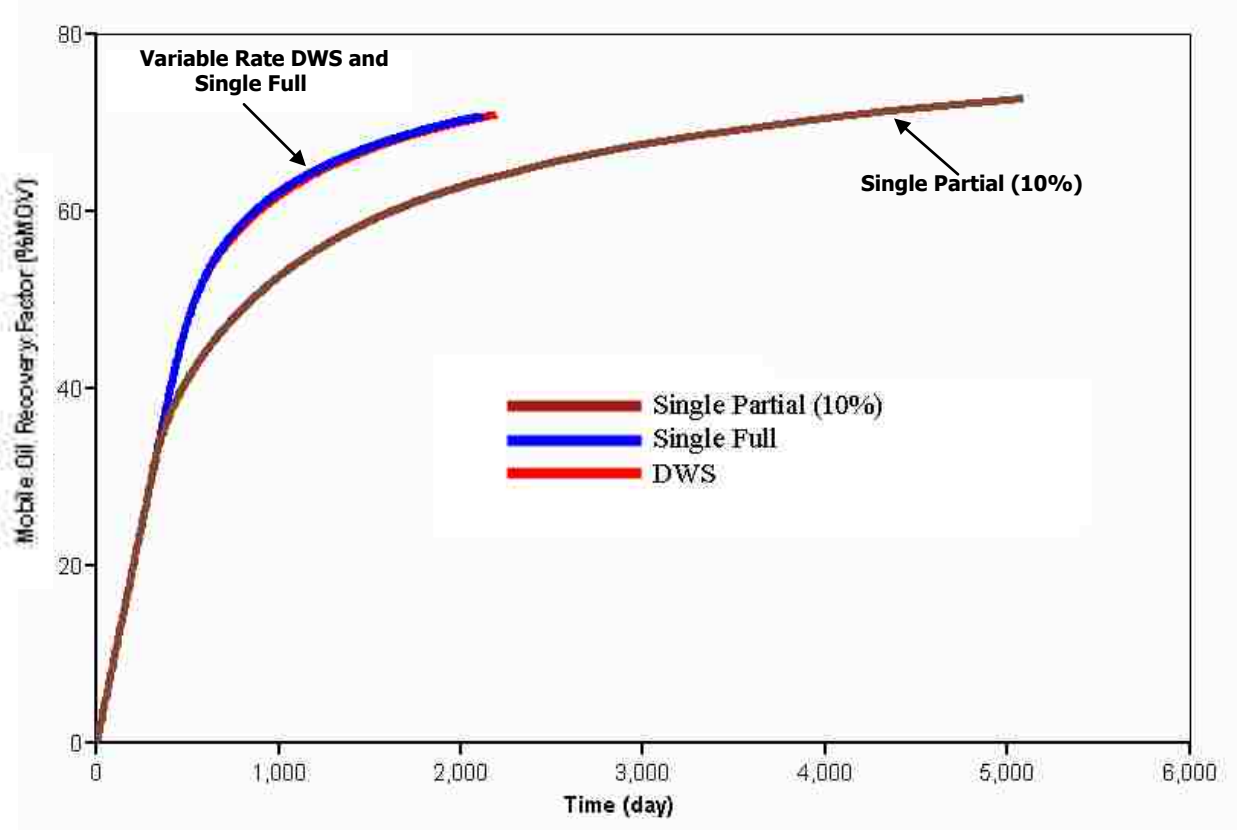

Figure 140: Oil Recovery vs. Time for a Homogeneous Average Reservoir

Both the full penetration and the DWS scenarios were able to produce at the assigned variable liquid rates and, therefore, they give approximately the same recovery development in

time. Due to the relatively high endpoint mobility ratio, there is a large dispersion or smearing of the oil-water interface as the displacement progresses. In other words, oil mixes with water before arriving to the well. As a consequence, the bottom completion in the DWS scenario produces oil. In other words, it is not possible to obtain segregated flow. Therefore, the expected increase in the overall mobility of the produced fluid due to segregated flow of oil and water in the DWS scenario was not as significant as desired.

These results suggest that there is not a significant difference in using DWS or full penetrations in edge-water reservoirs when both well completion strategies are produced at the same total rate. For cases with high end-point mobility ratios, the oil-water interface smears before encountering the well. This makes the separation of oil-and water, required for optimum operation of DWS systems, a difficult task. On the other hand, for low end-point mobility ratios there is no significant dispersion of the oil-water interface and the two fluids may flow separately to the well. However, low end-point mobility ratios are normally associated with stable interfaces and little oil bypassing and, therefore, there may not be a need for DWS installation.

5.1.3 Effect of Heterogeneity on the Performance of DWS and Conventional Wells

The same scenarios studied in the previous section for an "average" homogeneous reservoir were studied for the transgressive, regressive and serrated sequences introduced in Section 4.1.7. Variable bottom water rates, calculated using the new method described in previous sections, were used in all scenarios.

Table 37 shows oil recovery (expressed as a percentage of the movable oil volume, %MOV)) at abandonment for the four different types of depositional sequences. Abandonment is defined as 98% water cut in the top completion for the DWS scenario, or the equivalent overall water cut for the single completion scenarios. Also shown is the time at which the abandonment

conditions were reached. The following comments can be made from the table:

Table 37: Effect of Heterogeneity on Performance of DWS and Conventional Wells

Type of Sequence	Single Partial (10% penetration)		Single Full (100% penetration)		DWS	
	%Recovery	Time (days)	%Recovery	Time (days)	%Recovery	Time (days)
Homogeneous	72.8	5086	70.9	2113	71.0	2195
Transgressive	83.5	49279	71.7	5086	71.3	4748
Regressive	68.3	1925	68.3	1914	69.0	2205
Serrated	70.1	5451	68.5	2016	68.6	2098

- The full penetration and DWS scenarios always give approximately the same recovery and the same time of abandonment.
- Either full penetration or DWS are the best strategies for homogeneous and serrated sequences. They result in approximately the same recovery as the partial penetration scenario, but in less than half of the time. Because of a smaller area of contact with the reservoir, the partial penetration scenario was not able to achieve the assigned variable rates in these types of sequences, which resulted in slower recovery.
- Recovery for the partial penetration scenario was approximately 17% higher than for the other two scenarios when a transgressive sequence was modeled. However, both the full penetration and the DWS scenarios resulted in significant acceleration of recovery - abandonment was achieved in about one tenth of the time it took for the partial penetration scenario. It is obvious then that the full penetration and DWS are also the best alternative for transgressive sequences.
- The very slow recovery associated with the partial penetration scenario for the transgressive sequence is explained by the fact that permeability at the top layers of this

type of sequences is quite low. Because the well is only completed in the top layers, it requires a significant pressure drawdown to achieve the targeted production rates. However, because there is not enough reservoir energy to achieve such rates, production declines. The partial penetration scenario resulted in higher recovery because lower rates normally are translated into more stable displacements.

- All completion scenarios showed similar recoveries and abandonment times for regressive sequences. Because of their higher permeability, the top completions in regressive sequences are less restricted to flow and can achieve the targeted rates with lower pressure drawdown. Short completions may be the best alternative for this type of sequences, since they give the same performance at lower cost.

5.2. Bottom-Water Systems

5.2.1 Effect of Well Penetration on Oil Bypassing

5.2.1.1 Production Controlled by Maximum Total Rate

Figure 141 is an interaction plot showing the effect of well penetration for bottom-water systems. The plot was obtained using the 135 runs completed for the experimental design described in Chapter 4. For the sake of simplicity, only the main effects were considered in the plot. Similar to for edge-water systems, oil bypassing in bottom-water systems is stimulated by large well penetrations. Contrary to edge-water systems, however, the effect of well penetration in bottom-water systems controlled by maintaining a total (oil+water) production rate is - overall – statistically significant. This was shown in Figure 114 (Chapter 4).

Figure 141 also shows that the effect of well penetration in bottom-water systems is more pronounced for large G_v's (e.g., low production rates) and M's (e.g., large oil viscosity) and for small W_{sp}'s (e.g., small k_v/k_h and/or well spacing). These conditions are the equivalent to the

conditions that promote the effect of well penetration on oil bypassing in edge-water systems (Figure 119). It is also clear that end point mobility ratio is the group with the largest influence on the effect of well penetration.

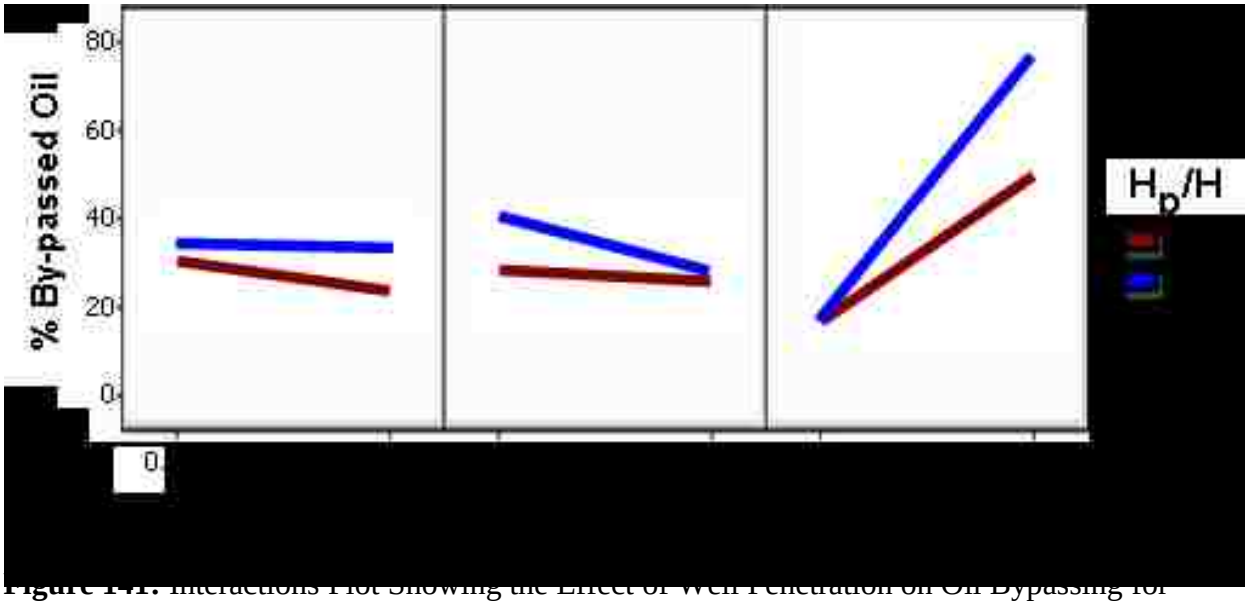

Figure 141: Interactions Plot Showing the Effect of Well Penetration on Oil Bypassing for Bottom-Water Systems

Figure 142 shows the effect of well penetration on oil recovery/bypassing for Case 61 of the design, a case defined by using the highest levels for G_v and M and the lowest level for W_{sp} (the levels used in the design are shown in Table 35). As expected from the results presented in Figure 141, the effect of penetration on oil bypassing for these conditions is of very large importance: the 10% penetration scenario recovered about 7.5 times more oil than the full penetration scenario. It is clear that oil bypassing for these conditions could be substantially reduced by using short penetrating wells. The figure also shows the effect of well penetration on the water breakthrough time: the short well penetrations resulted in later breakthrough times and the larger oil recoveries at breakthrough. For example, oil recovery at breakthrough for the 10% penetration scenario was about 35%, whereas the full penetration scenario showed almost no oil

recovery at breakthrough.

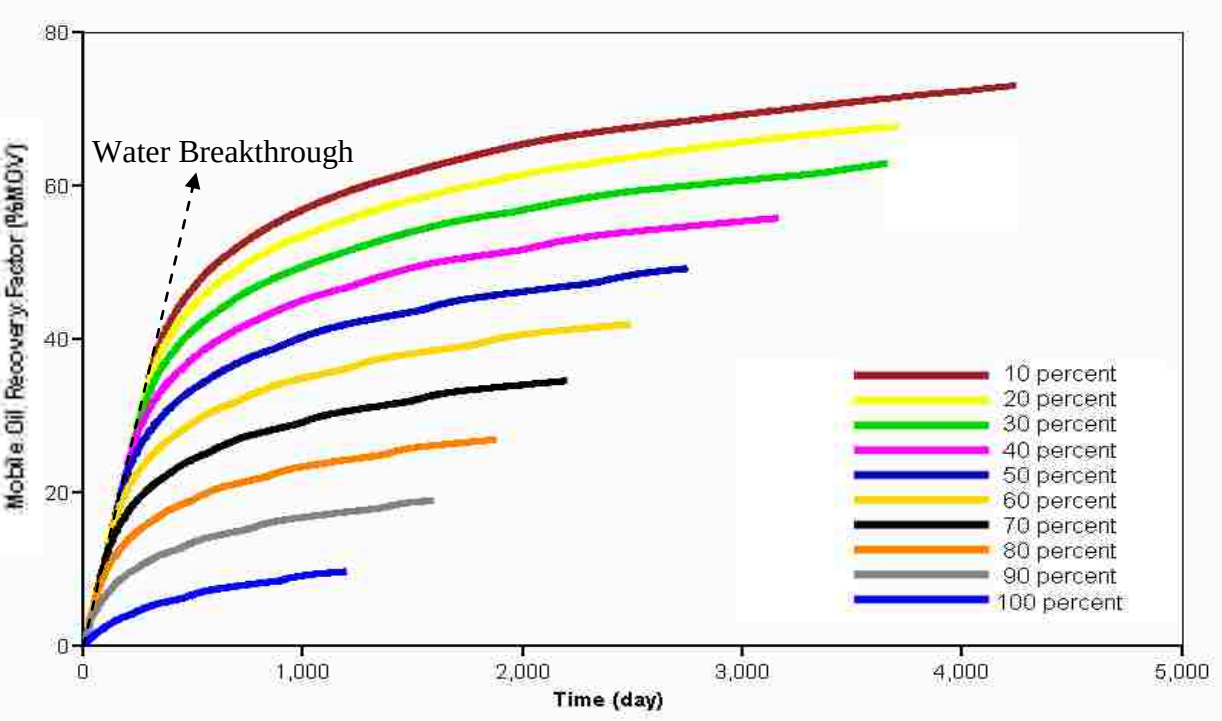

Figure 142: Effect of Well Penetration on Oil Recovery/Bypassing for Case 61 (G_v=20.21, W_{sp}=0.596, M=101.72)

Figure 143 displays the shape of the oil-water interface at breakthrough (3a) and at abandonment (3b) for Case 61. Water breakthrough time for the 10% penetration scenario is about 300 days, whereas water production for the full penetration scenario starts practically from day zero. It can also be seen that for the 10% penetration scenario there is a significant vertical movement of the OWC before breakthrough. As a consequence, there is an important displacement of oil by water and low oil bypassing. For the full penetration scenario, however, there is very little vertical movement of the OWC, which results in very little displacement of oil. By running Case 61 using different ratios of gravity to viscous forces (G_v), it was found that the small movement of the OWC for the full penetration scenario is related to the fact that gravity forces are significant. More movement of the OWC was obtained for cases with lower G_v, which

translated into higher recovery. This can be explained as follows: for high gravity forces, there is less fractional flow mixing (the higher the gravity forces the more the water fractional curve is shifted to the right) and, therefore, water saturation builds up more quickly once water encounters a well. Curiously, the same effect is beneficial for short penetrating wells, since most of the oil has already been displaced when water arrives to the well.

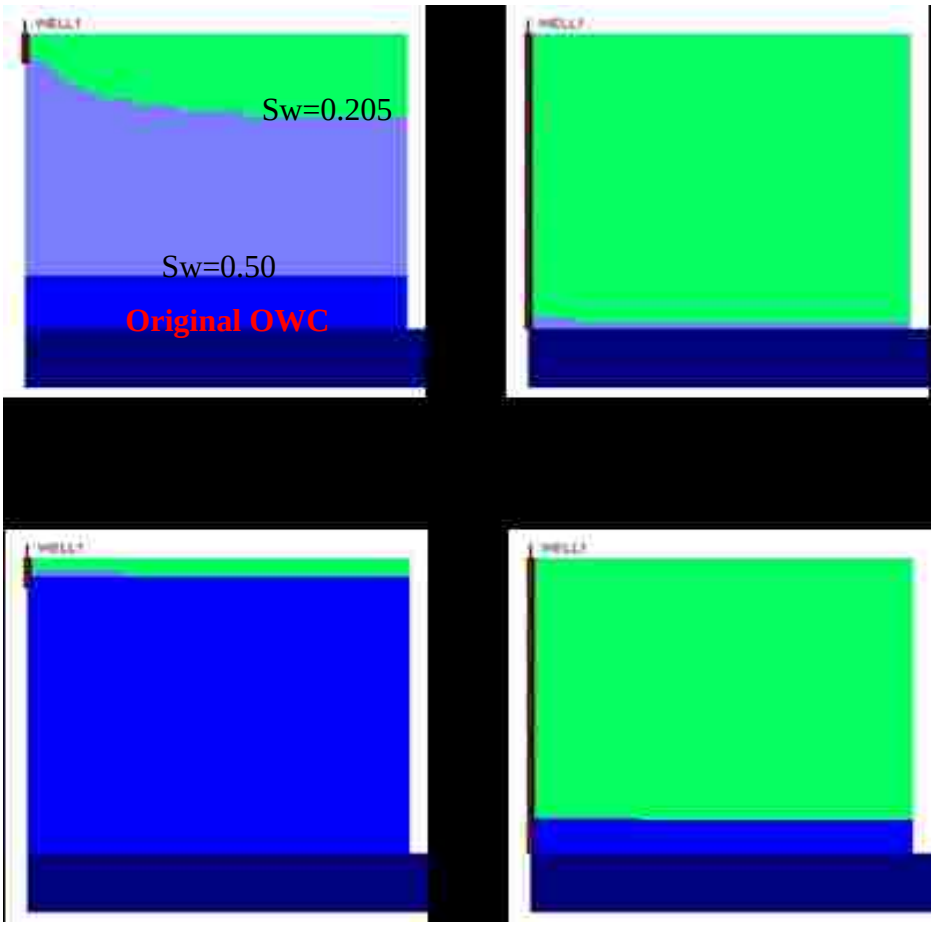

b) At Abandonment

Figure 143: 2D Shape of Oil-Water Interface at Water Breakthrough (a) and at Abandonment (b) for Case 61 at 10% Penetration (Left) and 100% Penetration (Right)

Figure 144 shows oil recovery vs. cumulative liquid production for Case 61. It is clear that displacement efficiency is significantly better for the scenarios with short well penetrations.

(short penetration scenarios show significantly higher oil production per barrel of water). A good explanation for this behavior is, obviously, that short penetrations delay water breakthrough: about 50% of the oil produced for the 10% penetration scenario was obtained before water breakthrough.

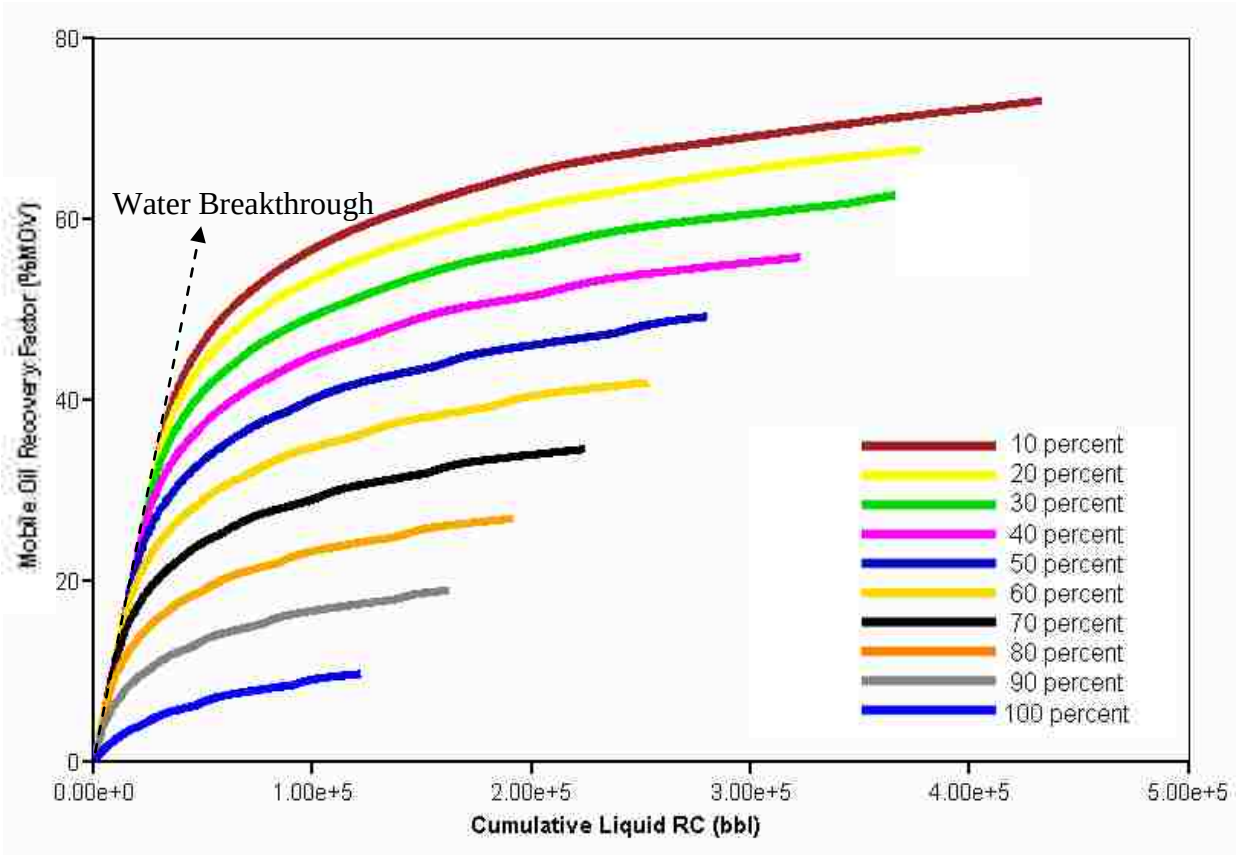

Figure 144: Oil Recovery vs. Cumulative Liquid Production for Case 61 (G_v=20.21, W_{sp}=0.596, M=101.72)

Figure 145 shows recovery versus time for a case with G_v=0.044 (i.e., high production rate), W_{sp}=24.05 (i.e., large well spacing and/or large ratio k_v/k_h) and M=10. As expected from the results presented in Figure 141, this case shows a very minimal effect of well penetration on oil bypassing. Figure 145 also show that, despite the high production rate associated with this case, oil recovery for this case is extremely slow: it takes more than 120 years to recover 80% of

the movable oil in place. This is undoubtedly because water breakthrough for this case was very rapid, regardless of the degree of penetration. After breakthrough, production was plagued with large water cut and, therefore, very little oil.

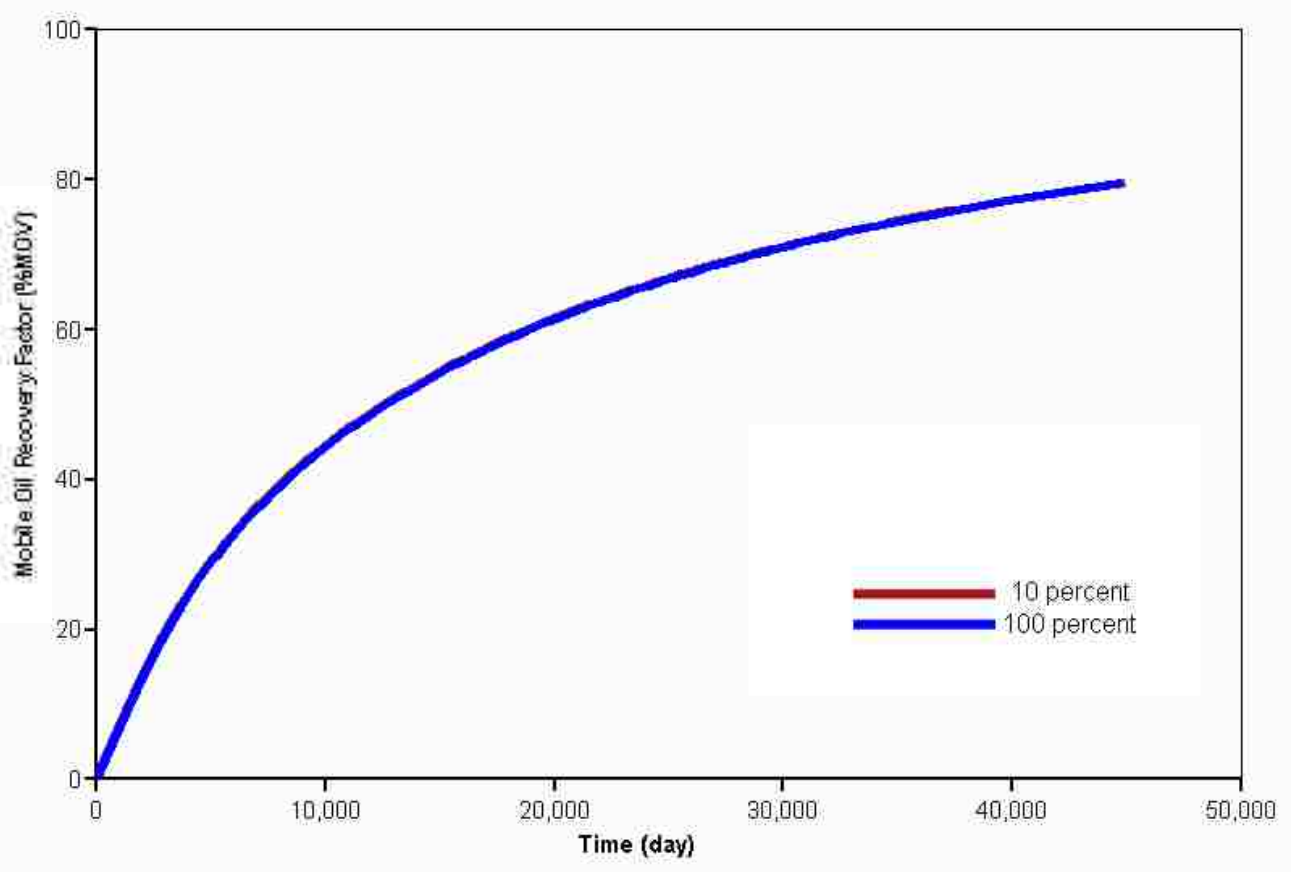

Figure 145: Effect of Well Penetration on Oil Recovery/Bypassing for a Case with G_v=0.044, W_{sp}=24.05 and M=10

Figure 146 displays the shape of the oil-water interface at breakthrough (6a) and at abandonment (6b) for the case with G_v=0.044, W_{sp}=24.05 and M=10. It can be seen that these conditions resulted in significant coning for the 10% penetration scenario. These results demonstrate that, under some specific reservoir conditions, shortening the well's completion does not significantly delay the formation of a water cone – water comes to the well so fast that it

would not make any important difference whether the well is partially or fully completed. This is especially true in cases with high values of mobility ratio (the substantial effect of well penetration for large values of M in Figure 141 occurs for cases with no significant water coning, where recovery is mainly a function of the uniform vertical movement of the oil-water contact). In fact, water breakthrough for the 10% penetration scenario occurred in just over 4 days.

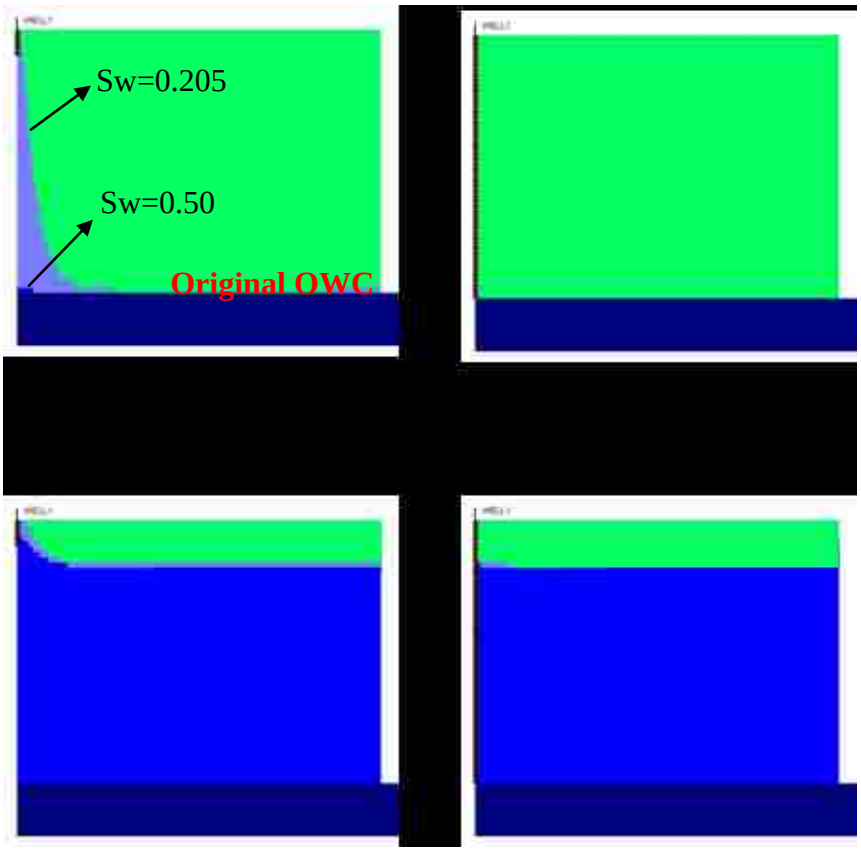

b) At Abandonment

Figure 146: 2D Shape of Oil-Water Interface at Water Breakthrough (a) and at Abandonment (b) for a Case with G_v=0.044, W_{sp}=24.05 and M=10 for 10% Penetration (Left) and 100% Penetration (Right)

Figure 147 shows oil recovery vs. cumulative liquid production for the case with G_v=0.044, Wsp=24.05 and M=10. It is obvious that the degree of well penetration does not have

any significant effect on the displacement efficiency for these conditions. The rapid formation of a very thin cone in the short penetration scenario resulted in poor displacement efficiency – similar to the long penetration scenario.

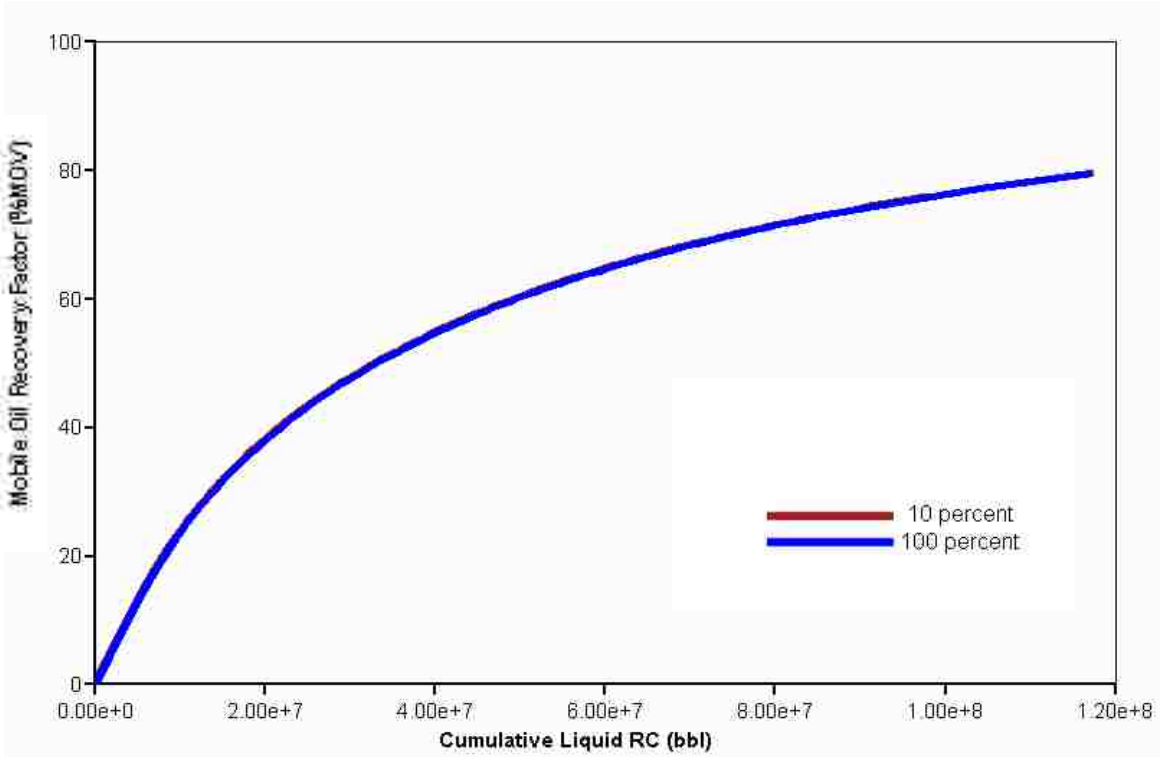

Figure 147: Oil Recovery vs. Cumulative Liquid Production for a Case with G_v=0.044, W_{sp}=24.05 and M=10

5.2.1.2 Production Controlled by Minimum Bottom Hole Pressure

Similar to what was done for the edge-water systems in Section 5.1.1.2, this section investigates the effect of well penetration on oil bypassing when the reservoir is produced at the maximum possible drawdown. Because no constant production rate target is defined in the simulations, it is not possible to calculate a single value for the ratio of gravity to viscous forces, G_v.

Figure 148 shows the effect of well penetration on oil recovery for Case 61, which

showed a significant effect of well penetration on oil bypassing in the previous section for constant-rate production. Recovery for the deep penetrating wells is faster than for the short penetration scenarios. As was indicated before, this is because long completions allow larger area of contact between the well and the reservoir. However, the figure also shows that total recovery at abandonment is smaller for the deep penetrating scenarios. For example, total recovery for the full penetration scenario is only half of the recovery for the 10% penetration scenario. This is mainly because using short penetrating wells would delay water breakthrough (e.g. water breakthrough time for the 10% penetration scenario occurred in about 183 days (%R=29), whereas for the full penetration scenario occurred in less than a day). One reason why the effect of well penetration in oil bypassing for bottom-water systems is more significant than for edge-water systems is that the time of cone development for bottom-water systems is a larger fraction of the total time water takes to get from the original OWC to the well.

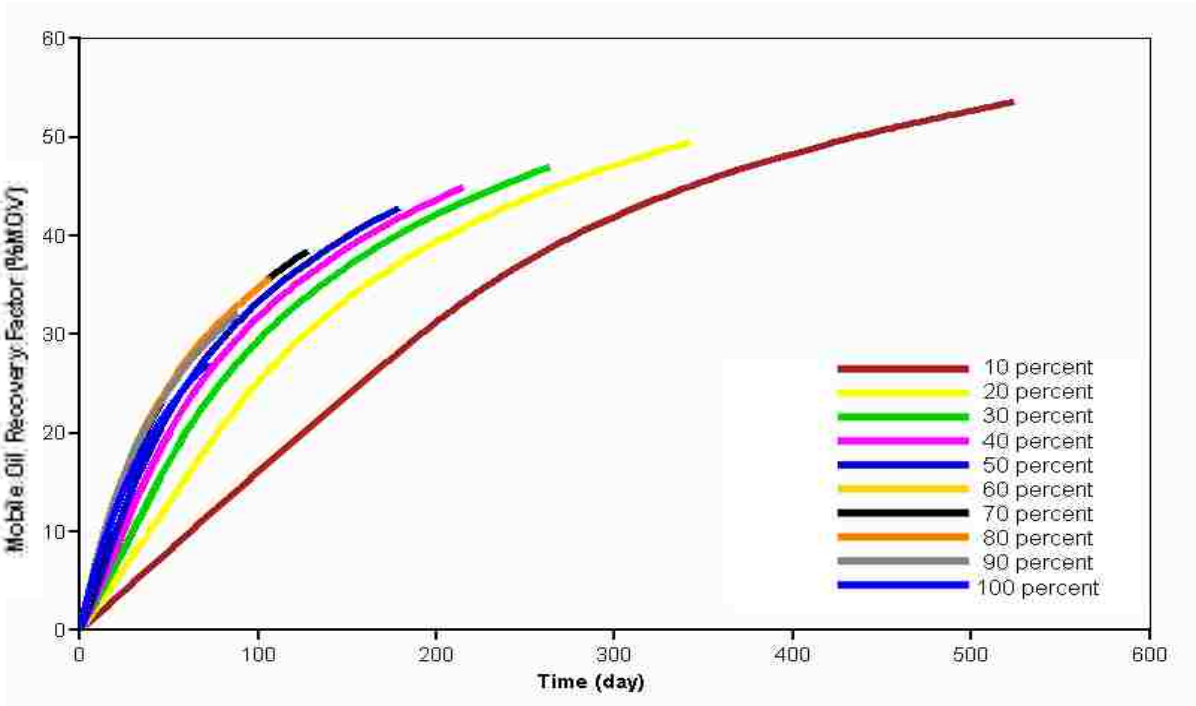

Figure 148: Effect of Well Penetration on Oil Recovery/Bypassing for Case 61 (W_{sp}=0.596, M=101.72)

Figure 149 displays oil recovery vs. cumulative liquid production for Case 61. As it was found for the cases controlled using a constant liquid rate, displacement efficiency is significantly better for the cases with short well penetrations. As explained before, this is because short penetrations delay water breakthrough time.

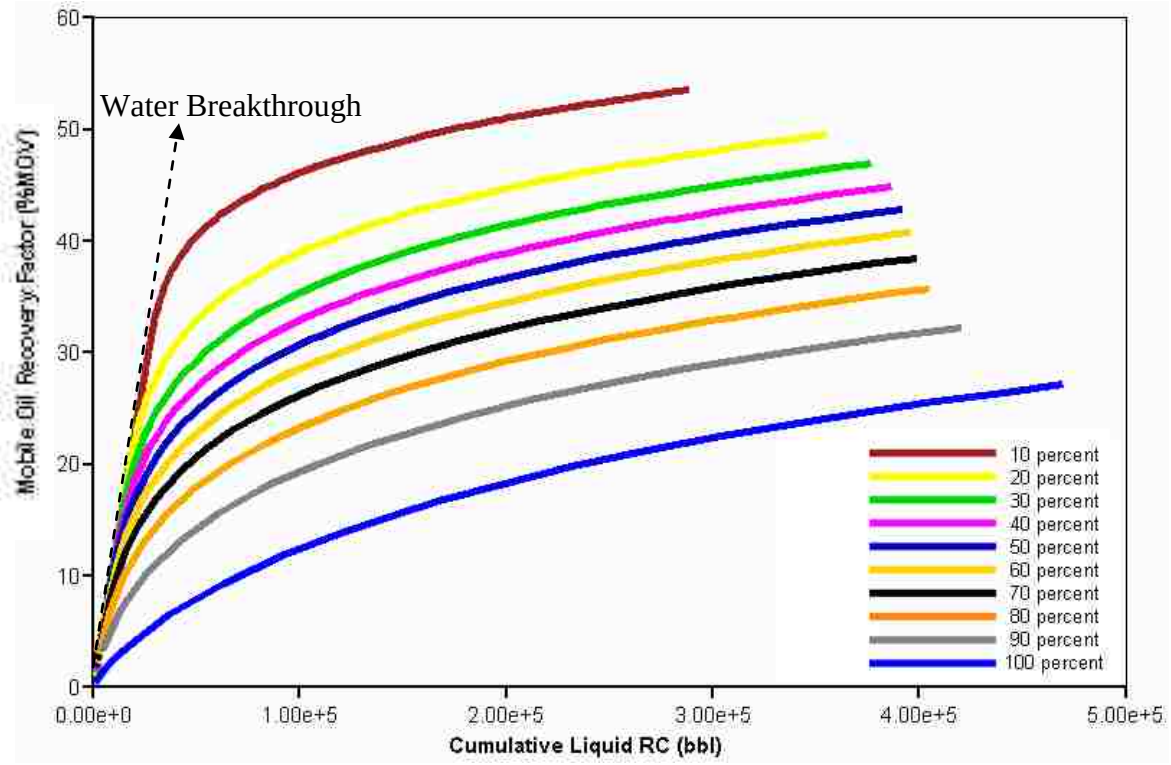

Figure 149: Oil Recovery vs. Cumulative Liquid Production for Case 61 (W_{sp}=0.596, M=101.72)

The effect of well penetration on oil recovery for a case with W_{sp} = 24.05 and M=101.72 is shown in Figure 150. A similar case showed almost no effect of well penetration on oil bypassing in the previous section (constant-rate production). Total recovery for the full penetration scenario (%R=71.7) is close to the recovery for the 10% well penetration (%R=78.6). The cone development for these conditions is so rapid that using short well penetrations does not

substantially delay water breakthrough when compared with full penetrations. As a consequence, total recovery is about the same for both scenarios. Recovery for the full penetration scenario, however, takes about a fourth of the time (75% shorter). As explained before, this is because long completions allow larger area of contact between the well and the reservoir.

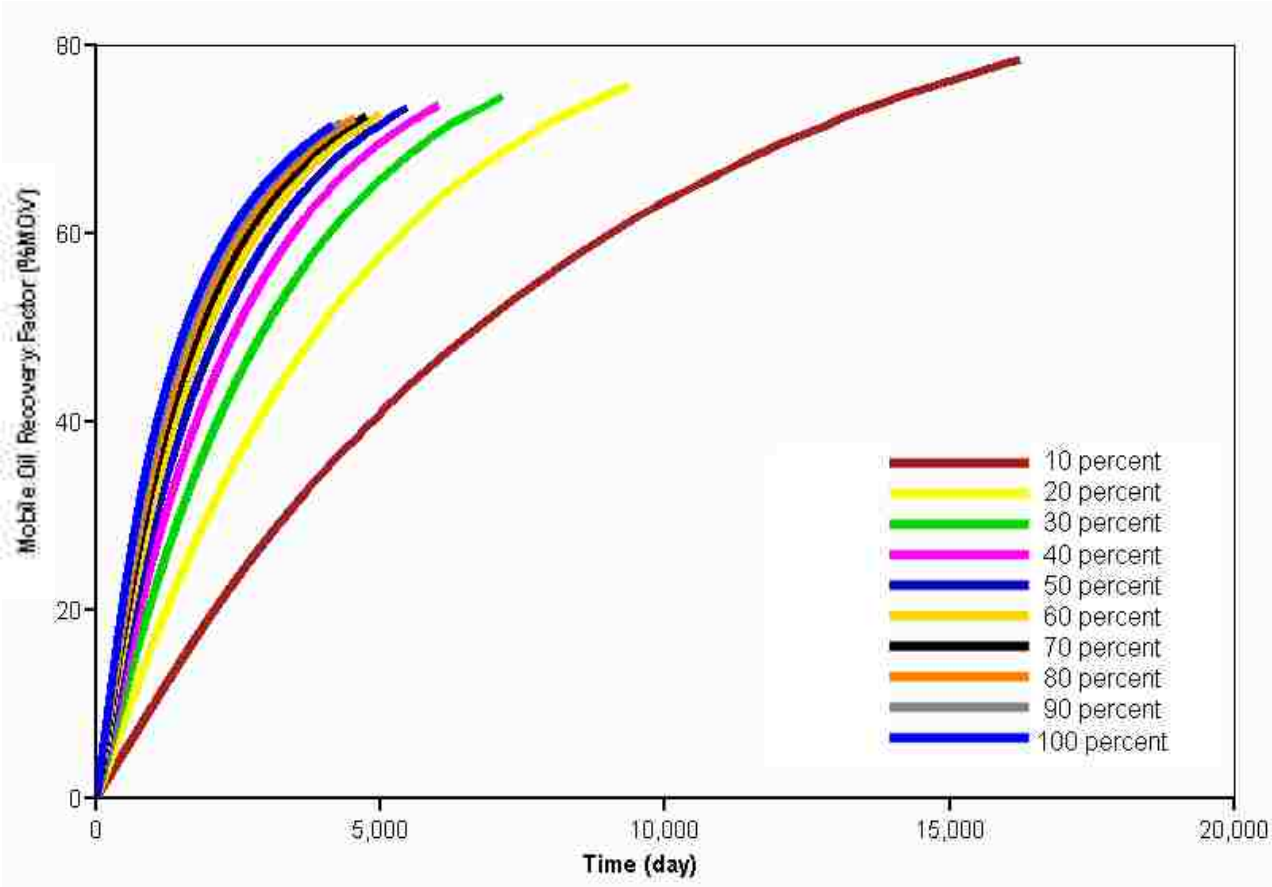

Figure 150: Effect of Well Penetration on Oil Recovery/Bypassing for a Case with W_{sp}=24.05 and M=10

Figure 151 shows oil recovery versus cumulative liquid production for the case with W_{sp}=24.05 and M=10. Similar to what was obtained for a similar set of conditions when the constant-rate production was used, it is clear that the degree of well penetration does not have any significant effect on the displacement efficiency.

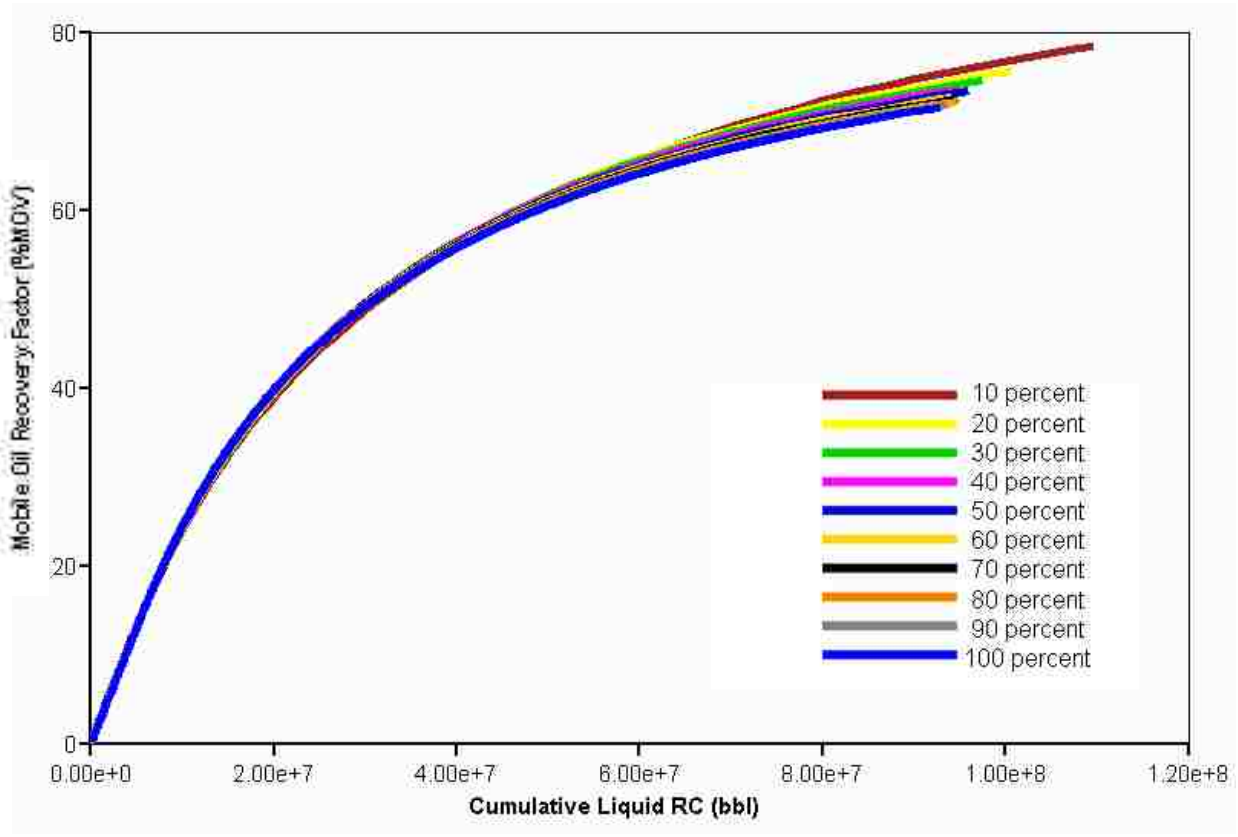

Figure 151: Oil Recovery vs. Cumulative Liquid Production for a Case with W_{sp}=24.05 and M=10

5.2.1.3 Summary on the Effect of Well Penetration

Results presented in the previous section suggest that, in general, the effect of well penetration for bottom-water systems shows a similar behavior as in edge-water systems. Some of the main findings are:

- For reservoirs with large G_v's (e.g. small production rates) and M's (e.g., large oil viscosity), as well as small W_{sp} (e.g., small k_v/k_h and/or well spacing), the effect of well penetration on oil recovery/bypassing could be important. Reservoirs with these conditions should be operated using short penetrating wells, since this may improve recoveries by delaying water breakthrough. It seems that substantial well penetration effects could be mainly obtained for very viscous oils (M ≈100).

- For reservoirs with small G_v's (e.g. large production rates), moderately small M's (e.g., M<10) and large W_{sp} (e.g., large k_v/k_h and/or well spacing), having different well penetrations would not substantially affect the amount of oil recovered per barrel of fluid produced. Reservoirs in this category could be produced using deep penetrating wells, since this could accelerate recovery. This appears to be the most common scenario since approximately 68 % of the reservoirs in the data set created for this study have an end-point mobility ratio lower than 10.

5.2.2 Comparison between Single and Dual Completions (DWS) Using the Same Total Rate

Similar to what was done for edge-water systems; this section presents a comparison between single and dual completions (DWS) in which all the scenarios are produced at the same total rate at all times, and production is finished at the same overall water cut. Also, all scenarios are operated at a bottomhole pressure just above the bubble point. The top completion in the DWS scenario penetrates 70% of the oil zone thickness and is operated at a specific constant rate. The bottom completion is operated at a variable bottom production rate estimated using the new method described in Section 5.1.2.1. Also, it is placed at about 5 ft below the OWC and has a length of 14 ft. Similar to what was found for edge-water systems in Section 5.1.2.2, the new method resulted in much higher recoveries than the conventional DWS approach in bottom-water systems. The cases considered for comparison are:

1. Single completion well penetrating 10% of the oil zone thickness
2. Single completion well penetrating 100% of the oil zone thickness
3. DWS Scenario (variable rate from the bottom completion).

Figure 152 shows recovery vs. time for a case with W_{sp}=24.05 (i.e., large well spacing and/or large ratio k_v/k_h) and M=10. This case showed a very minimal effect of well penetration on oil

bypassing in the results analyzed in previous sections. It can be seen that all scenarios recover approximately the same amount of oil at abandonment. It can also be noted; however, that the 10% penetration scenario resulted in slower recovery. The only reason why recovery for the 10% penetration scenario is slower is that, because of the smaller area of contact between the well and the reservoir, the well was not able to achieve the targeted assigned liquid production rates (the 10% penetration scenario showed no effect of penetration in Section 5.2.1.1 because the targeted "constant" liquid rates were achieved at all times). It can also be seen that the other two scenarios – full penetration and DWS - resulted in similar development of oil recovery with time.

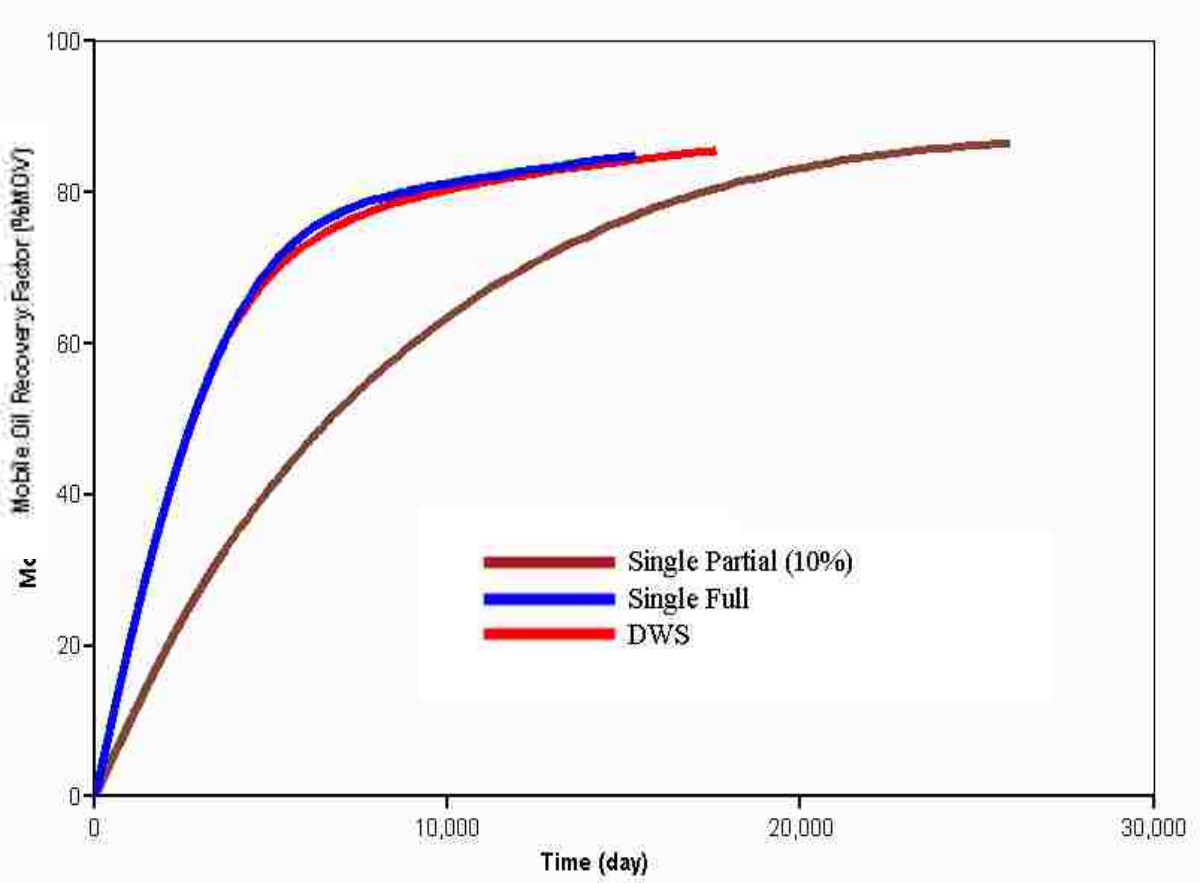

Figure 152: Oil Recovery for a Case with W_{sp}=24.05 and M=10

Figure 153 shows recovery vs. cumulative liquid production for the case with W_{sp}=24.05 (i.e., large well spacing and/or large ratio k_v/k_h) and M=10. It is obvious that the oil recovered per barrel of fluid produced for all scenarios is quite similar. The 10% penetration scenario shows slightly better recoveries at large volumes of liquid produced. This is probably because lower liquid production rates in this scenario resulted in a more stable cone. However, as shown in Figure 152, the higher liquid production rate in the other two scenarios resulted in substantial acceleration of recovery.

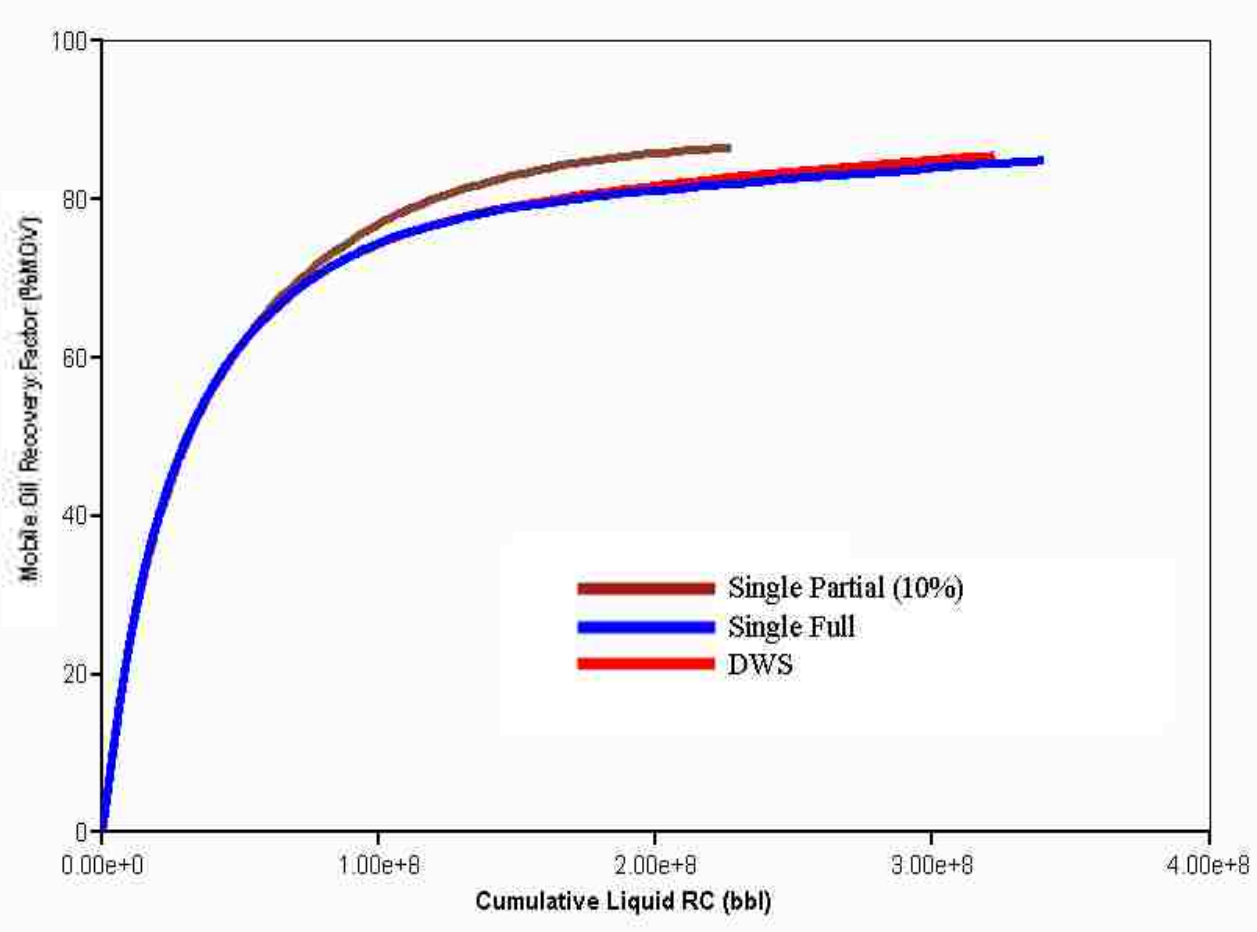

Figure 153: Oil Recovery vs. Cumulative Liquid Production for a Case with W_{sp}=24.05 and M=10

Figure 154 shows total water cut vs. time for the three scenarios. It is clear that the full

penetration and DWS scenarios give a faster development of water cut with time than the 10% penetration scenario. This is obviously because the 10% penetration scenario produced at a lower total production rate. These results clearly suggest that water production is needed in order to accelerate oil recovery. It is also interesting to observe that the water cut stabilizes at a value of approximately 0.67 in all cases, which is the ultimate water cut value calculated using Equation (2.43) at initial conditions (H_w=20 ft, H_o=100 ft, M=10). This confirms that the results of Equation (2.43) and, therefore, the method introduced in Section 5.1.2.1, can be reproduced in the simulator. Water cut remains stable at a value of 0.67 for as long as the cone grows laterally. Once there is vertical movement of the oil-water contact, the water cut starts to increase (zone at the right of the curve).

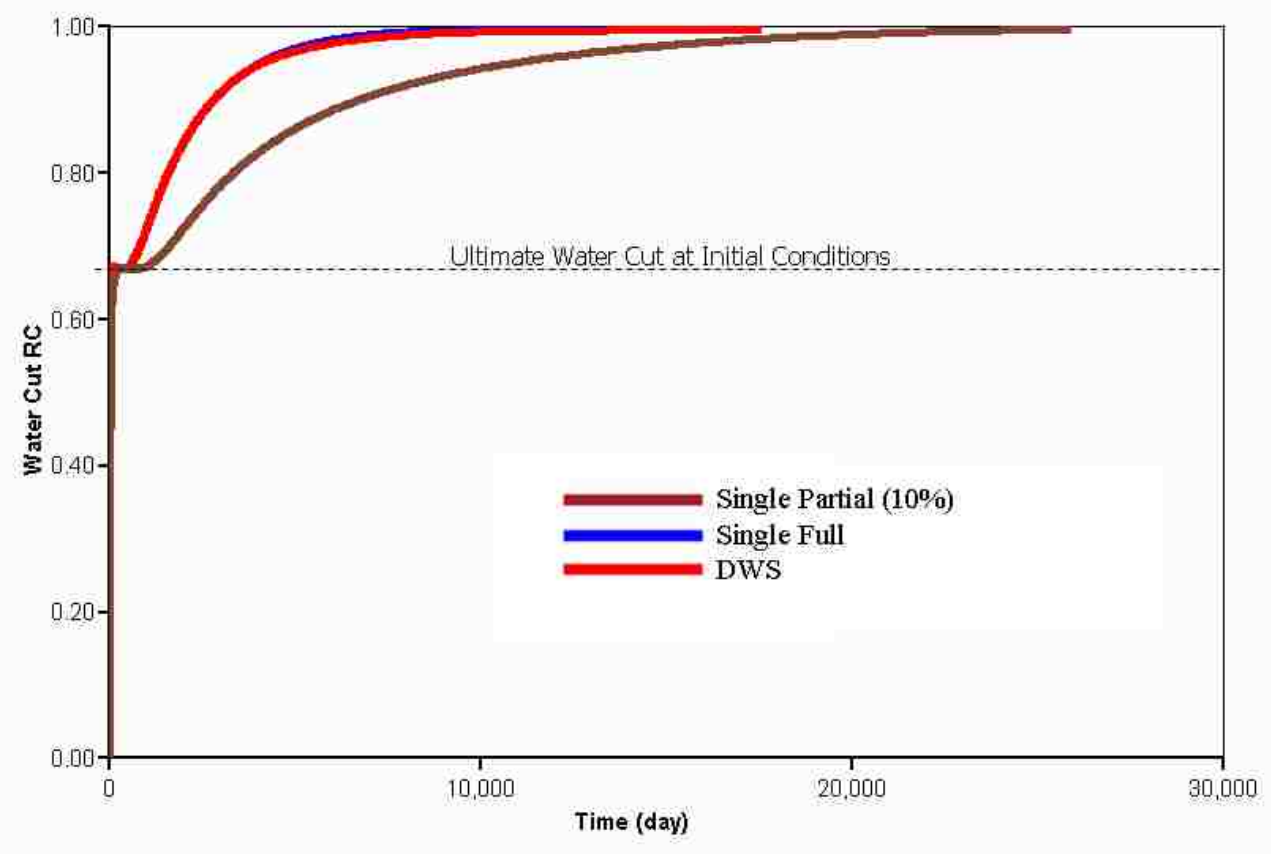

Figure 154: Water Cut vs. Time for a Case with W_{sp}=24.05 and M=10

Figure 155 shows oil recovery vs. time for a case created using the P50% values of each of the groups (W_{sp}=4.7 and M=2.6). This case can be regarded, therefore, as an "average reservoir". Similar to what was obtained for the case analyzed in the previous paragraphs, it can be seen that all scenarios recover approximately the same amount of oil at abandonment. It is also clear that the 10% penetration scenario resulted in slower recovery. As was explained before, this is because the 10% penetration scenario has a smaller area of contact between the well and the reservoir, therefore, the well was not able to achieve the targeted assigned liquid production rates.

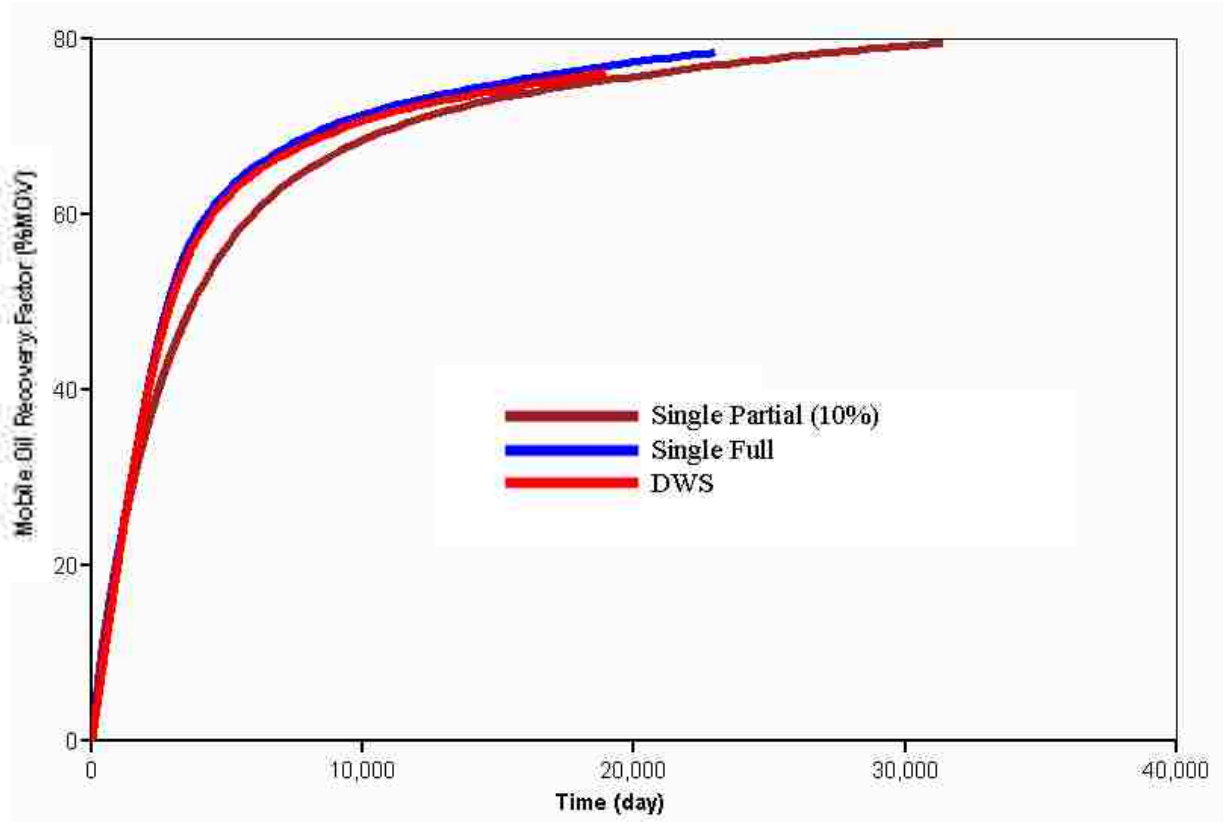

Figure 155: Oil Recovery for a Case with W_{sp}=4.7 and M=2.6 (Average Reservoir)

Figures 156 shows oil recovery vs. cumulative liquid for the "average" reservoir. Again,

it obvious that the amount of oil recovered per barrel of fluid produced for all scenarios is quite similar. Since the 10% penetration scenario is produced at smaller rates (it could not achieve the targeted assigned liquid rates), it resulted in slightly better recovery. However, as can be noted in Figure 155, lower rates also resulted in slower recovery, which may hamper the economics of the well.

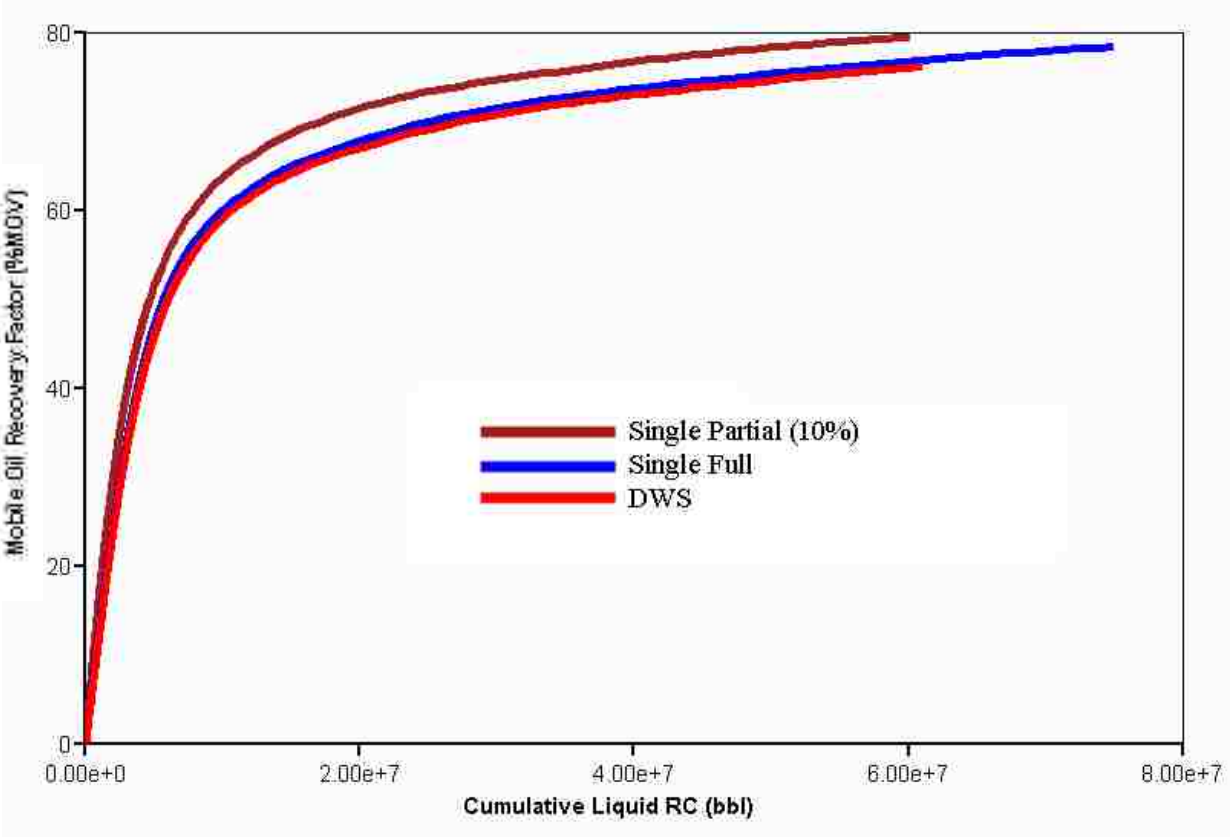

Figure 156: Oil Recovery vs. Cumulative Liquid Production for a Case with W_{sp}=4.7 and M=2.6 (Average Reservoir)

5.3 Summary and Further Discussion

The effect of well penetration on oil bypassing has been investigated using two different operating strategies: operation at a maximum total rate and operation at a minimum bottomhole

pressure. The first approach was considered since the ratio of gravity to viscous forces (N_g for edge-water system and G_v for bottom water systems), one of the dimensionless groups that describe immiscible displacement of oil by water drive systems, assumes constant total production rate. The second approach gives variable total production rate with time and; therefore, different values of the gravity to viscous forces ratio as time progresses.

Only a few cases were used to study the effect of well penetration on oil bypassing. However, both operating approaches (operation at maximum total rate and operation at minimum bottomhole pressure) show similar results. For example, it was found that for edge and bottom-water reservoirs with large end-point mobility ratios (e.g., large oil viscosities) and gravity forces (e.g., low liquid production rates), the best single completion strategy may be the use of short penetrating wells, since they may delay water breakthrough and improve oil recovery per barrel of fluid produced. This is true only if the reservoir has enough energy to maintain the targeted production rates. Short-penetration wells have smaller areas of contact between the well and the reservoir and, therefore, require more pressure drawdown to give a specific production rate than fully penetrating wells. The best single completion strategy for reservoirs with most of the other possible combinations of dimensionless groups seems to be the use of full penetrations. This is because fully penetrating well have a larger area of contact with the reservoir and, therefore, they could accelerate recovery.

A new method for DWS operation by using variable rates from the bottom completion has been introduced in this dissertation. The main advantage of the method is that only one simulation run is needed since the bottom completion water rates can be dynamically changed in the simulator by using multipliers. This provides a substantial advantage over Arslan (2005) method, which may require thousands of simulation runs to establish the optimum combination

of top and bottom rates at different times. The new method results in substantial acceleration in recovery over the conventional "constant rate at the top and bottom" approach by calculating the highest "clean" water rates at the bottom completion for a given "fixed" rate at the top completion. The new method, therefore, does not optimize the production rates from both completions. Since Arslan approach is based in an actual mathematical optimization problem, it is much more complete and should be used if detailed and accurate estimations of the optimum top and bottom completion rates are needed. The new method, thus, can be used for quick estimation of the potential of DWS over single completions and for rapid determination of the water production rates associated with improved DWS operation.

Contrary to what was expected, results presented in this study show that there is no significant difference between oil recovery rates obtained from DWS and long single completion wells if these two strategies are produced at the same total rates and ended at the same economic water cut. This study is unique in this sense. Previous studies have not compared DWS in terms of same total liquid production rate. It is important to indicate, however, that DWS allows independent operation of the completions. For example, each completion can be operated at a different pressure drawdown.

A tentative advantage of DWS over single penetrations is DWS can delay water breaktrough and give cleaner oil production from the top completion. DWS produces two stream of fluids having substantially different compositions. Fluid segregation may be desired to avoid the formation of emulsions and other effects that may affect well productivity and are not considered by the numerical simulation package used in this dissertation. Also, the simulation results presented here do not consider the effect of undesired water production on well tubing performance. Finally, no attempt has been made in this dissertation to evaluate the drainage-

injection variant of DWS. This variant would be benefitial since injecting the produced water may help to preserve the reservoir energy. Moreover, there may be cost reductions associated with the fact that water does not need to be taken to the surface.

CHAPTER 6. CONCLUSIONS AND RECOMMENDATIONS

6.1 Conclusions

In this dissertation, oil bypassing by water invasion in both edge-water and bottom-water reservoirs was studied in order to determine the magnitude of the problem and propose potential solutions. The main findings of the dissertation are:

Oil bypassing mechanisms:

- The main mechanisms leading to oil bypassing by water invasion in edge-water reservoirs is gravity underruning (formation of a water tongue). In bottom-water reservoirs, the main mechanism is water coning. The prejudicial effect of both mechanisms can be minimized if production is kept below the critical rates. However, the needed critical rates are usually too low to be economical.

Oil bypassing quantification:

- This research presents a statistical quantification, based on a database of reservoir properties, of the amount of bypassed oil in typical edge and bottom-water reservoirs. The results show that half of "homogeneous" edge-water reservoirs would bypass about 17% of the movable oil in place and one in five reservoirs (20%) would bypass 21% or more of the oil. Oil bypassing at abandonment was about 60% for the worst case scenario. When only reservoirs with end-point mobility ratios larger than 10 were considered, it was found that half of this new subset of reservoirs would bypass 26% or more of the movable oil volume and one in five would bypass 36% or more. These results suggest that the problem of oil bypassing in heavy oil reservoirs could be quite critical.

- The effect of permeability distribution on oil bypassing was studied by creating homogeneous, transgressive, regressive and serrated depositional sequences. The results show that oil bypassing is more significant for trangressive sequences. This is because high permeabilities at the bottom layers stimulate water tonguing. The average amount of by-passed oil for the homogeneous and transgressive sequences was found to be 19.3% and 25.4%, respectively.
- The effect of permeability distribution is more important for heavy oils. The average amounts of by-passed oil when only reservoirs with end-point mobility ratios higher than 10 were considered were 29.0% and 37.0% for homogeneous and transgressive sequences, respectively.
- It was found that oil bypassing for "typical" bottom-water reservoirs could be more significant than for "typical" edge-water reservoirs. Half of "typical" bottom-water reservoirs would bypass about 25% of the movable oil in place and one in five reservoirs (20% of the reservoirs) would bypass 40% or more of the oil. The worst case bottom-water scenario bypassed almost 80% of its oil. When only bottom-water reservoirs with end-point mobility ratios larger than 10 were considered, it was found that half of this new subset of reservoirs bypassed 44% or more of the movable oil volume and one in five bypassed 56% or more. These results confirm that the problem of oil bypassing in heavy oil reservoirs could be quite significant.

Oil bypassing prediction tools:

- This research presents new correlations for the prediction of oil bypassing in edge and bottom-water drive reservoirs. The correlations are not only easy to use, but they also remove many simplifying assumptions and problems implicit in the existing analytical

models. Also, since the new correlations were created using dimensionless groups and a large database of reservoir properties, they are general and can be used for oil bypassing prediction in a wide range of reservoirs.

Groups controlling oil bypassing:

- Three-dimensional water invasion to wells in a large variety of reservoirs with edge and bottom-water can be statistically modeled using only a few dimensionless groups and a small number of numerical experiments.
- The end-point mobility ratio (i.e., the viscosity contrast between oil and water) is the group with the strongest effect on oil bypassing for both edge and bottom-water reservoirs.
- For edge-water systems, it was found that oil bypassing is higher with high end-point mobility ratios (e.g. large oil viscosity) and Y-direction aspect ratios (e.g. large well spacing) and reduced by high X-direction aspect ratios (e.g. large L/H), high dip angle group (e.g. large dip angle) and high gravity numbers (e.g. low production rate).
- More oil will be left unrecovered in bottom-water reservoirs having high end-point mobility ratios, large well spacing and deep well penetration - particularly when they are produced at high rates (low values for the gravity to viscous forces group).

Effect of reservoir properties on oil bypassing:

- Aquifer strength, defined by its lateral extension, does not significantly affect the mechanisms of water invasion to wells, but could cause early end of production by natural drive. If artificially lifted, the wells in the same systems with weak aquifer and strong aquifer should leave the same amount of unrecovered oil.

- The effect of the Corey exponents on water invasion and oil bypassing could be significant. The choice of these exponents not only affects the shape of the oil-water interface, but also the thickness of the transition zone (separation between water saturation isosurfaces).
- Water breakthrough time can be substantially accelerated (up to 83% in this study) by the presence of a capillary transition zone in edge-water drive reservoirs.
- The maximum effect of capillary pressure on oil recovery at abandonment found in this study was 8%. This suggests that the capillary pressure effects can be neglected at abandonment. The effect of capillary pressure on oil recovery was found to be larger with low production rates.

Potential solutions:

- This study gives guidelines on the best well completion strategy for reservoirs affected by water invasion. It was found that edge and bottom-water reservoirs with large end-point mobility ratios and gravity forces should be operated using short penetrating wells, since this may improve oil recovery per barrel of fluid produced and delay water breakthrough. This is true only if the reservoir has enough energy to maintain the targeted production rates. Short-penetration wells have smaller areas of contact between the well and the reservoir and, therefore, require more pressure drawdown to give a specific production rate than fully penetrating wells.
- For reservoirs with most of the other possible combinations of dimensionless groups (most typical situation), having different well penetrations would not substantially affect the amount of oil recovered per barrel of fluid produced. Reservoirs in this category could be produced using deep penetrating wells, since this could accelerate recovery.

- A new method is proposed which would enhance DWS operation in vertical wells. The method involves using variable water production rates in time at the bottom completion. Variable rates are justified since the dynamics of water coning and the position of the horizontal oil-water contact change with time. Results show that the new method for DWS operation results in higher recoveries than the conventional approach.
- A comparison of DWS with long single completion of similar length based on the same total fluid rate does not give different recovery rates but shows that DWS well operates at different pressure drawdowns. It is, then, concluded that the recovery performance of the two types of wells may be different if the basis for comparison is a maximum pressure drawdown rather than same total fluid rate.
- A tentative advantage of DWS over single penetrations is DWS can delay water breaktrough and give cleaner oil production from the top completion. DWS produces two stream of fluids having substantially different compositions.

6.2 Recommendations

- Future work could involve using more levels per group in the experimental design. This would allow further exploring non-linear effects and increase the understanding of the effect of each group and the groups' interaction. The Central Composite, Box-Behnken, Fractional Factorial or any other design could then be used to optimize the process (minimize the number of runs).
- The dimensionless groups used in this dissertation to study oil bypassing were created for constant-rate conditions. It would be interesting to create new groups and repeat the work done in this dissertation for constant-pressure conditions.

- Additional work is required to study the potential for DWS application in watered out/marginal wells. Also, it would be prudent to study the optimum time for operation of the bottom (sink) completion.
- More work is needed to study the appropriate length for the top and bottom completions in DWS systems for different reservoir and operating conditions. A new experimental design could be performed to determine DWS potential over a wide range of reservoir/well parameters.
- The new correlations presented in this dissertation for the estimation of oil bypassing in edge and bottom-water reservoirs need to be tested against the existing analytical models and/or numerical simulations using different data than the one employed for their creation.
- The new method - based on the ultimate water cut concept - proposed in this dissertation for estimation of the bottom completion rates required for DWS application is simple and efficient. However, additional effort is needed to determine the exact conditions for which the assumptions implicit in the ultimate water cut equations are valid.
- It would be advisable to perform studies to determine the feasibility of the drainage-injection variant of DWS. These studies should include economic evaluations considering the cost of lifting water to the surface.
- It is important to study the impact of tubing effects, emulsions and other near wellbore effects on DWS performance.
- Results presented in this dissertation show that relative permeability curvatures can have a significant effect on oil bypassing, particularly for unstable displacements. It is recommended to consider this effect carefully. New dimensionless groups could be added

to include the impact of changes in relative permeability curvatures and/or relative permeability end-points.

- A similar study of oil bypassing than the one presented in this dissertation could be completed for gas reservoirs.

NOMENCLATURE

A = area

a = inter-well distance

BPO = by-passed oil (% of mobile oil volume)

g = gravity

H = thickness of the oil zone

h_p = penetration thickness

k = absolute permeability

k_h = horizontal permeability

k_v = vertical permeability

k_{ro}' = end-point relative permeability of oil

k_{rw}' = end-point relative permeability of water

k_x = X-direction permeability

k_y = Y-direction permeability

k_z = Z-direction permeability

L = length of the slab

n_o = Corey exponent to oil

n_w = Corey exponent to water

q = total (liquid) production rate

RF = recovery factor (% of movable oil volume)

r_w = well radius

S_{or} = residual oil saturation

S_w = water saturation

S_{wi} = initial water saturation

t = time

V = superficial velocity

W = width of the slab

α = dip angle of the reservoir

$\Delta\rho$ = density difference = water density – oil density

ϕ = porosity

λ^{o}_{ro} = end-point mobility permeability for oil

λ^{o}_{rw} = end-point mobility permeability for water

μ_o = oil viscosity

μ_w = water viscosity

ρ_o = oil density

ρ_w = water density

σ = interfacial tension

θ = contact angle

REFERENCES

Advanced Resources International: Undeveloped Domestic Oil Resources: The Foundation for Increasing Oil Production and a Viable Domestic Oil Industry. *Prepared for U.S. Department of Energy Office of Fossil Energy - Office of Oil and Natural Gas, February, 2006.*

Alden A.: Your Guide to Geology. *Found at: http://geology.about.com/library/bl/images/blanticline.htm, 2007.*

Armenta, M., White, C., Wojtanowicz, A.: Completion Length Optimization in Gas Wells; *Paper 2003-192, Canadian International Petroleum Conference, Calgary, Canada, June 2003.*

Arslan, O.: Optimal Operating Strategy For Wells With Downhole Water Sink Completions To Control Water Production And Improve Performance. *PhD Dissertation, Louisiana State University, May 2005.*

Begg S., Gustason E., Deacon M.: Characterization of a Fluvial-Dominated Delta: Zone 1 of the Prudhoe Bay Field. *SPE 24698, Annual Technical Conference and Exhibition, Washington DC, October 1992.*

Bournazel, C. and Jeanson B.: Fast Water-Coning Evaluation Method. *SPE 3628, 46th Annual Fall Meeting, New Orleans, Oct. 3-6, 1971.*

Bridgman. P.: Dimensional Analysis. *Encyclopaedia Britannica, Vol. 7, pp. 439-449, Chicago, 1969.*

Buckingham E.: On Physical Similar Systems; Illustrations of the Use of Dimensional Equations; *Phys. Rev. 2nd ser., 4, 1914.*

Catuneanu, O.: Sequence Stratigraphy of Clastic Systems: Concepts, Merits, and Pitfalls. *Journal of African Earth Sciences, Volume 35, Issue 1, Pages 1-43, 2002.*

Dake, L.P.: Fundamentals of Reservoir Engineering; *Elsevier Scientific Publishing Company, New York, 1978.*

Dietz, D.: A theoretical Approach to the Problem of Encroaching and By-Passing Edge Water. *Proceedings, series B, of the Koninklijke Nederlandse Akademie Van Wetenschappen, Amsterdam, 1953.*

Dunn, M. and Chukwu, G.: Simulation Based Dimensionless Type Curves for Predicting Waterflood Recovery. *SPE 68839, Western Regional Meeting, 26-30 March, Bakersfield, California, 2001.*

Fayers, F, Muggerldge, A.: Extensions to Dietz Theory and Behavior of Gravity Tongues in Slightly Tilted Reservoirs. *Paper SPE 18438, November 1990.*

Friedmann, F., Chawathe, A., Larue, D.: Assessing Uncertainty in Channelized Reservoirs Using Experimental Designs. *SPE 71622, SPE Annual Technical Conference and Exhibition, New Orleans, September 2001.*

Fleming, P., Mansoori, J.: An Accurate Numerical Technique for Solution of Convection-Diffusion Equations without Numerical Dispersion. *SPE 12714, July 13, 1986.*

Goda M., Behrenbruch P.: Using a Modified Brooks-Corey Model to Study Oil-Water Relative Permeability for Diverse Pore Structures. *SPE 88538-MS, Asia Pacific Oil and Gas Conference and Exhibition, Perth, Australia, October 18-20, 2004.*

Goda M., Behrenbruch P.: Two-Phase Relative Permeability Prediction: A Comparison of the Modified Brooks-Corey Methodology with a New Carman-Kozeny-Based Flow Formulation. *SPE 101150-MS, Asia Pacific Oil and Gas Conference and Exhibition, Perth, Australia, September 11-13, 2006.*

Henley D., Owens W., Craig F.: A Scale-Model Study of Bottom-Water Drives. *Journal of Petroleum Technology, Volume 13, Number 1, January 1961, Pages 90-98.*

Hernandez, J., Wojtanowicz, A.K., Qualification of Un-recovered Reserves Due to Production Process Dynamics in Water-Drive Reservoirs; *Paper 2005-237, Canadian International Petroleum Conference, Calgary, Canada, June 2005.*

Hernandez, J., Wojtanowicz, A.: Assessment of Un-Recovered Oil in Dipping Reservoirs From Analysis of Water Cut Development. *Paper 2006-200, Canadian International Petroleum Conference, Calgary, Canada, June 2006.*

Hernandez, J., Wojtanowicz, A., White, C.: Qualification of Un-recovered Reserves Due to Production Process Dynamics in Water-Drive Reservoirs. *Paper 2006-199, Canadian International Petroleum Conference, Calgary, Canada, June 2006.*

IMEX Manual, Version 2005.10. *Computer Modelling Group (CMG), Calgary, Canada, 2005.*

Inikori, S., Wojtanowicz, A.: Contaminated Water Production in Old Oil Fields With Downhole Water separation: Effects of Capillary Pressures and Relative Permeability Hysteresis. *SPE 66536, SPE/EPA/DOE Exploration and Production Environmental Conference, San Antonio, Texas, February 26-28, 2001.*

Inikori, S., Wojtanowicz, A., Siddiqi, S.: Water Control in Oil Wells With Down hole Oil-Free Water Drainage and Disposal. *SPE 77559, SPE Annual Technical Conference and Exhibition, San Antonio, Texas, Sep.29-Oct.2, 2002.*

Jensen, J., Lake, L.: The Influence of Sample Size and Permeability Distribution on Heterogeneity Measures. *SPE 15434, SPE Reservoir Engineering Journal, Volume 39, Number 9, May 1988.*

Ju, B. et al.: An Effective Method to Improve Recovery of Heavy Oil Reservoir with Bottom Water Drive. *Paper IPTC 10521, International Petroleum Conference, Doha, Qatar, November 21-23, 2005.*

Kalla, S., White.C.: Efficient Design of Reservoir Simulation Studies for Development and Optimization. *SPE 95456, Annual Technical Conference and Exhibition, Dallas, Texas, October 9-12, 2005.*

Kumar, A.: Drainage Areas for Wells in Edge Water-Drive Reservoirs. *SPE 4966, Journal of Petroleum Technology, December 1977, Pages 1673-1682*

Kuo, M. and DesBrisay, C.: A Simplified Method for Water Coning Predictions. *SPE 12067, SPE 58th Annual Technical Conference, San Francisco, Oct. 5-8, 1983.*

Lake, L.: Enhanced Oil Recovery. *Prentice-Hall, New Jersey, 1989.*

Lantz, R.: Quantitative Evaluation of Numerical Diffusion (Truncation Error). *SPE 2811, SPE 2nd Symposium on Numerical Simulation of Reservoir Performance, Dallas, Feb. 5-6, 1970.*

Lee, J.: Well Testing. *Society of Petroleum Engineers, Richardson, Texas, 2002.*

Lee, R. et al.: Strategies for Produced Water Handling in New Mexico. *New Mexico Water Resources Research Institute, October, 2002.*

Mattax C. and Dalton, R.: Reservoir Simulation. *SPE Monograph Volume 13, Richardson, Texas, 1990.*

Mitchum Jr.: Seismic Stratigraphy and Global Changes of Sea Level. Part 11: Glossary of Terms used in Seismic Stratigraphy: Section 2. Application of Seismic Reflection Configuration to Stratigraphic Interpretation. *A.A.P.G. Memoir 26, 1972, Pages 205 - 212.*

Novakovic D.: Numerical Reservoir Characterization Using Dimensionless Scale Numbers With Application In Upscaling. *Phd Dissertation, Louisiana State University, August, 2002.*

Outmans, H.: Transient Interfaces During Immiscible Liquid-Liquid Displacement in Porous Media. *SPE 210, California, July 1962.*

Poston, S. and Gross S.: Numerical Simulation of Sandstone Reservoir Models. *SPE 12135, Journal SPE Reservoir Engineering, Issue July, Pages 423-429, 1986.*

Rapoport, L. and Leas W.: Properties of Linear Water Floods. *SPE 213-G presented at the Fall Meeting of the Petroleum Branch in Houston, Texas, Oct. 1-3, 1952.*

Richardson, J., Blackwell, R.: Use of simple Mathematical Models for Predicting Reservoir Behavior. *SPE 2928, September 1971*.

Richardson, J., Sangree, J., Sneider, R.: Sand-Rich Deltas. *SPE 15779-PA, Journal of Petroleum Technology, Vol. 41, Number 2, February, 1989, Pages 157-158.*

Nau, R.: Additional Notes on Regression Analysis. *Found at: ttp://www.duke.edu/%7Ernau/ regnotes.htm*

Ruark, A.E.: Inspectional Analysis: A Method Which Supplements Dimensional Analysis. *Journal of the Mitchell Society, August 1935, Pages 127-133.*

SAS version 9.1.3. *SAS Institute Inc., Cary, NC, USA, 2003.*

Seright, R. et al.: A Strategy For Attacking Excess Water Production. *Petroleum Recovery and Research Center, New Mexico, 2003.*

Shaw, D., Dozzo, J.: Reducing Numerical Diffusion in the Modeling of Sharp Saturation Fronts: A Conservation - Law Approach. *SPE 21179, Latin American Petroleum Engineering Conferences, Rio de Janeiro, Oct. 14-19, 1990.*

Sheldon, J. and Fayers, F.: The Motion of an Interface Between Two Fluids in Slightly Dipping Porous Medium. *SPE 325, New York. September 1962.*

Shirman, E., Wojtanowicz, A.: More Oil with Less Water Using Downhole Water Sink Technology: A Feasibility Study. *SPE 49052-MS, Annual Technical Conference and Exhibition, New Orleans, Louisiana, September 27-30, 1998.*

Shook, M., Li, D. and Lake, L.: Scaling Immiscible Flow Through Permeable Media by Inspectional Analysis. *In Situ, 16 (4), Pages 311-349, 1992.*

Siddiqi, S.: A Study of Bottom Water Drive Reservoirs Using a Scaled Physical Model and a Numerical Simulator. *Thesis, Louisiana State University, 2001.*

Siddiqi, S., Wojtanowicz, A.: A Study of Water Coning Control in Oil Wells by Injected or Natural Flow Barriers Using Scaled Physical Model and Numerical Simulator. *SPE 77415-MS, SPE Annual Technical Conference and Exhibition, San Antonio, Texas, September 29 – October 2, 2002.*

Slobod, R., Howlett, W.: The Effects of Gravity Segregation in Laboratory Studies of Miscible Displacement in Vertical Unconsolidated Porous Media. *SPE 743, Calgary, June 1963.*

Sobocinski, D. and Cornelius, A.: A Correlation for Predicting Water Coning Time. *JPT, May 1975, Pages 594-600.*

Sonin, A.: The Physical Basis of Dimensional Analysis. *Department of Mechanical Engineering, MIT, Cambridge, 1997.*

White, C., Willis, B., Narayanan, K. and Dutton, S.: Identifying and Estimating Significant Geologic Parameters With Experimental Design. *SPE Journal, September 2001, Pages 311-324.*

Wojtanowicz, A.: Downhole Water Sink Technology. Taken from: http://www.pete.lsu.edu /faculty/akw/dws.htm.

Wojtanowicz, A.K., Shirman, E.I., Kurban, H.: Downhole Water Sink (DWS) Completion Enhance Oil Recovery in Reservoirs with Water Coning Problem. *SPE 56721, SPE Annual Technical Conference & Exhibition, Houston, TX, Oct. 3-6, 1999.*

Wood, D., Lake, L., Johns, R.: A Screening Model for CO2 Flooding and Storage in Gulf Coast Reservoirs Based on Dimensionless Groups. *Paper SPE 100021, SPE/DOE Symposium on Improved Oil Recovery, Tulsa, Oklahoma, April 22-26, 2006.*

Yaw Peng, C., Gupta, R.: Experimental Design in Deterministic Modelling: Assessing Significant Uncertainties. *SPE 80537, SPE Asia Pacific Oil and Gas Conference and Exhibition, Jakarta, Indonesia, September 2003.*

VITA

Juan C. Hernandez, son of Taide de Hernandez and Juan M. Hernandez, received a Bachelor of Science degree in petroleum engineering in 1998 in Barcelona, Venezuela. In 2001, he earned a Master of Philosophy degree, also in petroleum engineering, at Imperial College, London. His research interests include water production control in petroleum wells, numerical simulation, and reservoir engineering. Hernandez formerly worked at PDVSA (Venezuelan State Oil Company) as a numerical simulation engineer for over 3 years. He has completed summer internships with Unocal in Houston, Texas, where he acted as a numerical simulation engineer for a deep water project and Chevron Energy Technology Company in Bakersfield, California, were he worked in two thermal simulation projects. In 2005 he served as instructor of the course: "Numerical Simulation of Improved Recovery Processes (PETE 4056)" at LSU. He has also been a speaker at several Petroleum Technology Transfer Council (PTTC) workshops.